THE UNIVERSITY
of EDINBURGH

Dissecting the biological roles of Kdm3b and Kdm3a lysine demethylases

Ioannis Kasioulis

A thesis submitted for the degree of Doctor of Philosophy

The University of Edinburgh

2014

Στους γονείς μου

Decleration

I declare that this thesis has been composed by me, the work described is my own and contributions by others are clearly indicated. This work has not been submitted for any other degree or professional qualification except as specified.

Ioannis Kasioulis

May 2014

Abstract

Lysine demethylases are a newly discovered group of enzymes that have rapidly expanded over evolutionary time by the acquisition of multiple functional domains, in addition to the unifying catalytic JmjC domain. There are thirty members of the JmjC-domain family in humans. A proportion of lysine demethylases catalyse the removal of methyl modifications from lysine residues of histones and non-histone proteins.

The discovery of mutations in histone demethylase genes, in a number of human syndromes, stresses the functional importance of these enzymes in development and disease. Therefore, the phenotypic dissection of animal models of histone lysine demethylases will provide invaluable insights into the molecular mechanisms that underlie human disease.

In mammals, the *Kdm3* family of histone demethylases includes *Kdm3a, Kdm3b, Jmjd1c* and *Hairless*. However, in zebrafish, there are two *kdm3* genes, one of which encodes a protein similar to both the mammalian Kdm3a and Kdm3b. Morpholino knock-down of the *kdm3* gene in zebrafish faithfully recapitulates classical ciliary phenotypes, although the underlying causalities are still unclear. In recent years, *Kdm3a* function has been extensively dissected through the use of mouse models and cell culture studies, focusing on the nuclear histone demethylation function. Kdm3a gene-trap and knock-out mouse models present with obesity, infertility, sex reversal and predisposal to diabetes, reminiscent of a human ciliopathy syndrome. No mouse models for *Kdm3b* have been characterised yet.

In this study, I hypothesized that the murine Kdm3a and Kdm3b histone demethylases have diverged biological roles and that the zebrafish kdm3 fulfils the functions of both. The aims of my thesis were: 1) to compare the evolutionary conservation of the zebrafish kdm3 and murine Kdm3b in function and check their spatial expression, 2) to dissect the phenotype of *Kdm3b* gene-trapped mice and 3) to characterise an alternative murine *Kdm3a* isoform.

Protein sequence comparison studies show that the zebrafish kdm3 protein is closer in sequence to the mammalian Kdm3b. Both the zebrafish kdm3 and murine Kdm3b are di-methyl lysine 9 (H3K9me2) demethylases, however, they have diverged spatial expression during embryogenesis. In agreement with the phenotype of *kdm3* morphants, over-expression of the zebrafish kdm3 reduces ciliation efficiency when transfected into animal cells.

Notably, the phenotype analysis of *Kdm3b* gene-trapped mice does not resemble classical ciliary phenotypes, as one would expect from the zebrafish data. Homozygous *Kdm3b* gene-trapped mice are postnatally growth retarded, with plausible defects in thymus organ development.

Interestingly, an alternative murine Kdm3a isoform (Kdm3a-i2) shows both nuclear and cytoplasmic localisation. Over-expression studies revealed that Kdm3a-i2 retains its histone demethylation function, and a proportion of the over-expressed construct localises to the centrosome. In addition, over-expression of Kdm3a-i2 reduces ciliation efficiency.

Overall, the data from my studies suggests that: 1) the zebrafish kdm3 is more similar in sequence to the murine Kdm3b than Kdm3a, is a histone demethylase and has a distinct spatial expression during embryogenesis. However, the phenotype of *kdm3* zebrafish morphants is more closely related to the *Kdm3a*-than *Kdm3b*-deficient mice, 2) the murine *Kdm3a* and *Kdm3b* have distinct biological roles, as evidenced by the mouse models, 3) the Kdm3a-i2 isoform shares the same nuclear demethylation function as the full length Kdm3a and has a plausible centrosomal function.

Acknowledgements

There are so many people I would like to acknowledge, I hope I remember everyone! To begin, I would like to thank my supervisors Patricia and Ian for their advice, guidance and supprt throughout my PhD studies. Also, Ian Jackson and Veronica van Heyningen without whom the mouse work would have been impossible. To Pleasantine for all the input.

Special thanks to the microscopy people Matt and Paul for their help whenever I had throuble figuring out what I should be doing! Also, to John and Jacek for their cooperartion in maintaining the mouse stocks, their advice, and help on experiments. To Lizzie and Andrew Wood for their help with the FACS. To Rachel, not only for the advice, but also for the reagents of the immunohistochemistry experiment. To Carol-Anne for the provision of plasmids . To You-Ying Chau for all the help with the adipokine arrays☺.

Furthermore, lots of gratitude to Shipra, Adam, D.J., Kathy, Morad, Jackie, Anne, Carol-Anne, Maggie, Sarah, Abdel, Sylvia, Sara-the-spanish (and the forgotten others!!) for our daily chat in the office, the lab and the parking place on random stuff that had nothing to do with science!!

To all other people in the E2 and C2 lab for anything that I may be forgetting again! Furthermore, many thanks to the technical services personel for the provision of reagents, for sequencing and endless help and training for sectioning and staining-Allyson, you have been incredibly helpful, thank you so much!

And of course I could not forget my dear labmates Girish, Emma, Olivia, Matt, the super ex-labmate Shalini and the incredible Pedro for our day to day interactions in the lab, during lunchtime, in the pubs and....that's it! I wish you, all the good luck in your life and career, may your aspirations (whatever those can be!!) and wishes come true. May the force be with you!!

Coming towards the end, this PhD was mentally supported by Sofia and Costas. It is amazing how close friends can have such a positive impact on one's life

(in this case mine, don’t get carried away from the philosophical statement I just placed :D). I will be always in debt. And no, Costa, you are not going to Ibiza for free, you lost the bet!! Find another sponsor. :D

Last, my forever and ever love to my parents, who supported me throughout my life. Without you, I would not have been able to study abroad and experience a world, much different from Cyprus. Words become irrelevant when I reflect back to my everyday life and remember how much I was given.

Ok, it is about time I relax and enjoy the summer sun! Have an enjoyable 2014 summertime!!!!!

Table of contents

List of figures

List of Tables

Abbrevations

ARID	AT-rich interacting domain
ATP	Adenosine triphosphate
BAT	*brown adipose tissue*
BCIP	5-Bromo-4-chloro-3-indolyl phosphate
bp	base pair
BSA	bovine serum albumin
C. elegans	*Caenorhabditis elegans*
cDNA	complementary DNA
CH_2O	formaldehyde
CHAPS	3-[(3-Cholamidopropyl)dimethylammonio]-1-propanesulfonate
ChIP-seq	chromatin immunoprecipitation sequencing
CO_2	carbon dioxide
CoA	*co-activator*
CoR	*co-repressor*
cTEC	cortical thymic epithelial cells
DAB	3,3′-Diaminobenzidine tetrahydrochloride
DAPI	4',6-diamidino-2-phenylindole
dH_2O	distilled water
DIG	Digoxigenin
DMEM	Dulbecco's Modified Eagle's medium
DMEM/F12	Dulbecco's Modified Eagle Medium/Nutrient Mixture F-12
DN	Double negative
DNA	Deoxyribonucleic acid
DNase I	Deoxyribonuclease I

dNTP	Deoxyribonucleotide triphosphate
DOC	deoxycholate
DP	Double positive
dpf	days post fertilisation
DTT	Dithiothreitol
E18.5	Embryonic day 18.5
EDTA	Ethylenediaminetetraacetic acid
EGTA	ethylene glycol tetraacetic acid
ES	Embryonic stem
ESC	embryonic stem cells
EtOH	ethanol
EUCOMM	European Conditional Mouse Mutagenesis
FAD	flavin adenine dinucleotide
FCS	fetal calf serum
Fe(II)	iron
GFP	green fluorescent protein
H&E	haematoxylin and eosin
H1.4K26me2	dimethyl lysine 26 histone 1.4
H1.4K26me3	trimethyl lysine 26 histone 1.4
H_2O_2	hydrogen peroxide
H3K27ac	acetylation lysine 27 histone 3
H3K27me3	trimethyl lysine 27 histone 3
H3K4me1	monomethyl lysine 4 histone 3
H3K4me2	dimethyl lysine 4 histone 3
H3K4me3	trimethyl lysine 4 histone 3

H3K79me1	monomethyl lysine 79 histone 3
H3K79me2	dimethyl lysine 79 histone 3
H3K79me3	trimethyl lysine 79 histone 3
H3K9me1	monomethyl lysine 9 histone 3
H3K9me2	dimethyl lysine 9 histone 3
H3K9me3	trimethyl lysine 9 histone 3
HCl	Hydrochloric acid
Homo	homozygote
IPTG	Isopropyl β-D-1-thiogalactopyranoside
IFT A	Intraflagellar transport complex A
IFT B	Intraflagellar transport complex B
JmjC	JumonjiC
JmjN	Jumonji N
KCl	Potassium chloride
kDa	kilodalton
KDM3B-CT	antibody raised against the carboxyl-terminal of KDM3B
KDM3B-NT	antibody raised against the amino-terminal of KDM3B
KOH	Potassium hydroxide
LB	lysogeny broth
LiCl	Lithium chloride
Mb	mega base pairs
MEF	mouse embryonic fibroblasts
MeOH	methanol
mg	milligram
$MgCl_2$	Magnesium chloride

$MgSO_4$	Magnesium sulfate
ml	milliliter
mm	millimeter
mM	millimolar
mTEC	medullary thymic epithelial cells
n.s	not significant
NaCl	Sodium chloride
NBT	4-nitro blue tetrazolium chloride
NH_4Cl	Ammonium chloride
NLS	*nuclear localisation signal*
NP-40	nonyl phenoxypolyethoxylethanol
N-terminus	amino-terminus
NuRD	Nucleosome Remodeling Deacetylase
O_2	oxygen
^oC	degree Celsius
p14-28	postnatal day 14-28
p21	postnatal day 21
p3	postnatal day 3
p42	postnatal dat 42
p7	postnatal day 7
pA	poly A
PAS staining	periodic acid-schiff staining
PBS	phosphate buffered saline
PCR	polymerase chain reaction
PFA	paraformaldehyde

PI3K/Akt signaling pathway	phosphatidylinositol 3-kinase - v-akt murine thymoma viral oncogene homolog 1 signaling pathway
PMSF	phenylmethylsulfonyl fluoride
PPRE	peroxisome proliferator hormone response element
PRC2	*Polycomb Repressive Complex 2*
qRT-PCR	*real time quantitative polymerase chain reaction*
Ras/MAP signaling pathway	Rat sarcoma/mitogen-activated protein kinase signaling pathway
RFP	red fluorescent protein
RNA	Ribonucleic acid
RNase	Ribonuclease
rpm	rounds per minute
rRNA	ribosomal RNA
S. cerevisiae	*Saccharomyces cerevisiae*
SA	splice acceptor site
SAP	shrimp alkaline phosphatase
SDS	Sodium dodecyl sulfate
shRNA	short hairpin ribonucleic acid
SOC	Super Optimal Broth
SP	Single positive
SSC	saline-sodium citrate
SV40	Simian vacuolating virus 40
SWI-SNF	SWItch/Sucrose NonFermentable
T3	triidothyronine
T4	thyroxine
TBE	solution containing Tris, borate, and EDTA

TEG	buffer solution containing Tris base and EGTA
TEMED	Tetramethylethylenediamine
TERT-RPE1	Telomerase immortalised retinal pigmented epithelial cells
Th pathway	*thyroid hormone pathway*
Tris	tris(hydroxymethyl)aminomethane
tRNA	transfer RNA
TSS	transcription start site
t-test	Student's *t*-test
UTR	untranslated region
WAT	white adipose tissue
WT	wild type
X-Gal	5-bromo-4-chloro-3-indolyl-β-D-galactopyranoside
ZF	zinc finger
αKG	alpha ketoglutarate
β-gal	Beta-galactosidase
β-geo	Beta-galactosidase /neomycin
µCT	micro Computer Tomography
µg	microgram
µl	microlitre
µm	micrometer
µM	micromolar

Genes

Short name	Full name
Apoa4	*apolipoprotein A-IV*
ATR	*ataxia telangiectasia and Rad3 related*
Bbs4	*bardet-Biedl syndrome 4*
CD25	*interleukin 2 receptor, alpha chain*
CD4	*CD4 antigen*
CD44	*CD44 antigen*
CD8	CD8 antigen, alpha polypeptide
CEP152	*centrosomal protein 152kDa*
Chmp3	charged multivesicular body protein 3
CoREST	*REST corepressor*
Cyp26a1	cytochrome P450, family 26, subfamily a, polypeptide 1
Egr1	early growth response 1
EHMT1	*euchromatic histone-lysine N-methyltransferase 1*
EHMT2	*euchromatic histone-lysine N-methyltransferase 2*
Etf1	eukaryotic translation termination factor 1
Exoc6	exocyst complex component 6
Ezh2	*enhancer of zeste homolog 2 (Drosophila)*
Fam160b2	family with sequence similarity 160, member B2
Gapdh	*glyceraldehyde-3-phosphate dehydrogenase*
Gh	*growth hormone*
Ghih	*growth hormone inhibiting hormone*
Ghr	*Growth hormone receptor*
Ghrh	*growth hormone-releasing hormone*

Ghrhr	*Growth hormone releasing hormone receptor*
Gli1	*GLI-Kruppel family member GLI1*
Gli2	*GLI-Kruppel family member GLI2*
Gli2	*GLI-Kruppel family member GLI3*
H2A	*histone H2A*
H2B	*histone H2B*
H3	*histone 3*
H4	*histone H4*
Hbb-y	*hemoglobin Y, beta-like embryonic chain*
HR	*hairless*
Hspa4l	heat shock 70kDa protein 4-like
Ifgn	*interferon, gamma*
Ift88	*intraflagellar transport 88*
Igf1	*insulin-like growth factor 1*
Igf1r	*insulin-like growth factor 1 receptor*
Igf2	*insulin-like growth factor 2*
Igfals	*insulin-like growth factor acid labile subunit*
Igfbp3	*insulin-like growth factor binding protein 3*
Insr	*insulin receptor*
Irs	*insulin receptor substrate*
Jak2	*Janus kinase 2*
Jarid2	*jumonji, AT rich interactive domain 2*
Jhd1	*JmjC domain-containing Histone Demethylase*
Jhd2p	*JmjC domain-containing Histone Demethylase*
JMJD1C	*jumonji domain containing 1C*

JMJD6	*jumonji domain containing 6*
KDM1A	*lysine (K)-specific demethylase 1A*
KDM1B	*lysine (K)-specific demethylase 1B*
KDM2A	*lysine (K)-specific demethylase 2A*
KDM3A	*lysine (K)-specific demethylase 3A*
KDM3B	*lysine (K)-specific demethylase 3B*
KDM4A	*lysine (K)-specific demethylase 4A*
KDM4B	*lysine (K)-specific demethylase 4B*
KDM4C	*lysine (K)-specific demethylase 4C*
KDM4D	*lysine (K)-specific demethylase 4D*
KDM5A	*lysine (K)-specific demethylase 5A*
Kdm5b	*lysine (K)-specific demethylase 5B*
Kdm6b	*lysine (K)-specific demethylase 6B*
KDM7A	*lysine (K)-specific demethylase 7A*
Lmo2	*LIM domain only 2 (rhombotin-like 1)*
MDC1	*mediator of DNA-damage checkpoint 1*
Mrpl35	mitochondrial ribosomal protein L35
Ndufs8	NADH dehydrogenase (ubiquinone) Fe-S protein 8, 23kDa (NADH-coenzyme Q reductase)
NF-κB	*nuclear factor kappa-light-chain-enhancer of activated B cells*
NSD1	*nuclear receptor binding SET domain protein 1*
Nt5c1a	5'-nucleotidase, cytosolic IA
Nudt18	nudix (nucleoside diphosphate linked moiety X)-type motif 18
ORC	*origin recognition complex*
Pdgfra	*platelet-derived growth factor receptor, alpha polypeptide*
PHF2	*PHD finger protein 2*

PHF8	*PHD finger protein 8*
Pparα	*peroxisome proliferator-activated receptor alpha*
PKD2	*polycystic kidney disease 2*
PPARγ	*peroxisome proliferator-activated receptor gamma*
Ran	RAN, member RAS oncogene family
Reep1	receptor accessory protein 1
Reep2	receptor accessory protein 2
Reep3	receptor accessory protein 3
Reep4	receptor accessory protein 4
Rph1	*Regulator of PHR1*
SETD7	*SET domain containing (lysine methyltransferase) 7*
SETD8	*SET domain containing (lysine methyltransferase) 8*
Shc	*src homology 2 domain-containing transforming protein*
Smo	*Smoothened, frizzled class receptor*
SMYD2	*SET and MYND domain containing 2*
Sox2	*SRY (sex determining region Y)-box 2*
Src	*v-src avian sarcoma (Schmidt-Ruppin A-2) viral oncogene homolog*
Sry	*sex determining region Y*
Stat	*signal-transducer and activator of transcription*
SUV39H1	*suppressor of variegation 3-9 homolog 1 (Drosophila)*
SUZ12	*SUZ12 polycomb repressive complex 2 subunit*
Tbx21	*t-box 21*
Thra	*thyroid hormone receptor, alpha*
Thrβ	*thyroid hormone receptor, beta*
TP53	*tumor protein p53*

Trh	*thyrotropin-releasing hormone*
Tsh	*thyroid stimulating hormone*
Tshr	*thyroid-stimulating hormone receptor*
Ucp1	*uncoupling protein 1*
α-tubulin	*alpha tubulin*
γ-tubulin	*gamma tubulin*

Chapter 1. Introduction

1.1 Histone methylation as a chromatin modification

The core particle of chromatin is the nucleosome, an octamer composed of four pairs of histones called H2A, H2B, H3 and H4 (Kornberg, 1977). The histone tails are unstructured (Luger et al., 1997) and can be decorated with a number of post-translational modifications, for example methylation, acetylation, phosphorylation and ubiquitylation (Kouzarides, 2007).

Several lysine and arginine residues on histone tails can be methylated by histone methyltransferases. Each methyltransferase shows substrate and degree of methylation specificity: it methylates specific lysine or arginine residues without affecting others and can mono- (me1), di- (me2) and/or tri-methylate (me3) its histone substrate. For example, lysine methyltrasferase SETD8 monomethylates lysine 20 on H4 from an unmethylated state. Others, such as lysine methyltransferase SUV39H1 di- and trimethylates lysine 9 on H3 from a monomethylated state. Arginine residues on histone proteins can be symmetrically or asymmetrically dimethylated by a group of enzymes known as arginine methyltransferases (Black et al., 2012; Di Lorenzo and Bedford, 2011; Greer and Shi, 2012; Kouzarides, 2007).

Methylation on different lysine residues of histones has been associated with either transcriptional activation or repression (**Figure 1.1**). Methylation of lysine 4, 36 and 79 on H3 are generally associated with actively transcribed genes (Briggs et al., 2001; Santos-Rosa et al., 2002; Schaft et al., 2003; Steger et al., 2008). On the other hand, methylation of lysine 9 and 36 on H3, and lysine 20 on H4 are associated with transcription repression (Litt et al., 2001; Müller et al., 2002; Nakayama et al., 2001; Noma K et al., 2001; Plath et al., 2003; Schotta et al., 2004).

Moreover, regardless of their functional state, enhancers seem to be associated with H3K4me1 (Spicuglia and Vanhille, 2012). Active enhancers were found to be additionally marked by H3K27 acetylation (Pekowska et al., 2011; Spicuglia and Vanhille, 2012).

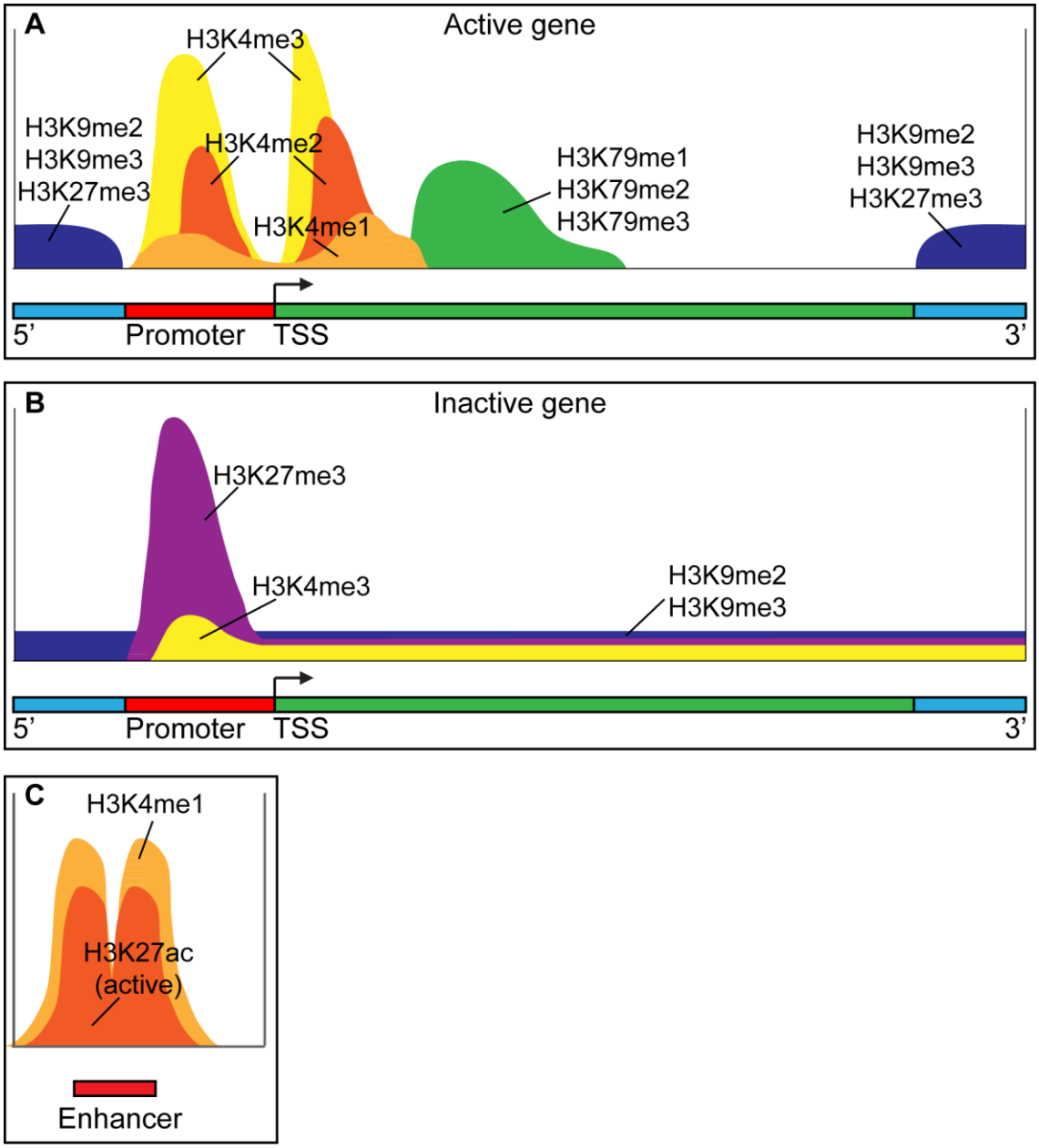

Figure 1.1: Occupancy of histone methylation marks on chromatin of active and inactive genes.

(A) When a gene is in an active state, it is characterised by the occupancy of H3K4me1/2/3 epigenetic marks within the promoter and transcription start site, as well as intragenic H3K79me1/2/3 in the intragenic region. Repressive H3K9me2/3 and H3K27me3 are excluded. **(B)** When a gene is in an inactive state, the promoter region is characterised by elevated H3K27me3 and decreased H3K4me3. The promoter and intragenic region is additionally occupied with H3K9me2. **(C)** Enhancers are marked by H3K4me1. Active enhancers are additionally characterised by the presence of H3K27ac.

In addition, the histone code, established in part by lysine methyltransferases and demethylases, provides a platform for the binding of chromatin remodelling complexes. These complexes can in turn affect the chromatin state and activate or repress transcription (Ho and Crabtree, 2010; Wu et al., 2009).

Therefore, histone modifications, including histone lysine methylation, and the action of lysine methyltransferases and demethylases, play key roles in the regulation of the chromatin state and consequently gene expression.

1.2 The two families of lysine demethylases

Lysine demethylases are divided into two evolutionary conserved families that catalyse the removal of methyl groups using distinct modes of action (**Figure 1.2**). The first family that includes lysine-(K) specific demethylase 1A and 1B (KDM1A and KDM1B) remove methyl groups utilising the amine oxidase domain using flavin adenine dinucleotide (FAD) as a cofactor. Formaldehyde and hydrogen peroxide are the products of this reaction (Karytinos et al., 2009; Shi et al., 2004).

The second family of demethylases is composed of 30 members in humans, which contain the catalytic JmjC domain and a diverse arrange of extra domains. Phylogenetic analyses have suggested that the acquisition of the motifs/domains of the ancestral JmjC-domain containing genes happened before the divergence of the major eukaryotic groups, that was later accompanied by gene duplication events (Zhou and Ma, 2008).

JmjC-domain lysine demethylases belong to the cupin metalloenzyme superfamily. Cupins are ancient protein domains, which are found in archaea, bacteria and eukarya (both animals and plants). The JmjC domain of lysine demethylases shows sequence similarities to other protein members of the superfamily that adopt the cupin fold. Different cupin metalloenzymes use different metal ions within the cupin fold to carry out their enzymatic functions, such as manganese, zinc, iron and nickel. Lysine demethylases use iron ions (Clissold and Ponting, 2001; Dunwell et al., 2001; Dunwell et al., 2004; Zhou and Ma, 2008).

In humans, JmjC-domain lysine demethylases have been divided into seven subfamilies according to their degree of homology and the presence of additional motifs/domains (Klose et al., 2006b). Due to their sequence similarities, members of the same subfamily often share the same or similar substrate specificities. For example, the KDM4 subfamily comprises of KDM4A, KDM4B, KDM4C and KDM4D. They all contain a Jumonji N (JmjN) domain, a JmjC domain, and, excluding KDM4D, the rest of the subfamily members also have CW-type zinc finger and TUDOR domains. All KDM4 subfamily members have H3K9me1/2, H3K36me1/2 and histone 1.4 di- and tri-methyl lysine 26 (H1.4K26me2/3) substrate specificities (Kooistra and Helin, 2012).

The demethylation reaction of JmjC-domain demethylases involves the hydroxylation of the methyl group in the presence of Fe(II) , oxygen and α-ketoglutarate to produce succinate, formaldehyle and cardon dioxide as by-products (**Figure 1.2**) (Klose and Zhang, 2007). Whereas FAD-dependent demethylases are only able to demethylate mono- and di-methyl groups, JmjC-domain demethylases can also demethylate tri-methyl post-translational lysine modifications.

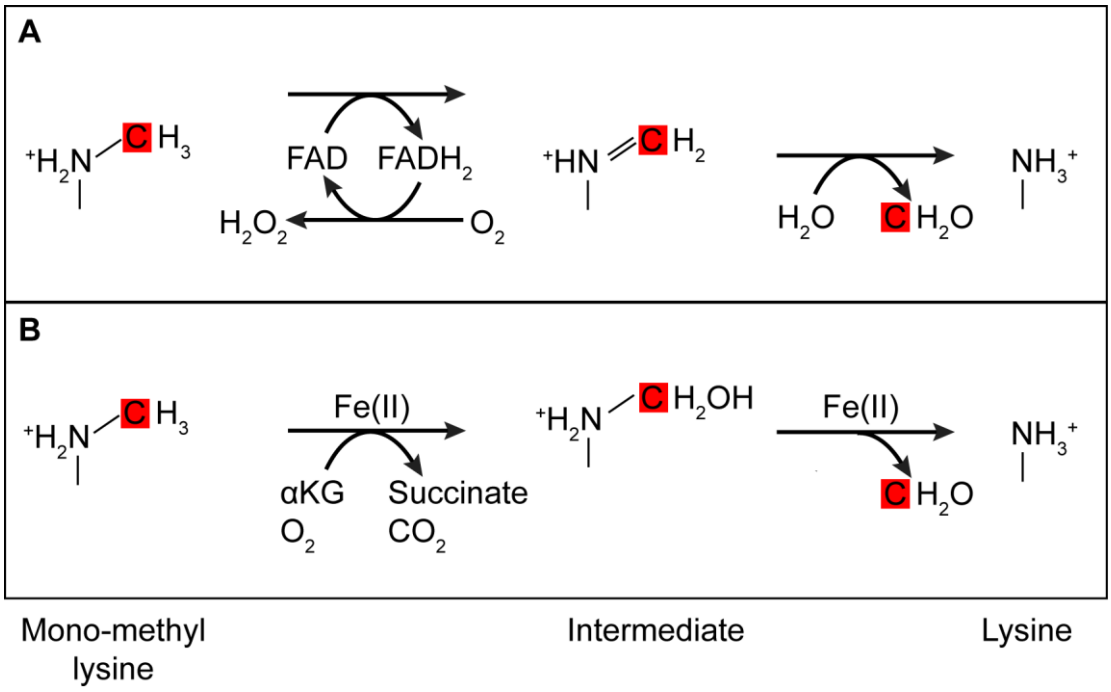

Figure 1.2: The demethylation reactions mediated by amine oxidase containing and JmjC-domain containing demethylases.

(A) Lysine demethylases, such as KDM1A, utilise the amine oxidase domain for lysine demethylation. In this reaction, FAD is used as a co-factor to reduce the mono-methyl lysine substrate to unmethylated lysine. Hydrogen peroxide (H_2O_2) and formaldehyde (CH_2O) are produced as a result of this reaction. **(B)** JmjC-domain containing demethylases utilise iron II (Fe (II)), alpha ketoglutarate (αKG) and oxygen for the reaction. Carbon dioxide (CO_2), succinate and formaldehyde form as by-products. In both the amine oxidase and JmjC-driven demethylations, the target methyl lysine goes through an intermediate state before it is fully demethylated.

1.3 Functions of histone demethylases

1.3.1 Chromatin regulation

1.3.1.1 Control of transcriptional activation

One of the best-studied functions of lysine demethylases is the control of transcription initiation. This is accomplished through both the histone lysine demethylation activity and the interaction of the demethylases with transcription factors, such as the androgen receptor (Metzger et al., 2005; Shin and Janknecht, 2007; Wissmann et al., 2007; Yamane et al., 2006). One such example is that of the H3K4me1/2 and H3K9me1/2 demethylase KDM1A and of the H3K9me2/3 and H3K36me2/3 demethylase KDM4C. For instance, the KDM1A and KDM4C demethylases interact with each other and with the androgen receptor, and co-localise at the androgen receptor-responsive elements in promoters and enhancers of target genes. Subsequently, KDM1A removes the H3K9me1 and H3K9me2 marks, whereas KDM4C removes the H3K9me3 marks from the androgen receptor-responsive elements, leading to the activation of androgen receptor targets. Interestingly, knock-down of either KDM1A or KDM4C reduces the expression of the androgen receptor target genes. Therefore, transcription initiation through the action of lysine demethylases is accomplished via the removal of repressive histone marks from gene regulatory regions (promoters and enhancers) (Metzger et al., 2005; Wissmann et al., 2007).

Given the importance of demethylases in the activation of the androgen receptor target genes, it will be interesting to investigate whether knock-out mice of each demethylase recapitulate the phenotype of the androgen receptor knock-outs (De Gendt et al., 2004; Notini et al., 2005; Yeh et al., 2002). However, one limitation

for this is the possible redundancy. Since many demethylases are known to be involved in the activation of androgen receptor targets, including many members of the same subfamily (KDM4), redundancy may lead to no observable phenotype, as illustrated by the *Kdm4d* knock-out mice (Iwamori et al., 2011). Therefore, in order to obtain a better insight into the importance of the demethylases in transcription initiation, it may be necessary to simultaneously knock-out more than one demethylases.

During development, the interaction of a lysine demethylase with transcription factors operates to promote the expression of the transcription factor target genes. This will also be influenced by the specific expression pattern of the lysine demethylase itself. Therefore, the activation of gene expression through histone lysine demethylation seems to be a common theme for a subset of lysine demethylases, which ultimately depends on their particular histone lysine substrates.

1.3.1.2 Control of transcriptional repression

Opposite to transcriptional activation, the histone demethylase function of lysine demethylases can result in transcriptional repression. This is due to the substrate specificity of a subset of these enzymes, removing transcriptionaly-activating marks from the enhancers and promoters of target genes. For instance, KDM1A was shown to localise at enhancer regions of embryonic stem cell (ECS) genes, including the enhancers of pluripotency factors. Differentiation of ESCs is accompanied by a reduction of H3K4me1 at the enhancer regions, including those of ESC pluripotency factors, thus repressing their expression (Whyte et al., 2012). The proposed function of KDM1A as a transcriptional repressor is not surprising since it is also associated with members of the NuRD remodelling protein complex, whose ATP-dependent and histone deacetylase activity represses the transcription of target genes (Reynolds et al., 2012). Members of this complex co-localise with KDM1A enhancer-bound regions on ESC chromatin (Whyte et al., 2012). In another example, the knock-down of the H3K4me2/3 demethylase KDM5A derepress the silencing of the embryonic-expressed β-globin gene *Hbb-y* in differentiated murine erythroid cells. KDM5A binds to the *Hbb-y* promoter, and this binding is lost upon KDM5A

knock-down, with concomitant H3K4me3 increase. Also, KDM5A interacts with the EHMT2 and EHMT1 methyltransferases and thus a cross talk between demethylases and methyltransferases activity is proposed to maintain gene silencing (Chaturvedi et al., 2012).

Therefore, lysine demethylases may mediate the repression of their target genes by being part of larger protein complexes that fulfill a range of enzymatic functions. Furthermore, depending on the biological context, it is also likely that each demethylase may associate with a range of different protein complexes, as illustrated by KDM1A (Rudolph et al., 2013).

1.3.1.3 Maintenance of transcriptional competence

In recent years, with the advent of genome wide studies, a new function has been proposed for lysine demethylases. Under this model, although lysine demethylases have the capacity to bind the regulatory regions of several genes, the knock-down of the demethylase only confers modest changes in gene expression (Schmitz et al., 2011). In particular, ChIP-seq for Kdm5b, a H3K4me2/3 demethylase, showed that Kdm5b is enriched on transcription start sites of embryonic stem cells. However, when Kdm5b is knocked-down, only 22 genes show more than 3-fold change in expression, despite a median 2.2-fold increase in H3K4me3. Therefore, a proposed function of lysine demethylases is not to directly affect gene expression *per se*, but rather to keep the chromatin in a desirable state, as to allow transcription, when necessary (Schmitz et al., 2011).

Although compelling, the proposed function still requires further investigation. In particular, apart from the ChIP-seq for the demethylase enzyme and its histone substrates, ChIP-seq should also be performed for other histone modifications, factors that affect transcription such as the RNA polymerase II, general transcription factors and chromatin remodelling complexes. These experiments will provide in-depth information of the target gene state, i.e. whether they are active or repressed. Furthermore, functional redundancy between demethylases of the same subfamily should be considered.

1.3.2 Modulation of non-histone protein function through methylation and demethylation

A less well-studied area of research is the modulation of non-histone protein function through methylation and demethylation. Despite that, there are some examples that illustrate the importance of the methylation-demethylation interplay, mediated by methyltransferases and demethylases.

The best and most well-studied example is that of the tumor protein p53 (TP53). TP53 is methylated and demethylated on a number of lysine residues that promote or inhibit its pro-apoptotic and cell-cycle checkpoint functions upon DNA damage. For example, upon DNA damage, SETD7 methyltransferase monomethylates lysine 372 of TP53, which leads to its activation and the induction of TP53 downstream effectors (Chuikov et al., 2004). On the other hand, the monomethylation of TP53 on lysine 370 and lysine 382 by SMYD2 and SETD8, respectively, represses its transcriptional inducing capacity (Huang et al., 2006a; Shi et al., 2007). Interestingly, TP53-K372 methylation by SETD7 (Chuikov et al., 2004) prevented TP53-370 methylation, suggesting antagonistic functions of the same post-translational medication (methylation) to finely control TP53 function (Huang et al., 2006b).

The dimethylation of TP53 at lysine 370 is counteracted by the KDM1A demethylase. KDM1A removed the dimethyl moiety, set by an unknown methyltransferase. This demethylation represses TP53-mediated gene expression, and siRNA knock-down of *KDM1A* resulted in upregulated of expression of the TP53 target genes (Huang et al., 2007).

Therefore, methylation and demethylation of lysine residues on TP53 represent a novel mode for the functional control of this protein.

In a similar fashion to p53, the p65 subunit of nuclear factor kappa-light-chain-enhancer of activated B cells (NF-κB) is methylated at lysines 218 and 221 by NSD1 in response to cytokines and demethylated by the H3K36me1/2 demethylase KDM2A (Lu et al., 2010). Methylation activates NF-κB, whereas demethylation

represses it. Therefore mutation of either lysine residue, or both, or the over-expression of KDM2A resulted in the reduced ability of NF-κB to drive the expression of its target gene *selectin E*. These observations led to the proposal that lysine methylation and demethylation of NF-κB presents a way to regulate the functions of this transcription factor (Lu et al., 2010).

Apart from transcription factors, the repertoire of proteins with diverse cellular roles, tightly regulated via methylation and demethylation, is expected to expand. This is highlighted by the identification of methylated residues on proteins of the translational apparatus, and the respective methyltransferases which deposit those methyl marks (Clarke, 2013; Egorova et al., 2010). Furthermore, large scale approaches are now being employed in order to identify several more proteins with lysine as well as arginine post-translational modifications (Bremang et al., 2013).Therefore, methylation and demethylation represents an additional level to control the functions of non-histone proteins, which have important cellular roles.

1.3.3 Demethylation-independent functions

Apart from their enzymatic capacity to demethylate lysine residues on histone and non-histone substrates, lysine demethylases display additional demethylase-independent functions. For example, the catalytically inactive Jarid2 demethylase (Klose et al., 2006b) was shown to be essential for development, by targeting the PRC2 complex, that possesses histone methyltransferase activity required for transcriptional gene silencing (Simon and Kingston, 2009), to its designated gene promoters. This function was mediated via the ARID domain of Jarid2. Chip-seq revealed that 90% of Jarid2 bound genomic sequences in mouse ESCs were also bound by the PRC2 complex protein Suz12. Knock-down of *Jarid2* by short hairpin RNA (shRNA) in mouse ESCs resulted in a significant reduction of Suz12 and Ezh2 binding to their target gene promoters. Most importantly, transient transfection of wild type Jarid2, but not of Jarid2 lacking the ARID domain, partly rescued the PRC2 targeting to its gene promoters (Pasini et al., 2010).

Another example illustrating the importance of demethylase-independent functions of demethylases is that of the H3K27me2/3 demethylase Kdm6b, required

for the T-box21 (Tbx21)-dependent chromatin remodelling, by acting as a link between Tbx21 and the SWI-SNF remodelling complex. Both a catalytically active and an inactive form of Kdm6b are able to induce the expression of the Tbx21 target gene *interferon, gamma* (*Ifng*). Subsequent, immunoprecipitation assays demonstrated that Kdm6b interacts with Tbx21, as well as with some members of the SWI-SNF remodelling complex. Thus, Kdm6b seems to function as a scaffold in order to bring together factors required for chromatin remodelling (Miller et al., 2010).

In summary, an array of distinct domains of the JmjC- containing have been shown to be essential for the histone demethylation function (Klose et al., 2006a; Whetstine et al., 2006). However, as exemplified above, they also provide the opportunity to expand the functions of these enzymes beyond lysine demethylation.

1.4 Conservation of function through evolution

Control of the chromatin state via the deposition and erasure of epigenetic histone marks is not only important in mammals but also in lower eukaryotes. This is exemplified by the capacity of demethylases, identified in *S. cerevisiae* and *C. elegans*, to erase methyl marks from their histone methyl targets (Klose et al., 2007; Liang et al., 2007; Tsukada et al., 2006; Kleine-Kohlbrecher et al., 2010; Lin et al., 2010).

The level of JmjC domain homology and the presence of additional domains within the full length proteins were used as parameters to trace homologues of the human JmjC-domain containing subfamilies in the mouse (*Mus musculus*), the worm (*Caenorhabditis elegans*), the fly (*Drosophila melanogaster*), the fission yeast (*Schizosaccharomyces pombe*) and the budding yeast (*Saccharomyces cerevisiae*). The search showed that some subfamilies had homologues up to *S. cerevisiae* (i.e. KDM2 and KDM5), whereas for other subfamilies, homologues were found up to *C. elegans* (PHF2/PHF8) or *D. melanogaster* (KDM3) (Klose et al., 2006b).

Five JmjC-domain containing demethylases have been identified in *S. cerevisiae*. Of those, Rph1 (a KDM4 orthologue), Jhd2 (a KDM5 orthologue) and

Jhd1 (a KDM2 orthologue) retained their histone demethylation potentials (Klose et al., 2007; Liang et al., 2007; Tsukada et al., 2006). *In vitro* studies, suggested that Rph1 and Jhd1 proteins function as H3K36 demethylases, and Jhd2 as an H3K4 demethylase. Further evidence supporting their demethylation potential came from the generation of mutant protein forms of the proteins, where critical residues within the JmjC domain, responsible for iron binding, were substituted. Under these conditions, the demethylation activity of the proteins was abolished. Interestingly, Rph1 was additionally shown to demethylate H3K9me3, just like its mammalian orthologues, although in the *S. cerevisiae* genome H3K9 is not methylated. This observation suggests that H3K9 methylation could have existed in *S. cerevisiae* and was subsequently lost. Therefore the methylation potential of Rph1 represented a functional vestige that was maintained due to the capacity of this enzyme as an H3K36 demethylase. Moreover, two independent studies demonstrated that a *C. elegans* orthologue of the mammalian PHF2/PHF8 subfamily, ceKDM7A, functioned as an H3K27me2 and H3K9me2 demethylase (Kleine-Kohlbrecher et al., 2010; Lin et al., 2010). Interestingly, similarly to its mammalian orthologue PHF8, targeting of ceKDM7A to chromatin was dependent on its PHD domain. Over-expression of a ceKDM7A mutant, lacking its PHD domain, abrogated its demethylation potential.

The conservation of histone demethylation function through evolution stresses the functional importance of these enzymes to modulate chromatin state. Therefore, it will not be surprising if more members of the histone demethylases in lower organisms display the same histone substrate specificities as those of the human counterparts.

1.5 Alternative isoforms of epigenetic regulators

To date, two demethylase genes are known to encode more than one functional protein isoform. Interestingly, different isoforms perform different functions, highlighting the need to study alternative isoforms, in addition to full length proteins (Verrier et al., 2011b).

The production of protein isoforms can be achieved via alternative splicing (Lois et al., 2007), as well as the use of different promoters (Cooper et al., 2006; Sandelin et al., 2007). About 70% of epigenetic modulators in humans can express isoforms by alternative splicing. The changes in the sequence of the alternative isoform(s) can partly or completely affect the catalytic domain, the interaction domain or even both leading to a drastic reduction of the protein size, affecting its function (Lois et al., 2007). Moreover, genes can have more than one active promoters, and the use of alternative promoters can affect the gene expression levels of the particular isoforms, giving rise to different expression patterns across tissues (Cooper et al., 2006). Further, alternative promoters can determine the inclusion/exclusion of the 5' prime exons while leaving the rest of the exons unaffected (Sandelin et al., 2007).

A shorter KDM4A isoform was shown to be important for skeletal muscle differentiation. The expression of this shorter isoform, but not of the full-length isoform, is elevated during terminal differentiation of mouse myoblast cells. The same was observed during the differentiation of human satellite cells (progenitor muscular cells). A comparison of siRNA knockdown of the full-length *KDM4A* isoform only versus the knockdown of both *KDM4A* isoforms revealed, by microarray technology, downregulation of genes related to muscle development and differentiation, specifically related to the shorter isoform. Since this short isoform is missing the catalytic JmjC domain, the demethylation function is presumably mediated via its interaction with full-length KDM4C, another member of the KDM4 sub-family, which removes the repressive H3K9me2/3 marks (Cloos et al., 2006; Verrier et al., 2011b).

Furthermore, alternative isoforms of the KDM1A protein have been discovered in mammalian neurons. In particular, alternative splicing generates the KDM1A-8a isoform, which is only expressed in the brain. KDM1A-8a expression in the brain is upregulated during the perinatal window up to p7 and is the predominant isoform over the other KDM1A isoforms. Interestingly, knock-down of the KDM1A-8a, but not the other isoforms, affects the neurite morphology (Zibetti et al., 2010). Phosphorylation of a threonine residue within the neurospecific exon 8 for KDM1A

results in the detachment of KDM1A-8a from the corepressor CoREST complex and as a result KDM1A-8a presumably functions in a dominant negative fashion, inhibiting the "conventional" KDM1A isoform repressor activity (Toffolo et al., 2014).

Alternative isoforms of lysine demethylases seem to play important roles in development. Fortunately, the sequence similarity of rodent and human genomes facilitates the discovery and functional characterisation of many more lysine demethylase alternative isoforms.

1.6 The KDM3 subfamily of JmjC-domain histone demethylases

In the present study, I concentrated on the Kdm3 subfamily demethylases Kdm3b and Kdm3a. In this section, I compare the sequence similarity of Kdm3 subfamily proteins, their biological roles from mouse studies and their substrate specificities, as described to present.

In humans and mice, the KDM3 subfamily consists of four genes: *KDM3A*, *KDM3B*, *JMJD1C* and *HAIRLESS* (**Figure 1.3)** (Klose et al., 2006b; Kooistra and Helin, 2012). Homologues for the *KDM3* subfamily are absent in the genomes of *Caenorhabditis elegans*, *Schizosaccharomyces pombe* and *Saccharomyces cerevisiae*. A homologue is present in *Drosophila melanogaster*, but has not been functionally characterised (Klose et al., 2006b).

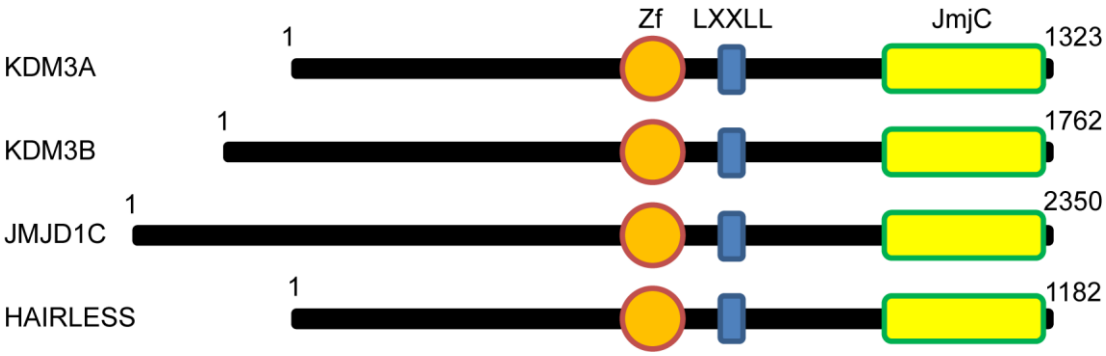

Figure 1.3: The human and mouse KDM3 protein family.

All members of the KDM3 protein family contain a C2HC4-zinc finger (Zf), followed by a nuclear receptor motif (LXXLL) and C-terminal JmjC domain. Proteins not drawn to scale. Numbers indicate sizes of mouse proteins.

1.6.1.1 Sequence identity of KDM3 subfamily members

Alignment of protein sequences of all human and mouse subfamily members in Uniprot shows that *KDM3A* and *KDM3B* are the closest paralogues and that *HAIRLESS* is the most distant. All human and mouse KDM3 members share only 5% sequence identity when full length proteins are aligned. Within the JmjC domain and the zinc finger, the sequences show greater conservation and share 25% and 38% identity, respectively. The nuclear receptor sequence is identical in 3 out of 5 positions (60% identity). Moreover, with the exception of HAIRLESS, all metal and α-ketoglutarate binding sites are conserved in KDM3A, KDM3B and JMJD1C (Klose et al., 2006b).

As mentioned above, KDM3A and KDM3B are the closest paralogues. The sequence identity across the full-length KDM3A and KDM3B proteins is 34% between human and mouse (**Figure 7.1** in Appendix). Interestingly, the sequence conservation within the JmjC and the zinc finger is 83% and 77%, respectively. The nuclear receptor sequence differs only by one residue (80% identity) (**Figure 1.4**).

Moreover, the cNLS mapper was used to predict the nuclear localisation signals (NLS) for the human and mouse KDM3A and KDM3B proteins. Both KDM3A and KDM3B have predicted NLS. The KDM3A and KDM3B homologues, in human and mouse, share a high percentage of sequence identity (86% and 92% for the predicted bipartite NLS of KDM3A and KDM3B homologues, respectively) within the predicted NLS, but there is no conservation in the predictions between KDM3A and KDM3B paralogues (**Figure 1.4**).

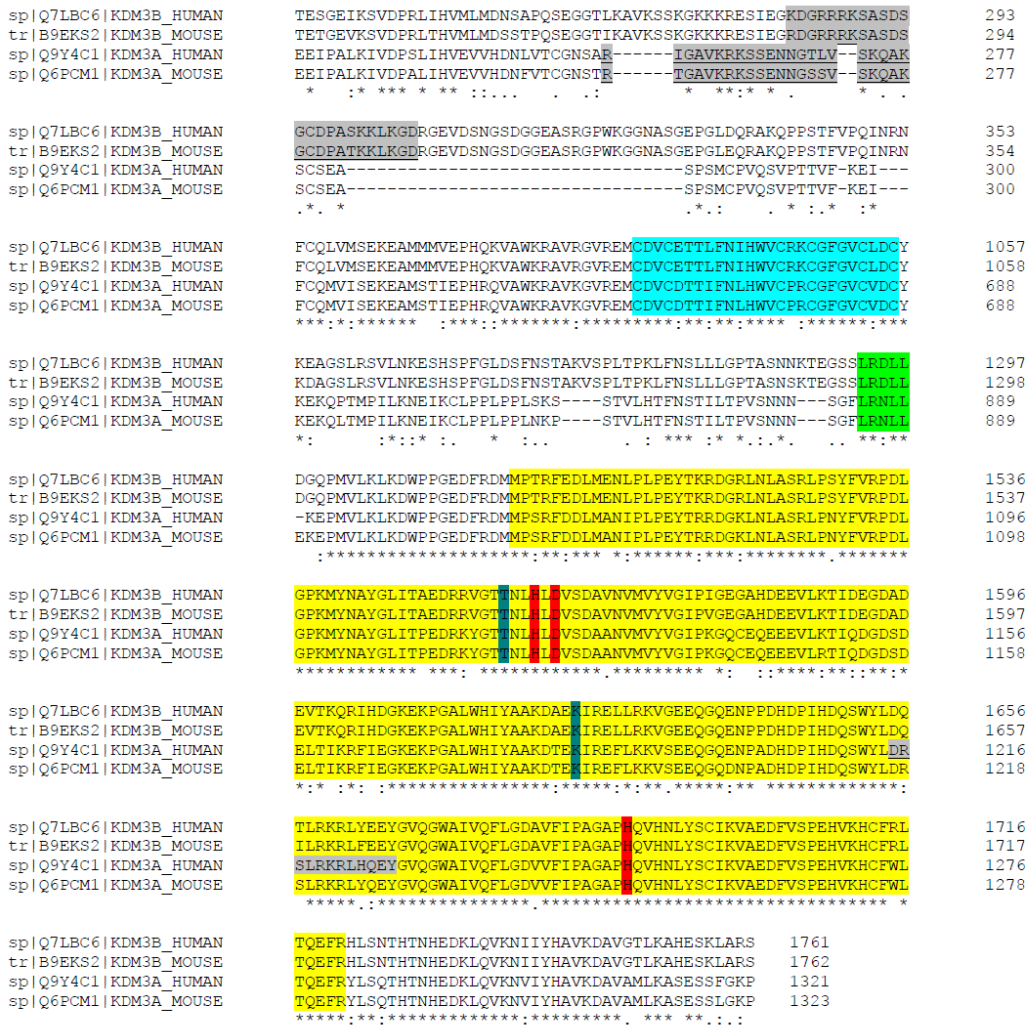

Figure 1.4: Alignment of the human and mouse KDM3A and KDM3B paralogue sequences with Uniprot identifiers: Q7LBC6, B9EKS2, Q9Y4C1 and Q6PCM1.

Highlights: Grey: predicted NLS; light blue- zinc finger; green- nuclear receptor motif; yellow-JmjC domain; red-predicted iron binding sites and dark blue- α-ketoglutarate binding sites.

* indicates fully conserved residue
: indicates residues of strongly similar properties
. indicates residues of weakly similar properties

Similar properties of amino acids are defined by the presence of: hydrophobic aliphatic side chains, hydrophobic aromatic side chains, polar neutral side chains, electrically charged-acidic side chains, electrically charged-basic side chains and covalent cross-linking (disulfide bonds).

1.6.2 The Kdm3 subfamily: diversity in biological roles

Although Kdm3a, Kdm3b, Jmjd1c and Hairless belong in the same protein sub-family, the characterisation of gene-trapped, knock-out and mutant mice demonstrates that each of these demethylases fulfils distinct/non-overlapping biological role(s). For example, both *Kdm3a* and *Jmjd1c* male knock-out mice exhibit infertility, although the time of infertility onset and the underlying causes are distinct. To date, mouse models have been characterised for Kdm3a, Jmjd1c and Hairless, but not for Kdm3b (this study). The phenotypes of gene-trapped and knock-out mice are summarised in **Table 1** and further discussed in sections 1.1.6.2.1-1.1.6.2.3.

Table 1-1: Phenotype of gene-trap, knock-out or mutant mice of the Kdm3 subfamily

Kdm3 subfamily member	Phenotype	References
Kdm3a (gene-trap and knock-outs)	Male infertility, obesity, predisposal to diabetes, frequent male sex-reversal	(Inagaki et al., 2009; Kasioulis et al., 2014; Kuroki et al., 2013a; Liu et al., 2010a; Okada et al., 2007; Okada et al., 2010; Tateishi et al., 2009)
Kdm3b	Not available/unpublished (this study)	Not available
Jmjd1c (knock-out)	Progressive age-dependent male infertility	(Kuroki et al., 2013b)
Hairless (mutants)	Permanent hair loss, reduced white adipose tissue, inner ear defects	(Cachón-González et al., 1999; García-Atares et al., 1998; Kumpf et al., 2012; Thompson, 2009)

1.6.2.1 The Kdm3a lysine demethylase

Kdm3a was initially identified in 1991 as a zinc finger-containing protein (known as testis specific gene A- TSGA), specifically expressed in the testis of rats, during the first wave of spermatogenesis (Höög et al., 1991). The characterisation of Kdm3a as a H3K9me1/2 demethylase enzyme was elucidated by Yamane et al. (2006) by means of biochemical and *in vivo* assays. Consistent with the fact that JmjC-domain proteins belong to the superfamily of 2-oxo-glutarate oxygenases (Loenarz and

Schofield, 2008), the demethylase activity of Kdm3a requires the Fe (II) and α-ketoglutarate as co-factors, with the release of formaldehyde. Both the catalytic JmjC domain and the zinc finger are essential for this demethylation function (Yamane et al., 2006).

To date, several gene-trap and knock-out mouse models for *Kdm3a* have been characterised. So far, it has been demonstrated that Kdm3a is essential for spermatogenesis (Kasioulis et al., 2014; Liu et al., 2010a; Okada et al., 2007; Okada et al., 2010), energy homeostasis and resistance to obesity (Inagaki et al., 2009; Okada et al., 2010; Tateishi et al., 2009) and regulation of sex determination (Kuroki et al., 2013a).

Kdm3a gene-trapped (Kasioulis et al., 2014; Okada et al., 2007) or knock-out (Kasioulis et al., 2014; Liu et al., 2010a) male mice are infertile, with significantly smaller testes. Spermatogenesis arrests around spermatid stage 9 (Liu et al., 2010a) or stage 11 (Okada et al., 2007) with very few mature spermatozoa in the epididymal ducts (a condition known as oligozoospermia) (Kasioulis et al., 2014; Liu et al., 2010a; Okada et al., 2007), most of which are immotile (Okada et al., 2007). Interestingly, spermatids of *Kdm3a*-deficient mice fail to condense their chromatin (Okada et al., 2007) and show aberrant acrosome and manchette formation (Kasioulis et al., 2014). The latter two structures are necessary for proper sperm-head shaping (Dam et al., 2007; Kierszenbaum and Tres, 2004). It is proposed that Kdm3a functions as a transcriptional co-activator by mediating the expression of protamines and transition proteins, essential for chromatin compaction in spermatids, via promoter H3K9me2 demethylation (Okada et al., 2007). Furthermore, tubulin and/or actin subunits may be necessary for the proper assembly of microtubular and actin-based structures seen altered during spermatogenesis of Kdm3a knock-out mice (Kasioulis et al., 2014). Kdm3a may also function as a non-histone protein demethylase, by demethylating lysine residues on tubulin and/or actin subunits.

Furthermore, adult *Kdm3a*-deficient mice are obese (Inagaki et al., 2009; Tateishi et al., 2009), with increased fat deposition in the muscles and liver and

increased brown adipose tissue (BAT). In addition, they show increased levels of blood triglycerides, cholesterol, insulin and leptin, resembling a pre-diabetic state.

By the use of microarray technology coupled with qRT-PCR, Tateishi et al. (2009) demonstrated that the expression of the *peroxisome proliferator-activated receptor alpha* (*Pparα*) and a number of its downstream pathway genes, involved in lipid metabolism, are significantly downregulated in skeletal muscle of *Kdm3a*-deficient mice. Kdm3a binds and removes H3K9me2 from the peroxisome proliferator hormone response element (PPRE) sequences of *Pparα*.

Moreover, *Kdm3a* knock-out mice are unable to maintain their body temperature when exposed to cold (Tateishi et al., 2009). In line with this result, BAT expression of *Uncoupling protein 1* (*Ucp1*), responsible for thermogenesis (Lowell and Spiegelman, 2000), is not upregulated during cold exposure in *Kdm3a*-deficient mice. Kdm3a binds to the *Ucp1* enhancer, and when not present, the H3K9me2 levels at the *Ucp1* enhancer are increased (Tateishi et al., 2009).

More recently, Kdm3a was shown to be important for sex determination in male mice (Kuroki et al., 2013a). A non-Mendelian proportion of *Kdm3a* male knock-out mice are often found to be sex reversed, either partially (with XY knock-outs having a testis and an ovary) or fully (with XY knock-outs having two ovaries). Sex reversal is presumably due to the reduced expression of the *Sex determining region Y* (*Sry*) transcription factor (driven by sertoli cell differentiation), essential for the development of male genitalia (Barrionuevo et al., 2006; Jäger et al., 1990). Consistent with the function of Kdm3a as a transcriptional co-activator, Kdm3a binds and reduces the H3K9me2 mark in the *Sry* regulatory regions of gonadal somatic cells, which is expected to promote the *Sry* expression (Kuroki et al., 2013a).

In summary, Kdm3a is involved in many different biological functions and reduced/absent levels of Kdm3a have been associated with infertility, obesity and male sex reversal. Finally, although most studies focus on the histone demethylation function of Kdm3a, work from our laboratory suggests that this demethylases may also function through non-histone demethylation.

1.6.2.2 The Jmjd1c lysine demethylase

To date, a single knock-out mouse for *Jmjd1c* has been generated and characterized (Kuroki et al., 2013b). *Jmjd1c* female knock-out mice are normal and fertile, whereas male mice are initially fertile but show an age-dependent infertility due to the progressive reduction of germ cells, commencing at about three months of age. The infertility in Jmjd1c-deficient male mice is attributed to increased apoptosis and by eight months of age, these mice are completely infertile. Jmjd1c is highly expressed in spermatogonial stem cells, which correlates with the infertility phenotype observed, provided that this demethylase performs an essential, yet unidentified function for the maintainance of male germ cells. Absence of Jmjd1c did not change the global H3K9me2 levels in the testes, suggesting that Jmjd1c controls the expression of a subset of genes via H3K9me2 demethylation or that it influences the function of non-histone substrates via lysine demethylation. The second statement is reinforced by *in vivo* demethylation assays, where over-expression of tagged-Jmjd1c does not result in global demethylation of H3K9me1/2, contrary to its orthologues Kdm3a and Kdm3b (Brauchle et al., 2013; Kuroki et al., 2013b; Sroczynska et al., 2014).

1.6.2.3 The Hairless lysine demethylase

Hairless is the best studied gene of the Kdm3 subfamily. Mutations in the *HAIRLESS* gene have been found in patients with Alopecia universalis and popular atrichia, hereditary forms of hair loss (Ahmad et al., 1998; Kruse et al., 1999; Sprecher et al., 1999). In the mouse mutants of *Hairless*, the initial hair growth is normal. However, when the hair is shed, it does not grow back owing to the inability of hair follicles to regenerate. Subsequently, the skin becomes wrinkled, the hair follicles widen near the epidermis, the lower part of the follicle eventually degenerates and cysts form in the dermis (Thompson, 2009). *Hairless* is expressed in the hair follicle after it is shed and during the initial stages of regeneration. Its expression is lost at stages of active hair growth. Hairless presumably controls hair regeneration/hair cycle by modulating Wnt signaling, whose action reinitiates hair growth (Beaudoin et al., 2005; Thompson et al., 2006).

In addition to its dynamic expression during hair regeneration, *Hairless* is highly expressed in the brain, and its absence results in neurological phenotypes, such as altered neuronal morphology and defects of the inner ear (Cachón-González et al., 1999; García-Atares et al., 1998).

Furthermore, *Hairless* mutant mice display reduced mass of the white, but not the brown adipose tissue (Kumpf et al., 2012). Hairless is upregulated during adipogenesis (Kumpf et al., 2012) and its knock-down results in the reduced expression of the early regulators of adipocyte differentiation, such as *Peroxisome proliferator-activated receptor gamma 1* (*PPARγ$_1$*) and *Peroxisome proliferator-activated receptor gamma 2* (*PPARγ$_2$*) (Rosen and MacDougald, 2006; Sarjeant and Stephens, 2012). As a result, the accumulation of lipids in differentiating *Hairless* knock-down 3T3-L1 preadipocytes is impaired. Hairless is thought to control the expression of *PPARγ$_1$ and PPARγ$_2$*, irrespective of the JmjC domain, suggesting that this demethylase interacts with other transcriptional co-activator proteins (Kumpf et al., 2012).

1.6.3 Substrate specificities for the Kdm3 subfamily members

A number of publications have, to date, attributed H3K9me1/2 substrate specificity for the Kdm3 subfamily members, although, in the case Jmjd1c, this is still unclear. Also, Jmjd1c was the first to show non-histone protein demethylation, but non-histone substrates for the other members have not yet been uncharacterised.

Kdm3a was the first of the Kdm3 subfamily to be attributed a H3K9me1/2 demethylase activity, as demonstrated by *in vitro* and *in vivo* assays (Brauchle et al., 2013; Yamane et al., 2006). It functions as a transcriptional co-activator through its H3K9me2 demethylase activity (Yamane et al., 2006). Additionally, the closest homologue of Kdm3a, Kdm3b, retains the same H3K9me1/2 substrate specificity (Brauchle et al., 2013; Kim et al., 2012). Kdm3b is potentially a transcriptional activator, as it promotes the expression of the haematopoietic transcription factor *LIM domain only 2 (rhombotin-like 1)* (*Lmo2*) via H3K9me2 promoter demethylation (Brandt and Koury, 2009; Kim et al., 2012).

The histone lysine demethylase activity of Jmjd1c is still debated. Although it was primarily shown to function as a H3K9me1/2 demethylase (Kim et al., 2010), later publications contradicted this finding (Brauchle et al., 2013; Kuroki et al., 2013b; Sroczynska et al., 2014), suggesting that Jmjd1c controls transcription via an indirect mechanism. It is possible that Jmjd1c may function as a H3K9me1/2 demethylase depending on the biological context, i.e. interaction with other transcriptional regulators. Thus, further research is necessary to clarify the histone demethylation potential of Jmjd1c. Interestingly, Jmjd1c was found to demethylate lysine 45 of Mediator of DNA-damage checkpoint 1 (MDC1), a protein involved in the DNA damage response (Coster and Goldberg, 2010; Watanabe et al., 2013). Hairless is known to function as a corepressor of liganded and unliganded nuclear receptors, and to interact with histone deacetylases (Hsieh et al., 2003; Potter et al., 2001; Potter et al., 2002; Thompson, 2009). *In vitro* and *in vivo* assays have indicated that Hairless has strong H3K9me1 and weak H3K9me2 demethylase activity (Liu et al., 2013), which further supports its function as a corepressor, as part of a multiprotein complex.

To date, the functions of H3K4, H3K9, H3K27, H3K36, H3K79 and H4K20 methylation on the chromatin state have been the focus of research (Black et al., 2012; Martin and Zhang, 2005). Lately, many more modifications on the histone tails have been identified, including methylation of additional lysine residues (Tan et al., 2011). Therefore, it is possible that members of the Kdm3 subfamily have additional, yet unidentified methyl histone substrates. Furthermore, given the importance of lysine methylation and demethylation as a means of non-histone protein-function control, it is also possible that Kdm3a, Kdm3b and Hairless, as already demonstrated by Jmjd1c, have non-histone nuclear and/or cytoplasmic substrates.

1.7 Growth

In this study, *Kdm3b* gene-trapped mice show a post-natal growth retardation phenotype. In this section the growth determinants as well as the pathways that regulate growth are discussed.

Growth is the increase in size, which is mainly accomplished via cell proliferation and cell size. In mammals, cell proliferation is the determining factor for body size, whereas in lower animals, such as the *C. elegans*, cell size is also important (Efstratiadis, 1998; Klingseisen and Jackson, 2011).

Two of the main determinants of growth are hormones and growth factors (Efstratiadis, 1998). Hormones are chemicals that signal away from their site of production. For example, the growth hormone-releasing hormone (Ghrh) is produced in the hypothalamus and exerts its effect at the anterior pituitary to promote the expression of the growth hormone (Gh). Growth factors, like the insulin-like growth factor 1 (Igf1), are polypeptides that can have an effect on the cell from which they are secreted or on neighbouring cells (autocrine and paracrine effect, respectively), as well as a systemic (endocrine) effect as they can be released in the bloodstream. Generally, prenatal growth is determined by growth factors, whereas postnatal growth is affected by both growth factors and hormones. In particular, mice knock-outs of the growth hormone and thyroid hormone pathways result in postnatal growth retardation, whereas mice knock-outs of growth factors or growth factor receptors result in prenatal and postnatal growth retardation. Insulin hormone is the exception to the "rule", since insulin receptor knock-out mice are prenatally mildy retarded. Furthermore, some mouse mutants or knock-outs of the growth hormone pathway display increased longetivity, whereas knock-out mice of the thyroid hormone receptor alpha and the insulin receptor die early in postnatal life (**Table 1-2**) (Alba and Salvatori, 2004; Coschigano et al., 2000; Coschigano et al., 2003; DeChiara et al., 1990; Efstratiadis, 1998; Flurkey et al., 2001; Fraichard et al., 1997; Holzenberger et al., 2003; Joshi et al., 1996; Kappeler et al., 2008; Liu et al., 1993; Louvi et al., 1997; Lupu et al., 2001).

Table 1-2: Knock-out mice with a growth retardation phenotype

Gene	Gene symbol	Commencement of growth retardation	Lifespan to WT mice	References
Growth hormone releasing hormone	*Ghrh*	Postnatal	n/a	(Alba and Salvatori, 2004)
Growth hormone releasing hormone receptor	*Ghrhr*	Postnatal	Increased	(Eicher and Beamer, 1976; Flurkey et al., 2001)
Growth hormone receptor	*Ghr*	Postnatal	Increased	(Coschigano et al., 2000; Coschigano et al., 2003; Zhou et al., 1997)
Thyroid hormone receptor alpha	*Thra*	Postnatal	Decreased	(Fraichard et al., 1997)
Insulin-like growth factor 1	*Igf1*	Prenatal	n/a	(Liu et al., 1993; Lupu et al., 2001)
Insulin receptor	*Insr*	Prenatal (mild)	Decreased	(Joshi et al., 1996; Louvi et al., 1997)
Insulin-like growth factor 2	*Igf2*	Prenatal	n/a	(DeChiara et al., 1990)
Insulin-like growth factor 1 receptor	*Igf1r*	Prenatal	Most die at birth, the rest survive	(Liu et al., 1993; Lupu et al., 2001)

1.7.1 Perturbation of pathways that affect growth

To date, perturbation of the Gh-Igf1 axis, Igf2, the thyroid hormone (Th) and the insulin pathways affect growth either prenatally, postnatally or both (Efstratiadis, 1998). Interestingly, Gh and insulin act through the same pathways and there is evidence of cross talk between them, as illustrated below.

1.7.1.1 The Growth hormone and insulin-like growth factor1 axis

Since growth is a fundamental biological process, then the Gh pathway (summarised in **Figure 1.5**), central for protein synthesis, cell proliferation, glucose metabolism and other processes, is tightly controlled at multiple levels via the secretion of hormones by different tissues, and the presence of negative feedback loops (Alba and Salvatori, 2004; Clemmons, 1997; D'Ercole et al., 1984; Efstratiadis, 1998; Guler et al., 1988; Mayo, 1992).

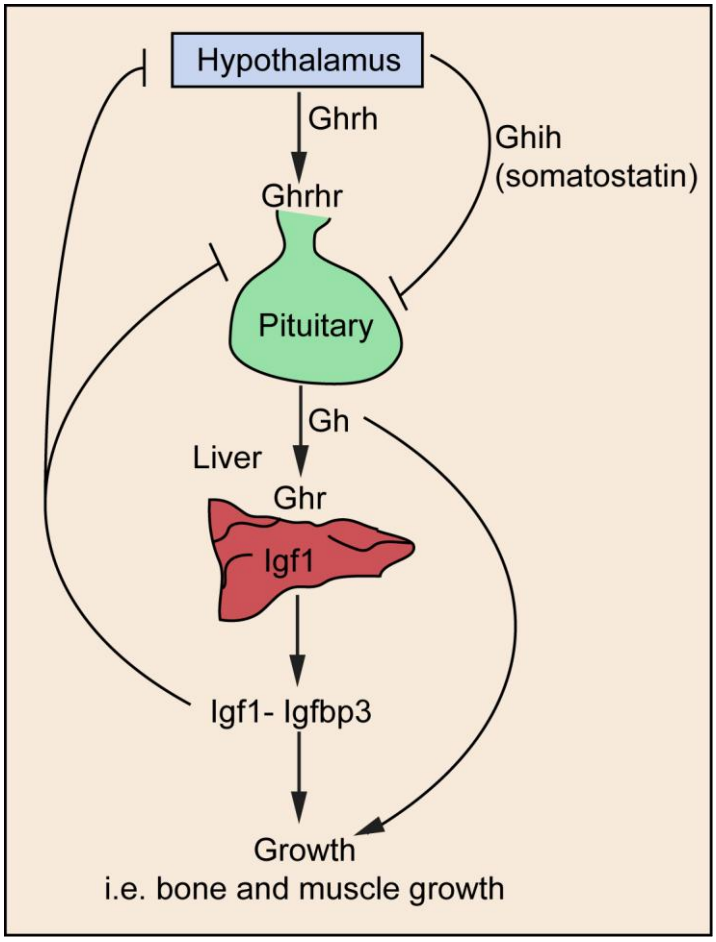

Figure 1.5: The growth hormone pathway.
The Gh pathway initiates in the hypothalamus by the expression of the Ghrh. The Ghrh binds to the Growth hormone-releasing hormone receptor (Ghrhr) in the pituitary gland and stimulates the expression of the Gh. The Gh is then released in the bloodstream and binds to the growth hormone receptor (Ghr) in several organs of the body. Growth hormone signaling in the liver results in the expression of Igf1, which acts as the mediator of Gh hormone action. Hepatic Igf1 does not only function in an autocrine and paracrine fashion, but is also secreted in the bloodstream and acts in a systemic way, similar to a hormone. Serum Igf1 is stabilised by IGF-binding proteins, mainly Igfbp-3. Gh release is inhibited via a negative feedback loop by Igf1 and also by the Growth hormone inhibiting hormone (or somatostatin).

At the molecular level, Ghr functions as a dimer. The binding of the Gh to its transmembrane receptor activates a number of signalling pathways that result in the transcription of target genes, necessary for growth (Brooks and Waters, 2010; Herrington and Carter-Su, 2001). **Figure 1.6** summarises the pathways activated by Gh binding on the Ghr.

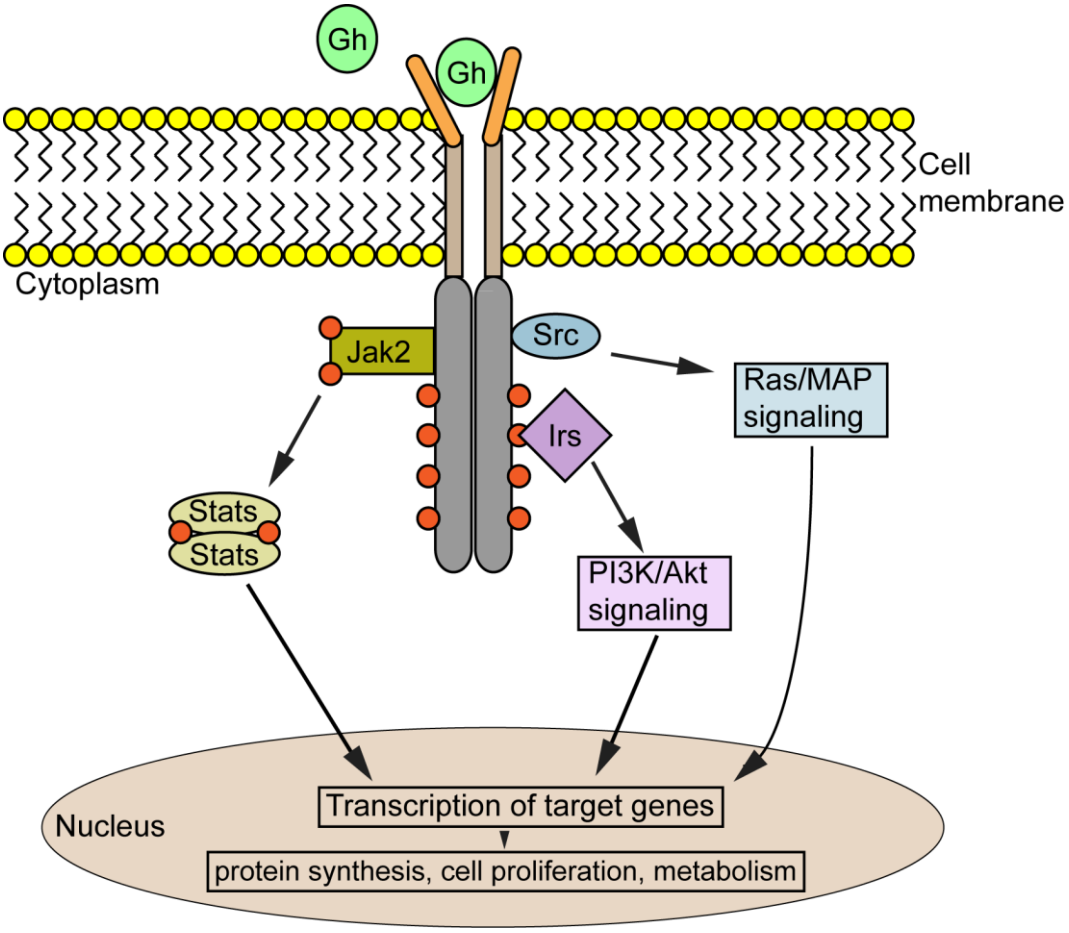

Figure 1.6: Signaling pathways activated by binding of the Gh on the Ghr.
Ghr functions as a dimer. Binding of its Gh ligand induces a conformational change in one of the receptor proteins, which in turn allows the binding of the Janus kinase 2 (Jak2). The Jak2 kinase phosphorylates itself and the Ghr, and these events allow the subsequent phosphorylation of signal-transducer and activator of transcription proteins (Stats). Finally, phosporylated Stats translocate to the nucleus and promote gene transcription of their target genes. Ghr phosphorylation can additionally activate the v-src avian sarcoma (Schmidt-Ruppin A-2) viral oncogene homolog (Src) and initiate the Rat sarcoma/mitogen-activated protein kinase (Ras/MAP) signaling pathway. Moreover, insulin receptor substrates (Irs), that function through the insulin binding, can also be activated and thus promote transcription of their target genes via the phosphatidylinositol 3-kinase - v-akt murine thymoma viral oncogene homolog 1 (PI3K/Akt) signaling pathway.

Hepatic Gh stimulation results in the expression and release of Igf1 in the bloodstream. However, the prenatal growth retardation of *Igf1*, *Igf1r*, as well as *Igf2* knock-outs implies that Igf1/2 are able to activate growth-promoting pathways in the absence of Gh stimulation. Furthermore, there is also a crosstalk between Igf1/2 and

the insulin pathway, as both growth factors bind the insulin receptor. The signalling pathways activated by Igf1/2 are depicted in **Figure 1.7** (Siddle, 2011; Zha and Lackner, 2010).

1.7.1.2 Insulin pathway

Insulin is a peptide hormone, which is expressed by the beta-cells of the pancreas and released in the bloodstream. Similarly to Igf1, insulin can bind the Igf1 receptor and activate common downstream signalling pathways. **Figure 1.7** summarises insulin action via signalling pathways (Siddle, 2011; Taniguchi et al., 2006).

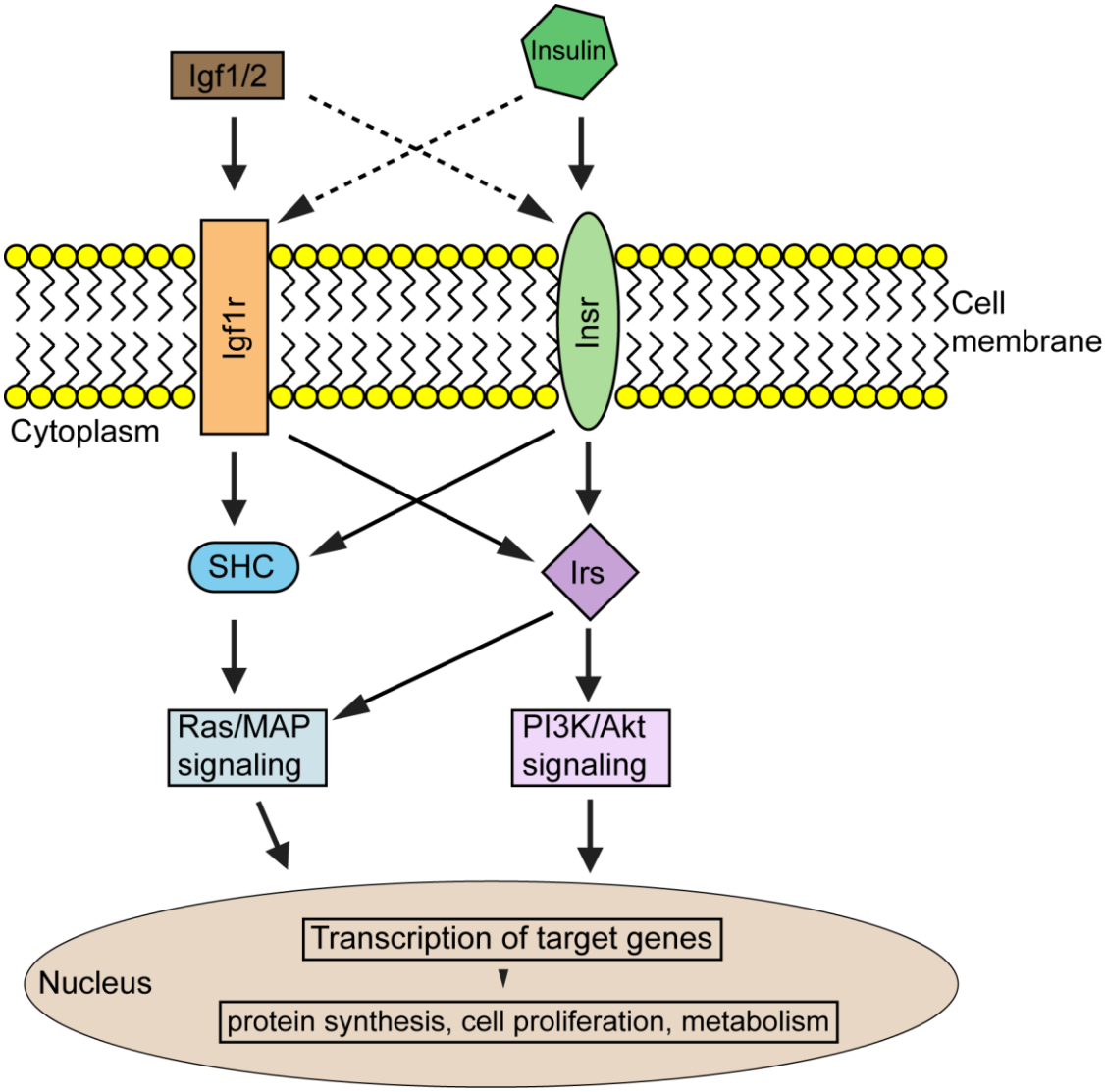

Figure 1.7: The signalling pathways activated by Igf1 and insulin.

Systemic Igf1/2 circulation binds to insulin-like growth factor 1 receptor (Igf1r) and also the insulin receptor (Insr), which leads to the activation of docking proteins (src homology 2 domain-containing transforming protein C) Shc and Irs, and the initiation of downstream Ras/MAP and PI3K/Akt signalling. Igf1/2 signaling drive protein synthesis, cell proliferation, glucose metabolism and other processes. Insulin binds Insr but can also bind the Igf1r. Reciprocally, Igf1 peptides can bind the insulin receptors. Activation of the receptors via insulin binding activates the adaptor proteins Shc and Irs, which initiate the Ras/MAP and PI3K/Akt signalling pathways, respectively. Therefore, signalling through insulin binding is also crucial for cell proliferation, glucose uptake, protein synthesis and other.

The convergence of the Gh, Igfs and insulin to common signalling pathways, as well as the ability of Igf1/2 and insulin to bind both Igf1r and insulin receptors,

demonstrates that the control of growth is complex and finely tuned. However, the differences in the commencement of growth retardation between the Igfs and insulin receptor knock-outs suggests that different growth-promoting factors may control the expression of a distinct subset of gene targets (in addition to common targets).

1.7.1.3 The thyroid hormone pathway

Like the Gh pathway, the thyroid hormone pathway is tightly regulated via a multistep hormone stimulation that initiates from the hypothalamus. Furthermore, the levels of T3 and T4 are balanced by a negative feeback loop to the pituitary, which suppresses the expression of the *Tsh*. The pathway is summarised in **Figure 1.8** (Brent, 2012; Dayan and Panicker, 2009; Oetting and Yen, 2007)**.**

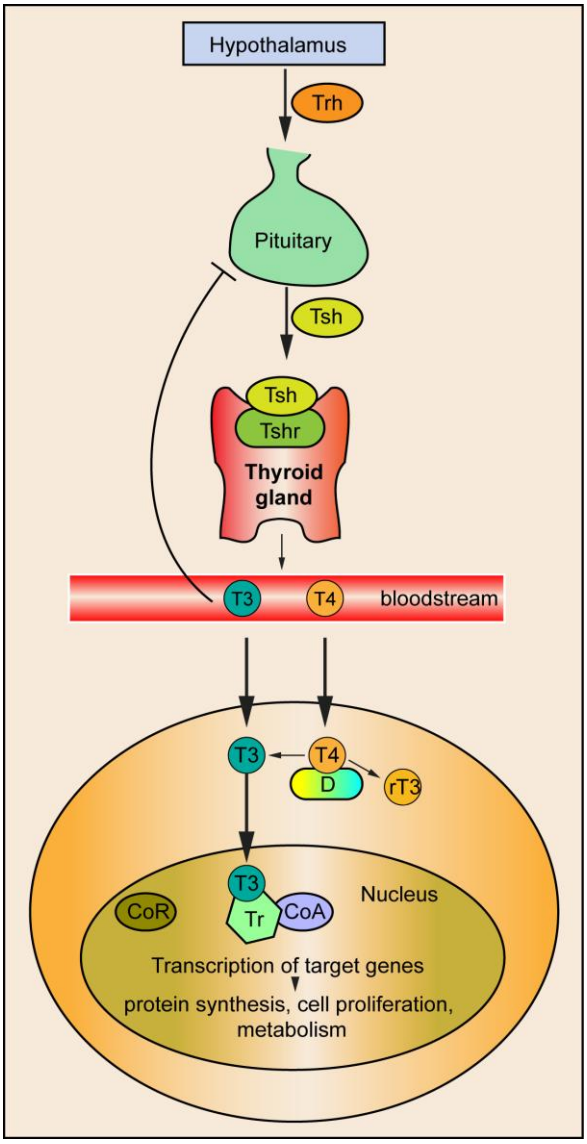

Figure 1.8: The thyroid hormone pathway

The thyroid hormone pathway initiates in the hypothalamus, by the expression and release of the thyrotropin-releasing hormone (Trh). Trh exerts its effect in the pituitary gland, which produces and releases the thyroid-stimulating hormone (Tsh). The latter hormone binds to the thyroid-stimulating hormone receptor (Tshr) into the thyroid gland and stimulates the release of triidothyronine (T3) and thyroxine (T4). They also exert a negative feedback to the pituitary gland to repress Tsh release.The thyroid signaling pathway functions through the T3 hormone. Thus, T4 is converted to T3 or an inactive form, known as rT3, by different deiodinase enzymes (D). In the nucleus, the thyroid hormone receptors (Tr) are kept in an inactive state by association with co-repressor complexes (CoR). In the presence and direct binding of T3 to the Tr, transcription is activated by the recruitment of co-activators (CoA). The thyroid hormone signalling pathway is important for growth, development and metabolism.

1.7.2 Proteins that directly affect cell proliferation and result in primordial dwarfism

The Gh, insulin and thyroid hormones discussed above promote cell proliferation by activating a number of downstream signalling pathways. Therefore, they modulate growth indirectly. Recently, downstream cell proliferation and cell survival proteins have also been identified. In humans, mutation of the latter genes can result in a distinct class of dwarfism, known as primordial dwarfism.

Primordial dwarfism initiates prenatally and continues postnatally. Affected individuals are characterised by an extreme global growth failure. Its most distinctive feature is the decrease in head size in proportion to body size (Klingseisen and Jackson, 2011).

Mutations in ten genes have been identified, whose protein products are involved in DNA damage control, centrosomal function and integrity, and DNA replication (Klingseisen and Jackson, 2011). For example, a homozygous mutation has been found that affected the splicing of the *ATR* gene. As such, patient-derived cells were unable to respond ATR-dependent damage induction (O'Driscoll et al., 2003). Mutations were also found in genes encoding centrosomal proteins such as *PERICENTRIN* and *CEP152* (Guernsey et al., 2010; Rauch, 2011). Patient cell lines with *PERICENTRIN* mutations exhibited abnormal mitosis due to their inability to correctly assemble the mitotic spindle (Rauch, 2011). Furthermore, mutations have also been identified in several *ORC* genes. These genes encode proteins that assemble as a complex at the origins of replication (Bicknell et al., 2011).

In summary, growth retardation can also result from mutations in genes that are directly involved in the control of cell division, irrespective of proper hormonal and growth factor signalling.

1.7.3 A dynamic postnatal genetic program to determine organ size

As discussed previously, several hormones and growth factors are essential for normal prenatal and postnatal growth. If hormones and growth factors were the sole determinants of organ/body size, then one would expect the levels of these

peptides to decline with age. However, this is not the case. For example, the levels of circulating GH and IGF1 remain high even postnatally (Kwan and Hartman, 2007; Rose et al., 1991). Therefore, if organ, and consequently body size, was a result of the systemic action of GH and IGF1, then body growth would never cease.

A current working hypothesis to explain how organs attain their final size and how this is orchestrated in a systemic fashion is through the existence of a common genetic program, operating in all organs (Finkielstain et al., 2009; Lui et al., 2010). This genetic program will promote cell proliferation (in this sense meaning growth), and will become limiting in postnatal life so that organs reach a certain final size.

Analysis of the gene expression profile in several mouse and rat organs shows that several genes are down regulated from an earlier to a later postnatal stage. Interestingly, there is extensive overlap of downregulated gene expression between organs, with many genes being involved in cell proliferation. A total of 235 genes are found to be downregulated in all mouse and rat tissues analysed, suggesting a common mechanism for organ growth control (Lui et al., 2010). Among the genes that show a sharp decline in expression with age include transcription and growth factors. Furthermore, when the expression of a selected number of genes is knocked down by siRNA, the proliferation of primary murine hepatocytes declines. Also, by inducing hypothyroidism, or putting young rats on a tryptophan-deficient diet (that results in growth retardation), the decline in the expression of the identified growth promoting genes is reduced. These results, suggest that: 1) the normal decline in the expression of growth promoting genes is mainly determined by growth *per se* and not by age and 2) postnatal growth deceleration is a result of a multiorgan genetic program that involves the decrease in gene expression of several growth promoting genes. This decrease occurs concurrently in multiple tissues, in a concerted fashion, in order to maintain body proportions (Finkielstain et al., 2009; Lui et al., 2010).

Therefore, growth is a process that requires: 1) the proper function of signalling pathways, regulated by hormones and growth factors and 2) underlying multigenetic programs that determine final organ size.

1.8 The formation of primary cilia and their functions

The primary cilium, an immotile organelle found in almost all eukaryotic cell types, has recently gained lots of attention. This is due to the appreciation that this organelle is vital for sensory perception and signal transduction. As such, perturbations in primary ciliary formation or function result in a group of disorders, collectively known as ciliopathies. Another type of cilia, the motile cilia are quite similar in structure to the primary cilia. Functional defects of the motile cilia give rise to primary ciliary dyskinesia, which also form another group of ciliopathies (Berbari et al., 2009; Gerdes et al., 2009b; Goetz and Anderson, 2010; Hildebrandt et al., 2011; Ishikawa and Marshall, 2011; Nigg and Raff, 2009).

1.8.1 Ciliogenesis

Primary cilia form following mitosis by the migration of the mother centriole near the cell surface to form the basal body. Ciliogenesis begins by the attachment of a Golgi-derived visicle at the distal region of the basal body, which will form part of the ciliary membrane. The basal body serves as a microtubule organising centre- the growing ciliary axoneme is composed of nine microtubule doublets that terminate to a singlet at the very tip of the cilium. The region just above the distal part of the basal body is called the transition zone, which is thought to function as a gatekeeper, controlling which proteins move into the cilium. In the meantime, attachment of more Golgi-derived vesicles extend the ciliary membrane to accommodate the elongating axomene. Anterograde transport of cargo proteins (from the ciliary base to the tip) is carried out by the intraflagellar transport protein complex B (IFT B) and the kinesin-2 heterotrimeric motor, and retrograde transport (from the ciliary tip to the base) is carried by the intraflagellar transport protein cimplex A (IFT A) protein complex and the dynein motor. IFT transport is essential for building up and maintaining the primary cilium, as well as for the localisation of proteins that signal through this organelle (Ishikawa and Marshall, 2011; Szymanska and Johnson, 2012).

1.8.2 Functions of primary cilia

Several functions have been proposed for the primary cilium. These functions include mechanosensation, light and odorant detection (Berbari et al., 2009). Mechanosensation is thought to be mediated via fluid flow through the renal tubules. Loss of ciliary proteins that reside in the renal epithilia such as polycystic kidney disease 2 (PKD2) result in the formation of kindey cysts (Mochizuki et al., 1996). Further, the retina photoreceptor outer segments represent a modified cilium responsible for light detection. Defects in the maintainance of photoreceptos caused by mutation of intraflagellar transport 88 (Ift88) (Pazour et al., 2002) or the loss of the Bardet–Biedl syndrome protein 4 (Bbs4) results in retinal degeneration (Abd-El-Barr et al., 2007) . Moreover, odorant detection is accomplished via specialised sensory neurons whose dendritic knobs end in ciliary clusters. The proteins responsible for odour sensation reside in the cilium (Berbari et al., 2009), therefore individuals with loss of function of the basal body BBS proteins present partial or complete anosmia (Kulaga et al., 2004).

The primary cilium also functions as a signalling centre, from where pathways operate in responce to external stimuli. The Hedgehog pathway is one of the best studied examples. When the hedgehog ligand is absent, the transmemberane protein Patched resides in the primary cilium and inhibits the cytoplasmic protein Smoothened (Smo). Upon Hedgehog binding, Smo inhibition is released, and Smo translocates in the cilium where it activates the Gli-Kruppel family zinc finger proteins 1, 2 and 3 (Gli1, Gli2 and Gli3) which also reside in the cilium. Activated Gli proteins translocate in the nucleus and stilumate gene expression (Berbari et al., 2009; Gerdes et al., 2009b; Goetz and Anderson, 2010). Another signalling pathway proposed to operate through the primary cilium is the Wnt pathway (Berbari et al., 2009). In addition, the platelet-derived growth factor receptor, alpha polypeptide (Pdgfra) was found to localise and proposed to signal through the primary cilia of mouse embryonic fibroblast NIH 3T3 cells (Schneider et al., 2005).

1.9 Aims and Objectives

Kdm3a and Kdm3b belong to the Kdm3 subfamily of JmjC-domain demethylases (Klose et al., 2006b). Work on knock-out and gene-trap mouse models have demonstrated that Kdm3a is important for spermatogenesis, metabolic gene expression and male sex-determination. These functions were accomplished by H3K9me2 demethylation of its target gene promoters (Inagaki et al., 2009; Kuroki et al., 2013a; Liu et al., 2010a; Okada et al., 2007; Okada et al., 2010; Tateishi et al., 2009). No mouse model has been characterised for Kdm3b, but was demostrated to function as a H3K9me1/2 histone demethylase. Interestingly, *kdm3b* is present in the zebrafish genome, but not *kdm3a*. The phenotype of morpholino *kdm3b* zebrafish knock-outs resembles a ciliary defect (Dr. Patricia Yeyati, Insitute of Genetics and Molecular Medicine, University of Edinburgh), as does the phenotype of Kdm3a knock-out and gene-trapped mice. Moreover, equally interesting is the fact that different isoforms of lysine demethylases can perform non-redundant functions (Verrier et al., 2011b; Zibetti et al., 2010).

The above observations are important because they suggest that lysine demethylases can have futher uncharacterised functions, which could possibly extend beyond histone lysine methylation. Furthermore, since the phenotype of the mouse models of Kdm3a, Jmjd1c and Hairless are non-redundant (Cachón-González et al., 1999; García-Atares et al., 1998; Inagaki et al., 2009; Kumpf et al., 2012; Kuroki et al., 2013a; Kuroki et al., 2013b; Okada et al., 2007; Tateishi et al., 2009), then it was interesting to investigate the functions of Kdm3b in a mouse model.

The aims of the present study were to:

- Compare the evolutionary conservation of the zebrafish kdm3 and murine Kdm3b in function and check their spatial expression
- Dissect the phenotype of *Kdm3b* gene-trapped mice
- Characterise an alternative murine *Kdm3a* isoform

The objectives were to:

- Investigate the protein sequence conservation of the zebrafish kdm3b with the human and mouse homologues
- Clone and check the demethylation function of the zebrafish kdm3b and of the mouse Kdm3a-i2 isoform
- Investigate the sub-cellular localisation of zebrafish kdm3b and mouse Kdm3a-i2
- Check if kdm3b and Kdm3a-i2 over-expression could result in a ciliation defect
- Check the spatial expression of the zebrafish and murine Kdm3b
- Quantify the levels of *Kdm3a-i2* transcription
- Provide a thorough phenotypic description of heterozygous and homozygous Kdm3b gene-trapped mice
- Understand in more depth the causes of the phenotype in homozygous gene-trapped mice

Chapter 2. Materials and methods

2.1 Generation of mouse lines

ES cell lines (**Table 2-1**) were obtained from the Sanger Institute Gene Trap Resource (http://www.genetrap.org) and EUCOMM (http://www.mousephenotype.org/martsearch_ikmc_project/about/eucomm), respectively. *Kdm3a* and *Kdm3b* gene-trapped mice were generated by microinjection of the ES cell lines into C57BL/6J blastocysts, with transmission of the mutation on a C57BL/ 6J background.

Table 2-1: ES cell lines for the generation of mouse gene-trap lines

Gene-trap mouse line	ES cell line
Kdm3a	XR0062 (129/ola)
Kdm3b-b07	EUCE305b07 (129P2/OlaHsd)
Kdm3b-g12	EUCE0244g12 (129P2/OlaHsd)

2.2 DNA extraction from murine tissues

Mouse ear clips were incubated with DirectPCR Lysis Reagent (Viagen, 401-E), supplemented with 0.4µg/ml proteinase K (Promega, V3021), overnight at 55^{o}C. The next day, proteinase K was then deactivated at 85^{o}C for one hour. 2µl of this crude DNA extract was used as input for the genotyping PCR.

2.2.1 Genotyping polymerase chain reaction

Each PCR was performed in a 25µl reaction, using 2 units of MyFi polymerase (Bioline, BIO-21117), 5x MyFi reaction buffer, 10µM forward and 10µM reverse primers (**Table 2-2**)(Sigma-Aldrich), 2µl of crude DNA and bought to the final volume with dH_2O. 2µl of dH_2O was used instead of DNA template as a negative control for all the primer sets. PCR products were amplified in DNA Engine tetrad 2 thermal cycler (Bio-Rad) using the protocol below (**Table 2-3**):

Table 2-2: Genotyping primers

Kdm3b-b07	5’- 3’
A	CTCTGACCGGCGTGGCTTCC
B	AGACCGAGGCAAGCGGCCAAA
C (common for both Kdm3b mouse lines)	CCCGAAAACCGCTTCTAGCAAC
Kdm3b-g12	5’- 3’
A	ACTTGAAGAAAGGCCCCTCCGATGT
B	TGGGGGATGGAGGCAGAGAAAAAGG
β-gal Forward	GCCGTCACTCCAACGCAGCA
β-gal Reverse	GTTGCGCAGCCTGAATGGCG

Table 2-3: Genotyping PCR conditions

Kdm3b-b07 line	A-B or B-C primers	B-gal primers
Initial denaturation	95°C for 1 minute	95°C for 1 minute
Denaturation	95°C for 15 seconds	95°C for 15 seconds
Annealing	65°C for 30 seconds	61°C for 30 seconds
Extension	72°C for 25 seconds	72°C for 20 seconds
Repeat denaturation, annealing and extension	34 cycles	29 cycles
Final extension	72°C for 1 minute	72°C for 1 minute
Holding	15°C forever	15°C forever

The same protocol was used for the genotyping of the Kdm3b-g12 line, except for the annealing temperature of the A-B and A-C primers at 58°C.

All PCR products were run on 2% agarose gels in 1% TBE (with 1% TBE running buffer) with 100bp molecular DNA size marker (Bio-Rad, 170-8202). Primer pair sizes: A-B- 800 base pairs; A-C- 650 base pairs; β-gal- 450 base pairs.

2.3 Tissue retrieval for wax embedding and sectioning

2.3.1 Tissue retrieval

Tissues from sacrificed mice were fixed in 4% formalin at 4°C on a roller. Eyes were fixed with Davidson's fix (EtOH, formalin, glacial acetic acid, distilled water) The next day, they were washed extensively with PBS (3 times, 30 minutes each) at room temperature. They were then dehydrated in a series of alcohols (30% → 50% → 70%) and stored at 4°C until embedding.

2.3.2 Wax embedding and sectioning

Wax embedding of tissues was accomplished with the Tissue-Tek VIP 5 Jr (Sakura). Details of the protocols are shown in **Table 2-4** below.

Table 2-4: Wax embedding protocols of mouse tissues

Station No.	Solution	Time (minutes)		
		Eyes	Testis, pancreas, kidney	Thymus
1	70% Ethanol	40	20	1
2	70% Ethanol	40	20	1
3	85% Ethanol	40	20	10
4	95% Ethanol	40	20	10
5	100% Ethanol	40	20	10
6	100% Ethanol	40	20	10
7	100% Ethanol	40	20	10
8	Xylene	30	20	10
9	Xylene	30	20	10
10	Xylene	30	20	10
11-14	Wax1-4 at 58 °C	30 each	20 each	10 each

Wax-embedded tissues were sectioned at 7µm and sections attached on superfrost slides. The slides were dried overnight at room tempetature and then baked overnight at 55°C.

2.4 Hematoxylin and eosin staining (H&E)

Tissue sections were deparaffinised in xylene (2 x 5 minute washes), and hydrated through graded alcohols (100% EtOH for 2 x 5 minutes and then 90% ➔ 70% ➔ 50% ➔ 30%, one minute each). The slides were washed in running water, haematoxylin stained (acidified Harris haematoxylin, Thermo Scientific, 6765003) for 4 minutes and then washed in running tap water for five minutes. The sections were differentiated in acid:alcohol for a few seconds, washed in running tap water and stained with lithium chloride for a few seconds. After brief washing in running tab water the sections were stained with eosin for two minutes, washed in tap water, placed in 100% alcohol for 10 minutes (2 x 5 minutes) and then to xylene for 10 minutes (2 x 5 minutes). The sections were mounted on DPX media.

2.5 Periodic acid-Schiff (PAS) staining

Tissue sections were deparaffinised in xylene (2 x 5 minute washes), and hydrated through graded alcohols (100% EtOH for 2 x 5 minutes and then 90% ➔ 70% ➔ 50% ➔ 30%, one minute each). The slides were washed in running water and incubated in 0.5% periodic acid for 7 minutes. They were then washed well in dH_2O and incubated in Schiffs solution for 25 minutes. After a thorough wash in running tap water for 10 minutes, the slides were counterstained with Harris haematoxylin for 45 seconds, differentiated in acid alcohol, and blued up in LiCl. Following a 3 minute wash in running water, the slides were dehydrated in 100% alcohol and then placed in xylene for 10 minutes (3 times for 3 minutes each). The slides were mounted in DPX.

2.6 Immunohistochemistry

Slides were placed in xylene overnight. They were then placed in 100% EtOH (3 changes of 10 minutes each) and then in 96% EtOH. The slides were then blocked for endogenous peroxidase (0.3% H_2O_2 in MeOH) and then washed in 96% and 70%

EtOH and dH_2O. Antigen retrieval was achieved by microwaving the slides for 15 minutes in TEG buffer (Tris base, EGTA, pH 9). After cooling down, the slides were incubated in NH_4Cl for 30 minutes and washed with wash buffer 1 (PBS with 1% BSA, 0.2% gelatine [Sigma, G1890], 0.05% saponin [Sigma, S7900]) for 30 minutes. The slides were then incubated overnight at 4°C, in a humidity chamber, with the Kdm3b-NT primary antibody (Sigma, 1/100) in antibody solution (PBS with 0.1% BSA and 0.3% Triton X-100). The following day, the slides were washed with wash buffer 2 (3 times, 10 minutes each) (PBS with 0.1% BSA, 0.2% gelatine and 0.05% saponin) and incubated for 1 hour at room temperature with peroxidase-conjugated antibody (1/200) (Jackson Immunoresearch, 111-035-003). The slides were then washed with wash buffer 2 (3 times, 10 minutes each). Antibody binding was revealed with DAB solution (1 DAB tablet [Kem-En-Tec Diagnostics, 4170] in 10ml of dH_2O and 10µl H_2O_2) for 10 minutes, and then the slides were rinsed in running water. They were then dehydrated with 1 minute incubations in graded EtOH (30% → 50% → 70% → 90%) and then in 100% EtOH (3 changes, 5 minutes each). The slides were incubated in xylene for 30 minutes (10 minute changes) and mounted on DPX.

2.7 Immunofluorescence

2.7.1 Antigen Retrieval

Eye and testis sections were deparaffinised for 10 minutes, hydrated through graded alcohols (90% → 70% → 50% → 30%), rinsed in distilled water and then PBS. Slides were placed in a staining dish and filled container with 10mM citrate buffer, 0.1% Tween-20, 1mM EDTA, pH 6.0. Slides were boiled in the microwave for 15 minutes at 900W, equilibrated to room temperature and then washed with PBS.

2.7.2 Immunostaining

The slides were incubated for 1 hours in block (1% BSA, 0.5% Triton-X100 in PBS), and then overnight with primary antibodies (**Table 2-7**) at 4^oC. The slides were then washed in PBS, incubated with fluorescent secondary antibodies (**Table 2-9**) for 1 hour, washed with PBS and then mounted in Vectashield/DAPI.

2.8 Alcian Blue and Alizarin Red staining of skeletal preparations

Sacrificed mice were skinned and eviscerated. They were then submerged in 95% EtOH for 5 days and then into 100% acetone for 5 more days to dissolve lipids. The skeletal preparations were then submerged in stain solution (1 part acetic acid, 1 part Alizarin red [0.1% in 96% EtOH, Sigma, A5533], 1 part Alcian blue [0.3% in 70% EtOH, Sigma, A5268] and 17 parts 70% EtOH) for a week. The staining solution was then replaced with 1% KOH in H_2O until the bones were fully visible. Once the bones were fully visible, the skeletal preparations were taken through a KOH/glycerol series (25%, 50%, 75% glycerol, changed after 1 week) until they were preserved in 100% glycerol.

2.9 Weight monitoring

E18.5 embryos were dissected out of their uteri in ice cold PBS. They were quickly put on whatman paper sitting on ice, photographed, then weighted and culled by decapitation. Weight of the embryos was rounded up to two decimal places. The weights, to 1 decimal place, of p14, p21 and p42 live mice was performed in the animal facilities.

2.10 Preparation of primary mouse embryonic fibroblasts (MEFs)

Mouse embryos E12.5 were obtained from female, sacrificed by cervical dislocation. Embryos were removed with the uterus and placed in sterile PBS. Individual embryos were exposed by cutting the uterus. Each embryo was then transferred in fresh PBS where its head and abdominal cavity were removed. The remaining part of each embryo was transferred in a $20cm^2$ culture dish (Corning) containing 10ml DMEM supplemented with 10% FCS, 1% penicillin/streptomycin and 0.1mM β-Mercaptoethanol. The embryos were severed into small pieces using sterile blades, and placed in a 3% O_2 incubator. Fresh media were added every twenty-four hours for two days. The cells in each plate were then trypsinised and all passed into 75 cm^2 plates. This was named as passage 1. About four days later, when MEFs had reached almost full confluence were passaged again. MEFs from passage 2 onwards were used for experiments.

2.11 Generation of SV-40 transformed MEFs

MEFs close to 70% confluency were transfected with 2µg of the SV-40 –expressing plasmid (Constructed by Dirk-Jan Kleinjan, School of molecular, Genetic and Population health sciences, University of Edinburgh), using Lipofectamine 2000 (Invitrogen). Transfected cells were selected with puromycin (2µg/ml) (Invitrogen, A11138-03). When transformed MEFs were close to confluency, they were passaged and maintained with growth media supplemented with puromycin at 2µg/ml. Transformed MEFs were used for experiments till passage 25.

2.12 Maintainance of TERT-RPE1 cells

Human telomerase immortalised retinal pigmented epithelial cells (hTERT- RPE1) (ATCC, CRL-400) were maintained in DMEM/F12 (Gibco, 31331-028) media supplemented with 10% FCS, 1% penicillin/ streptomycin, and sodium bi-carbonate. These cells are easy to transfect and also produce a cilium in low serum or upon serum srarvation. Thus, they were ideal for my cell culture studies.

2.13 RNA extraction and cDNA synthesis

2.13.1 Generation of cDNA libraries

Tissue from sacrificed mice or embryos was immediately incubated in RNAlater (Qiagen, 76104) or Trizol reagent (Life Sciences, 15596-026) to preserve RNA integrity.

2.13.2 RNA extraction

RNA extraction was performed with either the Trizol reagent or the RNeasy plus kit (Qiagen, 74134) according to manufacturer's instructions.

2.13.2.1 Trizol

Cells were lysed in Trizol reagent. Tissues were manually homogenised in TRizol reagent with micro pestles on a drive motor. Chloroform was added to separate the RNA from the DNA and proteins, by retaining only the upper aqueous phase. RNA precipitation was accomplished by the addition of RNase-free glycogen (Roche,

10899232103) and 100% isopropanol. After centrifugation, the RNA pellet was washed with 75% ethanol, briefly dried and resuspended in dH_2O.

2.13.2.2 RNeasy plus mini kit

Tissue was homogenised in RLT plus buffer with micro pestles on a drive motor, and DNA removed using the genomic DNA eliminator columns. RNA was precipitated with 70% ethanol, captured into RNeasy spin column and washed. RNA was eluted in dH_2O in a clean collection tube.

RNA concentration and quality was assessed using the nanodrop ND-1000 (Thermo Scientific). RNA quality was further validated by the presence of the 28S and18S rRNA bands and the absence of smearing when 1µl of RNA was run in a 2% TBE gel, supplemented with ethidium bromide, in 1x TBE running buffer.

2.13.3 DNA elimination

DNA elimination was accomplished with DNase I (Invitrogen, 18068-015). Up to 1µg of RNA was incubated with 1µl 10x DNase I reaction buffer, 1µl DNase I and dH_2O to 10µl for 15 minutes at room temperature. DNase I was deactivated with EDTA and a 10-minute incubation at 65°C.

2.13.4 Reverse transcription

cDNA was synthesized using Superscript III (Invitrogen, 18080-044). 1 µg RNA was mixed with 250ng random primers,10mM dNTP mix and dH_2O to 13µl. This was incubated at 65°C for 5 minutes, and placed immediately on ice. A reverse-transcriptase mix was then prepared in ice (4 µl reverse transcriptase 5x buffer, 1 µl Superscript III reverse transcriptase, 1 µl 0.1M DTT and 1 µl RNase inhibitor [Roche- 03335399001]) and mixed well with the RNA mix. The final mix was incubated for 60 minutes at 55°C and then at 70°C for 15 minutes to inactivate the reaction.

2.13.5 cDNA quality control

The 18S rRNA PCR was used to check the cDNA quality. The MyFi polymerase protocol was used, as described before, with 1µl of 1/10 dilution of the cDNA as

input. The PCR protocol was used as above, except for the annealing temperature at 61°C and the usage 30 cycles. The PCR products were run in 2% agarose gels in 1% TBE, with 1% TBE running buffer.

2.13.6 Confirming *Kdm3a-i2* transcript by RT-PCR

cDNA from Kdm3a homozygous gene-trapped MEFs was used for the RT-PCR. The Phision Flash polymerase (FINNZYMES, Cat. No. F-548) was used for the reaction as instructed by the manufacturer (**Table 2-5**). Primers are in **Table 2-6.**

Table 2-5: Kdm3a-i2 PCR protocol

Polymerase	Phusion Flash	
Step	Temperature (^{o}C)	Time
Initial denaturation	98	1 minute
Denaturation	98	1 second
Annealing	67	5 seconds
Extension	72	35 seconds
Repeat cycles	Back to step 2 for 29 more cycles	
Final extension	72	1 minute

Table 2-6: Primers to amplify *Kdm3a-i2* trancript

Primer	Sequence (5'- 3')
Kdm3a-i2ATGFwd	ATGTTTTGGGGGGACTGGAAGAAC
Kdm3aFL-18-19Rv	TCTGTCTTTGCTGTGGATGA
Kdm3a-FL-25Rv	CGCTCCTGCTGGGATAAACACCAC
Kdm3a-FL-27Rv	TGCCCAAACTGGATTCACTGGCTT

2.14 Protein extraction

2.14.1 Potein extraction from cultured cells and tissues

Proteins were extracted from cultured cells and tissues in RIPA buffer (50mM Tris-HCl, 200mM NaCl, 1% NP40, 0.5% DOC, 0.05% SDS, 2mM EDTA), supplemented with protease inhibitors (Roche, Cat. No. 11697498001) and Benzonase Nuclease (Novagen, Cat. No. 70746-4). Tissues were homogenised with micro pestles on a drive motor. Lysates were incubated on ice for about 20 minutes, vortexing 3-4 times during the incubation. They were then centrifuged at full speed (13,300rpm) for 15 (cultured cells) or 30 minutes at 4^{o}C and supernatants transferred in fresh chilled tubes. Protein concentration was determined with the Bradford assay.

2.14.2 Histone extraction from MEFs

MEFs were harvested by trypsinisation, washed twice with PBS and lysed in Triton lysis buffer (0.5% Triton X-100, 2mM PMSF, 0.02% sodium azide) on ice for 10 minutes, with gentle stirring. Nuclei were pelleted with centrifugation at 6,500 rpm for 10 minutes at 4^{o}C and the supernatant was discarded. The nuclear pellets were washed (resuspended) with Triton lysis buffer and re-centrifuged as before. Histones, in the pellet, were extracted with 0.2 N HCl overnight at 4^{o}C. The next day, the samples were centrifuged to pellet the debris and the histone extracts in the supernatant were transferred in fresh tubes.

2.15 Western blot

Protein extracts were mixed with 3x loading buffer (240mM Tris-HCl pH6.8, 6% SDS, 30% Glycerol, 2.1M β-Mercaptoethanol, 0.06% bromophenol blue), incubated at 95^{o}C for 5 minutes, loaded into 4-12% NuPAGE pre-cast gels (Invitrogen) or 15%-SDS in-house made gels (histone extraction) (Resolving gel: 2.3 ml H_2O, 5 ml 30% acrylamide mix, 2.5 ml 1.5M Tris pH 8.8, 0.1 ml 10% SDS, 0.1 ml 10% ammonium persulfate and 4 µl TEMED; Stacking gel: 3.4 ml H_2O, 0.83 ml 30% acrylamide mix, 0.63 ml 1M Tris pH 6.8, 0.05 ml 10% SDS, 0.05 ml 10% ammonium persulfate and 5 µl TEMED) and run at 150 volts at room temperature. The proteins were then transferred to nitrocelluloce membranes (Thermo Scientific, Cat. No. 88018) for 75 minutes at 4^{o}C at 100 volts. Membranes were blocked for 1

hour at room temperature with 5% milk (Marvel) in PBS/0.1%Tween and incubated overnight at 4°C with primary antibodies (**Table 2-7**). The next day, the membranes were washed with PBS/0.1% Tween-20, incubated with secondary antibody (**Table 2-8**) at room temperature for 1 hour, washed with PBS/0.1% Tween-20 and developed with ECL (Amersham, RPN2109).

2.16 Immunofluorescence

Cells grown on coverslips were rapidly but gently washed twice with ice-cold PBS and fixed with 4% formalin for 10 minutes at room temperature and washed with PBS/0.1% Tween-20. The fixed cells were permeabilised with PBS/0.2% Triton X-100 for 10 minutes and washed with PBS/0.1% Tween-20. They were then blocked for ≥ 1 hours at room temperature (blocking buffer: 1% BSA, 0.1% Triton X-100, 0.05% Tween-20). They were then incubated overnight with primary antibodies (**Table2- 8**) in blocking buffer, at 4^{o}C, in a humidity chamber. The next day, the cells were washed with PBS/0.05% Tween-20 and incubated with secondary antibodies (**Table 2-10**) in blocking buffer, for one hour at room temperature in a humidity chamber. Following secondary antibody incubation, the cells were washed with PBS/0.05% Tween-20 and mounted in Vectashield/DAPI (Vector Labs, H-1000). For the pre-extraction, cells were treated with PBS/0.2% Triton X-100 for 40 seconds followed by immediate fixing as above.

Table 2-7: Primary antibodies

Name	Host	Supplier, Catalog Number	Western blot dilution	Immunofluorescence dilution
Kdm3a	Rabbit	Proteintech, 13967-1-AP	1/600	----
Kdm3a-i2	Rabbit	Syd labs	1/2000	----
Kdm3b-NT	Rabbit	Sigma, HPA016610	1/500	1/100
Kdm3b-CT	Rabbit	Bethyl, A300-833A	1/500	1/100
α-tubulin	Mouse	Sigma, T6074	1/3000	----

Acetylated α-tubulin	Mouse	Sigma, T7451	----	1/500
γ-tubulin	Mouse	Sigma, T5326	----	1/500
Pericentrin	Rabbit	Abcam, ab4448	----	1/2,000
GFP	Mouse	Invitrogen, A11120	1/500	1/150
RFP	Rabbit	Evrogen, AB234	1/5000	----
H3K9me1	Mouse	Millipore, CMA306	1/1000	1/300
H3K9me2	Mouse	Abcam, ab1220	1/1000	1/300
H3K9me3	Mouse	Millipore, CMA308	1/1000	1/300
H3K27me3	Mouse	Abcam, ab6002	----	1/80
pan-H3-CT	Mouse	Millipore, 07-690	1/10,000	----
Islet 1	Mouse	DSHB, 39.4D5 (concentrated)		1/200

Table 2-8: Secondary antibodies used in Western Blot

Name	Host	Supplier, Catalog Number	Dilution
Anti-rabbit	Donkey	GE Healthcare	1/10,000
Anti-mouse	Sheep	GE Healthcare	1/10,000

Table 2-9: Secondary antibodies used in immunofluorescence

Name	Host	Supplier, Catalog number	Dilution
AlexaFluor anti-mouse 488	Goat	Invitrogen, A11017	1/800
AlexaFluor anti-mouse 594	Goat	Invitrogen, A11020	1/800
AlexaFluor anti-rabbit 488	Goat	Invitrogen, A11070	1/800
AlexaFluor anti-rabbit 594	Donkey	Invitrogen, A21207	1/800

2.17 Transfections

hTERT-RPE1 cells were seeded in plates close to confluency, with growth media devoid of penicillin and streptavidin and left to settle overnight. Transfections were performed with Lipofectamine 2000 (Invitrogen, 11668-027) according to manufacturer's instructions. Briefly, Lipofectamine 2000 and the constructs (**Table 2-10**) were incubated with OPTI-MEM separately, mixed and incubated at room temperature for 20 minutes. The latter mixes were added to cells for 6 hours. The cells were then incubated with growth media for 24 or 48 hours before fixing. For the demethylation assays, cells were fixed 24 hours post-transfection. For the ciliation experiments, the cells were grown in 0.25% FCS-containing media for 48 hours in order to induce ciliation, fixed and processed for immunofluorescence as on **section 2.16**. The table below shows the amount of each construct, in ng, transfected in each condition. For Western blot experiments, cells were lysed 24 hours post-transfection.

Table 2-10: Amount of construct transfections in ng

Construct	Per well in 24 well plate	20 cm^2 corning plate
Halo-Ms-Kdm3b	400	----
Halo vector	800	----
GFP-Kdm3a-i2	200	4000
GFP vector	40	2000
Kdm3a-i2-RFP	200	4000
Kdm3a-FL-RFP	200	4000
RFP vector	40	2000
GFP-γ-tubulin	1000	----
GFP-centrin2	1000	----

2.18 Cloning

2.18.1 PCR amplification and purification

The *Kdm3a-i2* and *Kdm3a-FL* isoforms were amplified from wild type testis and homozygous gene-trapped *Kdm3a* MEF cDNA. The zebrafish *Kdm3b* was amplified from an already ordered plasmid (Invitrogen). Primers are listed in **Table 2-11**. The amplification was a two-step process – firstly, the Kdm3 constructs were amplified using the Phusion Flash polymerase (Finnzymes, F-548) and then the PCR product were used in a second PCR round with Taq platinum polymerase (Invitrogen, 10966-034) to incorporate T-overhangs and the restriction enzyme cut sites (**Table 2-12 & 2-13**). For the zebrafish *kdm3b*, the first amplification step was omitted, thus the Taq platinum polymerase was directly used. The PCR products were purified with the QIAquick PCR purification kit (Qiagen, 28104). In case that the PCR contained unspecific bands, then, the band of the right molecular size was extracted using the QIAquick gel extraction kit (Qiagen, 28704)

Table 2-11: Primer sequences for cloning of Kdm3 constructs

Construct	Forward primer 5'- 3'	Reverse primer 5' – 3'
GFP-Kdm3a-i2	ATGTTTTGGGGGGACTGGAAGAAC	GCAGAGAAGAGTTAAGGTTTGCCC
Kdm3a-i2-RFP	ATGTTTTGGGGGGACTGGAAGAAC	GTCCACAGGAATCCTGCCTGAAGAG
Kdm3a-FL-RFP	ATGGTGCTCACGCTCGGAGAAAGTTGG	GTCCACAGGAATCCTGCCTGAAGAG

Table 2-12: PCR conditions for the amplification of Kdm3 constructs to be inserted in the P-Gem T-easy plasmid vector

Polymerase	Phusion Flash		Taq platinum	
Step	Temperature (^{o}C)	Time	Temperature (^{o}C)	Time
Initial denaturation	98	1 minute	94	2 minutes
Denaturation	98	1 second	94	30 seconds
Annealing	62	5 seconds	62	30 seconds
Extension	72	100 seconds	72	4.5-5.5 minutes
Repeat cycles	Back to step 2 for 29 more cycles		Back to step 2 for 29 more cycles	
Final extension	72	1 minute	----	----

Table 2-13: Primer sequences for subcloning of Kdm3 constructs.

Red highlight- Xho I restriction site; yellow highlight- Bam HI restriction site; green highlight- Sal I restriction site.

Construct	Forward primer 5'- 3'	Reverse primer 5' – 3'
GFP-Kdm3a-i2	CCGCTCGAGCTTTTTGGGGGGACTGGAAGAAC	CGGGGATCCTTAAGGTTTGCCCAAACTGGATTCACTGGC
Kdm3a-i2-RFP	CCCTCGAGCCATGTTTTGGGGGGACTGGAAGAAC	CGGGATCCCGAGGTTTGCCCAAACTGGATTCAC
Kdm3a-FL-RFP	CCCTCGAGCCATGGTGCTCACGCTCGGAGAAAG	CGGGATCCCGAGGTTTGCCCAAACTGGATTCAC
GFP-Zf-kdm3b	CCGCTCGAGCTGGGGACTCGCTCGGTCTGATCGGG	GGCGTCGACCTAAGAACGGCCTAATTTGGGCTCATG

2.18.2 Cloning/ligation in P-Gem T-Easy vector

The Kdm3 PCR products were then cloned/ligated in a P-Gem T-easy plasmid vector (Promega, A1360), with a single reaction as follows: 1µl P-Gem vector, 1µl T4 ligase (Promega, M180A), 1µl 10x buffer and 6µl dH_2O and 1µl of 1/10 diluted PCR reaction. Reactions were incubated overnight at 4^{o}C.

2.18.3 Transformation of library efficiency cells

Ligated constructs were transformed in Dh5α competent cells (Invitrogen, 18263-012) as follows: *E.coli* Dh5α cells were thawed in ice. 1µl of the ligation reaction was added to 50µl of Dh5α cells and incubated on ice for 30 minutes. The bacteria were then heat shocked for 45 seconds at 42^{o}C and replace on ice for 2 more minutes. SOC media (0.5% Yeast Extract, 2% Tryptone, 10 mM NaCl, 2.5 mM KCl, 10 mM $MgCl_2$, 10 mM $MgSO_4$, 20 mM Glucose) (950µl) was added to the cells, followed by an hour of incubation at 37^{o}C with shaking (250 rpm). Cells were plated in LB plates (with Ampicillin selection), to which X-Gal and IPTG were added for blue-white screening.

2.18.4 Minipreps and plasmid purification

Following blue-white screening, bacterial colonies were selected and grown overnight (37^{o}C with shaking at 250 rpm) in LB supplemented with 50mg/ml ampicillin. The next day, the plasmids were purified using the QIAprep spin miniprep kit (Qiagen, 27104) and sequenced.

2.18.5 Restriction enzyme digests and subcloning

The purified plasmids with the Kdm3 constructs, was well as the pEGFP-C1 (Clontech, 6084-1) and RFP (Evrogen, FP182) eukaryotic plasmid vectors (both with cytomegalovirus immediate early promoters- $P_{CMV\ IE}$), were restriction enzyme-digested overinight at 37^{o}C in a water bath. The Kdm3 fragments were then extracted using the QIAquick gel extraction kit. Digested vectors were purified with the QIAquick PCR purification kit. Digested vectors were then dephosporylated with shrimp alkaline phosphatase (SAP) (Affymetrix, 70092Y) for 1 hour at 37^{o}C in water bath as follows: 1µg digested vector, 4µl 10x SAP buffer, 2µl SAP and 24µl dH_2O.

Subcloning/ligation single reactions: 4µl dH_2O, 1µl 10x buffer, 1µl T4 ligase, vector and insert with a of 1:3 ratio. Ligation reactions were left overnight at 4^{o}C. The next day, ligations were transformed in Dh5α cells with antibiotic selection and colonies were pick-up for miniprep preparation. Kdm3 construct - vector control double digests were further performed for the RFP and GFP-Zf-Kdm3b cloning, and

the appropriate plasmids were then used for maxipreps (Qiagen, 12163). Vector maps are represented on **Figure 7.7**.

2.19 Quantitative reverse transcriptase PCR (qRT-PCR)

Performed with the Qiantitect SYBR Green kit (Qiagen, 204243) or Roche LightCycler 480 SYBR Green I Master (Roche, 04707516001) as per manufacturer's protocol. Individual reactions totalled 10µl (Qiagen) or 20µl (Roche) with a final primer concentration of 0.5mM. Input cDNA in reactions was diluted ½ for Kdm3a and 1/10 for the rest. qRT-PCR protocols as listed in **Tables 2-14** & **2-15**. Primers for qRT-PCT are listed in **Table 2-16**.Relative quantification of gene expression was obtained using the comparative C_T method.

Table 2-14: Qiantitect SYBR Green kit qRT-PCR protocol

Step	Temperature (^oC)	Time
Initial denaturation	95	15 seconds
Denaturation	95	15 seconds
Annealing	60	30 seconds
Extension	72	30 seconds
Back to step 2 for 39 more cycles		

Table 2-15: Roche LightCycler 480 SYBR Green I Master qRT-PCR protocol

Step	Temperature (^oC)	Time
Initial denaturation	95	5 minutes
Denaturation	95	10 seconds
Annealing	60	30 seconds
Extension	72	30 seconds
Back to step 2 for 44 more cycles		

Table 2-16: qRT-PCR primers

Primer name	Sequence (5'- 3')
Kdm3a-i2 Forward	GGGACTGGAAGAACATCATGGAAGGA
Kdm3a-i2 Reverse	GTGCCACGATGTTAACACAGGAGT
Kdm3a-FL Forward	TGGGAGCCATAACTTCTGTTCGGT
Kdm3a-FL Reverse	TCAGTAAGGGAAAGCCGAAGACTGT
Kdm3b-exon1 Forward	GCGGTAGTGAGCGGAGATCCTG
Kdm3b-exon2 Reverse	AGCACGTCTTCAGCGTGAACCTTA
Kdm3b-exon11 Forward	ACTGGGTCTGTCGGAAATGTGGAT
Kdm3b-exon12 Reverse	ATGATCTGGGTGGGCATGAGGTTT
Kdm3b-exon20 Forward	ATGGTGTATGTTGGGATCCCTGTC
Kdm3b-exon21 Reverse	TGCCATAAAGCTCCTGGCTTCTCT
Gh Forward	GAAACTGAAGGACCTGGAAGAG
Gh Reverse	GTTGGCGTCAAACTTGTCATAG
Ghrhr Forward	CCATCACTGGCTGGTCTAATC
Ghrhr Reverse	CACCGTGGAGAAGTACGATTT
Ghr Forward	CCCTACTGCATCAAGCTAACTAC
Ghr Reverse	CACGAATCCCGGTCAAACTAA
Igf1 Forward	TGGTGGATGCTCTTCAGTTC
Igf1 Reverse	CTCATCCACAATGCCTGTCT
Igf1r Forward	TAAATACGGGTCGCAAGTCG
Igf1r Reverse	GCTGTATAGTTCCCTGGGTTTAG
Igfbp3 Forward	AACCTGCTCCAGGAAACATC
Igfbp3 Reverse	GGAACTTGGAATCGGTCACT
Igfals Forward	GTATCAGGCAGTTAGGTGAGAAG

Igfals Reverse	ACGTTGAAGAGGCCAAAGAA
Tshb Forward	TACTGCCTGACCATCAACAC
Tshb Reverse	GACATCCTGAGAGAGTGCATATT
Apoa4 Forward	CAATGTGGTGTGGGATTACTTTAC
Apoa4 Reverse	GTTTGTCCTGGAAGAGGGTA
Gapdh Forward	CATGGCCTTCCGTGTTCCTA
Gapdh Reverse	CCTGCTTCACCACCTTCTTGAT

2.20 Zebrafish and Mouse Whole Mount *in-situ* Hybridisations (WISH)

2.20.1 Anti-sense riboprobe production

2.20.1.1 Polymease chain reaction

PCR products were amplified from cDNA. For zebrafish, the cDNA was derived from 4dpf embryos and for mice from wild type MEFs. The standard PCR Taq Platinum protocol was followed as in **Table 2-17**. The PCR products were subsequently cleaned using the PCR purification kit. Amplicons were run on a 1% TBE gel to verify the presence of a band of the correct size. Primer sequences for riboprobe production are listed in **Table 2-18**.

Table 2-17: PCR protocol for riboprobe production

Taq platinum	Mouse riboprobes		Zebrafish riboprobes	
Step	Temperature (^{o}C)	Time	Temperature (^{o}C)	Time
Initial denaturation	94	2 minute	94	2 minutes
Denaturation	94	30 seconds	94	30 seconds
Annealing	60	30 seconds	55	30 seconds
Extension	72	90 seconds	72	60 seconds
Repeat cycles	Back to step 2 for 34 more cycles			

Final extension	72	1 minute	72	1 minute

Table 2-18: PCR primer sequences for riboprobe production.

In capital letters are the gene primer sequences and in small letters the T7 RNA polymerase promoter sequence

Riboprobe	Primer sequences (5'-3')	
	Forward	Reverse
ZfExons15-16	ACGTCTACTTCATCCACAACCCGT	taagctttaatacgactcactatagggagaAACACTGGAGGAAATGGGAC
MsExon8-8	TGGCCTCTTCTGGATTTGGAGTGT	taagctttaatacgactcactatagggagaATCTGACAGGTCACTGTTGG
MsSenseExon8-8	taagctttaatacgactcactatagggagaTGGCCTCTTCTGGATTTGGA	ATCTGACAGGTCACTGTTGG

2.20.1.2 Digoxigenin (DIG) RNA labelling

The reactions were carried out as instructed by manufacturer (Roche, 11277073910). Single reactions were performed as follows: 2µl 10x T7 buffer (Roche), 2µl 10x DIG RNA labelling mix (Roche), 1µl RNase inhibitor (Promega, N2611), 2µl T7 polymerase (Roche, 10881767001), 5µl dH_2O. RNA labelling was carried out for 2 hours at 37^oC Removal of double stranded DNA was carried out by adding DNase for 15 minutes. The reactions were terminated by adding EDTA, followed by Lithium chloride and ethanol to precipitate the riboprobes on dry ice. The labelled riboprobes were pelleted by full speed centrifugation at 4^oC, washed with EtOH, air-dried and resuspended in RNase/DNase-free H_2O. The concentrations were determined by the Nanodrop 1000.

2.20.2 Zebrafish Whole mount *in-situ* hybridisation

2.20.2.1 Rehydration of embryos and hybridisation

Fixed zebrafish embryos stored in methanol (Dr. Shipra Bhatia, Institute of Genetics and Molecular Medicine, University of Edinburgh) were rehydrated in a methanol/PBS series (75%, 50%, 25%), proteinase K digested (1 dpf for 10', 2dpf for

17', 3dpf for 20' and 4dpf for 25') to assist riboprobe penetration. The embryos were then PFA re-fixed and blocked in pre-hybridisation mix (50% formadide, 5X SSC, 0.1% Tween-20, Citric acid at pH6, Heparin, tRNA) for several hours and then hybridised with the riboprobe (1/3000 dilution in pre-hybridisation mix) overnight at 65 °C (water bath).

2.20.2.2 Washes, blocking and antibody hybridisation

After the riboprobe hybridisation, the embryos were briefly washed in a hybridisation mix (withour tRNA and heparin) and then with an increasing 2x SSC series at 65°C (75% hybridisation mix: 25% 2x SSC, 50% hybridisation mix: 50% 2x SSC, 25% hybridisation mix: 75% 2x SSC and 2x SSC), followed by a 0.2x SSC-PBT series at room temperature (0.2x SSC, 75% 2x SSC: 25% PBT, 50% 2x SSC: 50% PBT, 25% 2x SSC: 75% PBT, 100% PBT). The embryos were then blocked for several hours (sheep serum and BSA in PBT) at room temperature, and incubated with anti-DIG antibody (1/5000) (Roche, 11214667001) overnight at 4°C.

2.20.2.3 Washes and staining

Following the antibody incubation, the embryos were washed extensively in PBT and then with the staining buffer (100mM Tris HCl pH9.5, 50mM $MgCl_2$, 100mM NaCl, 0.1% Tween-20). Staining was accomplished with NBT and BCIP (50 mg/ml NBT, 50 mg/ml BCIP in staining buffer). The embryos were monitored with a microscope. The staining reaction was terminated by aspirating the staining solution and adding PBS/ 1mM EDTA (3 washes, 5 minutes each).

2.20.3 Mouse whole mount *in-situ* hybridisation

2.20.3.1 Embryo collection and dehydration

Embryos at E9.5, E10.5 and E11.5 were dissected in PBS and fixed in 4% PFA overnight. They were then washed with PBT (PBS/0.1% Triton X-100), dehydrated through a MeOH- PBT series (25% MeOH: 75% PBT, 50% MeOH: 50% PBT, 75% MeOH: 25% PBT) and stored in 100% MeOH at -20°C.

2.20.3.2 Rehydration and prehybridisation

Embryos were rehydrated through a MeOH- PBT series (75% MeOH: 25% PBT, 50% MeOH: 50% PBT, 25% MeOH: 75% PBT), bleached with H_2O_2 for 1 hour, proteinase K treated (E9.5 for 10', E10.5 for 20' and E11.5 for 30') and re-fixed with 0.2% gluteraldehyde/4% PFA for 20 minutes at room temperature. They were then incubated overnight in pre-hybridisation mix (50% formamide, 5X SSC, 50µg/ml Heparin, 2% blocking powder [Roche, 11096176001], 0.5% CHAPS, 5mM EDTA, 100 µg/ml yeast tRNA, 0.1%Triton X-100 and H_2O to the desired volume) overnight at 65°C.

2.20.3.3 Hybridisation and post-hybridisation washes

Following incubation in the pre-hybridisation mix, the embryos were incubated overnight with the hybridisation mix (ribiprobe dilution 1/2000 in pre-hybridisation mix). They were then washed 2 time for 5 minutes with solution A (50% formamide, 5X SSC pH8, 0.1% Triton X-100, 0.5% CHAPS), and then with 50% solution A: 50% (2x SSC; 0.1% CHAPS) for 5 minutes, 2x SSC: 0.1% CHAPS for 1 hour, 0.2x SSC: 0.1% CHAPS for 1 hour and left overnight in 1X TBST at 4°C. All the above washes were performed at 65°C.

2.20.3.4 Blocking and antibody hybridisation

Embryos were blocked in 10% inactivated sheep serum in TBST buffer for several hours and incubated with anti-DIG antibody in blocking buffer (1/5000) overnight at 4°C.

2.20.3.5 Washes and staining

Following the antibody incubation, the embryos were washed extensively (1 full day of only washes) in TBST and then with the NTMT (100mM NaCl, 100mM Tris HCl pH9.5, 50mM $MgCl_2$, 0.1% Triton X-100) staining buffer. Staining was accomplished with NBT and BCIP in NTMT in the dark. For embryos >E10.5, levamisole was added in the staining buffer to block endogenous alkaline phosphatases. The staining was monitored with a microscope.Once the colour developed, embryos were further washed with NTMT and the staining reaction was

terminated by PBS/ 1mM EDTA (3 washes, 5 minutes each). The embryos were 0.1% gluteraldehyde/4% PFA post-fixed for 20 minutes at room temperature and stored in PBS at 4°C.

2.21 Protein alignments

Protein sequences were retrieved the from the Uniprot website (http://www.uniprot.org/) and aligned in Clusta; Omega (http://www.ebi.ac.uk/Tools/msa/clustalo/) Protein accession numbers are listed in **Table 2-19.**

Table 2-19: Uniprot protein accession numbers for Kdm3 subfamily members

Protein	Accession number
Human KDM3A	Q9Y4C1
Mouse Kdm3a	Q6PCM1
Human KDM3B	Q7LBC6
Mouse Kdm3b	B9EKS2
Human JMJD1C	Q15652
Mouse Jmjd1c	G3UZM1
Human HAIRLESS	O43593
Mouse Hairless	Q61645
Zebrafish kdm3	E7F3X7

2.22 Nuclear localisation signal predictions

The prediction of nuclear localisation signal was performed with the cNLS mapper (http://nls-mapper.iab.keio.ac.jp/cgi-bin/NLS_Mapper_form.cgi), which predicts importin α-dependent nuclear localisation signals, and also NLStradamus (http://www.moseslab.csb.utoronto.ca/NLStradamus/) which employs a hidden Markov model for nuclear localisation signal prediction.

2.23 Image acquisition and analysis

2.23.1 Macroscope

The Nikon AZ100 macroscope was employed for brightfield imaging of embryos.

Image acquisition was accomplished using Micropublisher 5.0 (Qimaging) camera and IPLab software (Scanalytics).

2.23.2 Fluorescence microscope

For visualisation of immunofluorescence in cultured cells, theAxioskop 2 fluorescence microscope (Carl Zeiss) was used, with Plan neofluar objectives(Carl Zeiss) and a triple-band filter set (Chroma technology, series 83000). Image acquisition was performed with the Coolsnap HQ_2 CCD camera (Photometrics) and scripts written for the IPLab (Scanalytics) software.

2.23.3 Dotslide microscope brightfield microscopy

The slide scanning system is based around an Olympus BX51 upright microscope (Olympus KeyMed, Southend on Sea, UK) with Marzhauser motorized stage (Marzhauser Wetzlar GmbH & Co, Wetzlar, Germany). The system uses Olympus plan Apochromat and UplanS Apochromat objective lenses with magnifications from 2x-40x. Images are acquired using an Olympus XC10 colour CCD camera, with a x20 magnification lens. All hardware is controlled through Olympus Dotslide VS-ASW software.

2.24 Fluorescence-activated cell sorting

The thymus was retrieved from p23 mice. It was mashed through a 40µm cell strainer in PBS and the cells were counted. The same number of cells were pipette in eppendorf tubes, the volume was brought to 100µl and the antibodies were added (for 5 million cells: 0.25µl CD4, 0.1µl CD8, 1µl CD25, 1µl CD44). OneComp beads (eBiosciences, 01-1111-42) were incubated with each antibody as positive controls. A negative cell control without antibodies was also used. The samples were incubated for 30 minutes in the dark at room temperature. Following antibody incubation, the samples were washed in 1ml PBS, centrifuged at 300g for 5 minutes

and then re-suspended in 200µl PBS (experimental samples) or 100µl PBS (control samples). FACS sorting was performed using a BD FACSAriaII cell sorter (Becton Dickinson). Data acquisition was performed with the BS FACSDiva software version 6.1.3 (Becton Dickinson) (Dr.Elizabeth Freyer, Institute of Genetics and Molecular Medicine, University of Edinburgh) and analysed with the FloJo software (FloJo LLC, 385 Williamson Way, Ashland, Oregon, 97520) (Dr. Andrew Wood, Institute of Genetics and Molecular Medicine, University of Edinburgh). All antibodies were from eBiosciences: CD4-FITC (11-0042-81), CD8-PE (12-0081-81), CD25-APC780 (47-0251-80) and CD44-e450 (48-0441).

2.25 Quantifications and statistics

2.25.1 Ciliation assays

Percentage ciliation in transfected cells was divided to the percentage ciliation in untransfected neighbouring cells. The resultant normalized ciliation in three repetitions was averaged and compared with the t test. If the p-value <0.05, then there is a significant difference between the datasets.

2.25.2 Demethylation assays

50-100 cells were counted and divided into two categories: 1) unchanged fluorescence and 2) reduced or absence fluorescence. Statistical analysis was performed with the Fisher's exact test (2x2 contingency table) using the results of the EGFP-C1 or RFP vectors as the comparison. If the p-value <0.05, then there is a significant difference between the datasets.

2.25.3 qRT-PCR

Normalised and calibrated values were compared with the t-test. If the p-value <0.05, then there is a significant difference in the gene expression between the genotypes.

2.25.4 Mouse weights

Mouse weights between genotypes were compared with one-way ANOVA test. If the p-value <0.05, then there is a significant difference in weight between genotypes.

2.26 Densitometric analysis

2.26.1 Western blot

Densitometric analysis of the western blots were performed using the Gel Analysis Tool from Image J (Rasband, W.S., ImageJ, U. S. National Institutes of Health, Bethesda, Maryland, USA, http://imagej.nih.gov/ij/, 1997-2014). The relative density of Kdm3a and histone epigenetic bands were normalized to the relative density of the corresponding α-tubulin or pan-H3 bands, respectively. Results for the histone extraction western blot were compared with the one-way ANOVA test. If the p-value <0.05, then there is a significant difference between genotype protein levels.

Chapter 3. The zebrafish and mouse Kdm3b: a comparative study

3.1 Introduction

At present, there is no information on whether the demethylase function for the KDM3 family members is conserved through evolution beyond the mouse and human studies. Previous synteny analysis, by Dr. Philippe Guatier (Institute of Genetics and Molecular Medicine, University of Edinburgh), show that the human and mouse genomes contain all four KDM3 family members: *KDM3A*, *KDM3B*, *JMJD1C* and *HAIRLESS*. However, the zebrafish genome only contains two of the four demethylases: *kdm3b* and *jmjd1c* (*kdm3a* and *hairless* are missing) (**Figure 3.1**). Through over-expression assays, it was shown that the human KDM3B functions as an H3K9me1 and H3K9me2 demethylase, whereas the demethylation potential of JMJD1C is still controversial (Brauchle et al., 2013; Kim et al., 2010; Kuroki et al., 2013b; Sroczynska et al., 2014). In this study: I investigate 1) whether the zebrafish kdm3b functions as histone demethylase, 2) how the human, murine and zebrafish KDM3B orthologues are related in terms of protein sequence and 3) the localisation of Kdm3b expression in murine and zebrafish embryos.

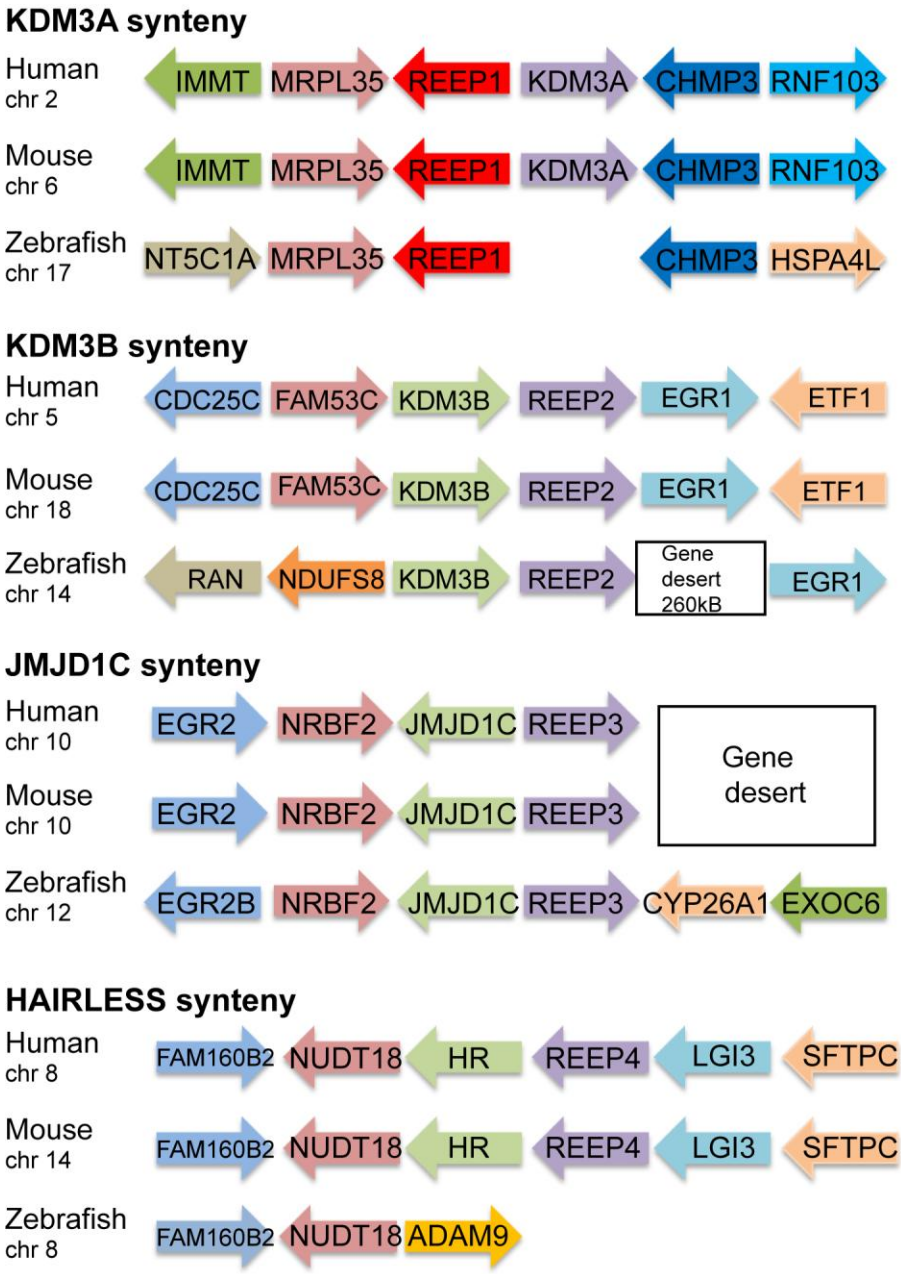

Figure 3.1: Genomic synteny in human, mouse and zebafish genomes suggest that KDM3A and HAIRLESS (HR) are absent from the zebrafish genome.

In human and mouse genomes, *KDM3* subfamily genes are in synteny with *receptor accessory protein* (*REEP*) genes, known to affect the endoplasmic reticulum shaping (Park et al., 2010; Schlaitz et al., 2013; Voeltz et al., 2006). In the zebrafish genome, *kdm3a* is absent from its genomic position, and the *hailess* genomic has been replaced by the *adam metallopeptidase domain 9* (*adam9*). It is a member of the ADAM (a disintegrin and metalloprotease domain) family of membrane anchrored proteins, which are involved in cell to cell and cell to matrix interactions (White, 2003). kdm3b and jmjd1c are uncharacterised genes in the zebrafish genome, with Ensembl annotations ENSDART00000089845 and ENSDART00000113148. Gene

deserts are areas of the genome that contain no genes. Gene symbols: *IMMT- inner membrane protein, mitochondrial*; *MRPL35- mitochondrial ribosomal protein L35; CHMP3- charged multivesicular body protein 3; RNF103- ring finger protein 103; NT5C1A- 5'-nucleotidase, cytosolic IA; HSPA4L- heat shock protein 4 like; CDC25C- cell division cycle 25C; FAM53C- family with sequence similarity 53, member C; EGR1- early growth response 1; ETF1- eukaryotic translation termination factor 1; RAN- RAN, member RAS oncogene family; NDUFS8- NADH dehydrogenase (ubiquinone) Fe-S protein 8, 23kDa (NADH-coenzyme Q reductase); EGR2- early growth response 2; NRBF2- nuclear receptor binding factor 2; CYP26A1- cytochrome P450, family 26, subfamily a, polypeptide 1; EXOC6- exocyst complex component 6; FAM160B2- family with sequence similarity 160, member B2; NUDT18- nudix (nucleoside diphosphate linked moiety X)-type motif 18; LGI3- leucine-rich repeat LGI family, member 3; SFTPC- surfactant protein C.*

3.2 Results

Searching for a *kdm3a* or *kdm3b* orthologue in the zebrafish genome

Previous data on genomic synteny around the KDM3 family members in humans, mice and zebrafish showed that zebrafish have lost *kdm3a* and *hairless* (Dr. Philippe Guatier, Institute of Genetics and Molecular Medicine, University of Edinburgh). To compare how similar the predicted zebrafish *kdm3b* is to the mouse *Kdm3a* and *Kdm3b*, I blast searched in the ZFIN website (zfin.org) using the mouse Kdm3a or Kdm3b protein as the query sequences. Both searches generated the same top hits (XP_005173195.1, XP_005173197.1, XP_005173198.1, XP_005173199.1, E7F3X7), which were labelled as uncharacterised proteins or predicted lysine demethylase 3B isoforms. Alignment of these predicted sequences resulted in 97% identity (data not shown), therefore all the entries encoded the same protein, with a small sequence variation between them. The results suggested that the zebrafish genome contains not both but one of the kdm3a or kdm3b paralogues.

To identify which paralogue is present in the zebrafish genome, I aligned the predicted zebrafish E7F3X7 protein sequence, which is the only one found in Uniprot (http://www.uniprot.org/), with the KDM3A or KDM3B human and mouse sequences. I chose the E7F3X7 sequence because an independent *in silico* prediction (by Philippe Gautier) resulted in 99% sequence identity with this zebrafish sequence.

Alignment of the human (Uniprot ID: Q9Y4C1) and mouse (Q6PCM1) KDM3A with the zebrafish E7F3X7 prediction resulted in 34.4% sequence identity (616 identical positions) (for complete alignments see **Figure 7.2**). The human and mouse KDM3A sequences were 91% identical (1209 positions). Based on the

sequence alignment of the human and mouse JmjC domain (both spanning 224 amino acids), I was able to identify zebrafish JmjC domain (232 amino acids). All species shared 78% identity (181 positions) (**Figure 3.2**- yellow and brown highlights), whereas human-mouse comparison yielded a 98.6% (221 positions) identity. Within the zinc finger, all species showed 77% (20/26) identity, with all cysteine residues conserved (**Figure 3.2**- blue and grey highlight). Notably, the human and mouse zinc fingers were 100% (26/26) identical. In addition, there was 80% (4/5) identity within the nuclear receptor motif between all three species (**Figure 3.2**- green highlight). Human and mouse nuclear receptor motifs were 100% (5/5) identical. All iron (II) [Fe (II)] and α-ketoglutarate (α-KG) binding sites within the JmjC domains, critical for the demethylase activity, were conserved in all species (**Figure 3.2**- red highlight and blue highlight, respectively).

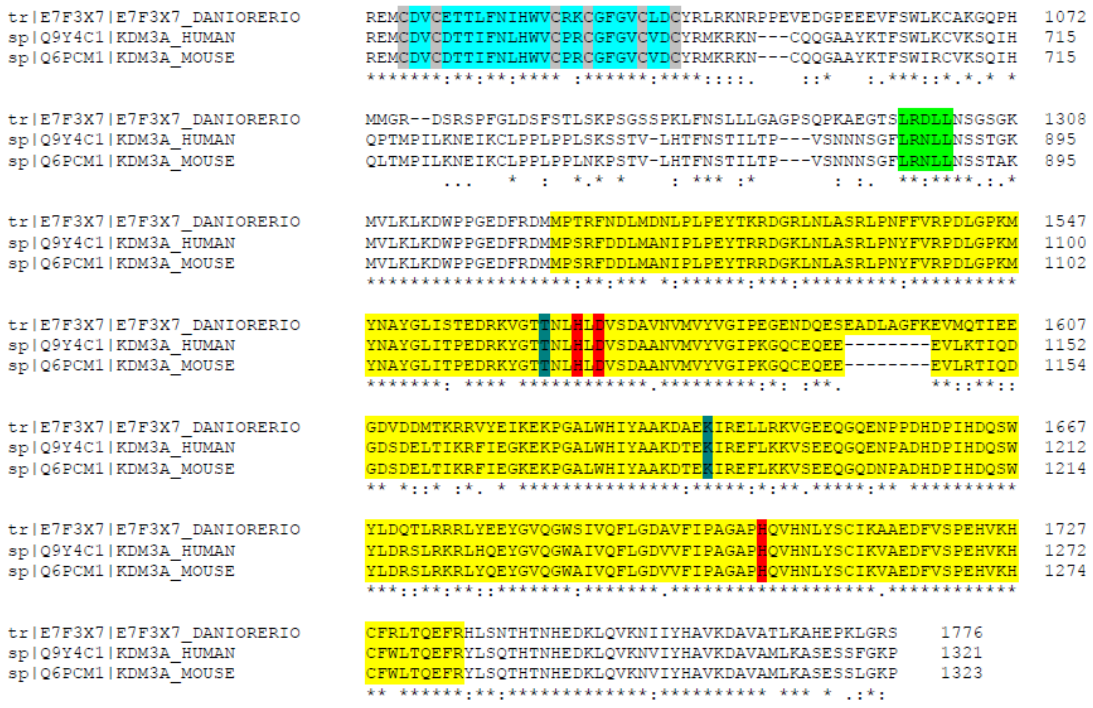

Figure 3.2: Alignments of the human and mouse KDM3A and zebrafish kdm3b domains and motifs.

Light blue highlight: zinc finger with cysteine residues in grey; green highlight: nuclear receptor motif; yellow and brown highlights: JmjC domain; red highlights: predicted iron binding sites; blue highlights: α-ketoglutarate binding sites; DANRE: *Danio rerio* (zebrafish) HUMAN: *Homo sapiens*, MOUSE: *Mus musculus*. Complete sequence alignments on **Figure 7.2**.

* indicates fully conserved residue

: indicates residues of strongly similar properties

. indicates residues of weakly similar properties

Similar properties of amino acids are defined by the presence of: hydrophobic aliphatic side chains, hydrophobic aromatic side chains, polar neutral side chains, electrically charged-acidic side chains, electrically charged-basic side chains and covalent cross-linking (disulfide bonds).

I then compared the human (Uniprot ID: Q7LBC6) and mouse (B9EKS2) KDM3B protein sequences with the zebrafish prediction (for complete alignments see **Figure 7.3**). All three homologues shared 48% identity (921 positions), whereas human and mouse homologues were 93% identical (1648 positions).

Within the JmjC domain, all three species shared 84% identity (195 positions) (**Figure 3.3-**yellow and brown highlights). Human and mouse domains were 98% identical (221 positions). The predicted Fe(II) and α-KG binding sites within the JmjC domain (**Figure 3.3-** red and blue highlights respectively) were conserved in all species. In addition, there was 100% sequence identity between species for the zinc finger (blue highlight- 26 amino acids) and the nuclear receptor sequences (green highlight- 5 amino acids).

Thus, zebrafish E7F3X7 has a higher level of sequence identity to mammalian KDM3B than KDM3A, both across the entire protein and within the key JmjC domain, the zinc finger and the nuclear receptor motif. Therefore I will refer it hereafter as kdm3b.

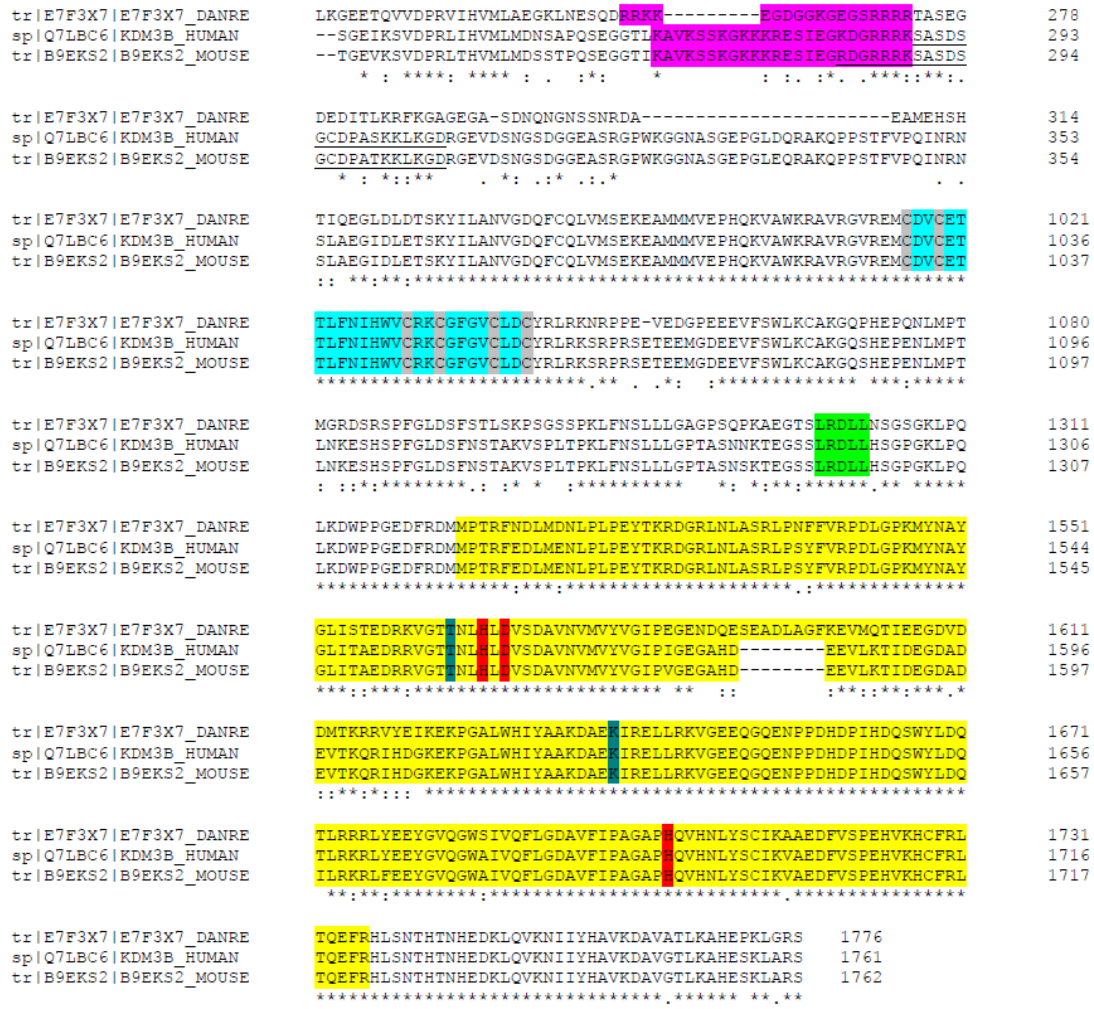

Figure 3.3: Alignments of the human, mouse and zebrafish Kdm3b domains, motifs and predicted nuclear localisation sequences.

Purple highlight: predicted nuclear localisation signal by NLStradamus; underline: predicted nuclear localisation signal by cNLS Mapper; light blue highlight: zinc finger with cysteine residues in grey; green highlight: nuclear receptor motif; yellow and brown highlights: JmjC domain; red highlights: predicted iron binding sites; blue highlights: α-ketoglutarate binding sites. DANRE- *Danio rerio* (zebrafish), HUMAN-*Homo sapiens*, MOUSE- *Mus musculus*. Complete sequence alignments on **Figure 7.3**.

* indicates fully conserved residue

: indicates residues of strongly similar properties

. indicates residues of weakly similar properties

Similar properties of amino acids are defined by the presence of: hydrophobic aliphatic side chains, hydrophobic aromatic side chains, polar neutral side chains, electrically charged-acidic side chains, electrically charged-basic side chains and covalent cross-linking (disulfide bonds).

3.2.1.1 Prediction of nuclear localisation signal in KDM3B orthologues

To carry out their histone demethylation function, all KDM3B orthologues must be imported to the nucleus, thus they should contain a nuclear localisation signal (NLS) (Lange et al., 2007). To predict potential NLS in the KDM3B orthologues, I primarily used the cNLS Mapper (Kosugi et al., 2009). The algorithm predicts classical importin α/β pathway NLS based on the yeast genome sequences (http://nls-mapper.iab.keio.ac.jp/cgi-bin/NLS_Mapper_form.cgi). cNLS Mapper predicted the bipartite NLS of human and mouse KDM3B to localise to 282-305 and 283-306 respectively (22 identical positions out of 24, thus 98% identity) (**Figure 3.3-** underlined regions**)**. The software was unable to predict any NLS in the zebrafish protein sequence.

Since the zebrafish kdm3b localises to the nucleus (for example see **Figure 3.7**), I used a second prediction algorithm called NLStradamus (Nguyen Ba et al., 2009) (http://www.moseslab.csb.utoronto.ca/NLStradamus/). The algorithm predicted NLS through a simple Hidden Markov model based again on yeast genome sequences. NLStradamus predicted the NLS of human, mouse and zebrafish KDM3B to localise to 265-288, 266-289 and 256-273, respectively (**Figure 3.3-**purple highlight). The NLS of all species show 21% identity (5 positions). Human and mouse NLS were 96% identical (23 out of 24 positions). A comparison between mouse and zebrafish sequences yielded 25% identity (6 positions) and 8 similar positions, showing the the zebrafish prediction could as well represent a NLS. Although the predicted NLS sequences derived from the two websites were not identical, they partly overlapped (human and mouse predictions) and combined covered a stretch of about 40 amino acids.

The data suggest that the human and mouse predicted NLSs are almost identical. The predicted zebrafish NLS has a different sequence, but could represent a true NLS.

3.2.2 Cloning of the zebrafish *kdm3b*

Human KDM3B functions as a mono- and di-methyl lysine 9 histone 3 (H3K9me1/2) demethylase (Brauchle et al., 2013; Kim et al., 2012). To test whether the demethylation function is maintained in the zebrafish *kdm3b,* I carried out over expression-based demethylation assays. For these experiments, *kdm3b* cDNA was synthesized on a plasmid vector (Life technologies, vector backbone pMA-T) based on an earlier *in silico* prediction (Dr. Philippe Gautier, Insitute of Genetics and Molecular Medicine, University of Edinburgh). I then sub-cloned it in an pEGFP-C1 vector, with a N-terminal GFP tag (GFP-Zf-kdm3bΔ2aa). When translated, this kdm3b protein prediction was missing two conserved amino acids, which were present in the current zebrafish Uniprot prediction (E7F3X7) and also in the human and mouse KDM3A and KDM3B homologues (**Figure 3.4-** yellow highlight). This two amino acid- deletion was closest to the zinc finger (**Figure 7.2** and **7.3-** dark grey highlight) Thus, the two amino acids were added (Dr. Patricia Yeyati, Insitute of Genetics and Molecular Medicine, University of Edinburgh), recreating a WT (GFP-Zf-kdm3b) and a deletion mutant (GFP-Zf-3bΔ2aa) GFP reporter constructs.

```
sp|Q7LBC6|KDM3B_HUMAN       CRECRLERYRKFKEQE--QDDSTVACRFFHFRRLIFTRKGVLRVEGFLSP 961
tr|B9EKS2|KDM3B_MOUSE       CRECRLERYRKFKEQE--QDDSTVACRFFHFRRLVFTRKGVLRVEGFLSP 962
tr|E7F3X7|E7F3X7_DANRE      CRECRLERYRKSREQDSDDDDPNVACRFFHFRRLAFTKKGVLRVEGFLSP 946
sp|Q9Y4C1|KDM3A_HUMAN       CRECRLDSLRKDKEQQ---KDSPVFCRFFHFRRLQFNKHGVLRVEGFLTP 592
sp|Q6PCM1|KDM3A_MOUSE       CRECRLDSLRKDKDQQ---KDSPVFCRFFHFRRLQFNKHGVLRVEGFLTP 592
                            ******:  ** ::*:   .*. * ********* *.::*********:*
```

Figure 3.4: The two amino acids absent in GFP-Zf-3bΔ2aa zebrafish kdm3b are evolutionarily conserved.
Alignment of human, mouse and zebrafish KDM3B and also of the human and mouse KDM3A orthologues around the site of mutation (yellow highlight) showed that the two amino acids absent in the zebrafish kdm3b mutant construct are conserved.

I validated the size of both GFP-tagged kdm3b constructs by over-expressions in TERT-RPE1 cells followed by Western blot. The GFP antibody detected the GFP-Zf-kdm3b band of about 250 kilodalton (kDa) and the GFP vector band of 30 kDa, but no bands in the untransfected cell lysate (**Figure 3.5 -** GFP). An antibody against a C-terminal epitope conserved in human, mouse and zebrafish Kdm3b (**Figure 3.5 -** KDM3B-CT) recognised only the GFP-Zf-kdm3b and GFP-Zf-3bΔ2aa. The two

lower bands in **Figure 3.5 B** may represent degradation products or the loss of the GFP tag from the over-expressed protein. An antibody against an N-terminal epitope of human KDM3B (**Figure 3.5 -** KDM3B-NT), not conserved in zebrafish kdm3b, was used as a negative control. As expected, it did not pick up the over-expressed GFP-Zf-kdm3b or GFP-Zf-3bΔ2aa, but recognised the endogenous human KDM3B in all three conditions/lanes of a predicted size of about 190 kDa.

I then validated the specificity of the antibodies by immunofluorescence. Both the GFP and KDM3B-CT antibodies recognised the GFP-Zf-3bΔ2aa over-expression (**Figure 3.5C,D**). When the KDM3B-CT was used, the low fluorescence nuclear signal in the neighbouring untransfected cells represented the endogenous KDM3B of the TERT-RPE1 cells. The KDM3B-NT antibody picked up only the endogenous KDM3B in all cells, as the KDM3B fluorescent intensity in transfected versus untransfected cells remained unchanged (**Figure 3.6E)**. Also, the KDM3B-CT antibody did not recognise the GFP protein tag (**Figure 3.6F**).

The results showed that kdm3b was correctly cloned and validated the specificity of KDM3B antibodies used throughout the study.

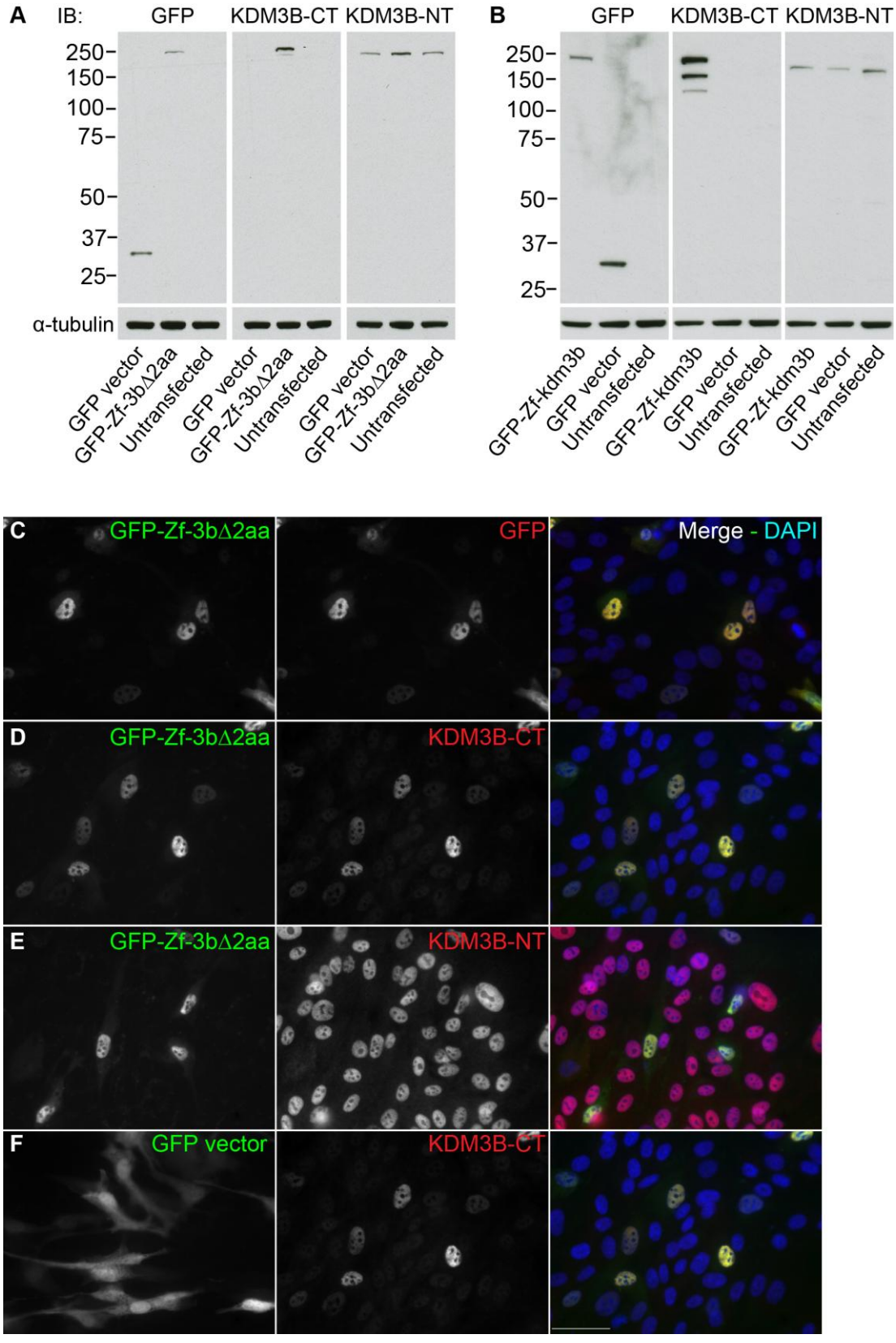

Figure 3.5: Size validation of the EGFP-C1 cloned zebrafish kdm3b constructs.

(A-B) Western blot of TERT-RPE1 cell lysates. TERT-RPE1 cells were tranfected with GFP-Zf-3bΔ2aa, GFP-Zf-kdm3b, GFP vector or left untransfected. The GFP antibody recognised the GFP-Zf-3bΔ2aa, GFP-Zf-kdm3b and the GFP vector protein. The KDM3B-CT antibody recognised the over-expressed GFP-Zf-3bΔ2aa and GFP-Zf-kdm3b. The two lower bands in the GFP-Zf-kdm3b blot may represent degradation products or the loss of the GFP tag from the over-expressed protein. The KDM3B-NT antibody whose epitope is not present in the zebrafish kdm3b picked up the endogenous KDM3B of the TERT-RPE1 cells. α-tubulin was used as a loading control. Numbers beside the Western blot are molecular weight markers in kDa. (**C-F**) GFP and KDM3B antibody validation. GFP-ZF-3bΔ2aa or the GFP vector were transfected in TERT-RPE1 cells. (**C**) The GFP antibody recognised the over-expressed GFP-Zf-3bΔ2aa. (**D**) The KDM3B-CT antibody recognised the over-expressed GFP-Zf-3bΔ2aa. The low nuclear fluorescence intensity in the untransfected cells represented the endogenous KDM3B. (**E**) The KDM3B-NT antibody, used as a negative control, recognised only the endogenous KDM3B. (**F**) The KDM3B-CT antibody did not recognise the over-expressed GFP tag. Scale bar: 20 μm.

3.2.2.1 The two amino acid deletion within GFP-Zf-3bΔ2aa affects its subcellular localisation

The GFP-Zf-kdm3b and GFP-Zf-3bΔ2aa transfections had a noticeable difference in relation to their subcellular localisation. **Figure 3.6** provides an example. In **Figure 3.6A**, GFP-control hTERT-RPE1 transfected cells showed both nuclear and cytoplasmic localisation (arrowheads). In **figure 3.6B** three out of five GFP-Zf-kdm3b transfected cells showed nuclear localisation (arrows), whereas the other two had both nuclear and cytoplasmic localisation (arrowheads). In contrast, all three GFP-Zf-3bΔ2aa transfected cells (**Figure 3.6C**) showed nuclear-cytoplasmic localisation (arrowheads). The difference in the distribution of these two constructs was quantified. While GFP-Zf-kdm3b was 69% (162/235) nuclear and 31% (73/235) nuclear-cytoplasmic, the GFP-Zf-3bΔ2aa was 28% (48/172) nuclear and 72% (124/172) nuclear-cytoplasmic (**Figure 3.6C**). The nuclear fluorescence in the nuclear-cytoplasmic category tended to be stronger than that of the cytoplasmic for both constructs. Fisher's exact test (2x2 contigency table) resulted in a significant difference between the localisation of the two constructs ($p < 0.0001$). The experiment was performed once and further replicates must be carried out to confirm the result.

The results suggested that the two amino acid deletion in GFP-Zf-3bΔ2aa affected its subcellular distribution. This could be due to changed folding of the mutant protein, affecting the binding of the nucleo-cytoplasmic shuttling complex.

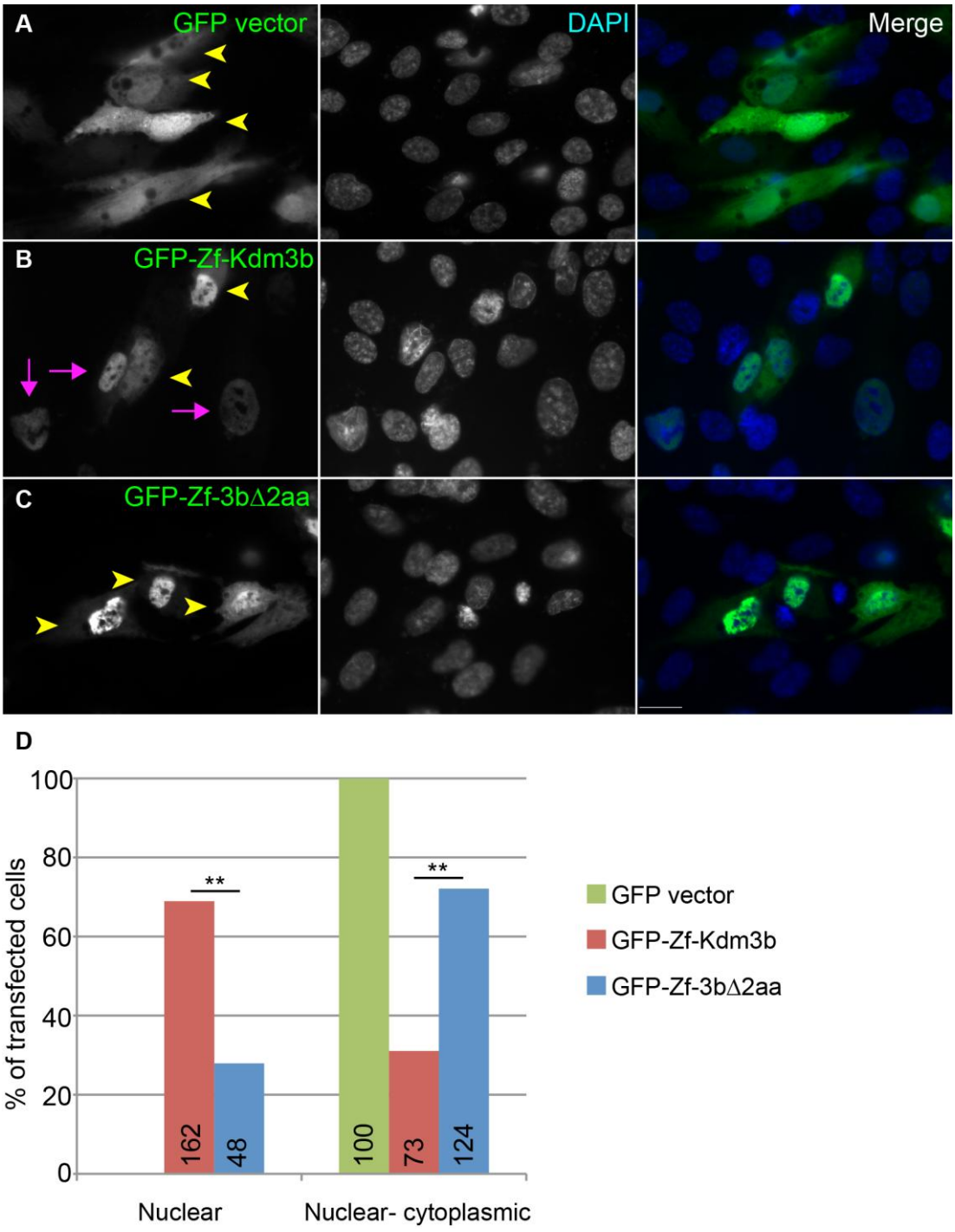

Figure 3.6: GFP-Zf-3bΔ2aa shows a higher nuclear-cytoplasmic localisation than GFP-Zf-kdm3b.

(A) All of the GFP vector transfected cells show nuclear and cytoplasmic localisation. (**B**) Three GFP-Zf-kdm3b transfected cells show nuclear localisation while the other two show nuclear-cytoplasmic localisation. (**C**) All three GFP-Zf-3bΔ2aa transfected cells showed nuclear-cytoplasmic localisation. Arrowheads indicate nuclear-cytoplasmic localisation whereas arrows indicate nuclear localisation. (**D**) The subcellular localisation of GFP-Zf-kdm3b and GFP-Zf-3bΔ2aa was quantified. GFP-Zf-kdm3b showed 69% nuclear localisation and 31% nuclear-cytoplasmic localisation. In contrast, GFP-Zf-3bΔ2aa showed 28% nuclear and 78% nuclear-cytoplasmic localisation. The GFP vector control showed 100% nuclear-cytoplasmic localisation. The numbers in bars represent the number of cells counted.The difference in sub-cellular localisation between the constructs is statistically significant. ** = significant, Fisher's exact test $p<0.0001$. Scale bar: 20 μm.

3.2.2.2 In low serum growth media, the zebrafish and human KDM3B can function as H3K9me2 demethylases

The human KDM3B functions as an H3K9me1/2 demethylase (Brauchle et al., 2013; Kim et al., 2012). To investigate the demethylation function of human KDM3B is evolutionary conserved, GFP-tagged zebrafish *Kdm3b* constructs were transfected in TERT-RPE1 cells, in low serum (0.25% FCS). Twenty-four hours post transfection, the cells were fixed and processed for immunofluorescence with antibodies against the epigenetic marks H3K9me1, H3K9me2 and H3K27me3. Cells were divided into two categories: a) transfected cells with unchanged fluorescence of the epigenetic marks and b) transfected cells with reduced or absent fluorescence of the epigenetic marks. Loss or reduction of the epigenetic mark fluorescence indicated that the zebrafish kdm3b constructs can function as demethylase enzymes. The results from the over-expressions were then compared to the results of their respective vectors by Fisher's exact test (2x2 contingency table). The fluorescence of H3K9me1/2 and H3K27me3 epigenetic marks was evaluated twenty four hours post-transfection. Quantifications were presented as the percentage of transfected cells with unchanged fluorescence. As a positive control, a murine Kdm3a isoform (GFP-Kdm3a-i2) was also transfected. The latter isoform functions as both a H3K9me1 and H3K9me2 demethylase (discussed in **Chapter 5**). One hundred cells (100) per category were evaluated, and the experiment was performed once.

Neither the GFP-Zf-kdm3b nor the GFP-Zf-3bΔ2aa transfections significantly affected the H3K9me1 fluorescence compared to the GFP vector (**Figure 3.7A,B,D,E-** Fisher's exact test: GFP-Zf-kdm3b, p= 0.77; GFP-Zf-3bΔ2aa, p= 0.33). The GFP-Kdm3a-i2 positive control transfection resulted in 65% (65/100) decreased/absent H3K9me1 fluorescence. The difference was statistically significant (Fisher's exact test, p< 0.0001) (**Figure 3.7C,E**). Moreover, the Halo-Hm-Kdm3b (Kazusa, pFN21A HaloTag CMV Flexi vector), used as another positive control for the assay, did not significantly affect the H3K9me1 fluorescence (**Figure 3.7E-** Fisher's exact test, p= 0.37). This result could be due to low expression levels for the *Kdm3b* constructs, which do not suffice to cause the demethylation effect.

In contrast, 39% (39/100) of the GFP-Zf-kdm3b transfected cells showed reduced the H3K9me2 fluorescence intensity compared to neighbouring untransfected cells (**Figure 3.9A,E-** Fisher's exact test- p< 0.0001). Notably, the GFP-Zf-3bΔ2aa was unable reproduce this effect (0%- 0/100) (**Figure 3.9B,E-** Fisher's exact test- p=1). As expected, GFP vector transfection did not affect the H3K9me2 fluorescence (0%- 0/100). The GFP-Kdm3a-i2 construct, used as a positive control for the assay, caused global demethylation of the H3K9me2 mark (**Figure 3.8C,E-** Fisher's exact test, p < 0.0001).

The Halo-Hm-Kdm3b transfection reduced the H3K9me2 fluorescence intensity in 9% (9/100) compared to neighbouring untransfected cells, whereas the Halo vector did not (0%- 0/100) (**Figure 3.8E-** Fisher's exact test, p < 0.0001).

The fluorescence of H3K27me3 mark, used as a negative control, was unchanged for all transfections (0%- 0/100). The p-value for all comparisons was 1; therefore none of the transfections produced a significant result (**Figure 3.9A-E**).

Under the experimental conditions used, both GFP-Zf-kdm3b and Halo-Hm-Kdm3b can function as H3K9me2, but not H3K9me1, demethylases. GFP-Zf-3bΔ2aa was unable to decrease H3K9me2 fluorescence. To further validate this result, the fluorescence signal in transfected versus untransfected cells should be quantified and compared. Alternatively, *in vitro* demethylation assays can be

employed. Furthermore, in agreement with previous published data, Halo-Hm-KDM3B was able to demethylate both H3K9me1 and H3K9me2, when the cells were maintained in 10% FCS (**Figures 7.4 – 7.6**).

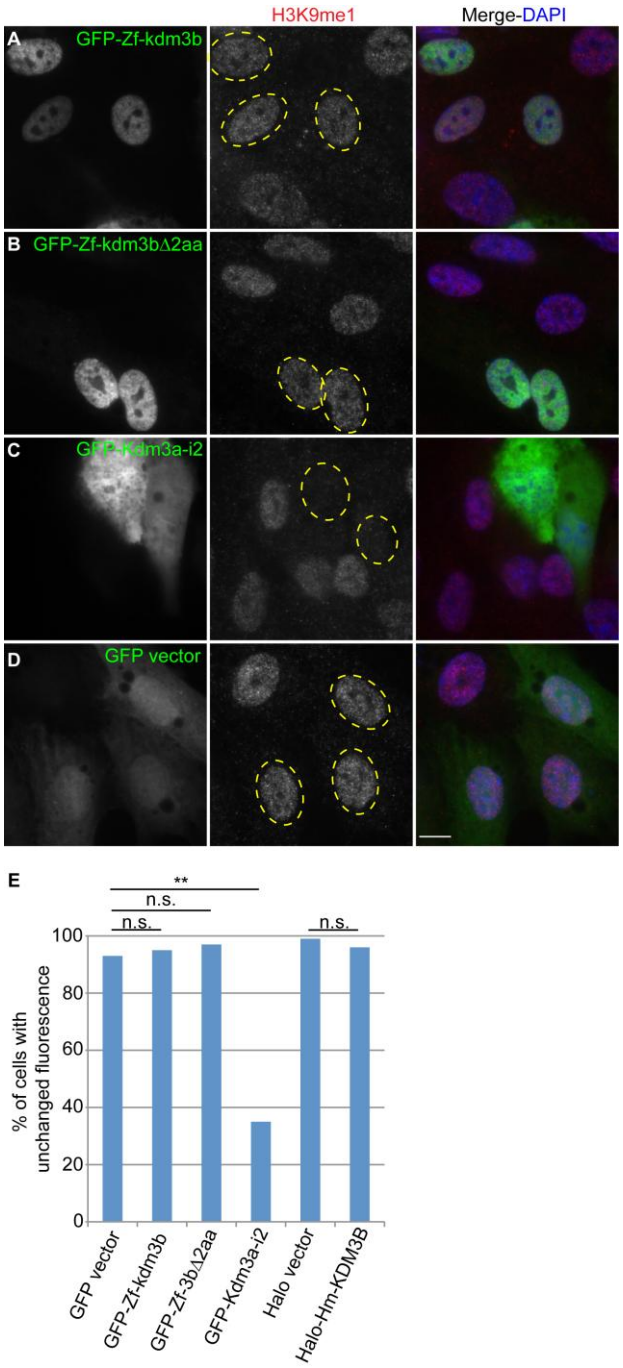

Figure 3.7: In low serum growth media, over-expressed zebrafish and mouse Kdm3b do not affect the fluorescence signal of the H3K9me1 mark.

(**A-B)** The GFP-Zf-kdm3b and GFP-Zf-3bΔ2aa transfections did not reduce the H3K9me1 fluorescent intensity. (**C**) The GFP-Kdm3a-i2 construct, used as a positive

control for the assay, caused global demethylation of the H3K9me1 mark, whereas (**D**) the GFP tag protein had no effect. (**E**) Bar chart showing the percentage of cells with unchanged H3K9me1 fluorescence for all transfections. ** = significant, Fisher's exact test $p<0.05$. Yellow circles indicate nuclei of transfected cells. Scale bar: 10 μm.

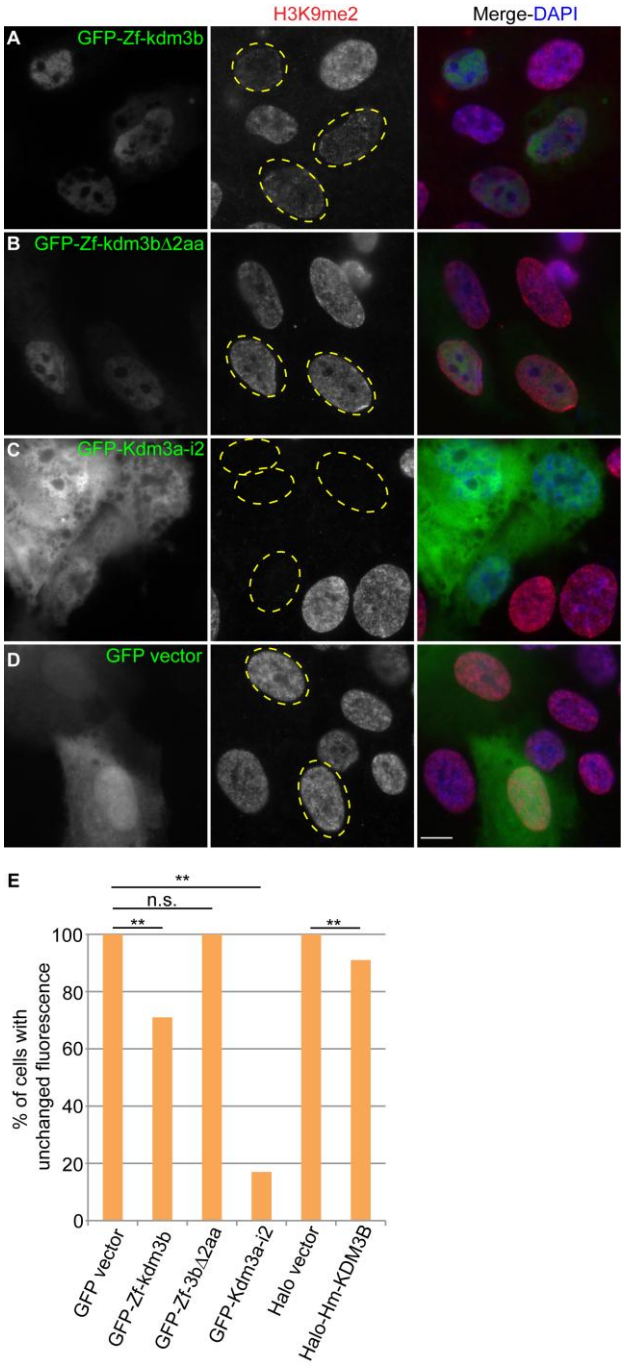

Figure 3.8: In low serum growth media, over-expressed zebrafish and mouse Kdm3b can function as H3K9me2 demethylases.

(**A**)The GFP-Zf-kdm3b construct decreased the fluorescence of the H3K9me2 mark compared to neighbouring untransfected cells, but (**B**) the GFP-Zf-3bΔ2aa did not. (**C**) The GFP-Kdm3a-i2 construct, used as a positive control for the assay, caused global demethylation of the H3K9me2 mark, whereas (**D**) the GFP-tag protein had no effect. (**E**) Bar chart showing the percentage of cells with unchanged H3K9me2 fluorescence for all transfections. ** = significant, Fisher's exact test $p<0.05$. Yellow circles indicate nuclei of transfected cells. Scale bar: 10 μm.

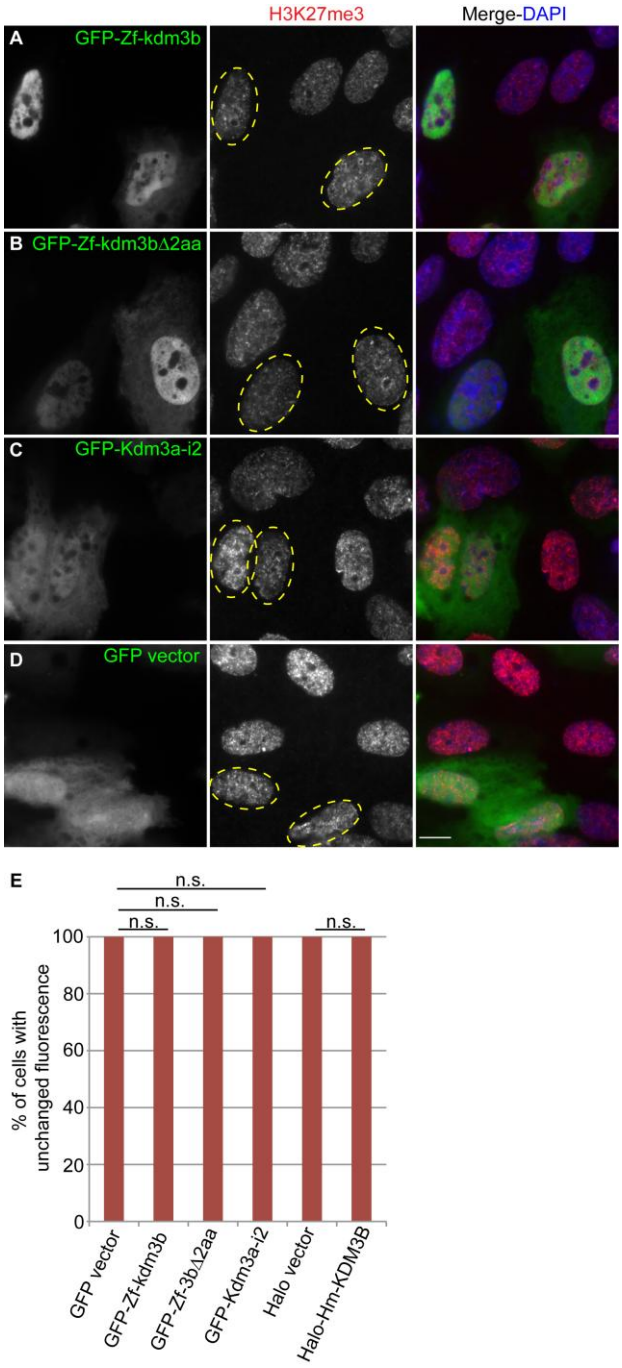

Figure 3.9: In low serum growth media, the zebrafish and mouse Kdm3b do not affect the fluorescent intensity of the H3K27me3 mark.

(**A-D)** Transfections with GFP-Zf-kdm3b, GFP-Zf-3bΔ2aa, GFP vector, Halo-Ms-Kdm3b and the Halo vector did not affect the H3K27me3 fluorescence intensity. (**E**) Bar chart showing the percentage of cells with unchanged H3K27me3 fluorescence for all transfections. Yellow circles indicate nuclei of transfected cells. Scale bar: 10 μm.

3.2.2.3 Over-expressions of GFP-Zf-kdm3b and GFP-Zf-3bΔ2aa result in reduced ciliation efficiency

Unpublished data by Dr. Patricia Yeyati (Insitute of Genetics and Molecular Medicine, University of Edinburgh) showed that morpholino knock-down of *kdm3b* in zebrafish recapitulates ciliary phenotypes such as body curvature, hydrocephalus, *situs inversus* and reduced number of otoliths (personal communication). However, it is unknown if this effect is due to the histone lysine demethylation potential of kdm3b or through a demethylase-independent function.

To investigate the putative role of kdm3b in ciliation, I over-expressed GFP-Zf-kdm3b, GFP-Zf-3bΔ2aa, and the controls GFP-Kdm3a-i2 and GFP vector inTERT-RPE1 cells. The cells were allowed to ciliate in 0.25% FCS growth media for forty-eight hours before fixation. Ciliation was assessed by using the ciliary marker IFT88. The percentage of ciliated transfected cells was then normalised to the percentage of ciliated neighbouring untransfected cells to obtain a normalised percentage of ciliation.

Compared to a 10% ciliation reduction in GFP vector transfected cells (37/112) when normalised to ciliation in neighbouring untransfected cells (50/137), the GFP-Zf-kdm3b and GFP-Zf-3bΔ2aa transfections resulted in 59% and 58% reduction, respectively (GFP-Zf-kdm3b: transfected cells – 13/133; untransfected cells – 33/140, GFP-Zf-3bΔ2aa: transfected cells – 11/101; untransfected cells – 30/116) (**Figure 3.10**).

The results show that increased levels of zebrafish kdm3b in the cell hinder its ability to ciliate. Since both the GFP-Zf-kdm3b and GFP-Zf-3bΔ2aa were able to produce the same effect, and GFP-Zf-3bΔ2aa did not decrease histone methylation (**Figure 3.7 and 3.8**), it can be suggested that the effect on ciliation loss is disconnected from the histone demethylase/enzymatic function of kdm3b. The experiment was performed once, therefore, more replicas are necessary to further confirm the result.

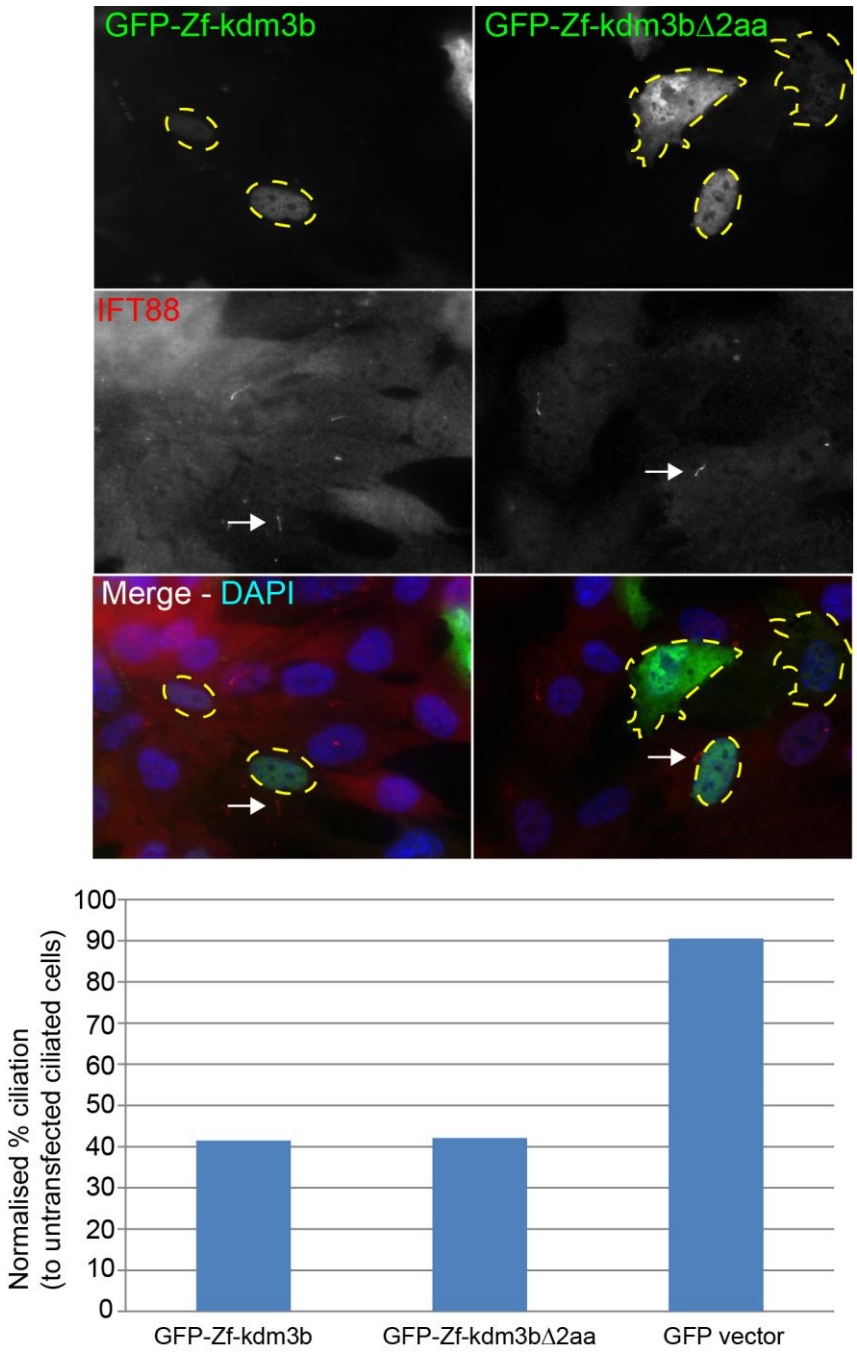

Figure 3.10: Over-expressing GFP-Zf-kdm3b and GFP-Zf-3bΔ2aa results in reduced ciliation efficiency.

Representative images of ciliated and non-ciliated GFP-Zf-kdm3b and GFP-Zf-3bΔ2aa transfected cells. One out of two GFP-Zf-kdm3b and one out of three GFP-Zf-3bΔ2aa transfected cells (circled with yellow dashed lines) are ciliated (arrows). Cilia were marked with the intraflagellar transport protein 88 (IFT88). Transfected cells are circled with yellow dashed lines and cilia of transfected cells are indicated by the white arrows. The GFP vector transfected cells showed only 10% ciliation

reduction, whereas the GFP-Zf-kdm3b and GFP-Zf-3bΔ2aa transfections resulted in 59% and 58% reduction, respectively.

3.2.3 Investigating *Kdm3b* spatial expression in zebrafish and mouse by whole mount *in situ* hybridisation

Spatial gene expression is often conserved between species during development, since the proteins has to fulfil the same (evolutionary conserved) functions. One such example is *Sox2*. Within the developing retina, *Sox2* is expressed in retinal neural progenitors and as development proceeds, it is downregulated. Its expression is maintained in some amacrine cells both in mice and zebrafish. However, some differences between species exist. That is, although Müller glial cells maintain *Sox2* expression in mice, these cells are *sox2* negative in zebrafish (Pujic et al., 2006; Taranova et al., 2006).

To check the spatial expression of Kdm3b in zebrafish and mice during development, I performed whole mount *in situ* hybridisation in a number of embryonic stages for both species. For zebrafish, I used 1-4 days post fertilisation (dpf) and for mice, the embryonic stages 9.5-11.5 (E9.5-E11.5).

kdm3b was widely expressed in zebrafish at 1 dpf, with elevated expression levels in the hindbrain (**Figure 3.12A**-hb). At 2 dpf, expression was restricted to the brain region with higher expression in the otic vesicles (**Figure 3.12B and B'**-ov). At 3 dpf expression in the brain and otic vesicles was still present. In addition, *kdm3b* expression appeared in the gut (or intestinal bulb) (**Figure 3.12C**-gut). At 4 dpf, *kdm3b* was maintained in the brain and gut and possibly appeared in the swim bladder and pronephric duct (**Figure 3.12D-**gut, sb, pd).

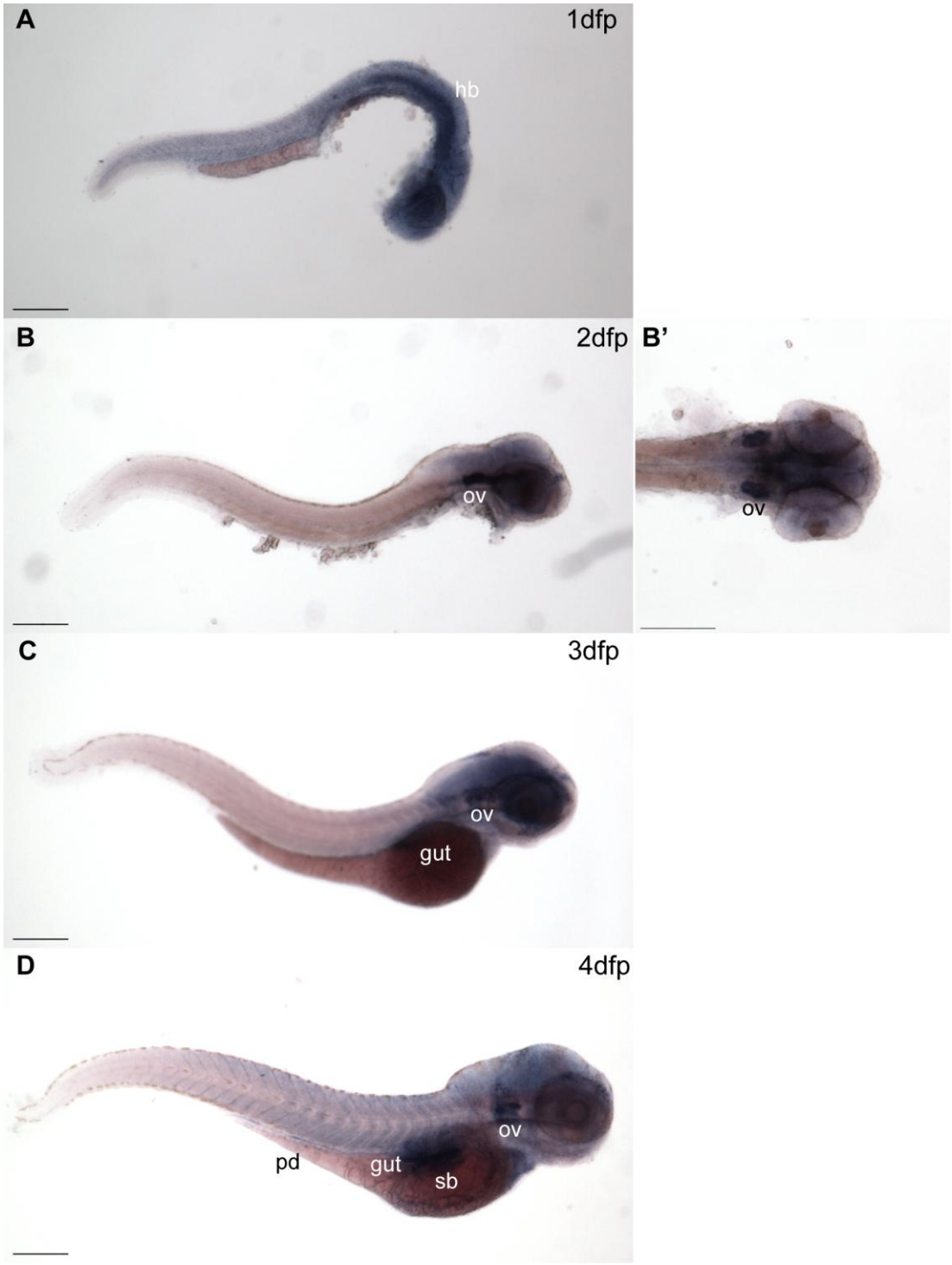

Figure 3.11: Whole mount *in situ* hybridisation on zebrafish embryos.
(**A**) At 1dpf, *kdm3b* was widely expressed with higher levels in the hindbrain (hb). (**B, B'**) The expression became restricted in the brain at 2 dpf, with increased expression in the otic vesicles (ov). (**C**) At 3 dpf, expression was still present in the brain and otic vesicles. In addition, it also appeared in the gut. (**D**) *kdm3b* expression

in the brain, otic vesicles and gut was maintained at 4 dpf . It was possibly expressed in the swim bladder (sb) and the pronephric duct (pd). Scale bars: 250 μm.

In mouse embryos, *Kdm3b* was widely expressed at all stages (**Figure 3.13A-C**). The sense probe (for the *Kdm3b* probe) was used as a negative control and resulted in no staining (**Figure 3.13D-F**). *Sox2* probe was used as a positive control for the technique. It displayed the expected *Sox2* expression in the brain, eyes and neural tube (**Figure 3.13G-I**) (Ellis et al., 2004).

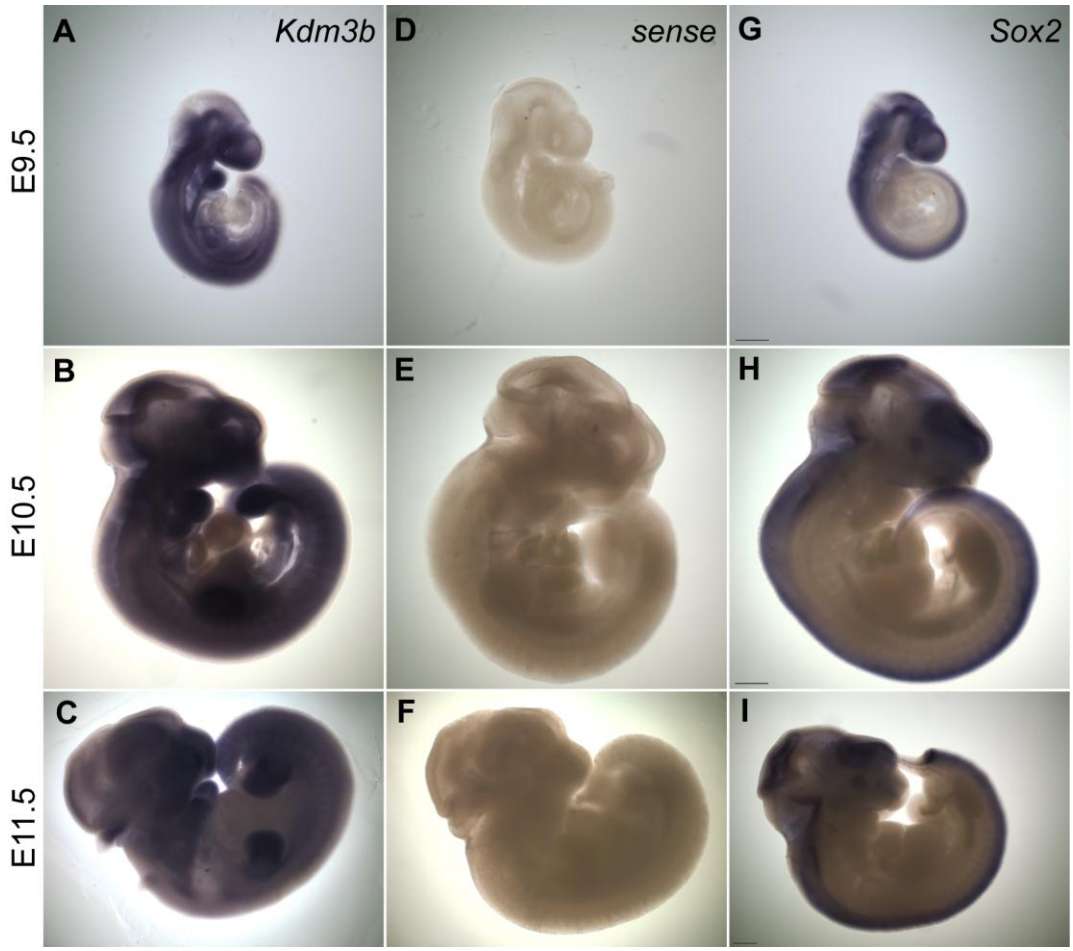

Figure 3.12: *Kdm3b* expression in mouse embryos.
(**A-C**) *Kdm3b* was widely expressed at all stages. (**D-F**) The sense probe (of the *Kdm3B* probe) was used as a negative control and resulted in no staining. (**G-I**) The *Sox2* probe was used as a positive control. Scale bars: 500 μm.

Alongside, I checked the expression of Kdm3b in tissues of adult mice by Western blot, loading 100 μg of protein for all tissues except the white adipose tissue (WAT) where I loaded 50 μg.

The Kdm3b band between 150 and 250 kDa (as determined by the MEFs Western blot in **Figure 3.13**) was present in lysates from many tissues such as the pituitaty gland, spleen, testis, eye, heart, lungs, WAT and thymus. Long exposure times of membranes also brought up Kdm3b in the pancreas, brown adipose tissue (BAT) and the brain (**Figure 3.13A,B**). Kdm3b was not detected in the kidney and liver under the experimental conditions used.

Another prominent band at about 55 kDa was present in a number of tissues such as the spleen, testis, eye and the thymus. This band may represent a Kdm3b alternatively spliced isoform that includes both N- and C-terminal Kdm3b sequences present in the full-length isoform. This was supported by the thymus Western blot, where the N- and C-terminal KDM3B antibodies revealed the same band on two different nitrocellulose membranes (**Figure 3.13B**).

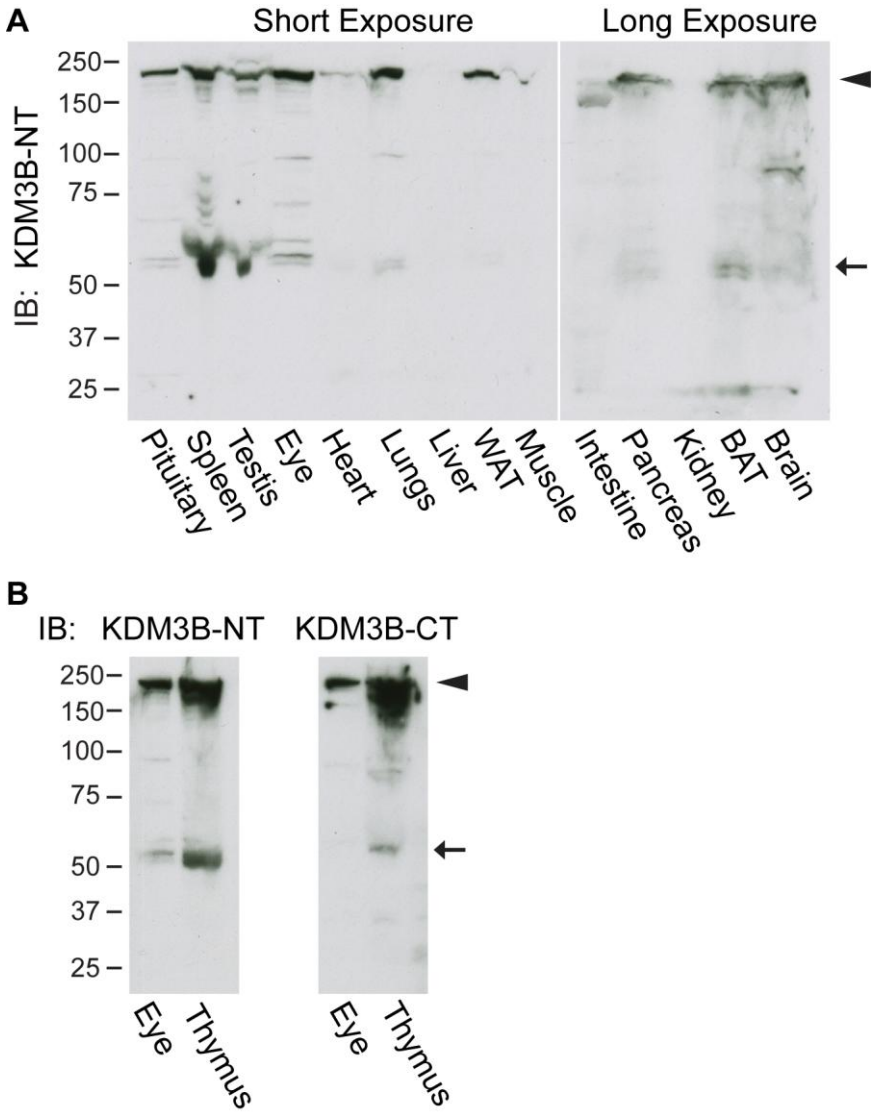

Figure 3.13: Kdm3b was expressed in many adult tissues.

Western blot of tissue lysates from wild type adult mice. (**A**) Using the KDM3B-NT antibody, Kdm3b protein (arrowhead) was expressed in the pituitary gland, spleen, testis, eye, heart, lungs and WAT. Long exposures of membranes also showed Kdm3b expression in the pancreas, BAT and the brain. (**B**) Both the KDM3B-NT and KDM3B-CT antibodies picked up Kdm3b in the thymus. The 55 kDa band (arrow) recognised by both antibodies may represent an alternative Kdm3b isoform. Numbers beside the Western blot are molecular weight markers in kDa.

Under the experimental conditions used, zebrafish showed a more restricted, while mice showed a widespread *Kdm3b* expression.

3.2.4 Summary of chapter 3

Based on the genomic synteny data by Philippe Gautier *kdm3a* was lost from the zebrafish genome, whereas *kdm3b* was present. Through blast searches and protein alignments, I showed that the zebrafish orthologue is closest to the mouse Kdm3b than Kdm3a. I subcloned and tagged the zebrafish *kdm3b* with GFP and found that it shows mainly nuclear localisation, whereas a deletion mutant was predominantly both nuclear and cytoplasmic. In addition, demethylation assays showed that the zebrafish kdm3b could function as a di-methyl lysine 9 histone 3 (H3K9me2) demethylase, whereas a deletion mutant could not. Based on previous unpublished data that kdm3b zebrafish morphants recapitulate ciliopathy phenotypes, over-expression of tagged kdm3b in cultured cells resulted in ciliation reduction. Finally, *Kdm3b* whole mount *in situ* hybridisations showed that zebrafish had a restricted spatial expression whereas mouse embryos a widespread expression. Murine Kdm3b is widely expressed, both in embryogenesis and adulthood. (Dr. Patricia Yeyati, Insitute of Genetics and Molecular Medicine, University of Edinburgh)

Chapter 4. Phenotyping *Kdm3b* gene-trapped mice

The aim of this study was to dissect the phenotype of *Kdm3b* gene-trapped mice. The decision for the phenotypic dissection was based on previous unpublished data (Dr. Patricia Yeyati, Insitute of Genetics and Molecular Medicine, University of Edinburgh) that the zebrafish *kdm3b* morphants show the classical ciliopathy phenotypes, such as body curvature, hydrocephalus, *situs inversus* and reduced number of otoliths. A potential involvement of Kdm3b in ciliary function is novel, as no other demethylase gene trap or knock-out mouse model was previously shown to affect the ciliary structure or function.

4.1 Results

4.1.1 Gene trap and validation of Kdm3b depletion

4.1.1.1 The *Kdm3b* gene-trap and genotyping strategy

To investigate the biological role(s) of Kdm3b in development and adult life, a mouse model was generated, from ES cells that contained the gene trap in intron 1 of the *Kdm3b* locus (ES cell clone: EUCE305b07, EUCOMM). It consisted of a strong splice acceptor site, a β-gal/neomycin (β-geo) sequence that allowed the selection of positive embryonic stem (ES) cells by G418 treatment and the visualisation of the targeted gene expression *in vivo* (**Figure 4.1A**).

Genotyping was accomplished by three independent PCR reactions. One amplified the wild type allele (A-B), the other the gene-trapped allele (A-C) and the last PCR amplified part of the β-gal sequence within the gene trap. Wild type mice whose *Kdm3b* alleles do not contain the gene trap only amplify the A-B primer pair band. Heterozygous gene-trapped mice have a wild type allele and a gene-trapped allele. For this reason, all three primer pairs produced a band. As expected, homozygous gene trapped mice, whose both alleles contained the gene trap failed to amplify the A-B (wild type) primer pair, but did amplify the other two (A-C and β-gal) (**Figure 4.1B**).

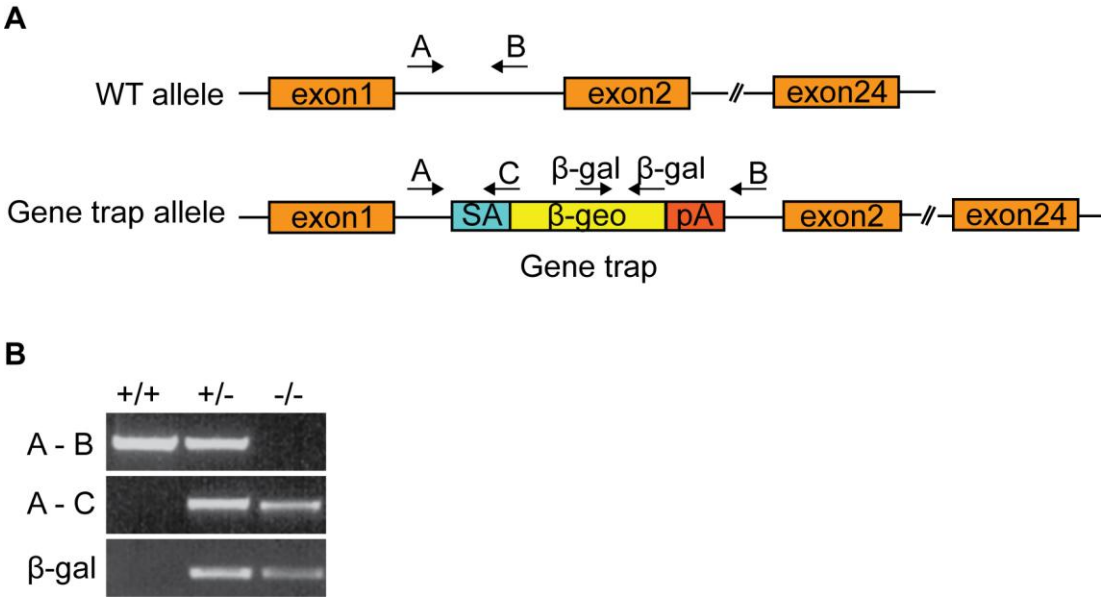

Figure 4.1: The *Kdm3b* gene trap and genotyping strategy.
(**A**) The gene-trap was inserted in intron 1 of the *Kdm3b* locus and consisted of a strong splice acceptor site (SA), a β-gal/neomycin (β-geo) sequence and a poly A (pA) sequence. Positions of genotyping primers are indicated. (**B**) The wild type allele was amplified by a PCR reaction with the A-B primer pair, present in wild type and heterozygous gene-trapped mice. The gene trap allele, present in heterozygous and homozygous gene-trapped mice was amplified by the A-C primer pair. The A-C primer pair results were confirmed with the β-gal PCR reaction.

4.1.1.2 E18.5 homozygous embryos closely follow Mendelian ratios but mice more than two week old do not

Chimeric male *Kdm3b* gene-trapped mice were crossed with C57BL/6J females to generate heterozygous gene-trapped offspring. Heterozygous males were backcrossed for one generation with C57BL/6J females. I started setting up crosses from generation one heterozygous male and females, to obtain homozygous gene-trapped mice.

To check if homozygotes follow Mendelian ratios prenatally, I genotyped six litters of E18.5 embryos. The chi-square test, comparing observed to expected numbers, resulted in p=0.038, which suggests a statistically significant difference between the three genotypes (**Table 4-1**). The significant difference result is possibly due to the small number of litters analysed. Homozygotes, however, closely followed the Mendelian ratios.

Table 4-1: Homozygous E18.5 embryos closely follow Mendelian ratios.
N represents the total number of mice from 6 litters.

N= 42, p=0.038	**Wild type**	**Heterozygote**	**Homozygote**
Observed	5	29	8
Expected	10.5	21	10.5

In addition, I counted the numbers of postnatal mice of all three genotypes, earclipped from postnatal week two onwards. The number of homozygous gene-trapped mice was reduced compared to the expected value. I carried out a chi-square test of observed versus expected numbers (for all three genotypes) for a total of 19 litters. The chi-square test showed that there is a significant difference (p= 0.007) and therefore the genotypes did not follow Mendelian ratios. (**Table 4-2**).

Table 4-2: More than two week old earclipped mouse litters of heterozygous pairs do not follow Mendelian ratios.
N represents the total number of mice from 19 litters.

N= 116, p=0.0007	**Wild type**	**Heterozygote**	**Homozygote**
Observed	25	74	17
Expected	29	58	29

The analysis of Mendelian ratios of pre-natal embryo and post-natal mouse litters indicates that the reduction in the numbers of homozygous mice can be narrowed to the first two weeks of post-natal age. Further analysis of genotypes during the first two post-natal weeks is important to investigate the possibility of peri-natal lethality; for example, genotyping of litters at post-natal day 2 (p2).

Moreover, I checked whether backcrosses to C57BL/6J females generated wild type to heterozygous mice at a ratio of 1:1, for a total of 42 litters. The p-value was 0.9, suggesting that there is no statistically significant difference between the observed and expected frequencies (**Table 4-3**).

Table 4-3: Backcrosses generated the expected 1:1 ratio of wild type to heterozygous mice

N represents the total number of mice from 42 litters.

N= 268, p= 0.9	**Wild type**	**Heterozygote**
Observed	134	132
Expected	133	133

4.1.1.3 Kdm3b is significantly reduced in homozygous gene-trapped mice

In order to investigate whether the gene-trap results in significant reduction of Kdm3b expression, quantitative reverse-transcriptase PCR (qRT-PCR), Western blot and immunofluorescence experiments were employed.

To check the transcript levels in all three genotypes, I performed qRT-PCR using cDNA from E9.5 embryos. Three primer pairs across the *Kdm3b* transcript (exons 1-2, exons 11-12 and exons 20-21) were used. The first primer pair flanked the gene trap (exons 1-2) and the other two were more 3' (exons 11-12 and exons 20-21). The purpose of using three primer pairs along the transcript was to check whether transcription continued after the gene-trap sequence or the presence of possible transcripts with alternative start sites not affected by the gene-trap insertion. The qRT-PCR results were analysed pairwise, using the t-test.

There was reduced *Kdm3b* expression in heterozygous and no expression in homozygous E9.5 embryos (**Figure 4.2**). The results were not significant for the exons 1-2 primer pair possibly due to variation in the Ct values of wild type and heterozygous biological replicas (+/+ vs -/-, p= 0.50; +/+ vs +/-, p= 0.06; +/- vs -/-, p= 0.05). For exons 11-12, there was a statistically significant difference between wild types and heterozygotes (p=0.004), wild types and homozygotes (p< 0.0001) and heterozygotes and homozygotes expression levels (p= 0.0012). The same was true for the exons 20-21; there as a statistically significant difference between wild types and heterozygotes (p=0.0005), wild types and homozygotes (p< 0.0001) and heterozygotes and homozygotes expression levels (p< 0.0001).

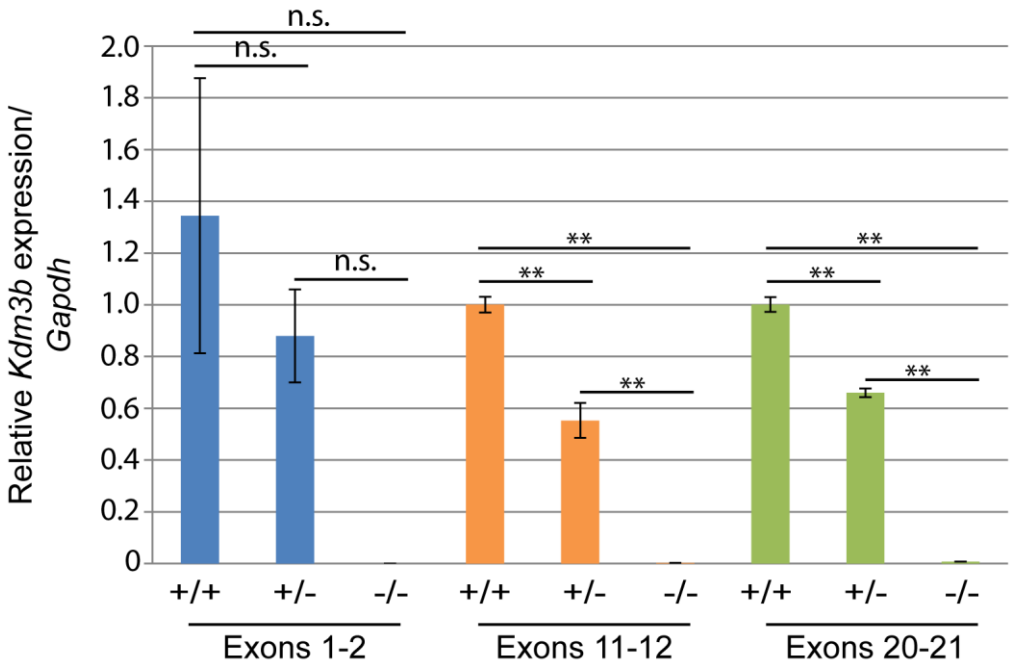

Figure 4.2: *Kdm3b* expression is reduced in heterozygous and absent in homozygous gene-trapped E9.5 embryos.
qRT-PCR across the *Kdm3b* transcript using three primer pairs. For each primer pair, the wild type *Kdm3b* expression was used as a calibrator. In all three primer pairs, heterozygous *Kdm3b* expression is reduced and the homozygous expression is barely detectable. The results were not significant for the first primer pair, but were highly significant for the other two primer pairs. ** = significant, t-test $p<0.05$. Error bars represent ± standard error. +/+ : wild type; +/- : heterozygotes; -/- : homozygotes.

Western blot on MEF lysates (**Figure 4.3**), using both an N-terminal (KDM3B-NT) and a C-terminal (KDM3B-CT) antibody, showed that compared to the wild type Kdm3b protein levels, there was less Kdm3b protein in the heterozygous MEFs (the band between 150 and 250 kDa, with a predicted size of 190 kDa). No Kdm3b protein was detected with either antibody in Kdm3b homozygous MEF lysates.

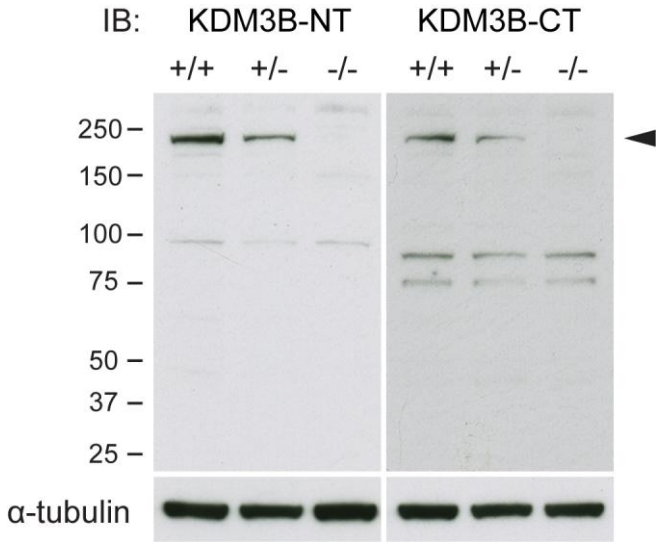

Figure 4.3: The Kdm3b protein is reduced in the heterozygous and is absent in the homozygous gene-trapped MEFs.
Western blot using antibodies against an N-terminal (KDM3B-NT) and a C-terminal (KDM3B-CT) epitope of Kdm3b. Compared to the wild type MEFs Kdm3b protein band (arrowhead), there was less Kdm3b protein in the heterozygous MEFs and no Kdm3b protein in the homozygous MEFs. The bands of lower molecular weight possibly represent unspecific bands. α-tubulin was used as a loading control. Numbers beside the Western blot are molecular weight markers in kDa.

Further, Western blot on adult tissues (eyes and spleen) validated the significant reduction of Kdm3b protein levels (**Figure 4.4**). Although no Kdm3b band was present in homozygous-derived extracts under short exposures when blotting with the KDM3B-NT antibody (arrowhead for the full length protein), a faint band was in some cases visible when the membranes were exposed for a longer time. The significant Kdm3b reduction in homozygous tissues was further confirmed with the KDM3B-CT antibody, again with a faint full length band in the eye extract of the first homozygote. In addition, the loss of the ~55 kDa band in homozygous tissues (arrows) suggested the presence of an alternative isoform that could be tissue specific.

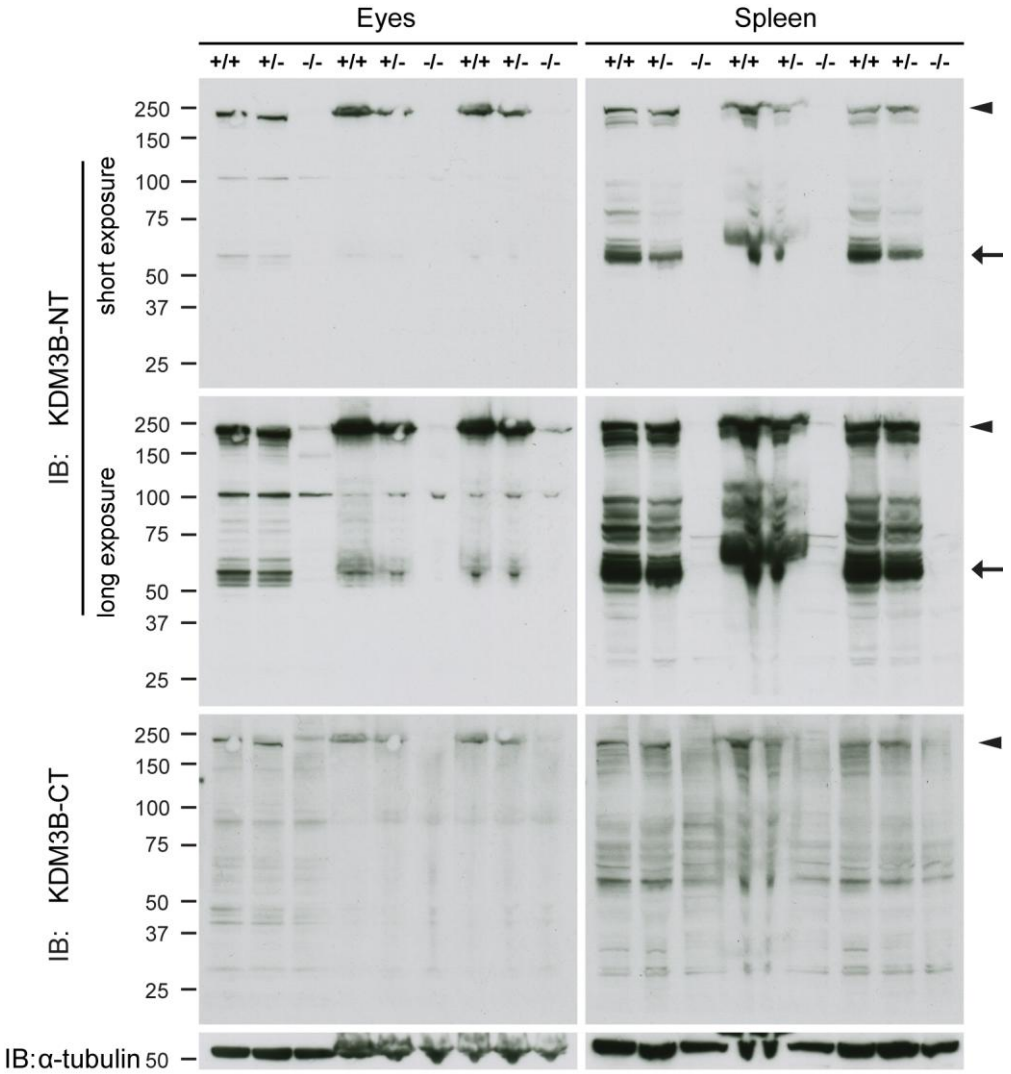

Figure 4.4: Kdm3b is significantly reduced in adult tissues of homozygous Kdm3b gene-trapped mice.

A Western blot for Kdm3b was performed using eye and spleen extracts of adult mice of all genotypes. Both the N-terminal (KDM3B-NT) and C-terminal (KDM3B-CT) antibodies were used. Kdm3b full-length protein (arrowheads) is significantly reduced in homozygous gene-trapped mice, as evidenced by the long exposure with the KDM3B-NT antibody. An additional band at about 55 kDa (arrows), was lost in homozygous-derived tissues, and therefore appeared to be Kdm3b-specific, representing a shorter isoform. Numbers beside the Western blot are molecular weight markers in kDa.

In wild type MEFs, immunofluorescence revealed strong nuclear Kdm3b localisation with both antibodies, as confirmed by DAPI staining (**Figure 4.5A,B,E,F**). The result was not surprising since it is already known that the human KDM3B functions as an H3K9me1/2 demethylase (Brauchle et al., 2013; Kim et al.,

2012). In homozygous MEFs the nuclear localisation of Kdm3b was absent (**Figure 4.5C,D,G,H**).

Further immunofluorescence on wild type or heterozygous adult tissues, eyes and testis, revealed that Kdm3b is expressed in the nucleus of pachytene spermatocytes in testis (**Figure 4.6**), and also in the ganglion cell layer (faint staining), inner nuclear layer and outer nuclear layer in the eyes (**Figure 4.7**). Under this experimental method, Kdm3b expression was absent in the tissues of homozygous gene-trapped mice.

The results from the qRT-PCR, Western blot, immunofluorescence experiments indicated that the homozygous *Kdm3b* gene-trapped mice had significantly reduced *Kdm3b* transcript and Kdm3b protein levels.

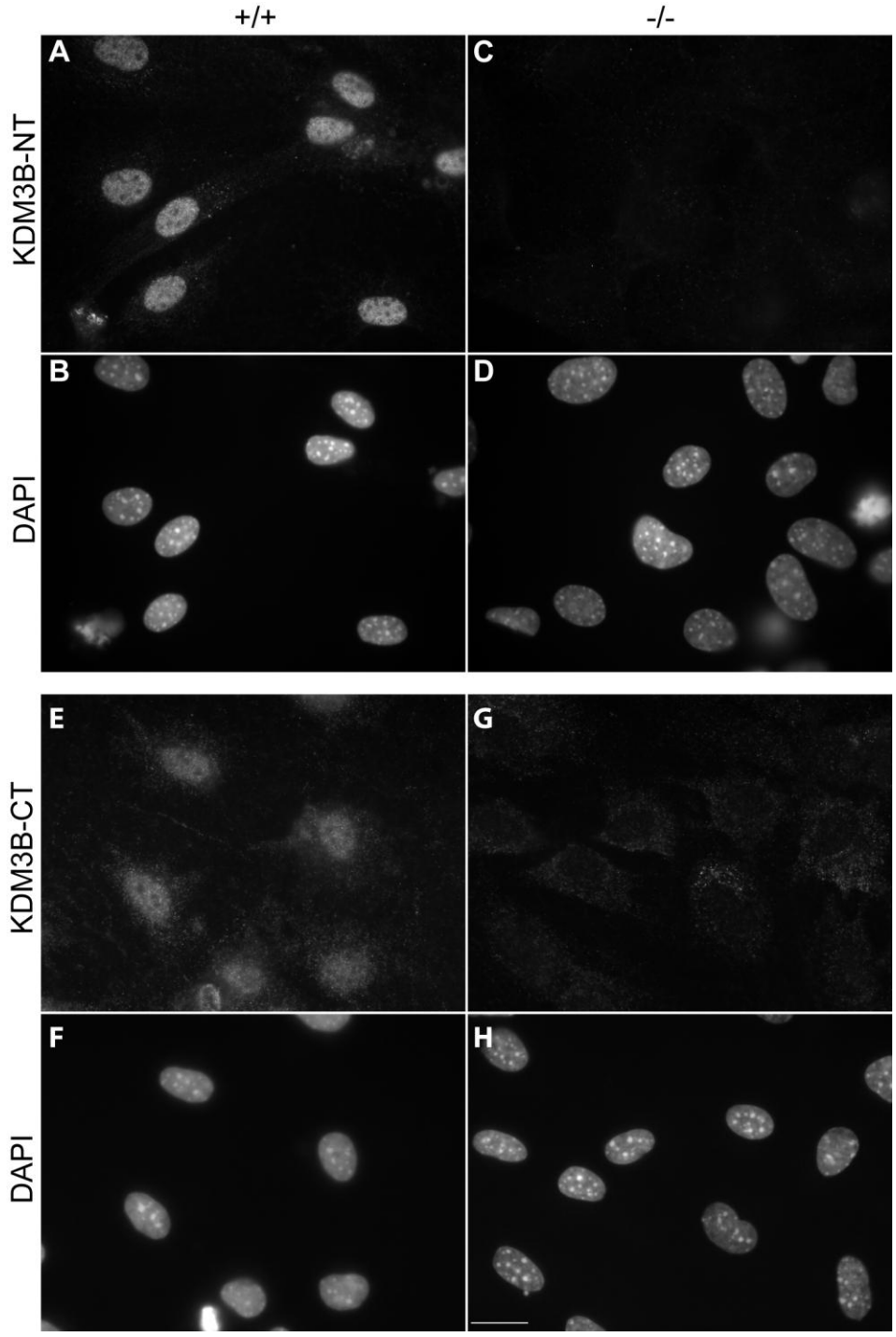

Figure 4.5: The Kdm3b protein is absent in homozygous MEFs.

Immunofluorescence of wild type (+/+) and homozygous (-/-) gene-trapped MEFs using both KDM3B-NT and KDM3B-CT antibodies. (**A-B, E-F**) Both antibodies show strong nuclear localisation in wild type MEFs. (**C-D, G-H**) The nuclear localisation is lost in homozygous MEFs. Scale bar: 20 μm.

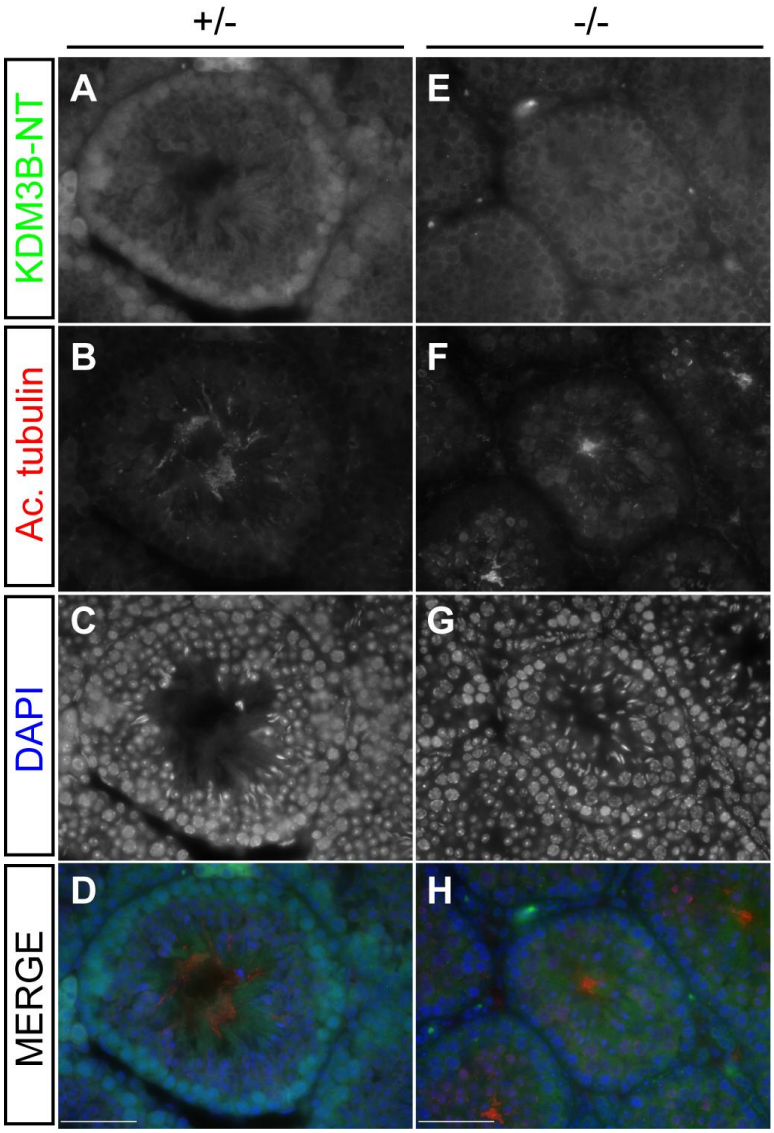

Figure 4.6: Immunofluorescence Kdm3b expression is testis.

(**A,C,D, E,G,H**) In heterozygous (+/-) adult testis, Kdm3b is expressed in pachytene spermatocytes and is absent in the testis of homozygous (-/-) gene-trap mice. (**B,F**) Acetylated alpha tubulin was used as a positive control for the assay, and marks the spermatid flagellae. Scale bars: 50 μm.

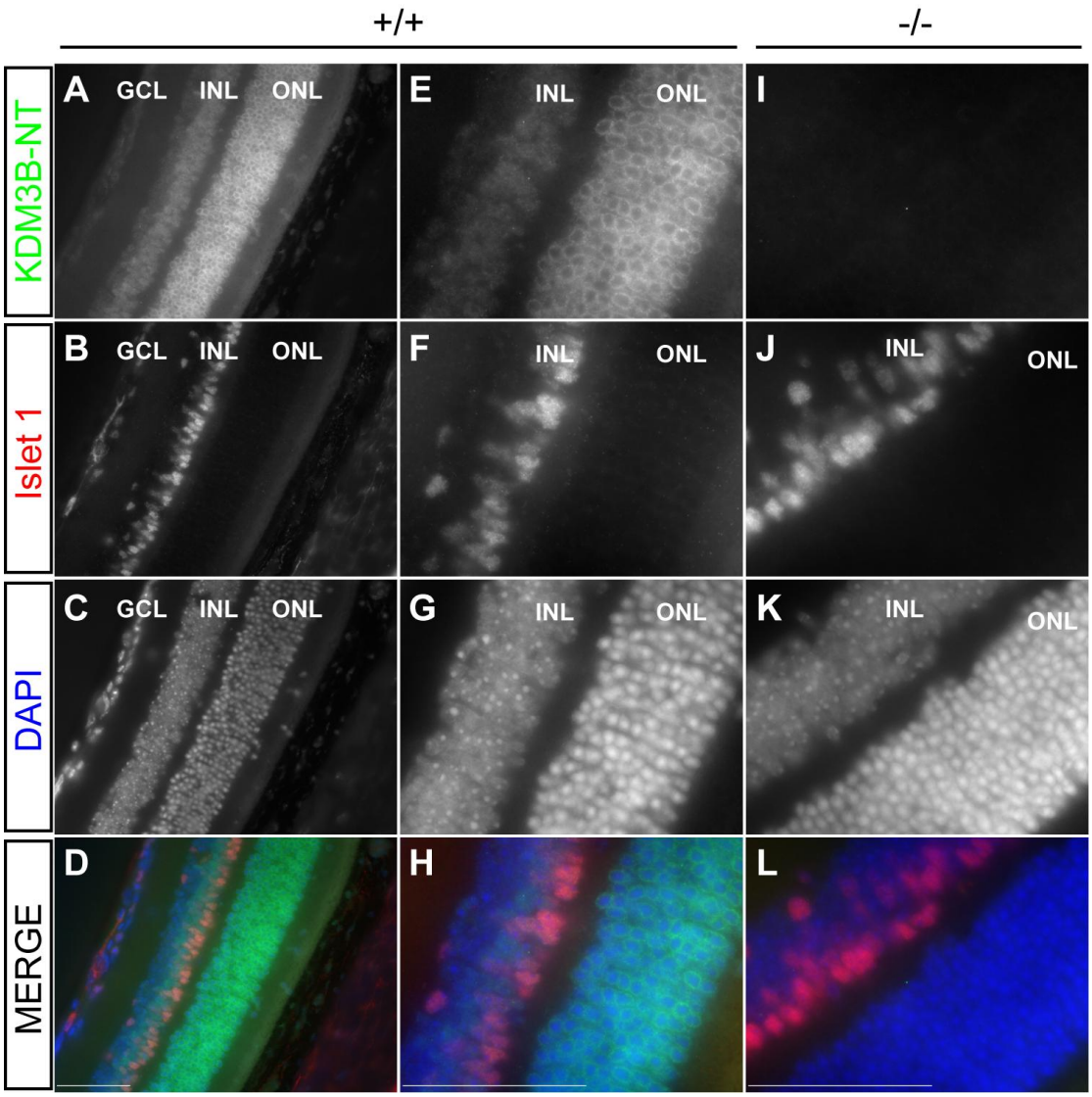

Figure 4.7: Immunofluorescence of Kdm3b expression in the eyes.

(**A,C,D**) In the eyes of wild type mice, Kdm3b is expressed in the ganglion cell layer (GCL), the inner nuclear (INL) and outer nuclear layer (ONL). (**E,G,H**) A higher magnification showed that Kdm3b is nuclear in the INL but cytoplasmic in the ONL. (**I,K,L**) Kdm3b was absent in the eyes of the homozygous mice. (**B,F,J**) Islet 1 was used as a positive control for the assay, and marks a subset of the GCL and INL cells. Scale bars: 50 μm.

4.1.2 Adult homozygous gene-trapped mice are small

The next step was to characterise the phenotype of heterozygous and homozygous gene-trapped mice. Homozygous mice presented a small body size compared to wild type and heterozygous littermates (**Figure 4.8A)**. Both sexes were affected (data not shown). Mice of all three genotypes were weighted at six weeks of

age. The homozygous mice were significantly underweight compared to wild type (Tukey, p= 0.0000009) and heterozygous (Tukey, p= 0.0000009) mice. There was no statistically significant difference in weight between wild type and heterozygous mice (Tukey, p= 0.4301627) (**Figure 4.8B**).

The small size phenotype of the homozygous gene-trapped mice was further validated by Alcian blue- Alizarin Red skeletal preparations (**Figure 4.9**). The preparations showed no gross skeletal abnormalities in homozygous mice.

Furthermore, the homozygous mice failed to thrive and died, for example some died at 2 weeks, others at 4, 6 or 10 weeks. Although no survival curve was produced for the time of death, only one homozygous gene-trapped mouse survived up to 10 weeks post-natally. No alternation in behaviour or locomotion was observed.

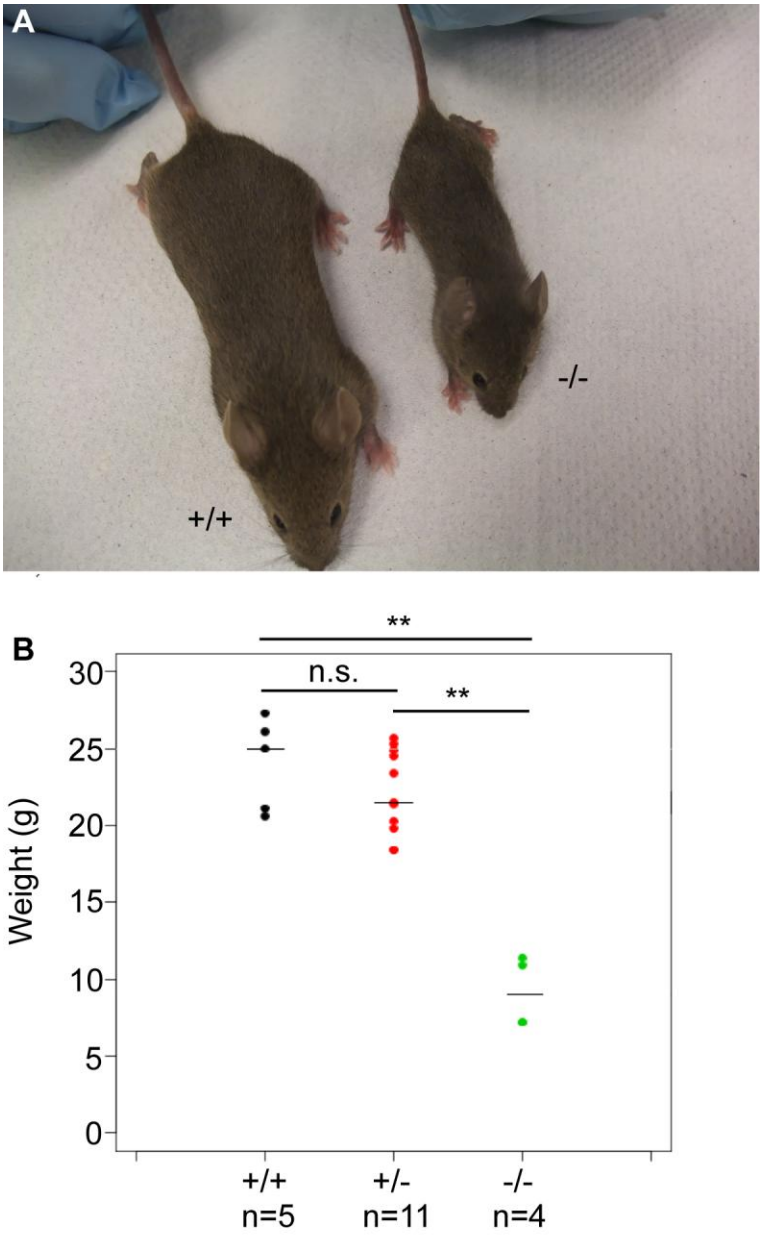

Figure 4.8: Homozygous gene-trapped mice presented a small body size and are lighter than wild type and heterozygous gene-trapped mice.

(**A**) Homozygous mice were small compared to their wild type and heterozygous littermates. (**B**) Dot plot of weight (at six weeks of age) versus genotype. The lines represent the median values. Homozygous mice were significantly underweight when compared to wild type or heterozygous mice. There was no statistically significant difference in weight between wild type and heterozygous mice. The numbers below each genotype represent the number of mice. ** = significant, Tukey, $p<0.05$.

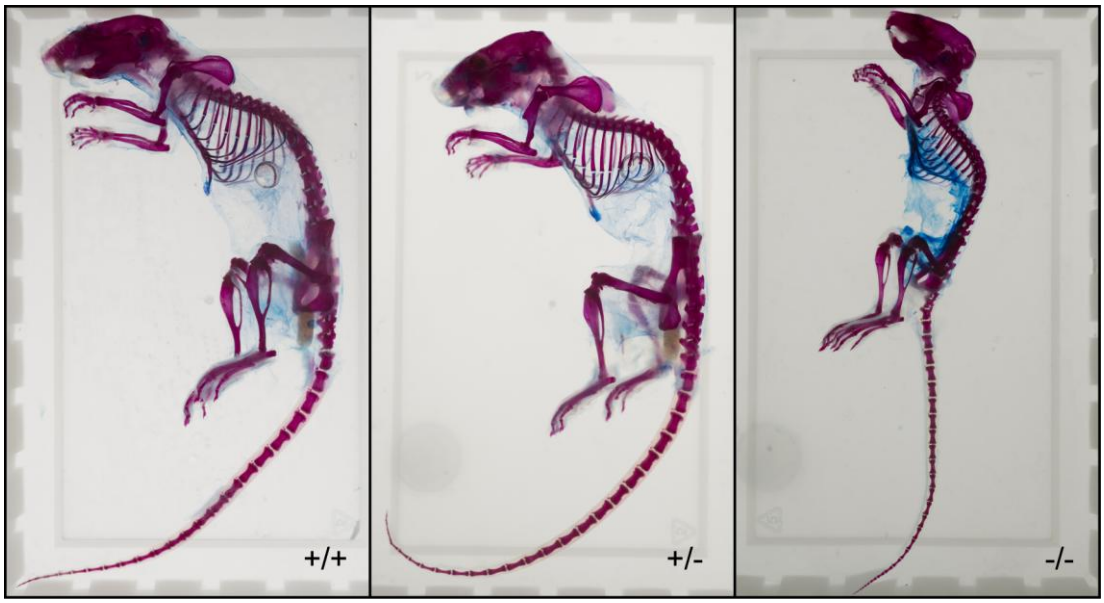

Figure 4.9: The skeleton of gene-trapped mice is not grossly deformed.
Alcian blue- alizarin red skeletal preparations were performed for 6-week old wild type, heterozygous and homozygous gene-trapped mice. The preparations revealed no gross skeletal abnormalities in gene-trapped mice.

The reduced body size phenotype of the *Kdm3b* homozygous mice was confirmed by a second gene-trap mouse line (ES cell clone: EUCE0244g12, EUCOMM) (**Figure 4.10C**). In this mouse line, the gene trap was inserted in intron 11 of the *Kdm3b* locus (**Figure 4.10A**). The gene trap has the same features as the one inserted in intron one: a strong splice acceptor site (SA), a β-geo sequence and a poly A (pA) tail. Again, genotyping followed the same logic: an A-B primer pair for the amplification of the wild type allele, an A-C primer pair for the amplification of the gene-trap allele and a β-gal primer pair to further confirm the presence of the gene trap (**Figure 4.10B**). No further work has been undertaken with this mouse line.

Collectively, the data show that the reduction in body size is due to the significant Kdm3b reduction.

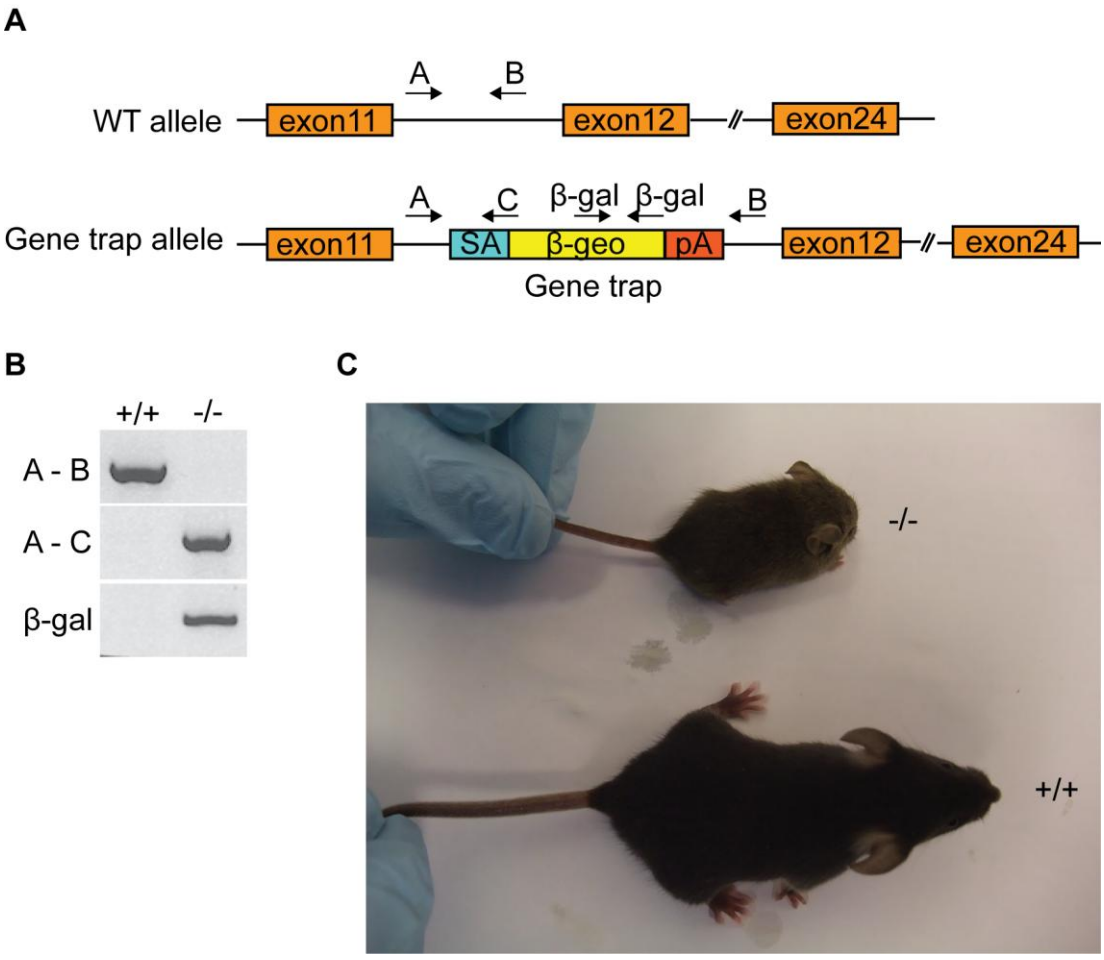

Figure 4.10: A second gene-trap line for Kdm3b confirms the small body size phenotype of the homozygous mice.

(**A**) The gene-trap was inserted in intron 11 of the *Kdm3b* locus and consisted of a strong splice acceptor site (SA), a β-gal/neomycin (β-geo) sequence and a poly A (pA) sequence. Positions of genotyping primers are indicated. (**B**) The genotyping strategy. The wild type allele was amplified by a PCR reaction with the A-B primer pair, present in wild type mice. The gene trap allele, present in homozygous gene-trapped mice was amplified by the A-C primer pair. The A-C primer pair results were confirmed with the β-gal PCR reaction. (**C**) Picture of a homozygous small mouse (top) and a wild type littermate (bottom).

4.1.2.1 Growth retardation commences post-natally

To determine whether the growth retardation of homozygous mice commences pre-natally or post-natally, I initially weighted (to two decimal places) E18.5 embryos from six litters of heterozygous pairs (**Figure 4.11A**). One-way ANOVA test showed that there was no statistically significant difference in weight between the three genotypes (p= 0.69) (**Figure 4.11B**).

Having established that homozygous embryos are not growth retarded *in utero*, I carried out weight monitoring of heterozygous pair litters at post-natal day 14 (p14) and p21, to determined the timing of growth retardation.

The data showed that growth retardation was already evidenced at p14 and was maintained at p21. The difference in weight between wild type or heterozygous to homozygous mice was statistically significant at p14 (One-way ANOVA, $p= 0.02$ and $p= 0.01$). The same was true for p21 (One-way ANOVA, $p< 0.001$ and $p< 0.001$) (**Figure 4.12**). Also, between p14 and p21, homozygous mice gained minimal, if any, weight and this was reflected from the p-value result of 0.97.

Pre-natal and post-natal weight measurements indicate that growth retardation commences post-natally. Further weight monitoring at younger post-natal ages is required to determine when growth retardation begins.

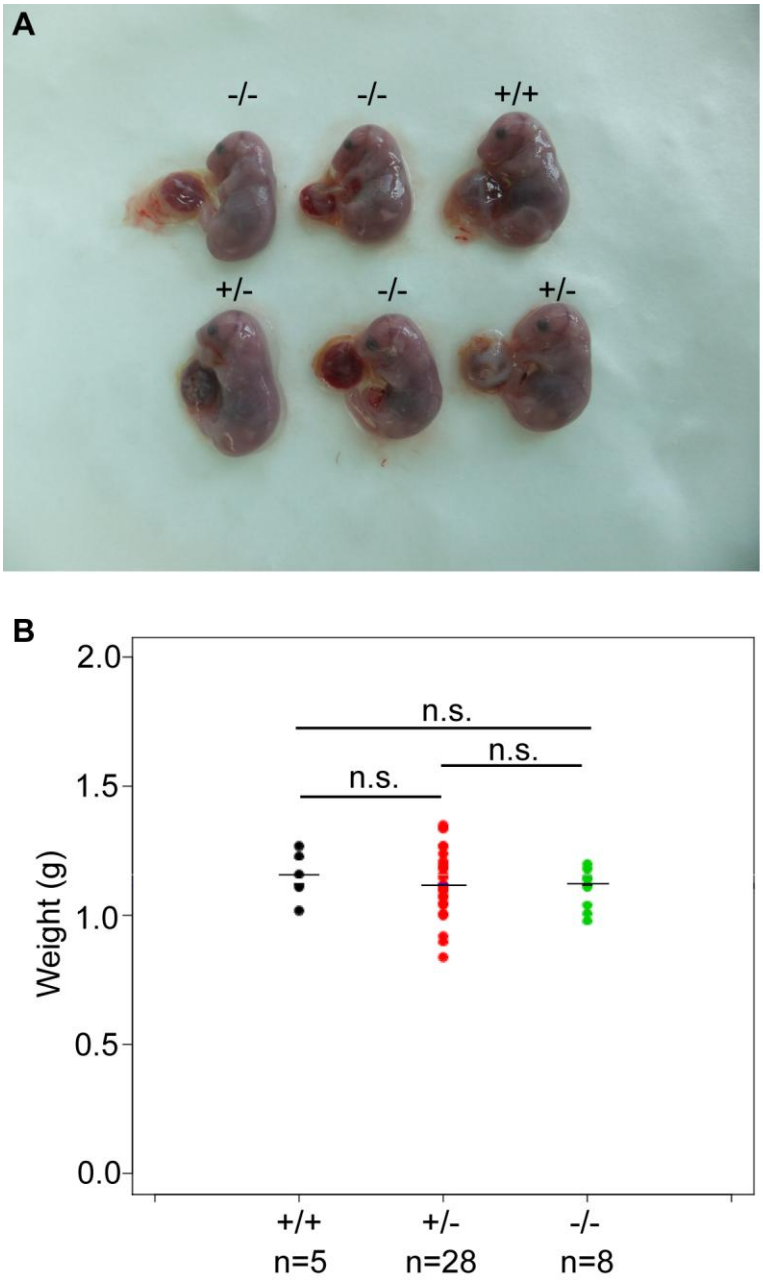

Figure 4.11: Growth retardation of homozygous mice does not commence pre-natally.

(**A**) Picture of E18.5 embryos of all genotypes. (**B**) Dot plot of E18.5 embryo weights (from six litters) versus genotype. There was no statistically significant difference in weight between genotypes. The lines represent median values. Numbers below genotypes represent number of embryos. One-way ANOVA test, p= 0.69.

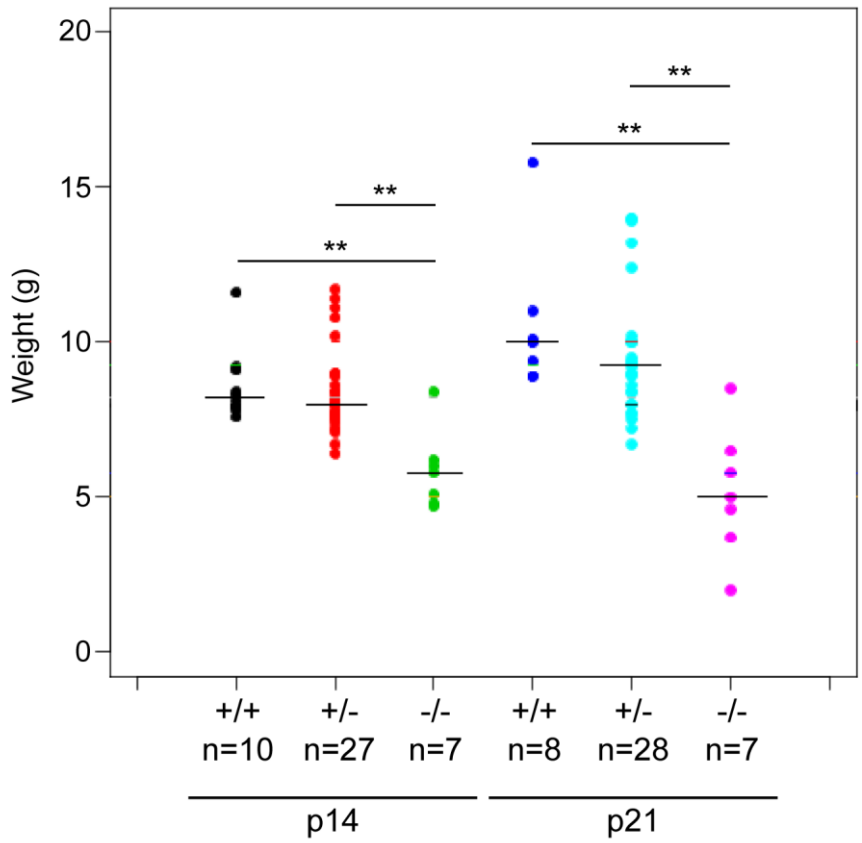

Figure 4.12: Growth retardation is already evidenced from p14.
Mice of all genotypes were weighted on p14 and p21. Both at p14 and p21, wild type or heterozygous mice were significantly heavier than homozygous mice. The lines represent median values. Numbers below genotypes represent number of embryos. One-way ANOVA, **= p< 0.05

4.1.3 Investigating perturbations of the growth hormone and thyroid hormone pathways

4.1.3.1 Kdm3b does not function as a global H3K9me1/2 demethylase

Previous knock-out mouse models have shown that post-natal growth is determined by the expression of hormones (Alba and Salvatori, 2004; Efstratiadis, 1998; Eicher and Beamer, 1976; Fraichard et al., 1997; Zhou et al., 1997). The reduced size, weight and post-natal growth retardation of *Kdm3b* homozygous mice

prompted me to investigate possible perturbations in the expression of the growth and thyroid hormone pathway genes.

Firstly, I checked in more detail Kdm3b localization in MEFs. Kdm3b showed a widespread nuclear localisation. It was depleted from the nucleoli regions (dark regions in DAPI staining indicated by the yellow circles) and the pericentric heterochromatin regions, which are transcriptionally silent (bright DAPI staining, few indicated by the red asterisks) (**Figure 4.13**).

The immunofluorescence results suggested that Kdm3b localised in euchromatic regions of the MEFs nuclei.

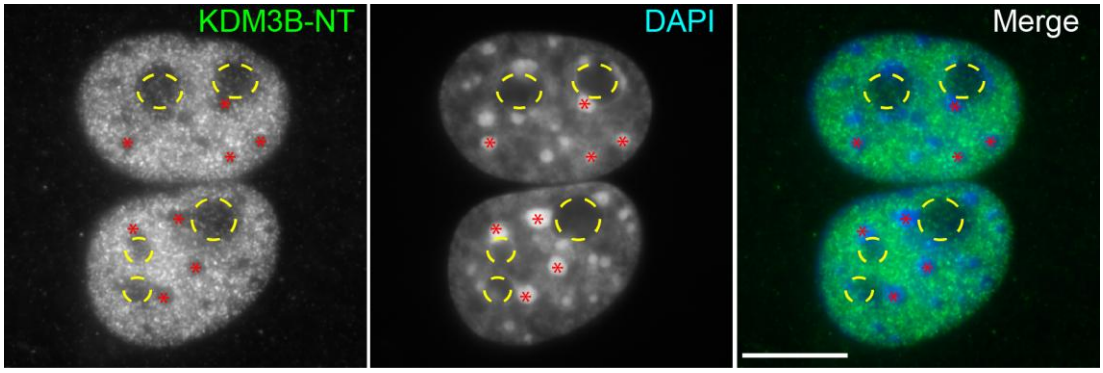

Figure 4.13: Kdm3b shows a widespread nuclear localisation and is excluded from nucleoli and heterochromatic regions.
Immunofluorescence on wild type MEFs with the KDM3B-NT antibody. Nuclear Kdm3b localisation was assessed by comparison to DAPI staining. The Kdm3b protein showed a widespread nuclear localisation. It was excluded from the nucleoli (yellow circles) and heterochromatic regions (red asterisks). Scale bars: 10 μm.

The 93% sequence identity between the human and mouse KDM3B orthologues,and a further 98% and 100% identity within the JmjC and Zinc finger domains, respectively, suggests that the mouse Kdm3b can function as a H3K9me1/2 demethylase, although no demethylation assays were carried out. To test whether Kdm3b loss can result in global alternations of H3K9me1/2 levels, I carried out a Western blot of MEF histone protein extracts from all genotypes. I used the antibodies for the H3K9me1/2 epigenetic marks and also H3K9me3 as control (**Figure 4.14A**). The results of the Western blot were quantified and then normalised

to pan-histone 3, used as a loading control, for all genotypes and epigenetic marks, to derive to the adjusted relative density. Three biological replicates were used for wild type, two for heterozygous and two for homozygous gene trapped MEFs. An ANOVA test for each epigenetic mark showed that there was no statistically significant difference in the adjusted relative density between genotypes (H3K9me1: p= 0.38; H3K9me2: p= 0.72; H3K9me3: p= 0.99) (**Figure 4.14B**).

The results showed that Kdm3b loss does not have detectable effects on the global H3K9me1/2 methylation. However, its sequence similarity with the human orthologue suggests a potential demethylation function.

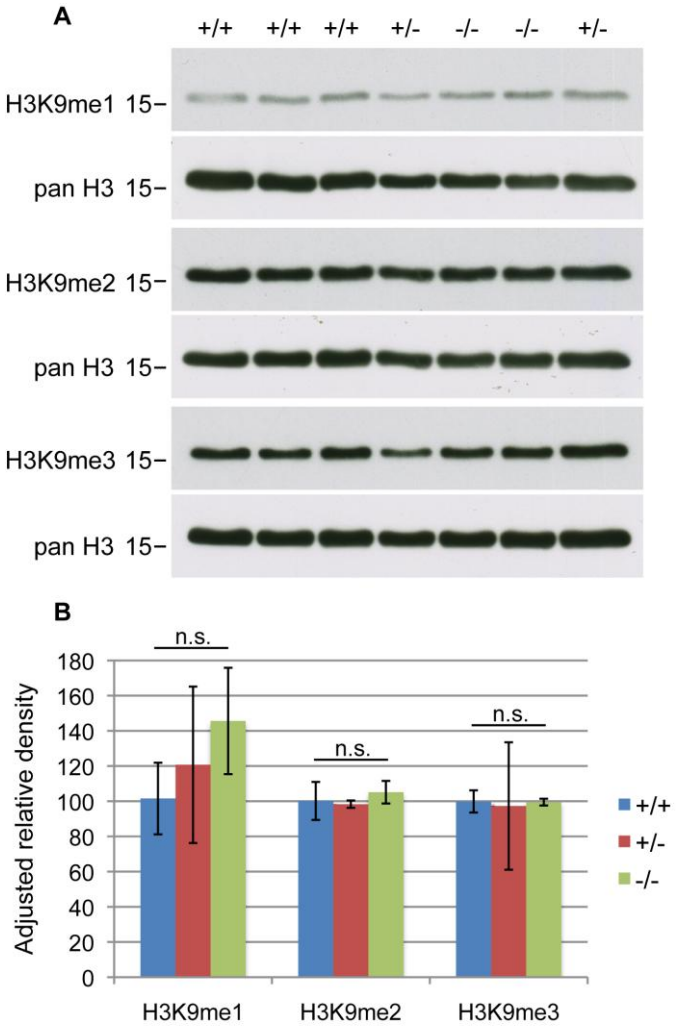

Figure 4.14: Kdm3b does not have a detectable effect on the global H3K9me1/2 methylation.

Histone proteins from MEFs of all genotypes were isolated by acid extraction. (**A**) Western blot analysis of H3K9me1/2/3 epigenetic marks resulted in no differences between genotypes. Pan-histone 3 antibody was used as a loading control. Numbers beside the Western blot are molecular weight markers in kDa. (**B**) The western blot results were quantified and compared for all genotypes. There was no statistically significant difference in adjusted relative intensity between genotypes for any epigenetic mark. One-way ANOVA test. Error bars represent ± standard deviation.

4.1.3.2 Investigating perturbation in the growth and thyroid hormone pathways

I checked the expression levels of genes involved in the growth hormone pathway. qRT-PCR results from wild type and heterozygous mice were pooled together (Co= control), as heterozygous mice do not show a growth retardation phenotype. I analysed gene expression from three wild type, three heterozygous and four homozygous mice. The expression levels were compared with the t-test.

Ghrhr (p= 0.08) and *Gh* (p= 0.20) expression, in the pituitary glan was not statistically significant between controls and homozygotes. In the liver, the expression of the *Ghr* (p= 0.33), *Igf1* (p= 0.22), *Igf1r* (p= 0.06) and *Igfbp3* (p= 0.80) were again not statistically significant.. However, the expression of *Igfals* was statistically significant between controls and homozygotes (p= 0.0098) (**Figure 4.15**).

Moreover, the levels of *Tshb*, involved in the thyroid hormone pathway, were significantly increased in homozygous pituitary glands (p= 0.028), but the levels of the thyroid hormone pathway target gene *Apoa4* (Weitzel et al., 2003) were not significantly altered. (p= 0.11) (**Figure 4.16**).

Altogether, the qRT-PCR results suggest not significant perturbations of the growth hormone pathway, whereas the thyroid hormone pathway seems to be affected.

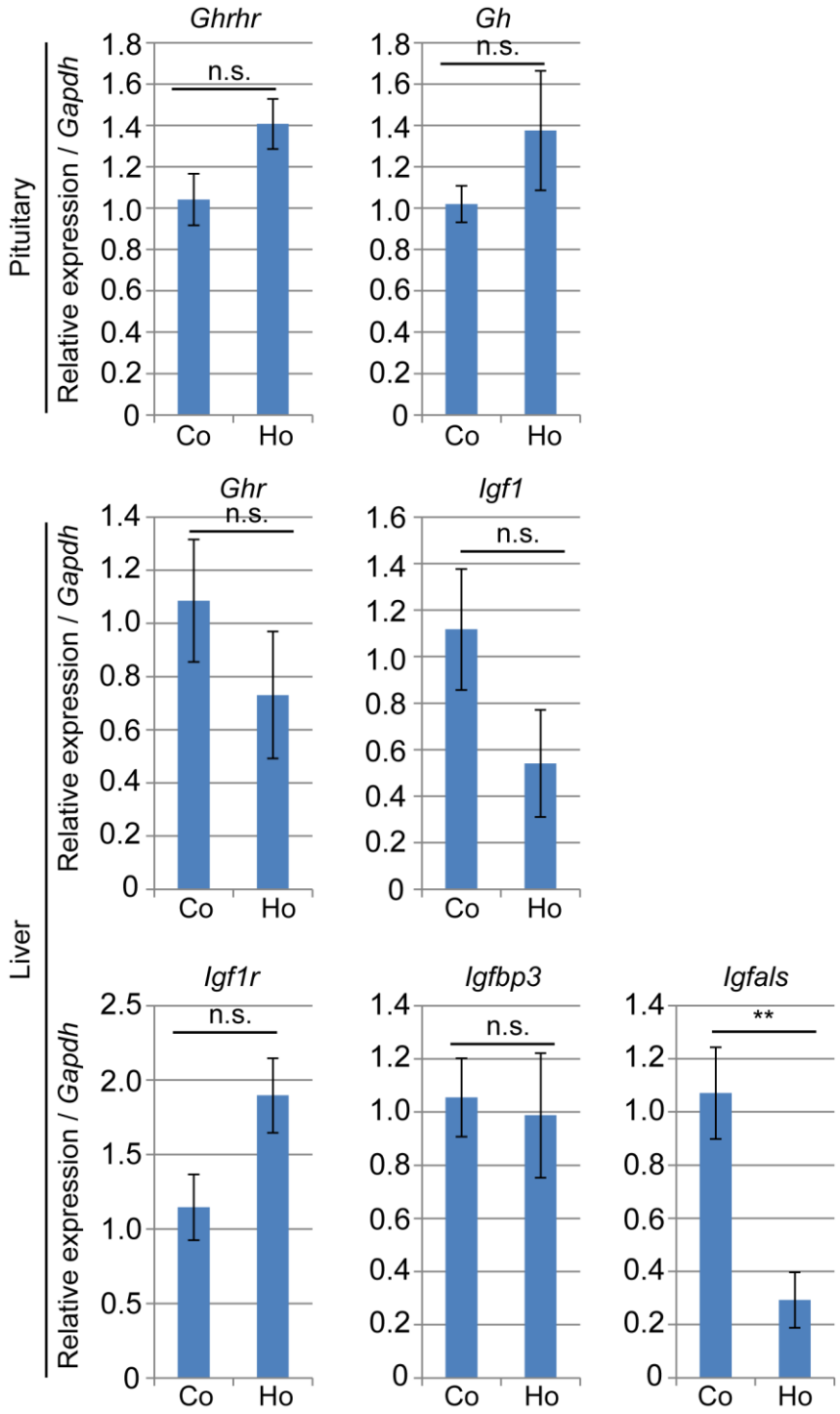

Figure 4.15: Gene expression analysis for the growth hormone pathway. qRT-PCR of pituitary gland and liver. In the pituitary gland, there was no statistical change in the levels of the *Ghrhr* and *Gh* between controls and homozygotes. In the liver, expression of the *Ghr*, *Igf1*, *Igf1r* and *Igfbp3* were again not statistically significant, while *Igfals* levels were significantly reduced in homozygues liver. t-test, ** $p < 0.05$. Error bars represent ± standard error. Co= wild type and heterozygous; Ho= homozygous.

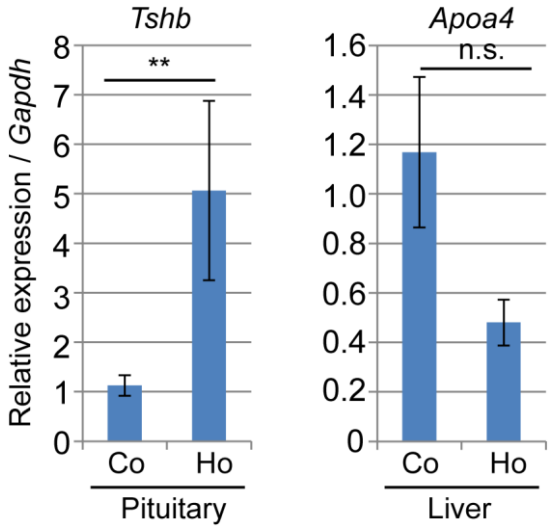

Figure 4.16: Gene expression analysis for the thyroid hormone pathway
qRT-PCR of pituitary gland and liver RNA extracts. *Tshb* expression levels were significantly increased in homozygous mice pituitary glands and *Apoa4* levels were not significantly altered in controls and homozygous liver extracts. t-test, ** $p < 0.05$ Error bars represent ± standard error. Co= wild type and heterozygous; Ho= homozygous.

4.1.4 The gross morphology of several organs of *Kdm3b* gene-trapped homozygous mice was unaffected

To check whether any organs of the Kdm3b homozygous gene-trapped mice were affected by the absence of Kdm3b protein, I paraffin embedded and sectioned several organs.

Hematoxylin and eosin staining (H&E) of eyes, kidney, pancreas and testis grossly suggested no changes in the overall tissue organisation of homozygous mice. In the eye sections, retinal layers such as the ganglion cell layer (GCL), the inner nuclear layer (INL) and the outer nuclear layer (ONL) were present (**Figure 4.17A**). The kidneys contained the characteristic round renal corpuscles located in the renal cortex (**Figure 4.17B-** arrowheads), while the pancreas contained the white coloured islets of Langerhans (**Figure 4.17C-** circles) and the ducts that carry digestive enzymes to the stomach (**Figure 4.17C-** arrows). Moreover, spermatogenesis is not affected in homozygous mice as they produce mature spermatozoa (**Figure 4.17D**), as revealed by the presence of stage 6-7 spermatids and mature spermatozoa (stage 15-16) exposed to the lumen of seminiferous tubules.

The small size of homozygous mice could imply reduced feeding and subsequent utilisation of fat stores for energy provision. To check for the presence of fat depots, p28 mice were dorsally skinned (Jacek Mendrychowski, Transgenics facility) (**Figure 4.18**). I chose weaned mice to eliminate the mother effect (as a food provider) and to check whether the homozygous mice could independently feed sufficiently to maintain their fat depots. I compared wild type, heterozygous and homozygous littermates of the same sex (all females). The comparison showed that homozygous mice maintained all the fat depots that were visible from the dorsal side, such as the brown adipose tissue (BAT), the anterior subcutaneous, the visceral retroperitoneal and the posterior subcutaneous. The weight of fat depots in proportion to total body weight was not recorded.

Therefore, apart from the small body size phenotype, examination by hematoxylin and eosin of several organs of homozygous mice revealed the gross morphology was unaffected. In addition, fat deposits were still present suggesting that the inability to feed was not the cause of death.

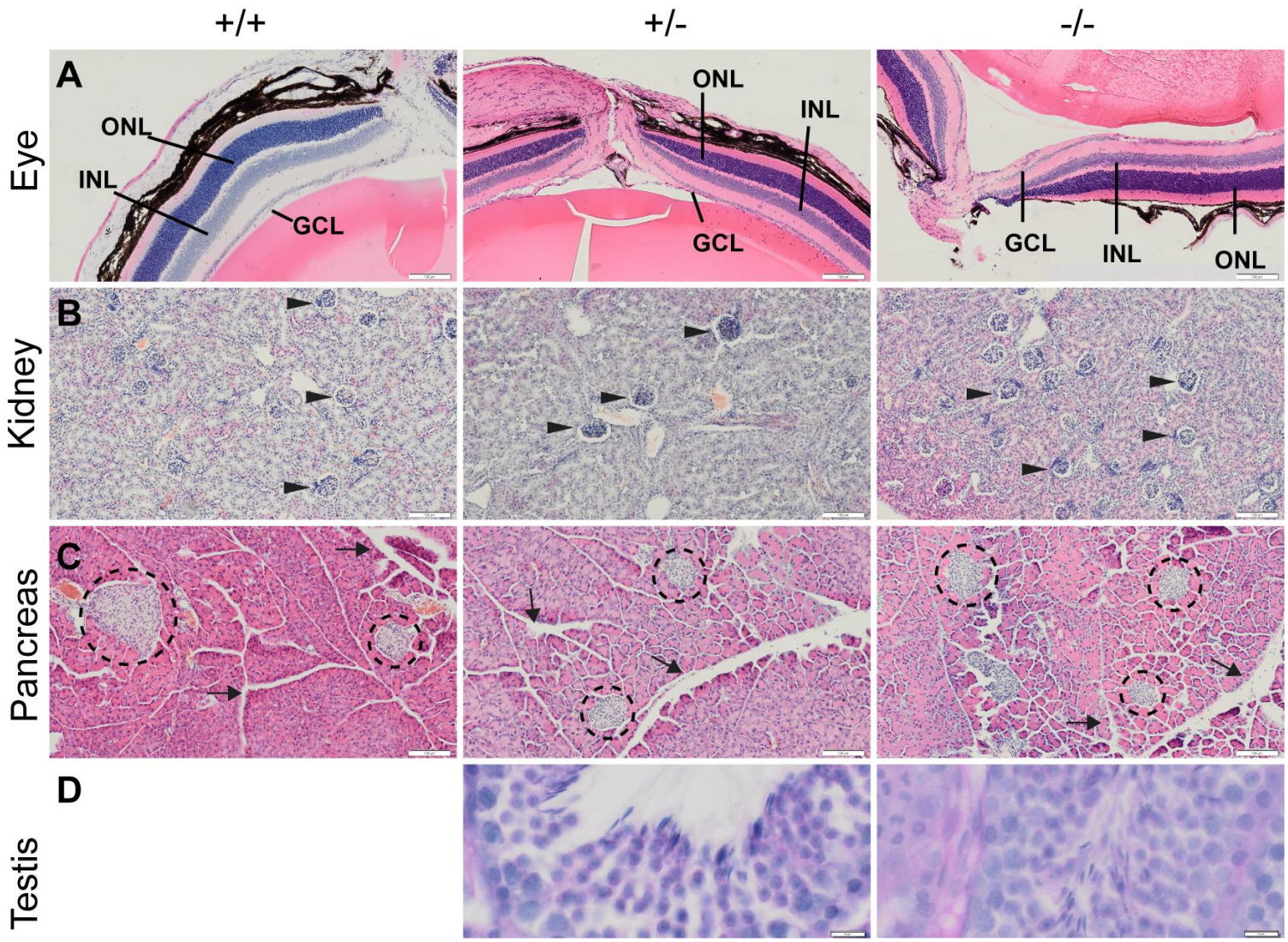
+/+
+/-
-/-
Eye
Kidney
Pancreas
Testis
A
B
C
D
ONL
INL
GCL
ONL
INL
GCL
GCL
INL
ONL

Figure 4.17: The gross morphology of several organs of homozygous adult mice was unaffected, as determined by hematoxylin and eosin staining.

(**A**) All cell layers are present in the of homozygous eye section; GCL-ganglion cell layer, INL- inner nuclear layer, ONL- outer nuclear layer. (**B**) Kidneys contained renal corpuscles (arrowheads). (**C**)The Islets of Langerhans (circles), as well as the ducts (arrows) for digestive enzyme excretion, were present in the pancreas. (**D**) Spermatogenesis was completed in the testes. Scale bar: **A-C**:100 µm; D: 10 µm.

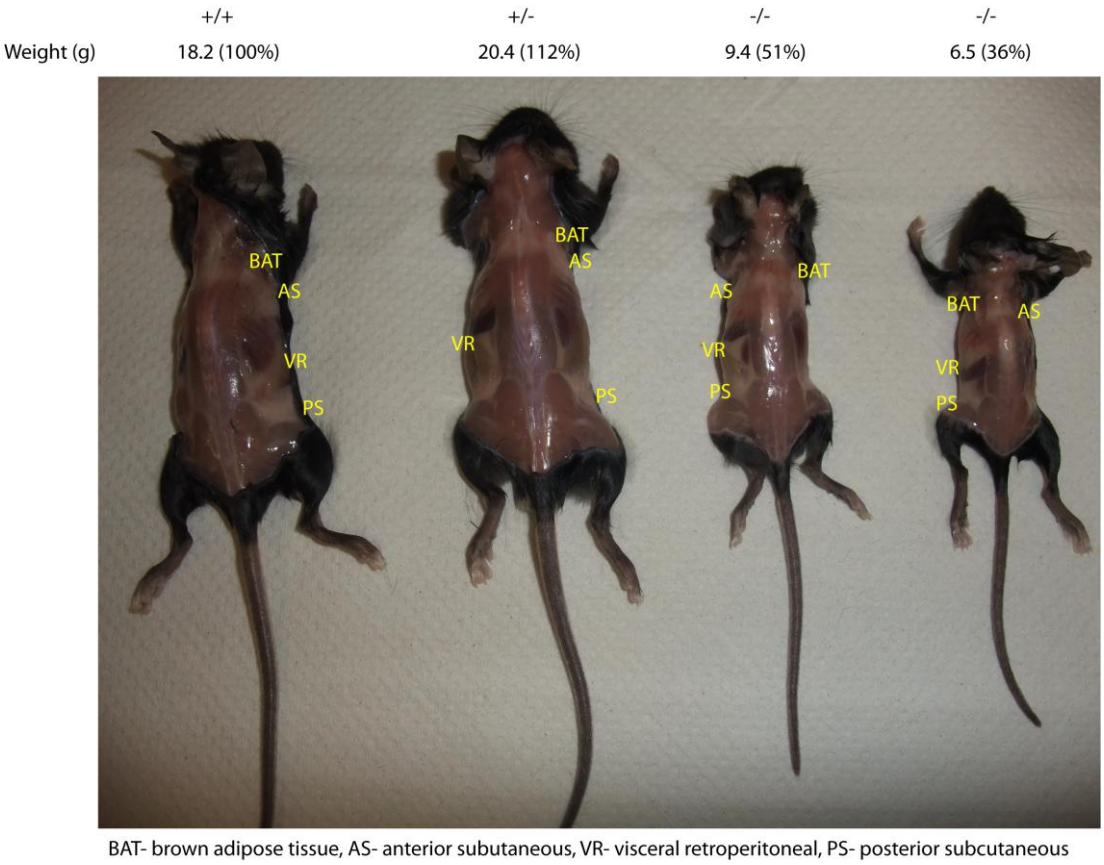

Figure 4.18: Homozygous gene-trap mice maintain their fat deposits.

Female littermates (one wild type, one heterozygote and two homozygote) at p28 were skinned dorsally and presence of fat deposits was assessed. Homozygous mice, like the wild type and heterozygous littermates, maintain their brown adipose tissue (BAT), anterior subcutaneous (AS), visceral retroperitoneal (VR) and posterior subcutaneous (PS) deposits. Genotype, weight in grams and percentage weight relative to the wild type are indicated above the picture.

4.1.5 Reduced weight and heterogeneous thymus phenotype in homozygous gene-trapped mice

To gain insights into the phenotype causation, a litter of mice, which included two homozygotes, was sent for necropsy analysis (Dr. Mary Diaz, Centre for Cardiovascular Science, University of Edinburgh). The analysis confirmed the previous H&E results of **Figure 4.17** that the majority of organs remain grossly unaffected. However, an interesting finding from the necropsy analysis was that the thymuses of both homozygotes were missing the cortical cell layer (**Figure 4.19B**), whereas thymuses of wild type mice consisted of both the cortical and medullary cell layers (**Figure 4.19A-** Co, Me). Moreover, the thymuses of both mice were reduced in weight, which was validated by normalising the thymus weight to total body weight; in other words, the weight of the thymuses in homozygous mice was not in proportion to the body weight when compared to the values obtained for the wild type and heterozygous gene-trapped mice. The ratio revealed a 3-4 times reduction in homozygous gene trapped-mice (**Table 4-4**). Unpaired t-test statistics revealed that there was no significant difference in thymus weight between the wild type and heterozygous gene trapped mice ($p= 0.51$). However, there was a significant weight difference between wild type and homozygous ($p= 0.02$), as well as between heterozygous and homozygous gene trapped mice ($p< 0.0001$).

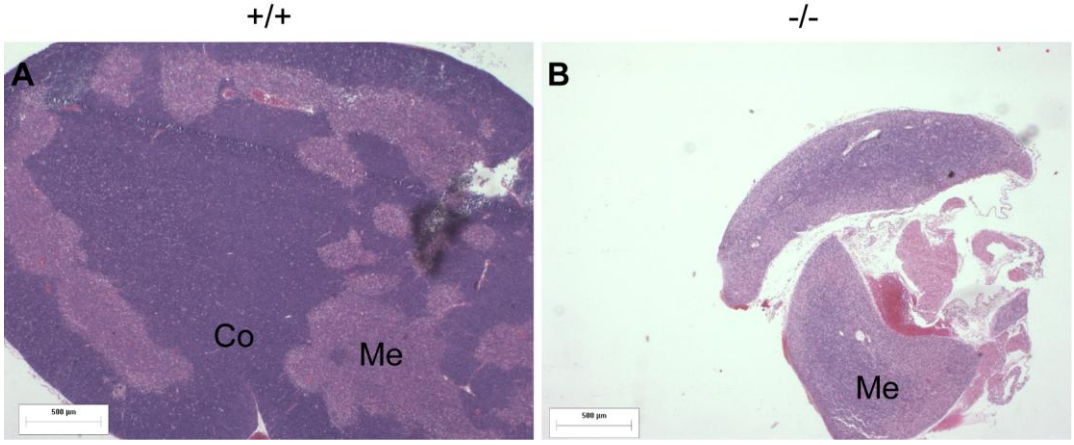

Figure 4.19: *Kdm3b* homozygous gene-trapped mice were missing the cortical cell layer.
Thymuses of homozygous and wild type littermates were sectioned and stained with H&E (Dr Mary Diaz, Centre for Cardiovascular Science, University of Edinburgh).

(**A**) The thymus of wild type mice comprised of the cortical (Co) and medullary (Me) cell layers. (**B**) The thymus of homozygous mice was reduced in size and was missing the cortical cell layer. Scale bar: 500 μm.

Table 4-4: Thymus weight and thymus weight\body ratio were reduced in homozygous gene trapped mice

Genotype	Body weight (g)	Thymus (mg)	Thymus/body weight ratio	Average ratio (± standard deviation)
+/+	11.8	80.9	6.9	6.25 (± 0.92)
+/+	13.2	74	5.6	
+/-	14.4	96	6.7	6.63 (± 0.21)
+/-	13.5	87	6.4	
+/-	16.2	110	6.8	
-/-	5.6	8.7	1.6	1.70 (± 0.14)
-/-	6.7	12	1.8	

To confirm the abnormal thymus phenotype in homozygous gene-trapped mice, more thymuses from all three Kdm3b genotypes were isolated, sectioned and H&E stained (**Figure 4.20**). The stains revealed a normal thymic cell layers for the heterozygous thymuses, like the wild type (**Figure 4.20A, B**). The thymuses of homozygous gene-trapped mice showed a heterogeneous phenotype, including normal cortical and medullary layers (**Figure 4.20C**), reduced cortical layers (**Figure 4.20D**) and loss of the two layers' identity to what seems more cortical-like in **Figure 4.18E** and more medullary like in **Figure 4.20F**.

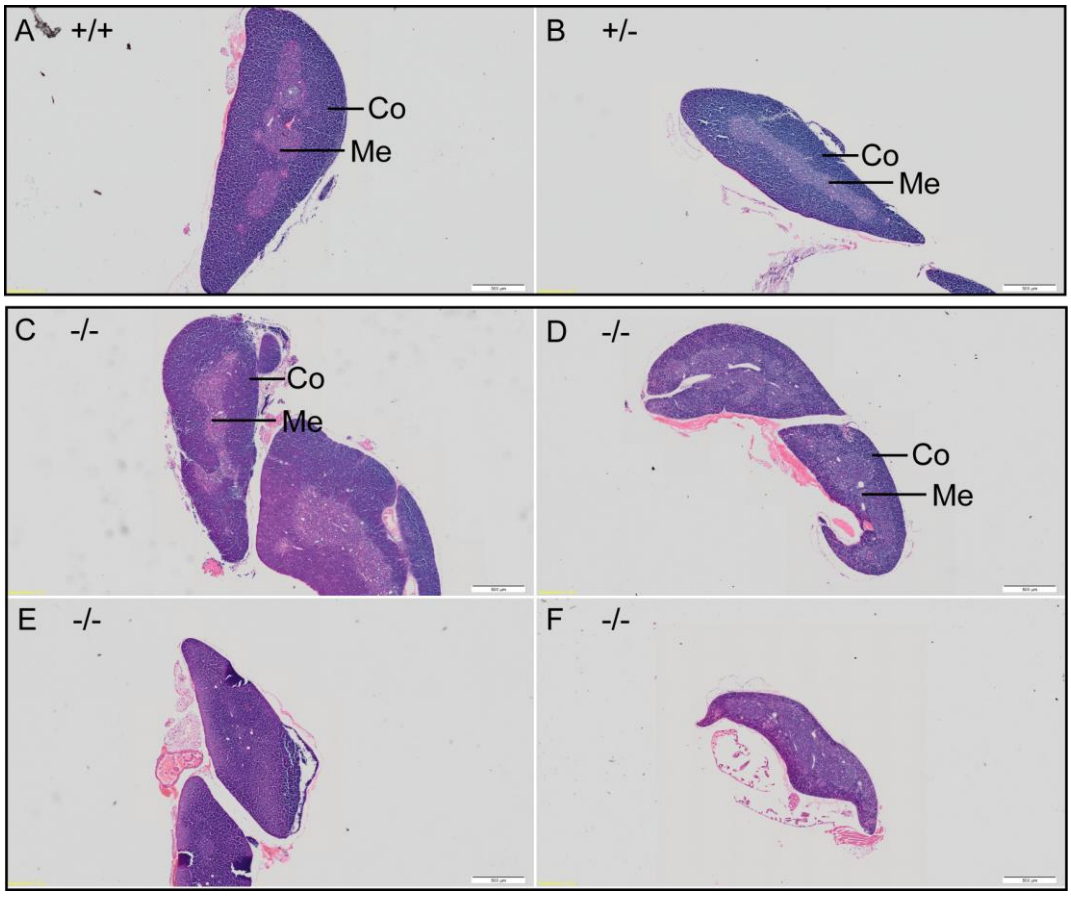

Figure 4.20: Thymuses of homozygous gene-trapped mice show a range of phenotypes.

H&E stains of thymus sections of wild type, heterozygous and homozygous gene-trapped mice. (**A, B**) wild type and heterozygous gene-trapped mice show normal thymic cell layering, with the cortical layer sourrounding the internal medullary layer. (**C - F**) The thymuses of homozygous gene-trapped mice show a range of phenotypes, such as normal cortical-medullary layers (**C**), reduced cortical layer (**D**) and loss of thymic layer identity (**E, F**). Co= cortex, Me= medulla. Scale bar: 500 μm.

Furthermore, immunohistochemistry on thymus sections revealed that Kdm3b is expressed in both the medullary and cortical layers, with more positive cells in the medulla. In line with the significant reduction of Kdm3b gene expression in homozygous gene-trapped mice, as demonstrated before, the thymuses of the latter mice were negative for Kdm3b staining, irrespective of the thymus phenotype (**Figure 4.21**).

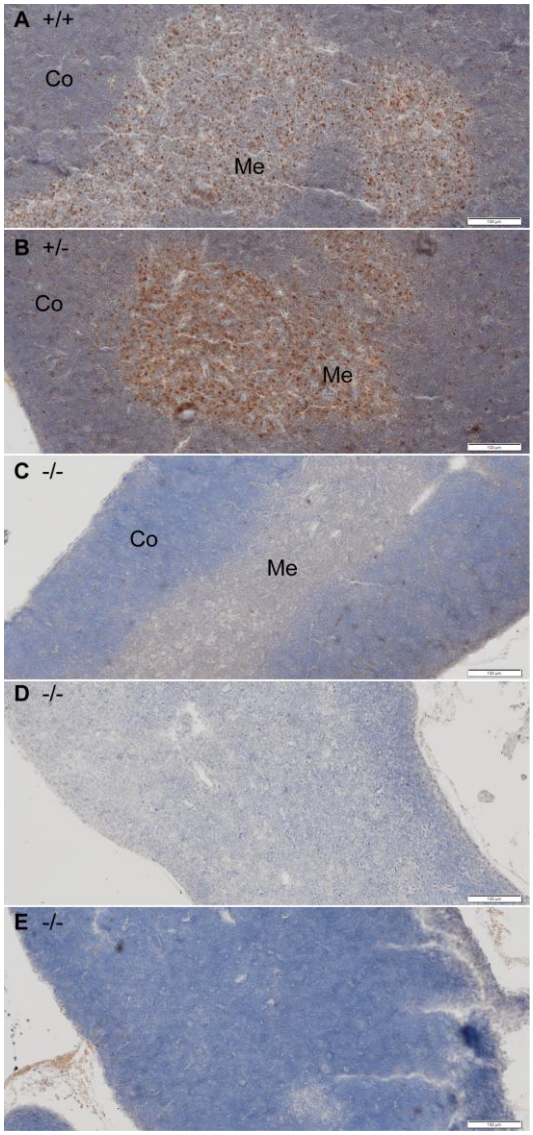

Figure 4.21: Kdm3b is densly expressed in the medulla and more sparsly expressed in the cortex.

(**A, B**) Immunohistochemistry for Kdm3b revealed that it is expressed both in the cortical and medullary layers. Its expression is more dense in the medulla. (**C- E**) Kdm3b expression is lost in the homozygous mice, irrespective of normal or abnormal thymic cell layering. Co= cortex, Me= medulla. Scale bar: 100 μm.

In summary, a proportion of *Kdm3b* homozygous gene-trapped mice show abnormal thymic cell layering. This observation suggests possible defects in T-cell development and maturity.

4.1.6 T-cell maturation is maintained in the thymuses of homozygous gene-trapped mice

The abnormal thymic architecture in a proportion of homozygous mice implied a plausible perturbation of T-cell maturation. For this season, I characterised the profile of maturing T-cells in the thymus of p23 mice, using the cell surface markers CD4, CD8, CD25 and CD44.

The thymus is a specialised organ of the immune system, responsible for the commitment and education of early lymphoid progenitors to the T-cell lineage. These processes are accomplished through an elaborate course of positive and negative selection, which ensures the elimination of T-cells that are reactive to self-presenting antigens (**Figure 4.22**) (Bhandoola et al., 2007; Ciofani and Zúñiga-Pflücker, 2007; Lind et al., 2001; Petrie and Zúñiga-Pflücker, 2007; Zlotoff and Bhandoola, 2011).

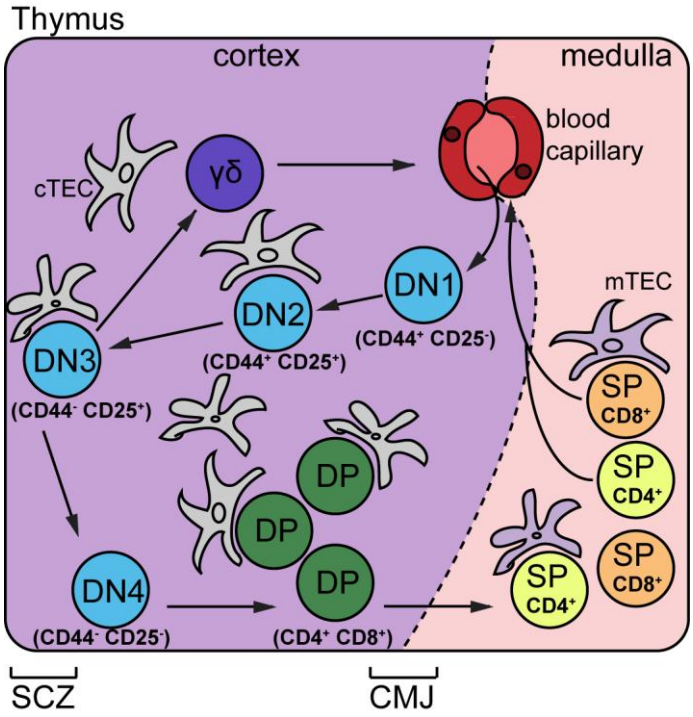

Figure 4.22: Maturation and selection of T-lymphocytes

The lymphoid progenitors, known as double negative 1 (DN1), enter the thymus at the cortico-medullary junction (CMJ) and proliferate extensively. They are characterised by the presence of CD44 and the absence of CD25 surface markers

(CD44+ CD25-). DN1 cells differentiate into DN2 cells (CD44+ CD25+), which continue to proliferate in order to further expand the cell population. DN2 cells then migrate to the cortical subcapsular zone (SCZ) and become DN3 cells (CD44- CD25+). The latter cells are now terminally committed to the T-lymphocyte lineage. At this stage, the cells can further differentiate to become αβ-lineage or γδ-lineage T cells by rearranging their β, γ and δ T-cell receptor (TCR) gene loci. T-lymphocytes towards the γδ lineage do not require further differentiation. DN4 (CD44- CD25-) become double positive (DP), defined by the expression of the surface markers CD4 and CD8 (CD4+ CD8+), further proliferate. Double positive cells undergo T-cell receptor alpha rearrangement, downregulate one of the two cell surface markers (either CD4 or CD8) to become single positive cells (SP) and enter the medulla. They then undergo negative selection to remove cells that show strong reaction to self-antigens. SP cells that pass the negative selection, exit the thymus and move to the periphery (Bhandoola et al., 2007; Ciofani and Zúñiga-Pflücker, 2007; Zlotoff and Bhandoola, 2011). cTEM= cortical thymic epithelial cells; mTEC= medullary thymic epithelial cells.

Since heterozygous mice present with a normal thymic architecture, I combined the results of the wild type and heterozygous thymuses together. I analysed the data from two wild type, six heterozygous and two homozygous-derived thymuses. **Figure 4.23A** shows that all stages of T-cell maturation are present in heterozygous and homozygous mice, with a similar profile in terms of percentage of cells (**Figure 4.23B**).

The results show that the thymuses of *Kdm3b* homozygous gene-trapped mice allow T-cell maturation, despite a possible abnormal thymic architecture.

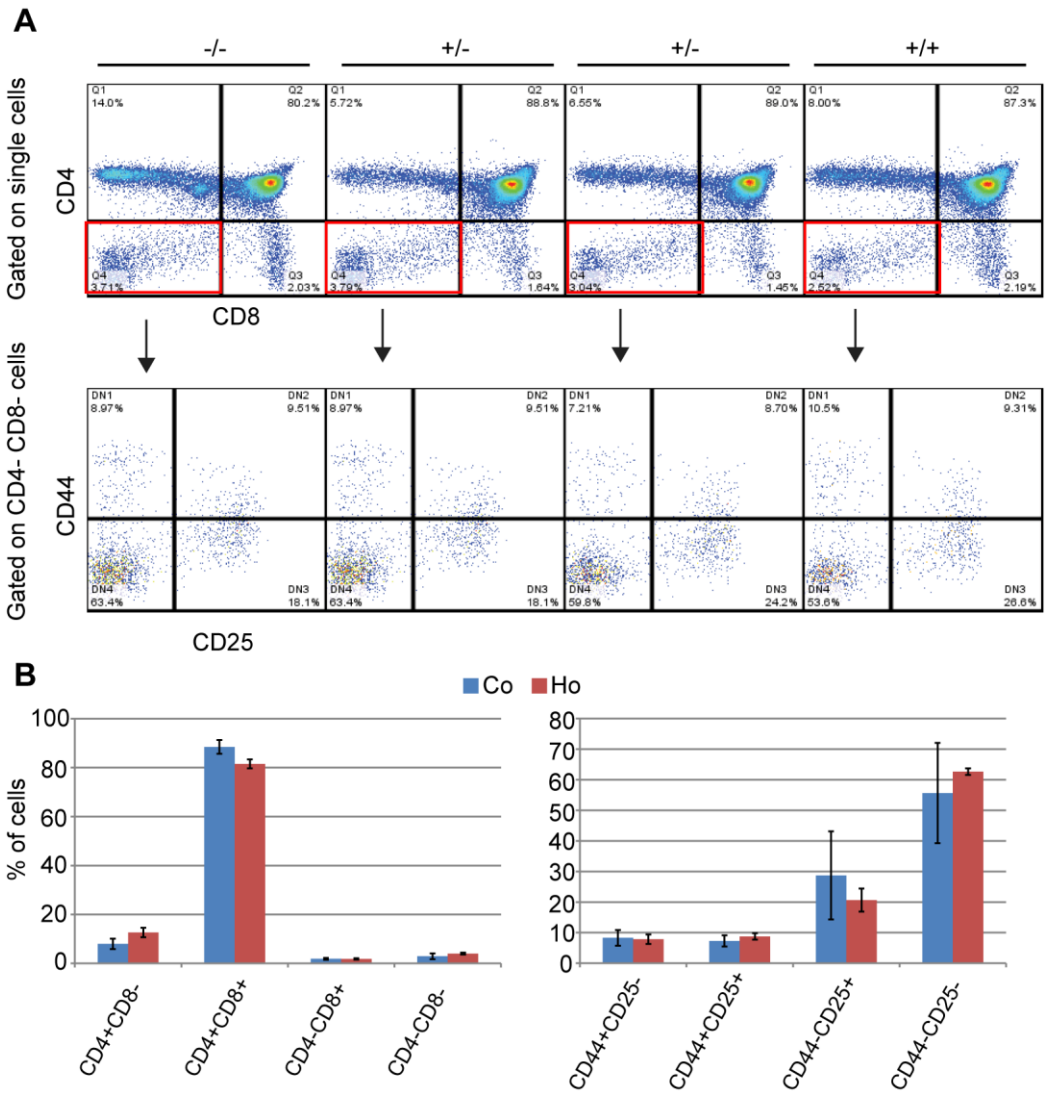

Figure 4.23: T-cell maturation completes in the thymuses of homozygous *Kdm3b* gene-trapped mice.

(**A**) A representative profile of thymic maturation, using the cell surface markers CD4 vs CD8 and CD44 vs CD25. The CD4 vs CD8 profile was gated on single cells. The CD44 vs CD25 profile was gated in CD4- CD8- cells (red boxes). (**B**) The thymuses of homozygous gene-trapped mice (Ho) presented a similar profile to the controls. Co= wild type and heterozygous.

4.1.7 Summary of chapter 4

In this chapter, significant reduction of *Kdm3b* expression resulted in postnatal - but not prenatal- growth retardation in *Kdm3b* homozygous gene-trapped mice, possibly attributed to perturbations in the thyroid hormone pathway. Several organs were grossly unaffected; however, the thymus showed reduced cortical layer or

undefined cortico-medullary boundaries. T-cell maturation completed, with no significant changes in the profile at any stages.

Chapter 5. Investigating the function of an alternative Kdm3a isoform

5.1 Results

As discussed in section 1.5 of the introduction, isoforms of chromatin-binding proteins can perform specialised functions (Verrier et al., 2011a; Zibetti et al., 2010). *Kdm3a* gene-trap and knock-out mice present with obesity, infertility, pre-disposal to diabetes and frequent partial sex reversal (Inagaki et al., 2009; Kasioulis et al., 2014; Kuroki et al., 2013a; Liu et al., 2010a; Okada et al., 2007; Okada et al., 2010; Tateishi et al., 2009). The aim of this project was to verify the existence and investigate the putative function/s for a predicted alternative murine *Kdm3a* isoform (*Kdm3a-i2*) that had not been experimentally characterised before.

5.1.1 The cloning of an alternative Kdm3a isoform from an Ensembl prediction

Apart from the full-length *Kdm3a* isoform (*Kdm3a-FL*), the Ensembl build software (http://www.ensembl.org/index.html) predicted an alternative Kdm3a isoform (Ensembl transcript ID ENSMUST00000101304). This isoform, which I named *Kdm3a-i2*, is missing the first eleven exons of *Kdm3a-FL* and contains a unique exon one within intron eleven of *Kdm3a-FL* (**Figure 5.1A** - asterisks). I confirmed by RT-PCR that this isoform is expressed in MEFs. For this, I used a common forward primer within the unique exon1 of *Kdm3a-i2* and reverse primers to exons18-19, exon 25 and exon 27 (numbering according to the *Kdm3a-FL* transcript). I observed a band of the correct size to the *Kdm3a-i2* prediction for all RT-PCRs (**Figure 5.2**).

I designed primers based on the Ensembl prediction to specifically amplify the coding sequence, cloned the *Kdm3a-i2* isoform in p-Gem T-easy vector (Promega) and confirmed its nucleotide sequence by sequencing and aligning. The *Kdm3a-i2* isoform was PCR amplified from homozygous *Kdm3a* gene-trapped MEFs cDNA (gene trap discussed in section 5.2).

Additionally, I confirmed that *Kdm3a-i2* is a transcribed gene by amplifying and sequencing from its 5' untranslated region (UTR) into the coding regions. The forward primer hybridised 200 base pairs within the predicted 5' UTR. By

sequencing from the 5' UTR, the predicted translation start site, as well as the splicing pattern was confirmed (data not shown). These experiments validate the *Kdm3a-i2* prediction and show that it is expressed in homozygous gene-trapped MEFs.

When translated, this newly cloned cDNA lacks the first 492 N-terminal amino acids of the full-length Kdm3a protein, but retains the zinc finger (ZF), the nuclear receptor (LXXLL) motif and the catalytic JumonjiC (JmjC) domain. The predicted protein size of *Kdm3a-i2* is 91 kDa (**Figure 5.1B**).

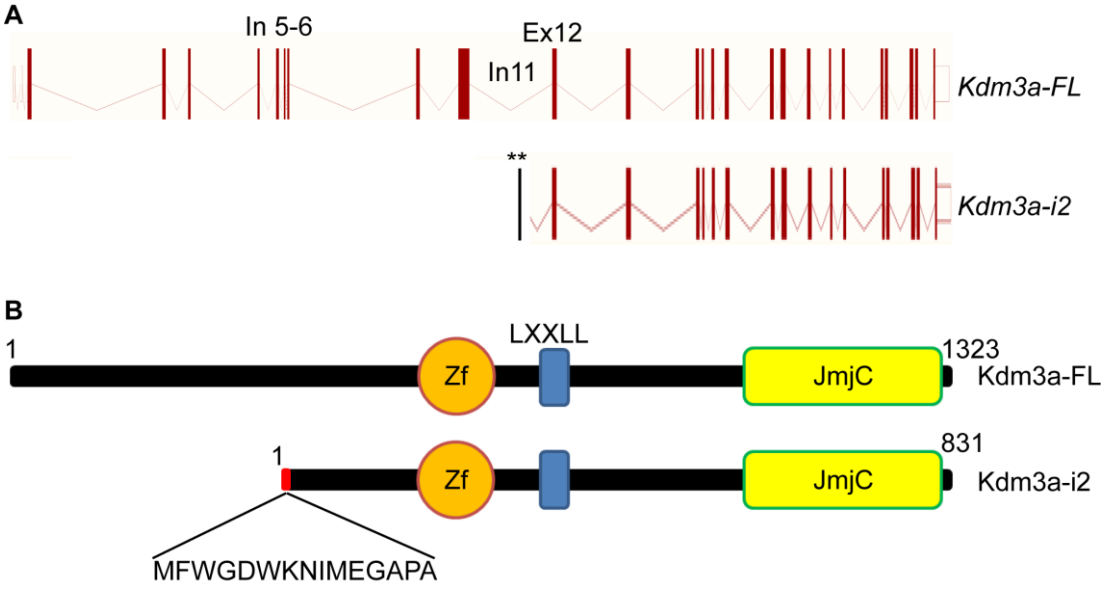

Figure 5.1: The *Kdm3a-i2* isoform genomic locus.
(**A**) The predicted *Kdm3a-i2* was missing the first eleven exons of *Kdm3a-FL* and contained a unique exon one within intron eleven, as indicated by the asterisks. (**B**) The Kdm3a-i2 protein retained all domains/motifs, present in Kdm3a-FL: the zinc finger (ZF), the nuclear receptor (LXXLL) and the catalytic JmjC domain. In red is the translation of the unique Kdm3a-i2 exon one, comprising of fifteen amino acids.

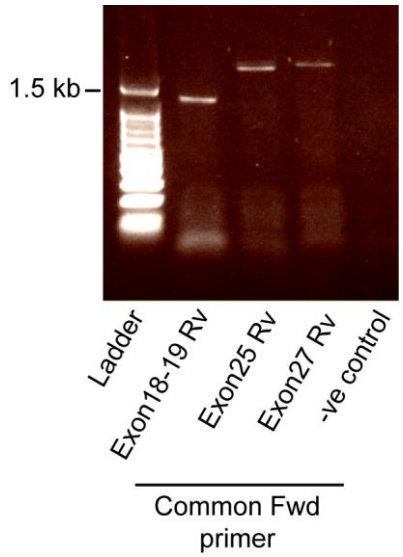

Figure 5.2: *Kdm3a-i2* is expressed in MEFs.

RT-PCR from MEF cDNA. A common forward primer was used to the unique exon1 of *Kdm3a-i2*and reverse primers to exons 18-19, exon 25 and exon 27. Numbering of reverse primers according to the *Kdm3aFL* transcript.

5.1.1.1 Sub-cloning of the predicted *Kdm3a-i2* isoform into tag vectors

To investigate the subcellular localisation of Kdm3a-i2, the cloned *Kdm3a-i2* described above was subcloned and GFP-tagged at the amino (N-) terminus (GFP-Kdm3a-i2) or RFP-tagged at the carboxyl (C-) terminus (Kdm3a-i2-RFP) (**Table 5-1**).

Table 5-1: *Kdm3a-i2* cloning primers.

Highlighted nucleotides represent the restriction enzyme cut sites; red- Xho I, green- Bam HI

Primer	Sequence (5'- 3')
GFP-Kdm3a-i2 Forward	CCGCTCGAGCTTTTTGGGGGGACTGGAAGAAC
GFP-Kdm3a-i2 Reverse	CGGGGATCCTTAAGGTTTGCCCAAACTGGATTCACTGGC
Kdm3a-i2-RFP Forward	CCCTCGAGCCATGTTTTGGGGGGACTGGAAGAAC
Kdm3a-i2-RFP Reverse	CGGGATCCCGAGGTTTGCCCAAACTGGATTCAC

I also subcloned and RFP-tagged, at the C-terminus, the *Kdm3a-FL* (Kdm3a-FL-RFP) and a deletion mutant of *Kdm3a-FL* missing exons 2-18 (Kdm3a-Δ2-18-

RFP). This deletion mutant of Kdm3a encodes a protein missing most of the N-terminus, the zinc finger and the nuclear receptor motif (Kdm3a-Δ2-18-RFP) (**Figure 5.3A**).

I validated the subcloning (data not shown) by sequencing and over-expressions in TERT-RPE1 cells, followed by Western blot. An antibody raised against the unique exon one epitope of Kdm3a-i2 detected a band of about 120 kDa, the expected size for GFP-Kdm3a-i2. The antibody did not recognise the GFP- tag protein (GFP vector) or any bands in the untransfected cell lysates (**Figure 5.3B**). The pre-bleed of the Kdm3a-i2 antibody, used as a negative control, did not detect the over-expressed GFP-Kdm3a-i2, although it detected an unspecific band close to 60 kDa, present in all cell lysates. The GFP antibody detected both the GFP-tag protein and GFP-Kdm3a-i2 and gave no bands in the untransfected cell lysates (**Figure 5.3B**).

Similarly, the Kdm3a-i2 antibody recognised the predicted over-expressed Kdm3a-i2-RFP of 115 kDa (**Figure 5.3C**). The lower band is possibly a cleavage product, where over-expressed Kdm3a-i2-RFP was cleaved from RFP tag at the connecting hinge region. The size of the band did support this hypothesis, although no cleaved RFP protein was seen in the RFP-antibody blot. The RFP antibody recognised all the over-expressed constructs: the RFP-tag protein of 25 kDa, Kdm3a-FL-RFP of 175 kDa, Kdm3a-i2-RFP of 115 kDa and Kdm3a-Δ2-18-RFP of 75 kDa. A non-specific faint band of about 100 kDa was present in all lanes. The pre-bleed did not recognise the over-expressed Kdm3a-i2-RFP but brought up some unspecific bands in all lanes (**Figure 5.3C**).

Thus, the Western blots validated the correct subcloning of all the constructs and the specificity of the Kdm3a-i2 antibody towards the over-expressed GFP-Kdm3a-i2 and Kdm3a-i2-RFP.

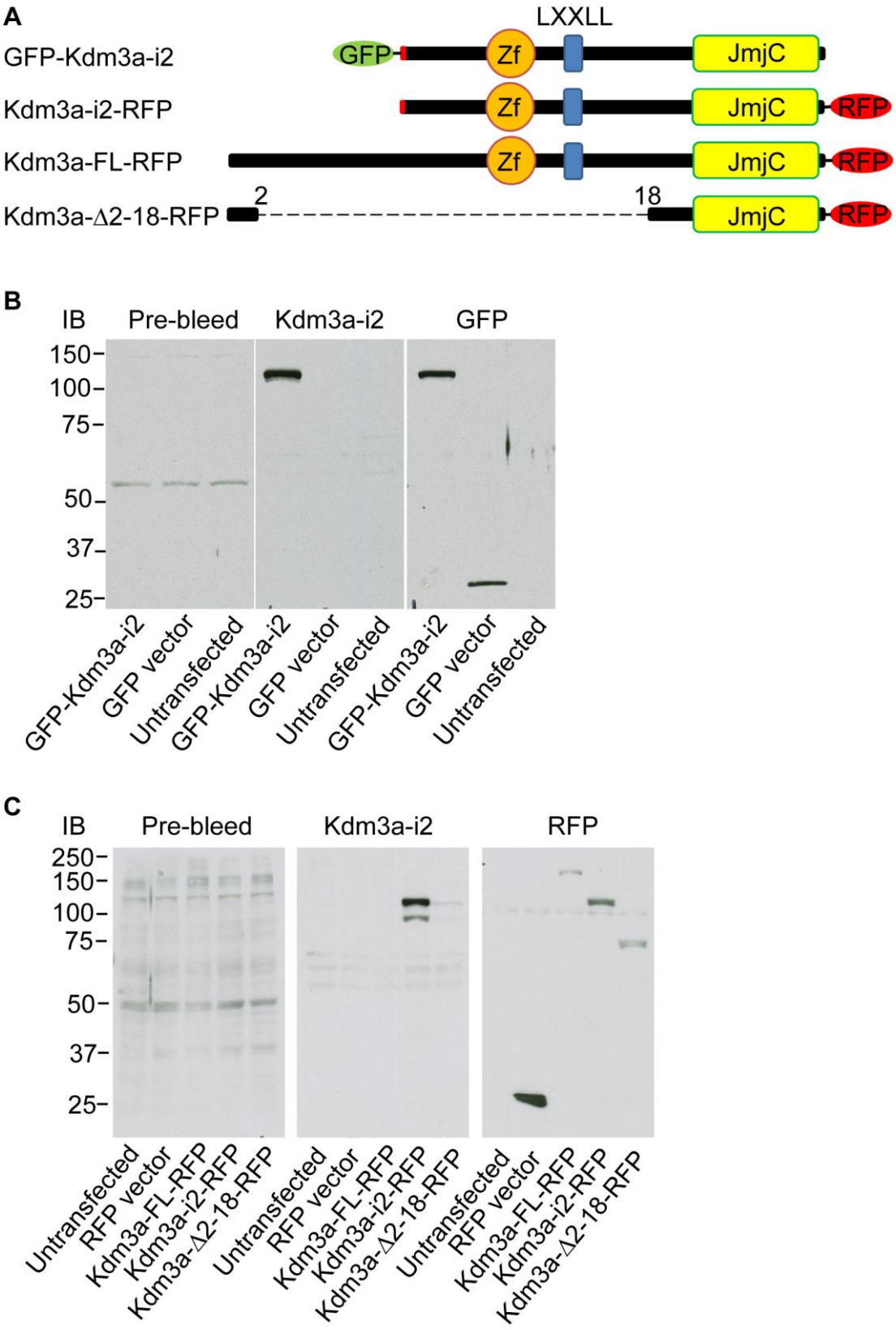

Figure 5.3: Cloning of Kdm3a isoforms and mutant, and size validation by Western blot.

(**A**) The Kdm3a-i2 isoform was GFP-tagged at the N-terminus and RFP-tagged at the C-terminus. Further, Kdm3a-FL and a deletion mutant missing exons 2-18, resulting in a protein missing most of the N-terminus, the zinc finger and the nuclear receptor motif were also RFP tagged at the C-end (Kdm3a-FL-RFP and Kdm3a-Δ2-18-RFP respectively). The red colour on Kdm3a-i2 represents the unique exon 1 of this isoform. (**B**) The size of the GFP-Kdm3a-i2 tagged protein was validated by Western blot. The Kdm3a-i2 antibody detected only the GFP-Kdm3a-i2 over-expression, the pre-bleed of the polyclonal antibody an unspecific band close to 60 kDa and the GFP antibody both the GFP-tag protein and GFP-Kdm3a-i2. (**C**) Size of RFP-tagged Kdm3 proteins validated by Western blot. The Kdm3a-i2 antibody detected only the Kdm3a-i2-RFP over-expression and a possible cleavage product. The RFP antibody detected all over-expressions and the pre-bleed did not detect the over-expressed Kdm3a-i2-RFP, but brought up some unspecific bands in all lanes. Numbers beside the Western blot represent molecular weight markers in kDa.

5.1.1.2 The over-expressed Kdm3a-i2 can function as an H3K9me1 and H3K9me2 demethylase and distorts the nuclear localisation of the H3K9me3 mark

Previous publications have demonstrated that Kdm3a-FL functions as an H3K9me1/2 demethylase (Yamane et al., 2006).

Since, Kdm3a-i2 protein retains the catalytic JmjC domain, I hypothesised that the Kdm3a-i2 isoform will retain the H3K9me1/2 demethylation function. To test this hypothesis, I over-expressed the GFP- and RFP-tagged Kdm3a-i2 in TERT-RPE1 cells and assessed the state of H3K9me1, H3K9me2, H3K9me3 and H3K27me3 methyl marks, by comparing transfected and untransfected neighbouring cells. I assessed 100 cells per experiment. Additionally, I transfected Kdm3a-FL-RFP as positive control for the assay and the Kdm3a-Δ2-18-RFP mutant as a negative control since the zinc finger is essential for the demethylation function (Yamane et al., 2006) .The experiment was performed in triplicate under 0.25% FCS growth conditions. The demethylation potential of Kdm3a-Δ2-18-RFP mutant was assessed in two experiments.

Over-expression of GFP-Kdm3a-i2 resulted in global loss or decrease of H3K9me1 fluorescence (**Figure 5.4A,E**) in 31% (94/300) of transfected cells. The GFP vector resulted in 0% (0/300) HeK9me1 global loss or decrease (**Figure 5.4E**). The result was statistically significant with a p-value of $p<0.0001$. Similarly, Kdm3a-i2-RFP transfections resulted in 34% (103/300) of decreased/lost fluorescence versus

0% (300/300) for the RFP vector. The result was again statistically significant with a p-value of p<0.0001 (**Figure 5.4B, E**). Over-expression of the control Kdm3a-FL-RFP resulted in 12% (36/300) of transfected cells with decreased or no fluorescence, which gave a Fisher's exact test p-value of 0.0001. (**Figure 5.4C,E**). However, Kdm3a-Δ2-18-RFP over-expression resulted in 1% (198/200) H3K9me1 fluorescence change which was not statistically significant (Fisher's exact test, p= 0.5) (**Figure 5.4D,E).**

Similar results were obtained for the H3K9me2 mark. Over-expression of GFP-Kdm3a-i2 and Kdm3a-i2-RFP resulted in reduced or absent fluorescence in 40% (121/300) and 30% (90/300) of transfected cells, respectively. GFP and RFP vectors did not affect the fluorescence intensity (0%- 0/300) (**Figure 5.5A,B,E**). The difference in the percentages of cells with reduced/absent fluorescence between the GFP-Kdm3a-i2 or Kdm3a-i2-RFP and their corresponding vectors was statistically significant, with a p-value of p< 0.0001. As expected the Kdm3a-FL-RFP control transfection resulted in 15% (45/300) of cells showing reduced or absent H3K9me2 (p< 0.0001) (**Figure 5.5C,E**). Kdm3a-Δ2-18-RFP over-expression resulted in no H3K9me2 fluorescence change (0/200- Fisher's exact test, p= 1) (**Figure 5.5D,E**).

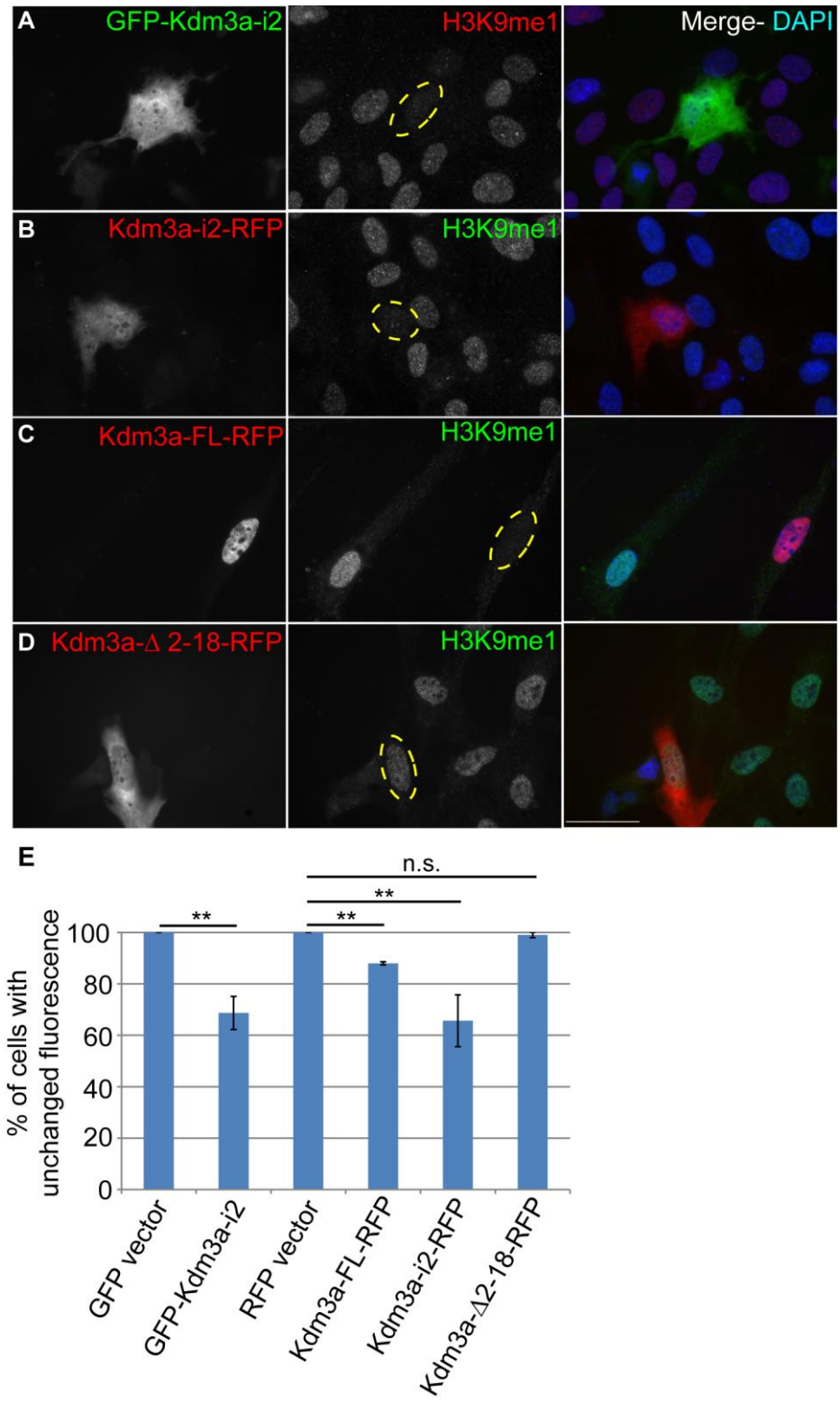

Figure 5.4:The Kdm3a-i2 isoform can function as an H3K9me1 demethylase.
TERT-RPE1 cells were transfected with GFP-Kdm3a-i2, Kdm3a-i2-RFP, Kdm3a-FL-RFP or Kdm3a-Δ2-18-RFP. The cells were then fixed and stained with H3K9me1 antibody. (**A,B**) Over-expression of both GFP-Kdm3a-i2 and Kdm3a-i2-

RFP resulted in global loss or decrease of the H3K9me1 fluorescence. (**C**) The Kdm3a-FL-RFP control transfection resulted in H3K9me1 fluorescent loss. (**D**) The Kdm3a-Δ2-18-RFP mutant was unable to reduce H3K9me1 fluorescence. (**E**) Compared their control vector transfections, the percentage of cells with unchanged H3K9me1 fluorescence was significantly reduced in GFP-Kdm3a-i2, Kdm3a-i2-RFP and Kdm3a-FL-RFP transfections. Kdm3a-Δ2-18-RFP transfections resulted in no significant difference. Yellow circles indicate nuclei of transfected cells. ** = significant, Fisher's exact test $p<0.05$. Error bars represent ± standard error. Scale bar: 40μm.

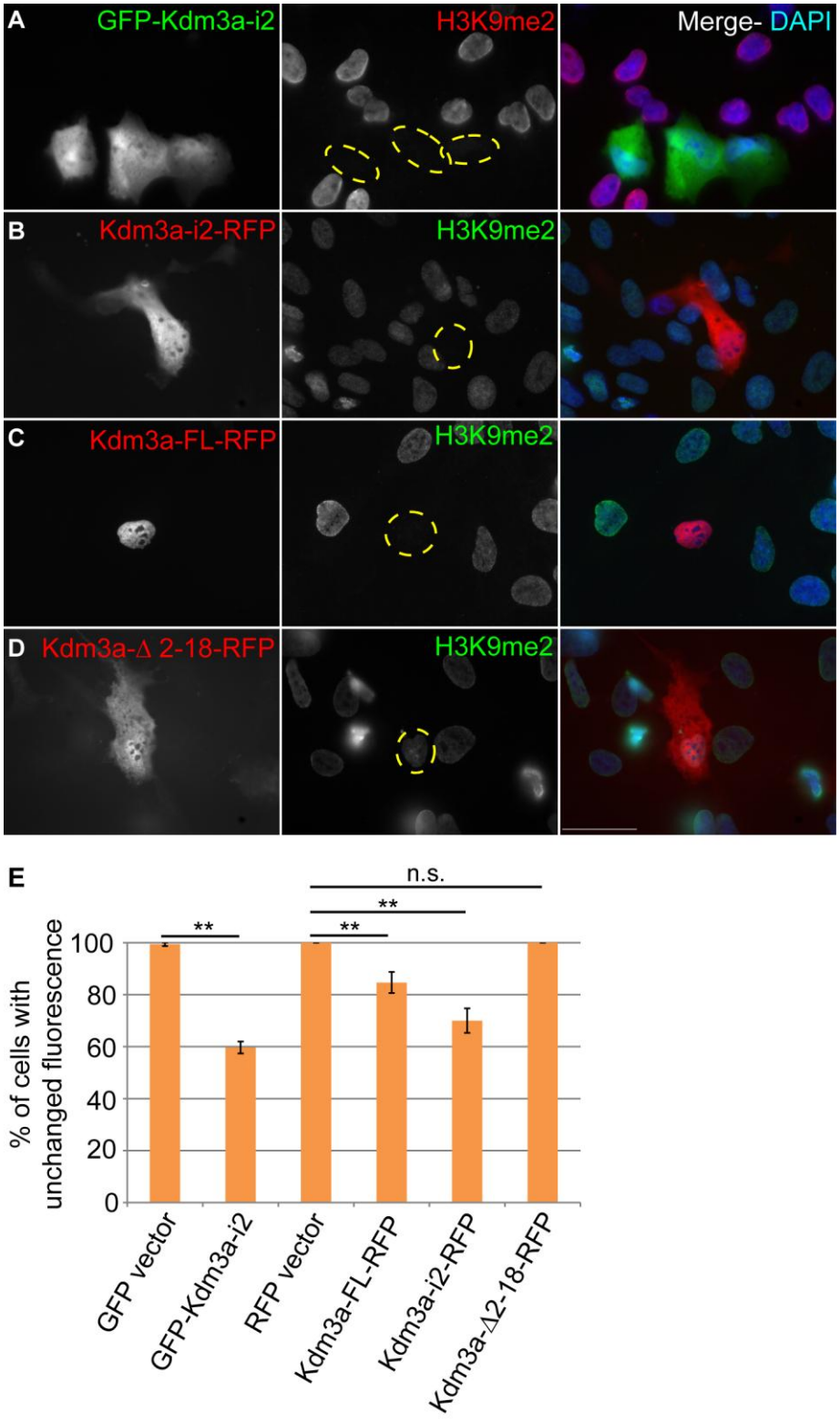

Figure 5.5: The Kdm3a-i2 isoform can function as an H3K9me2 demethylase.
TERT-RPE1 cells were transfected with GFP-Kdm3a-i2, Kdm3a-i2-RFP, Kdm3a-FL-RFP or Kdm3a-Δ2-18-RFP. The cells were then fixed and stained with H3K9me2 antibody. (**A,B**) Over-expression of both GFP-Kdm3a-i2 and Kdm3a-i2-

RFP resulted in global loss of the H3K9me2 fluorescence. (**C**) As expected the Kdm3a-FL-RFP control transfection resulted in H3K9me2 fluorescent loss. (**D**) The Kdm3a-Δ2-18-RFP mutant was unable to change H3K9me2 fluorescence. (**E**) Compared their control vector transfections, the percentage of cells with unchanged H3K9me2 fluorescence was significantly reduced in GFP-Kdm3a-i2, Kdm3a-i2-RFP and Kdm3a-FL-RFP transfections. Kdm3a-Δ2-18-RFP transfections resulted in no significant difference. Yellow circles indicate nuclei of transfected cells. ** = significant, Fisher's exact test $p<0.05$. Error bars represent ± standard error. Scale bar: 40μm.

In TERT-RPE1 untransfected cells, the H3K9me3 mark spread evenly through the nucleus. Sometimes, puncta were visible but were not very prominent. However, in GFP- Kdm3a-i2, Kdm3a-i2-RFP and Kdm3a-FL-RFP transfected cells, the methyl mark became punctuated with a decrease of fluorescent intensity in the rest of the nucleus (**Figure 5.6A-C**). This effect was evidenced in 67% (200/300) of GFP-Kdm3a-i2 transfected cells, as well as for 47% (140/300) and 40% (120/300) of Kdm3a-i2-RFP and Kdm3a-FL-RFP transfected cells, respectively. Compared to the GFP and RFP vector transfections that had no effect on H3K9me3 (0%- 0/300), the difference in the percentage of affected cells was statistically significant ($p< 0.0001$, all comparisons) (**Figure 5.6E**). Again, this was not the case for Kdm3a-Δ2-18-RFP where the nuclear H3K9me3 remained unchanged (0%- 0/200- Fisher's exact test, $p= 1$) (**Figure 5.6D,E**). This effect on H3K9me3 may be due to the significant decrease of H3K9me1/2, resulting in the remodelling of the epigenetic landscape.

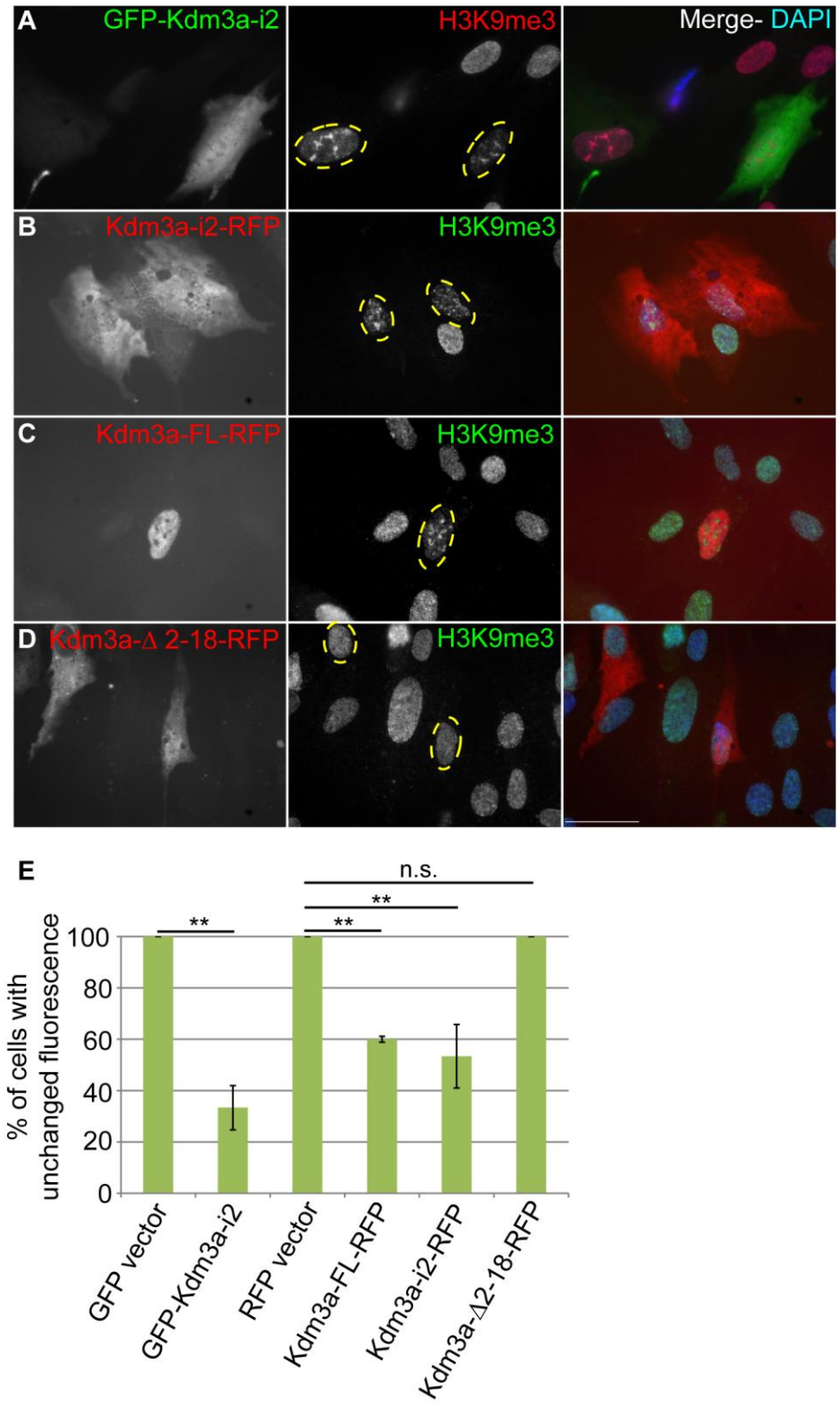

Figure: 5.6: Over-expression of Kdm3a-i2 and Kdm3a-FL distorted the nuclear H3K9me3 localisation.

TERT-RPE1 cells were transfected with GFP-Kdm3a-i2, Kdm3a-i2-RFP, Kdm3a-FL-RFP or Kdm3a-Δ2-18-RFP. The cells were then fixed and stained with

H3K9me3 antibody. (**A-C**) Over-expression of GFP-Kdm3a-i2, Kdm3a-i2-RFP and Kdm3a-FL produced a punctuated H3K9me3 phenotype. (**D**) Over-expression of Kdm3a-Δ2-18-RFP resulted in no distortion of the H3K9me3 mark. (**E**) Compared their control vector transfections, the percentage of cells with unchanged H3K9me3 fluorescence was significantly reduced in GFP-Kdm3a-i2, Kdm3a-i2-RFP and Kdm3a-FL-RFP transfections. Kdm3a-Δ2-18-RFP transfections resulted in no significant difference. Yellow circles indicate nuclei of transfected cells. ** = significant, Fisher's exact test $p<0.05$. Error bars represent ± standard error. Scale bar: 40μm.

The H3K27me3 mark was used as a negative control and resulted in no change (0%- 0/300) of the fluorescent intensity in any of the transfections (Fisher's exact test: GFP-Kdm3a-i2, p = 1; Kdm3a-i2-RFP, p= 1; Kdm3a-FL-RFP, p= 1, Kdm3a-Δ2-18-RFP, p= 1) (**Figure 5.7A-E**).

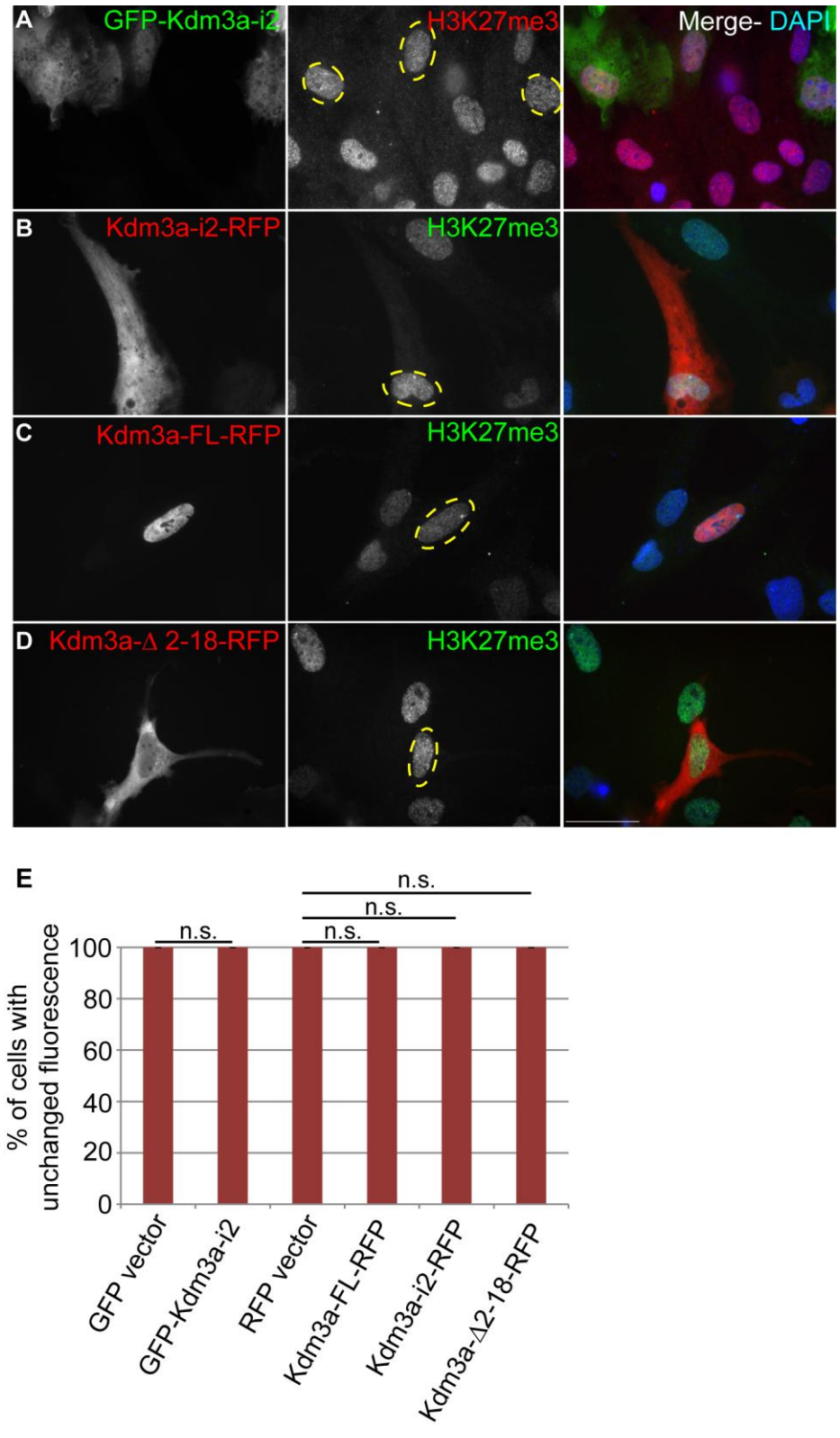

Figure 5.7: Over-expression of Kdm3a constructs did not affect the fluorescent intensity of H3K27me3.

TERT-RPE1 cells were transfected with GFP-Kdm3a-i2, Kdm3a-i2-RFP, Kdm3a-FL-RFP or Kdm3a-Δ2-18-RFP. The cells were then fixed and stained with H3K27me3 antibody. (**A-D**) There was no change in the fluorescent H3K27me3 intensity of the transfected cells for any of the constructs. (**E**) There was no significant difference in the percentage of Kdm3a transfected cells with unchanged fluorescence in comparison to their vector transfections. Scale bar: 40 μm.

The results suggest that Kdm3a-i2 can function as an H3K9me1/2 demethylase, having the same substrate specificity as Kdm3a-FL. In addition, the presence of excess Kdm3a-FL or Kdm3a-i2 protein in the cell nucleus disrupted the H3K9me3 nuclear distribution. Deletion of the exons 2-18 resulted in the loss of demethylase activity.

5.1.2 The murine Kdm3a gene trap

To test the expression levels of *Kdm3a-i2* upon *Kdm3a-FL* reduction, I took advantage of a gene-trap mouse model where the gene trap was inserted upstream of the *Kdm3a-i2* start site but within the genomic locus of *Kdm3a-FL*. As shown in **Figure 5.8**, the gene trap was inserted in intron 5-6 of the *Kdm3a-FL* locus and consisted of a splice acceptor site and a β-gal/neomycin (β-geo) sequence that allowed the selection of positive embryonic stem (ES) cells by G418 treatment and the visualisation of the targeted gene expression *in vivo.*

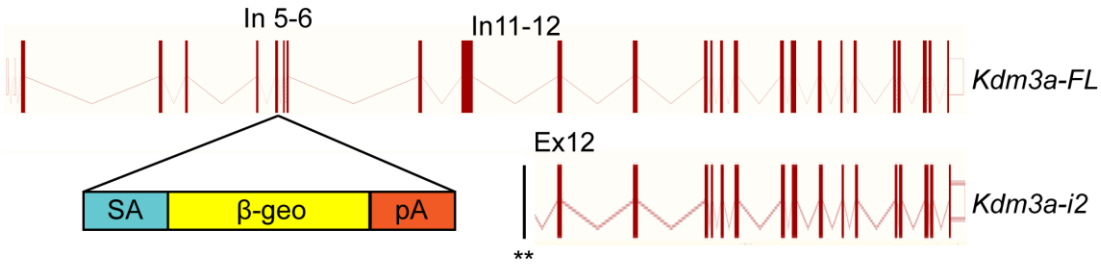

Figure 5.8: The gene trap within the Kdm3a locus.
The gene trap was inserted within intron 5-6 of the *Kdm3a* locus. It consisted of a strong splice acceptor site (SA), a β-gal/neomycin (β-geo) and a poly A (pA) sequence. The genomic *Kdm3a-i2* locus was unaffected.

I tested the efficiency of the gene trap by Western blot and qRT-PCR. Western blot with an antibody against the N-terminus of Kdm3a-FL (not present in Kdm3a-i2) showed minimal levels of Kdm3a-FL protein in homozygous gene-trapped MEFs

(GT Homo) compared to the wild type (WT) MEFs. In addition, in GT Homo MEFs a β-gal positive band was detected, possibly reflecting a Kdm3a/β-geo hybrid fusion protein. Densitometry analysis, with the Image J software, revealed 3-4% residual Kdm3a-FL protein remaining in GT Homo MEFs after normalising with α-tubulin and comparing with WT Kdm3a-FL expression (**Figure 5.9A-B**).

qRT-PCR was performed with a primer pair in exons 5-6 that flanked the gene trap (forward primer in exon 5 and reverse primer in exon 6). I used the t-test to check whether the reduction of Kdm3a transcript was statistically significant. The qRT-PCR showed a statistically significant ($p= 0.004$) decrease of 74% in *Kdm3a-FL* transcript of primary gene-trapped homozygous MEFs (Primary GT Homo MEFs) compared to primary wild type MEFs (Primary WT MEFs) (**Figure 5.9C**). In SV40 large T antigen-immortalised MEFs, there was a 70% decrease in homozygous (GT Homo-SV40) versus the wild type (WT-SV40) MEFs ($p= 0.03$). *Kdm3a-FL* transcripts from homozygous liver, kidney and testis showed a statistically significant reduction of 98%, 85% and 99% decrease compared to their wild type counterparts, respectively (liver, $p= 0.0005$; kidney, $p= 0.03$; testis, $p< 0.0001$). The qRT-PCR results confirmed previous publications where *Kdm3a* was found to be expressed at high levels in the testis (Tateishi et al., 2009) (**Figure 5.9C**).

The results of the Western blot and the qRT-PCR show that gene-trapped mice are hypomorphs as there was variable residual *Kdm3a-FL* expression in tissues and cells.

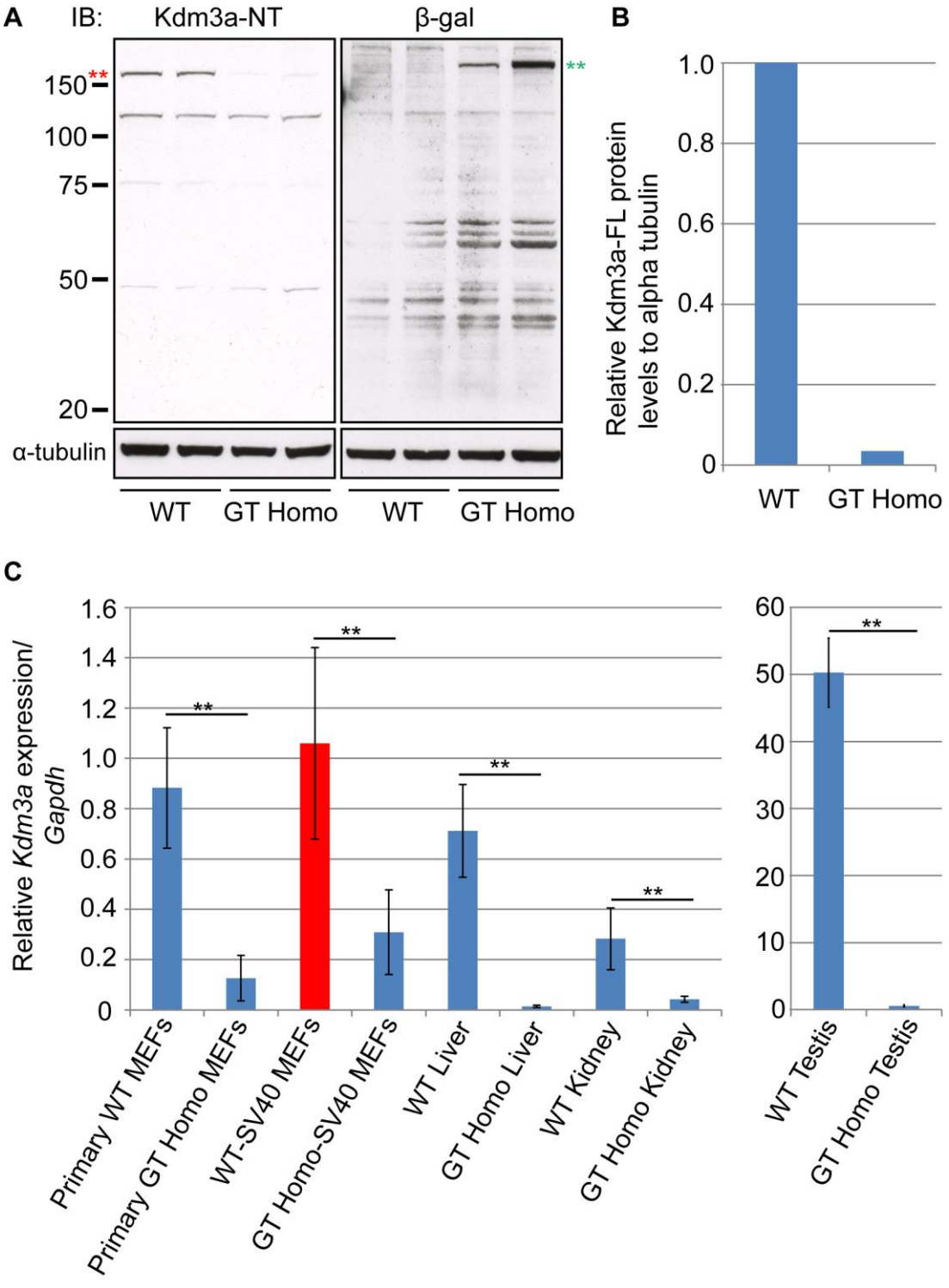

Figure 5.9: Validation of the gene trap efficiency in *Kdm3a* gene-trapped MEFs and tissues.

(**A**) Western blot of cell lysates from wild type (WT) and homozygous gene-trap (GT Homo) MEFs. Full length Kdm3a (band above 150 kDa) is expressed at low levels in GT Homo MEFs (red asterisks). A positive β-gal band in homozygous MEFs points

to a possible Kdm3a-FL/β-geo fusion protein containing the first five translated Kdm3a exons and the β-geo hybrid protein. Numbers beside the Western blot are molecular weight markers in kDa. (**B**) Densitometry analysis of the Western blot showed that after normalisation with the alpha tubulin (α-tubulin) loading control and comparison to WT Kdm3a-FL, about 4% of the full length Kdm3a protein is expressed in the homozygous gene-trapped MEFs. (**C**) qRT-PCR in WT, GT Homo MEFs and adult-derived tissues such as the liver, kidney and testis. Results from wild type-SV40 MEFs (WT-SV40 MEFs) were used as the calibrator (red bar). ** = significant, Tukey, $p<0.05$. Error bars represent ± standard deviation.

5.1.2.1 Comparing *Kdm3a-i2* expression in wild type and homozygous-derived cells and tissues

As shown above, *Kdm3a-FL* expression was significantly reduced in MEFs and tissues of homozygous mice. To check whether *Kdm3a-i2* expression is altered in response to the significant reduction of the *Kdm3a-FL* transcript and protein levels, I performed qRT-PCR on MEFs and tissues of WT and GT Homo mice. The forward primer bound to the unique exon one of Kdm3a-i2 transcript and the reverse in the shared exon two of *Kdm3a-i2* (that corresponds to exon 12 of *Kdm3a-FL*).

As shown in **Figure 5.10**, *Kdm3a-i2* transcript levels were significantly reduced by 48%in primary GT Homo MEFs compared to primary WT MEFs ($p= 0.009$). *Kdm3a-i2* transcript levels remained unchanged in immortalised MEFs (Tukey, $p= 0.94$), as well as in testis (Tukey, $p= 0.92$) of wild type and homozygous gene-trapped mice when compared to the wild type. The minimal expression of *Kdm3a-i2* observed in WT kidneys is lost in GT Homo. The result was significant ($p= 0.009$). No *Kdm3a-i2* expression was detected in the liver.

Although a comparison between the *Kdm3a-FL* and *Kdm3a-i2* transcript levels cannot be made due to the qRT-PCR experimental design, it should be noted that the *Kdm3a-i2* appeared be expressed at lower levels than *Kdm3a-FL*. For example, in wild type-SV40 MEFs, the average Ct value for *Kdm3a-FL* was 27.89 and for *Kdm3a-i2* was 33.94. Likewise, in the wild type testis, the average Ct value for *Kdm3a-FL* was 24.8 and for *Kdm3a-i2* was 39.96 (data not shown).

The qRT-PCR experiment showed that the SV40 transformation reduced the *Kdm3a-i2* levels in WT-SV40 MEFs. Also, MEFs expressed higher *Kdm3a-i2* levels

than tissues. In two cases, (primary MEFs and kidney) there was a correlation between *Kdm3a-FL* and the *Kdm3a-i2* levels in wild types and homozygotes; that is, reduction of *Kdm3a-FL* expression resulted in the reduction of *Kdm3a-i2*. In contrast, there was no difference in *Kdm3a-i2* levels in SV40 MEFs and testis of wild type and homozygotes, despite the *Kdm3a-FL* reduction in homozygotes.

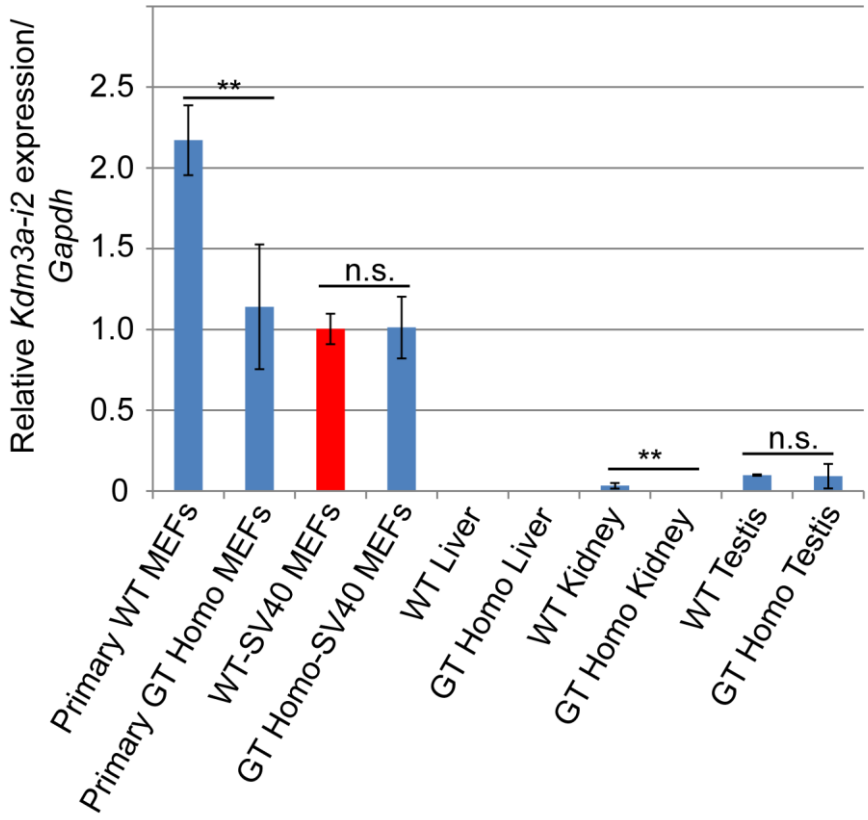

Figure 5.10: *Kdm3a-i2* expression is unaffected or decreased/absent in homozygous MEFs and tissues.

There was a significant decrease in *Kdm3a-i2* expression in primary GT Homo MEFs compared to WT MEFs (Tukey, p= 0.0009). This decrease was not evident in SV-40 immortalised homozygous MEFs (Tukey, p= 0.99). Compared with MEFs, WT kidneys express minimal *Kdm3a-i2*. The expression is lost in GT Homo Kidney however the difference was not significant (Tukey, p=0.72). WT and GT Homo testis show similar levels of *Kdm3a-i2* expression (Tukey, p= 0.99). No expression was detected in liver extracts. ** = significant, Tukey, p<0.05. Error bars represent ± standard deviation.

5.1.3 Subcellular localisation of Kdm3a constructs

Previous studies report nuclear as well as cytoplasmic Kdm3a localisation (Okada et al., 2007; Yamada et al., 2011). To investigate the subcellular localisation of Kdm3a-i2, I over-expressed GFP-Kdm3a-i2 and Kdm3a-i2-RFP in TERT-RPE1 cells for 24 hours, and fixed with formaldehyde. GFP- and RFP- vector transfections were used as a control.

I first investigated the localisation in cells that were kept in 10% FCS growth media. In 100% (300/300) of the RFP and GFP vector transfected cells the signal was present evenly throughout the nucleus and the cytoplasm (nuclear-cytoplasmic localisation) (**Figure 5.11A** and **D**). However, 64% (193/300) of Kdm3a-i2-RFP transfected cells showed nuclear-cytoplasmic localisation (**Figure 5.11B,D**) whereas 36% (107/300) showed strong cytoplasmic with none or limited nuclear localisation (**Figure 5.11C,D**). Similarly, 78% (235/300) of Kdm3a-i2-GFP transfected cells showed nuclear-cytoplasmic and 22% (65/300) showed strong cytoplasmic localisation (**Figure 5.11D**). The similar percentage between GFP and RFP Kdm3a-i2 constructs suggests that the tags do not affect the Kdm3a-i2 subcellular distribution.

When transfected cells were kept in 0.25% FCS growth media, there was an increase in the nuclear presence of Kdm3a-i2. More precisely, RFP-Kdm3a-i2 and GFP-Kdm3a-i2 transfected cells showed 94% (282/300) and 98% (6/300) nuclear cytoplasmic localisation respectively, with a significant decrease in the strong cytoplasmic category (**Figure 5.11E**).

The data suggested that subcellular localisation of GFP-Kdm3a-i2 and Kdm3a-i2-RFP was dependent on the growth conditions used.

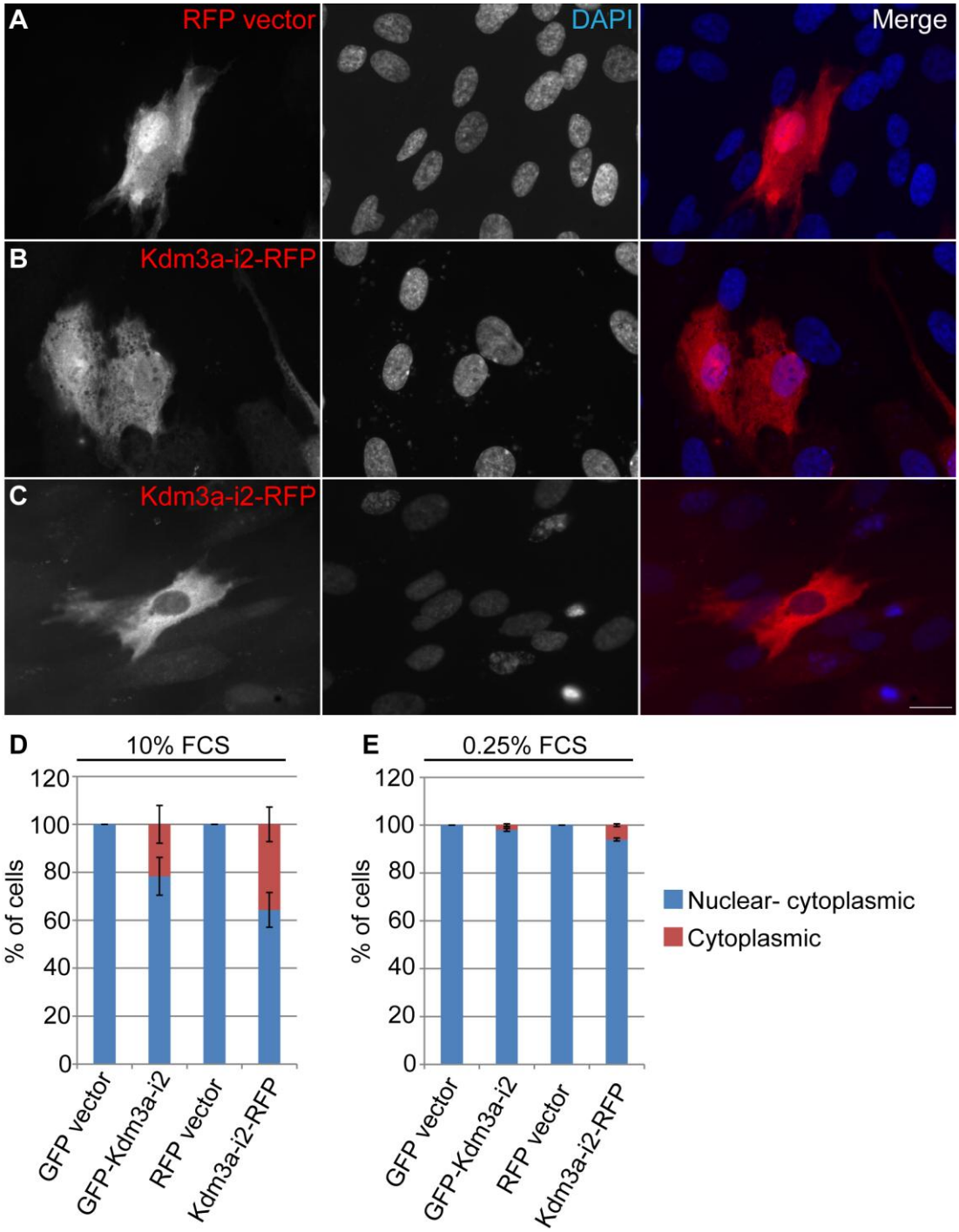

Figure 5.11: Subcellular localisation of Kdm3-i2 over-expressions.

TERT-RPE1 cells were transfected separately with either Kdm3a-i2-RFP or GFP-Kdm3a-i2 and their control vectors. (**A**) Localisation of RFP vector is nuclear-cytoplasmic. (**B**) Kdm3a-i2-RFP showed nuclear-cytoplasmic or (**C**) strong cytoplasmic localisation. (**D**) The subcellular localisation of the over-expressions under 10% FCS and 0.25% FCS growth media was quantified. Bars represent the mean of three independent experiments ± standard error.

5.1.3.1 Over-expressed GFP-Kdm3a-i2 is a potential centrosomal protein

Apart from the widespread cytoplasmic localisation of GFP-Kdm3a-i2 and Kdm3a-i2-RFP, I noticed that the signal was also concentrated as a single or two dots next to the nucleus (**Figure 5.12A,D)**. To check whether this specific localisation represented the centrosome, I used the centrosomal marker gamma-tubulin (γ-tubulin) (Fuller et al., 1995; Stearns et al., 1991) on methanol-acetone fixed TERT-RPE1 cells. Indeed, GFP-Kdm3a-i2 and Kdm3a-i2-RFP co-localised with γ-tubulin at the centrosomal material (**Figure 5.12B-C, E-F** and insets).

The above experiment suggested that GFP-Kdm3a-i2 is a potential centrosomal protein.

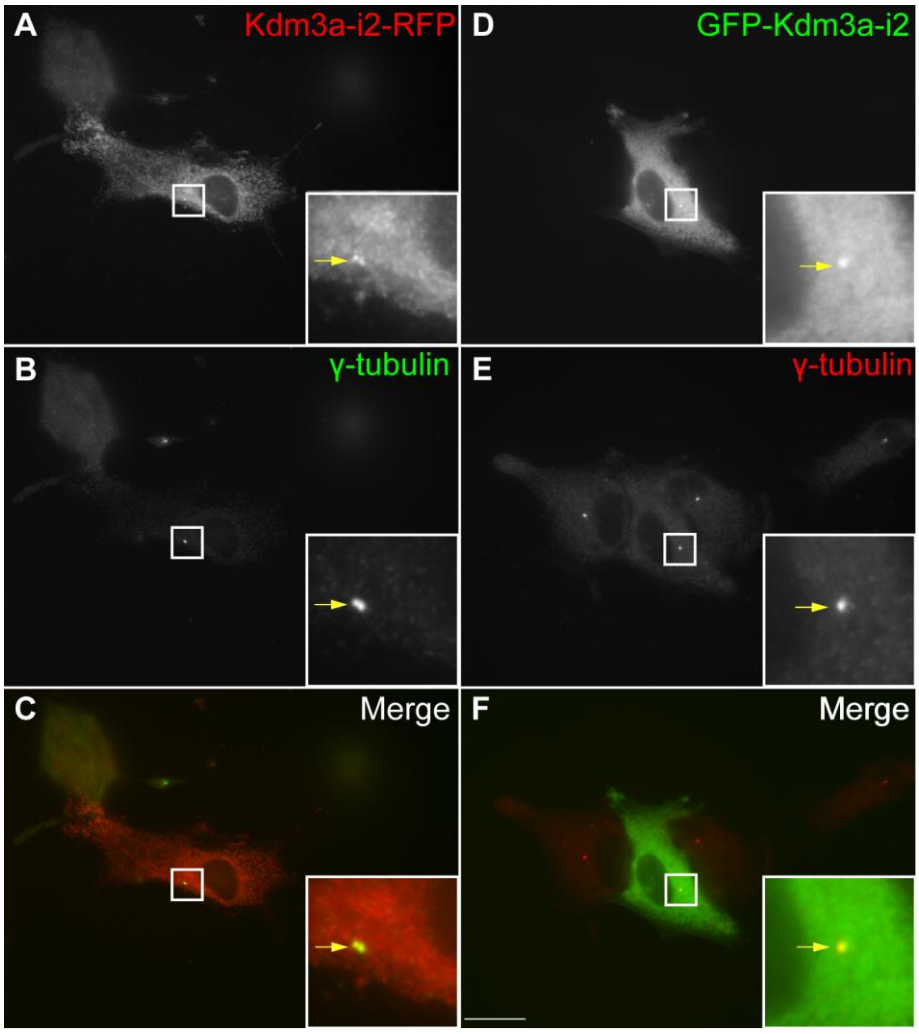

Figure 5.12: Over-expressed Kdm3a-i2 localises at the pericentriolar region.

TERT-RPE1 cells were transfected with GFP-Kdm3a-i2, methanol-acetone fixed and labelled using a γ-tubulin antibody. (**A-C**) Over-expressed Kdm3a-i2-RFP localised diffusely in the cytoplasm and the pericentriolar material, as marked by γ-tubulin. (**D-F**) Cytoplasmic and pericentriolar localisation was also evidenced for GFP-Kdm3a-i2. Scale bar: 20 μm.

5.1.3.2 A fraction of GFP-Kdm3a-i2 retained its centrosomal localisation after detergent pre-extraction

To further characterise the centrosomal localisation of GFP-Kdm3a-i2, I over-expressed GFP-Kdm3a-i2 in TERT-RPE1 cells. The cells were briefly pre-extracted with 0.2% Triton X-100 in PBS and fixed with 4% formaldehyde. **Figure 5.13A** shows that GFP-Kdm3a-i2 co-localised with the pericentriolar marker pericentrin (Delaval and Doxsey, 2010). Centrosomal co-localisation of Kdm3a-i2 was observed in about 5% (30/546) of the transfected and pre-extracted cells (**Figure 5.13E**), based on a calculated transfection efficiency of 58% for GFP-Kdm3a-i2 (not pre-extracted). As positive controls for the assay, I over-expressed GFP-centrin-2 and GFP-γ-tubulin, which are centriolar and pericentriolar markers, respectively (Lee and Huang, 1993; Stearns et al., 1991). GFP only over-expression was used as a negative control. Both GFP-centrin-2 and GFP-γ-tubulin maintained their centriolar and pericentriolar localisation, while the GFP vector did not show pericentriolar localisation after detergent pre-extraction (**Figure 5.13B-D**).

Under the experimental conditions used, a small percentage of GFP-Kdm3a-i2 was tightly associated with the centrosome.

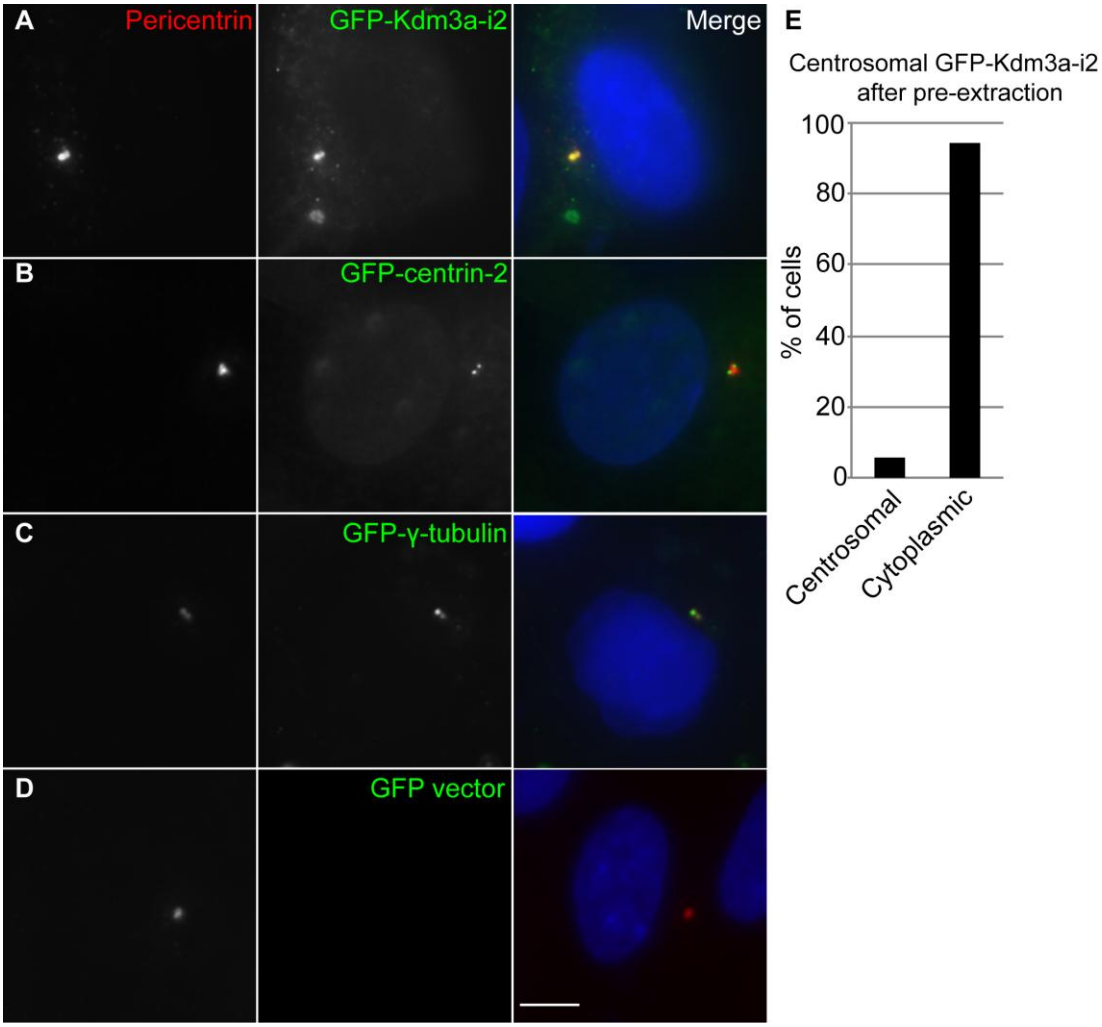

Figure 5.13: A fraction of GFP-Kdm3a-i2 retained its centrosomal localisation after detergent pre-extraction.
GFP-Kdm3a-i2, GFP-centrin-2, GFP-γ-tubulin and the GFP vector were transfected in TERT-RPE1 cells, detergent pre-extracted and then formaldehyde fixed. Pericentrin was used as a marker of the pericentriolar material. (**A-C**) GFP-Kdm3a-i2, GFP-centrin-2 and GFP-γ-tubulin localised at the centrosomes but (**D**) the GFP protein was no longer present. (**E**) About 5% of GFP-Kdm3a-i2 transfected cells retained their centrosomal localisation. Scale bar: 5 μm.

5.1.3.3 Kdm3a-i2 over-expression reduces the number of ciliated cells

The presence of GFP-Kdm3a-i2 at the centrosome prompted me to investigate whether over-expression of GFP-Kdm3a-i2 could affect ciliation. Thus, I over-expressed the GFP-Kdm3a-i2 isoform or the GFP vector in TERT-RPE1 cells, and following transfection, I replaced the 10% FCS growth media with 0.25% FCS media to induce ciliation. Forty-eight hours later, I quantified the percentage ciliation

of transfected cells and normalised that value to the percentage ciliation of neighbouring untransfected cells. The derived values were then compared.

Whereas ciliation was reduced by 34% in the GFP vector-transfected cells compared to their neighbouring untransfected cells, a 64% reduction in ciliation was observed in GFP-Kdm3a-i2 transfected cells. The reduction in ciliation, caused by the GFP-Kdm3a-i2 transfections, was statistically significant according to Student's *t*-test (t-test, p=0.01) (**Figure 5.14**).

The results show that over-expression of Kdm3a-i2 hinders the cell's ability to promote ciliation.

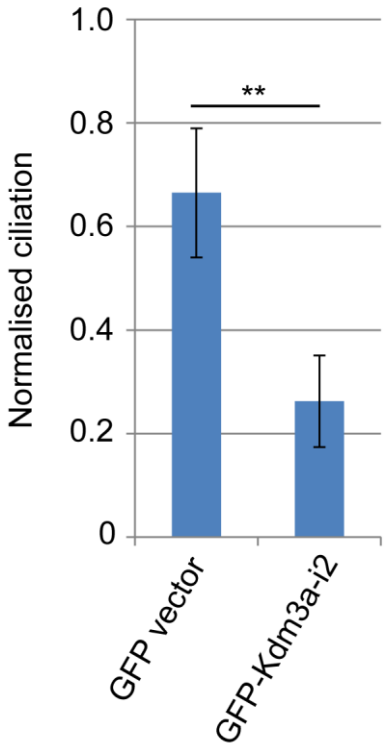

Figure 5.14: Over-expression of GFP-Kdm3a-i2 reduces the number of ciliated cells.
GFP-Kdm3a-i2 or the GFP vector constructs were transfected in TERT-RPE1 cells, and following transfection, 10% FCS media were replaced with 0.25% FCS media to induce ciliation. Forty-eight hours later, the percentage ciliation in transfected cells was quantified and normalised to the percentage ciliation of neighbouring untransfected cells. The reduction in ciliation by the GFP-Kdm3a-i2 transfections was statistically significant. ** = significant, t-test p= 0.01. Error bars represent ± standard deviation from three independent replicas.

5.1.4 Summary of chapter 5

In this study, *Kdm3a-i2* was cloned and shown to retain the H3K9me1/2 demethylase function. Interestingly, over-expressed Kdm3a-i2 localised both at the nucleus and the cytoplasm and co-localised with the centrosomal marker γ-tubulin. Further, over-expression of Kdm3a-i2 resulted in ciliation loss. Therefore, these results suggest a novel centrosomal function for Kdm3a-i2.

Chapter 6. Discussion

In the present study, I utilised model organisms and cell culture to investigate: 1) the conservation of *Kdm3b* function and spatial expression through evolution 2) the phenotype of *Kdm3b* gene-trapped mice and 3) plausible functions of an alternative murine Kdm3a isoform. Understanding the biological roles and molecular functions of lysine demethylases is important, since mutations in a subset these genes have already been identified in a number of diseases, such alopecia universalis, popular atrichia, X-linked mental retardation and cancer (Ahmad et al., 1998; Jensen et al., 2005; Kruse et al., 1999; Laumonnier et al., 2005; Sprecher et al., 1999; Tzschach et al., 2006; van Haaften et al., 2009). Furthermore, by dissecting the molecular pathways that Kdm3b participates in, I aimed to gain an insight into how Kdm3b controls a number of biological processes, such as growth and maintenance of immune system organs.

6.1 Conservation of demethylation function through evolution

The conversation of the demethylation function through evolution has already been demonstrated for a number of lysine demethylase protein families. In those instances, the *S. cerevisiae* demethylase homologues of the KDM2, KDM4 and KDM5 subfamilies possess histone lysine substrate specificities identical to the already characterised human proteins (Klose et al., 2007; Liang et al., 2007; Yamane et al., 2006). The same principle applies to non-vertebrate eukaryotic organisms such as *C. elegans*, where ceKDM7A shows histone lysine demethylase activity, like its human counterparts (Lin et al., 2010).From an evolutionary perspective, this observation demonstrates the essential need for control of the chromatin state via histone lysine demethylation, from low to higher eukaryotic organisms, such as the vertebrates.

In this study, I demonstrated that the zebrafish kdm3 protein, most closely related to the murine Kdm3b in protein sequence, retains H3K9me2 demethylation function when over-expressed in human cells. Interestingly, neither the zebrafish kdm3b nor the human homologue display H3K9me1 demethylase activity in low serum conditions. However, H3K9me1/2 demethylase activity is observed when the human KDM3B is over-expressed in cells incubated in growth media supplemented with 10% FCS (normal serum conditions). This is in agreement with publications that show that the human KDM3B is a H3K9me1/2 demethylase (Brauchle et al., 2013; Kim et al., 2012). It is unclear how serum levels may affect the demethylase potential of Kdm3b; however, further validation of these results is

essential since the experiment was performed only once. It is possible that the level of over-expression was not sufficient to drive global H3K9me1 demethylation, or that H3K9me1 demethylation within the KDM3B-over-expressed cell was counteracted by the accumulation of H3K9me1, via H3K9me2 demethylation. Alternatively, it is also possible that the zebrafish kdm3b has lost its H3K9me1 demethylase potential.

Furthermore, I showed that a mutant zebrafish kdm3b construct, lacking two amino acids, does not show any demethylase activity. Interestingly, the mutation does not localise within the catalytic JmjC domain or the zinc finger, which are necessary for histone lysine demethylation (Brauchle et al., 2013; Yamane et al., 2006), but is close to the zinc finger domain. Furthermore, over-expression of this mutant construct, results in a greater cytoplasmic, in addition to the nuclear localisation of the protein. Therefore, the mutation may distort the protein conformation, reducing its ability to bind the nuclear import-transport machinery and impeding its demethylation capacity by affecting the structure of the substrate-binding site. Alternatively, its histone binding capacity may be reduced.

Moreover, I demonstrated that the murine Kdm3a-i2 isoform can function as a H3K9me1/2 demethylase, as the already characterised full length isoform (Yamane et al., 2006). The Kdm3a-i2 isoform is missing the N-terminal domain of the full length isoform, and instead contains a unique exon one. This result is interesting because it shows that the N-terminal domain of the full length Kdm3a isoform is dispensible for the demethylase enzymatic function.

The demethylation potential of the zebrafish kdm3b can be further investigated by *in vitro* experiments. Purified kdm3b can be incubated with methylated peptides or nucleosomal substrates and the demethylation potential can be checked by western blot, using antibodies to methylated lysines (Liu et al., 2010b; Tsukada et al., 2006). Given: 1) the high percentage similarity of the human, mouse, and zebrafish KDM3B protein sequences within the JmjC domain and the zinc finger (78% and 77%, respectively), 2) the retention of the α-KG and Fe (II) binding sites in the zebrafish kdm3b protein, and 3) the histone lysine demethylase activity of the human KDM3B (Klose et al., 2006b), I am in favour of the zebrafish kdm3b as a true histone lysine demethylase.

6.2 Kdm3a and Kdm3b: novel ciliary candidate proteins?

Ciliation is a highly regulated process, in a spatiotemporal manner, that requires the gradual building of the axoneme and the selective trafficking of signaling proteins within the cilium (Gerdes et al., 2009a; Plotnikova et al., 2009). Although, in recent years, the processes of ciliary assembly and disassembly have been under intense scrutiny, the functional control of ciliary proteins via post-translational modification has not been thoroughly investigated. Interestingly, the over-expression of the Kdm3a-i2 isoform, as well as the zebrafish kdm3b, in cultured cells results in the reduction of ciliary assembly under conditions of low serum (that encourages ciliation).

Furthermore, the over-expression of both the wild type, as well as the mutant zebrafish kdm3b, shows the same ciliary-inhibiting efficiency, suggesting that the potential lysine demethylation function of kdm3b could be dispensible for this process. In addition, the over-expression of both constructs results in a proportion of cells with cytoplasmic kdm3b localisation, although their ciliary or centrosomal localisation was not investigated. Furthermore, whole mount in-situ hybridisation in zebrafish embryos showed that *kdm3b* is expressed in the otoliths, whose formation is dependent on fluid flow, generated by beating (motile) cilia (Stooke-Vaughan et al., 2012). These results correlate with unpublished data (Dr. Patricia Yeyati, Insitute of Genetics and Molecular Medicine, University of Edinburgh personal communication), where zebrafish *kdm3b* morphants recapitulate classical ciliary phenotypes, such as body curvature, *situs inversus* and reduced number of otolithis. How the knock-down of *kdm3b* in zebrafish morphants results in ciliary phenotypes is still unclear. Several models can be put forward such as: 1) kdm3b, via H3K9me2 promoter demethylation, allows the expression of genes involved in ciliation, 2) kdm3b promotes ciliation by demethylating lysine residues on ciliary proteins, thus controlling their function and 3) kdm3b functions as a scaffold to assist the interaction of ciliary proteins.

Moreover, as mentioned above, the over-expression of the murine Kdm3a-i2 isoform results in a reduction in ciliation efficiency. Strikingly, detergent pre-extraction resulted in about 5% of transfected cells retaining their Kdm3a-i2 binding on the centrosome. This is an interesting result, as no demethylase protein has yet been reported to localise to the centrosome. The plausible centrosomal function of Kdm3a-i2 at the centrosome is still unclear. Although an antibody was raised against the unique exon one of Kdm3a-i2, I was

unable to detect a band at the correct molecular size by Western blot, possibly due to its low expression levels compared to the full length isoform. Furthermore, this antibody still needs optimisation for immunofluorescence experiments. It is, however, very interesting that the phenotype of *Kdm3a* gene-trapped and knock-out mice (obesity, infertility and predisposal to diabetes) also recapitulates ciliary phenotypes. Kdm3a has been shown to localise to the nucleus and cytoplasm of spermatids (Okada et al., 2007), as well as the acrosome of mature sperm (Kasioulis et al., 2014). Loss of Kdm3a in knock-out mice results in disrupted acrosome and manchette formation. Testis extracts from Kdm3a knock-out mice show altered fractionation of γ-tubulin and β-actin. The unaltered levels of these proteins between wild type and homozygous Kdm3a knock-out mice suggests that the localisation but not the expression of these proteins is affected by the knock-down of Kdm3a.

Bearing in mind that the over-representation of Kdm3a-i2 and the zebrafish kdm3b leads to a reduced ciliation, these proteins may be involved in ciliary assembly. Methylation of ciliary proteins may be critical for the assembly and maintenance of the ciliary structure. Therefore, the demethylation of lysine residues on ciliary proteins may inhibit ciliary assembly. Alternatively, we cannot reject the hypothesis that reduction in ciliation could also be mediated through H3K9me1/2 demethylase activity. On the other hand, these ciliation assays should be approached with caution, as reduction in ciliation may be an indirect effect, owing to the global H3K9me1/2 demethylation or the high levels of these proteins in the cytoplasm. A negative control should also be incorporated in future experiments, for example, a protein that is not involved in the modulation of ciliation.

6.3 The Kdm3b mouse model

6.3.1 The Kdm3b mouse model: non-redundant biological roles compared to the other Kdm3 family members

The phenotype analysis of gene-trap, knock-out or mutant mouse models for the Kdm3 family (Kdm3a, Jmjd1C and Hairless) suggests minimal overlap in their biological roles:

a) Kdm3a is involved in male fertility, control of metabolic gene expression and sex determination (Inagaki et al., 2009; Kasioulis et al., 2014; Kuroki et al., 2013a; Liu et al., 2010a; Okada et al., 2007; Okada et al., 2010; Tateishi et al., 2009)

b) Jmjd1c is important for the maintenance of male fertility in age-dependent fashion (Kuroki et al., 2013b)
c) Hairless controls hair regeneration and white adipose tissue maintenance (Cachón-González et al., 1999; García-Atares et al., 1998; Kumpf et al., 2012; Thompson, 2009)

In the present study, I dissected the phenotype of heterozygous and homozygous gene-trap mice for *Kdm3b*, the only member of the *Kdm3* family whose function has not been studied using mouse models. The data suggest that Kdm3b is involved in promoting growth and thumic-tissue maintenance, which represent unique biological roles among the Kdm3 subfamily.

6.3.2 The thyroid hormone pathway as candidate for the growth retardation phenotype in *Kdm3b* homozygous gene-trapped mice

Homozygous *Kdm3b* gene-trapped mice are not prenatally growth retarded, as their weight at E18.5 is indistinguishable from their wild type and heterozygous gene-trap littermates. Growth retardation is evidenced from p14 (two weeks), and from that time point, the homozygous mice will gain little or no weight, as evidenced by the weight monitoring performed at p21 (three weeks) and p42 (six weeks). Monitoring litter weights at earlier stages, such as p3 and p7, will provide more information on when growth retardation commences.

Moreover, at prenatal stage E18.5, homozygous embryos are found at Mendelian ratios, in contrast to p14 and onwards, where homozygous mice are under-represented compared to wild type and heterozygous mice. These data suggest that a proportion of homozygous mice die during the first two postnatal weeks. In postnatal life, the health of homozygous mice deteriorates, and the majority do not thrive past p28.

To complement the results on growth, based on weight, and further dissect the phenotype observed in homozygous *Kdm3b* gene-trapped mice, the following experiments are necessary:

a) Check the development of the proximal growth plate of long bones, such as the tibia, to investigate if *Kdm3b* homozygous gene-trapped mice show delayed development of secondary ossification centres (Fraichard et al., 1997; Lupu et al., 2001)

b) Perform apoptosis and proliferation assays on tissue sections of organs. In particular, investigate proliferation on organs that show high cell turn-over in adult life, i.e. intestines
c) Investigate apoptosis and cell proliferation on MEFs
d) Measure the average cell size and area
e) Organ weights to body weights, apart from the thymus

6.3.2.1 The growth hormone pathway

The commencement of growth retardation, as assessed by weight monitoring, in *Kdm3b* homozygous mice is reminiscent of the growth retardation observed in knock-out mice of the growth and thyroid hormone pathways. For example, knock-out mice for *Ghrhr*, *Ghrh* and *Ghr* show post-natal growth retardation that is already evidenced at p14. These mice, however, follow Mendelian ratios in their adult life and are not short lived (Alba and Salvatori, 2004; Coschigano et al., 2000; Coschigano et al., 2003; Flurkey et al., 2001; Lupu et al., 2001). Absence of *Ghrh* and *Ghr* expression results in the perturbation of the growth hormone pathway, as the serum levels of Igf1 are significantly reduced (Alba and Salvatori, 2004; Lupu et al., 2001). In *Kdm3b* homozygous gene-trapped mice, I found that the expression of the *Ghrhr*, *Gh*, *Igf1*, *Igf1r* and *Igfbp3* are not significantly reduced compared to the control wild type and heterozygous gene-trapped mice. The *Igfals* expression, necessary for the stabilisation of Igf1 in the serum (Clemmons, 1997) was significantly reduced in homozygous mice. However, reduction of *Igfals* expression in homozygous mice cannot explain the growth retardation phenotype, since *Igfals* knock-out adult mice show a minor weight decreases (Ueki et al., 2000). Therefore, based on the qRT-PCR data, the growth hormone pathway is not perturbed in *Kdm3b* homozygous gene-trapped mice.

If necessary, further work that can be undertaken to dissect any possible perturbation of the growth hormone pathway in the homozygous mice includes:

a) Check the serum levels of Igfs, Igf-binding proteins and Igfals in adult mice
b) Investigate the protein levels of Igf1, Igfals and Ghr in liver protein extracts of adult mice

6.3.2.2 The thyroid hormone pathway

In the thyroid hormone pathway, Trh from the hypothalamus promotes the expression of Tsh in the pituitary, which binds the Tshr in the thyroid gland. Thyroid hormones (T3 and T4) are synthesized, which enter the blood stream and then are imported into cells. There they enter the nucleus, where the active T3 binds Thrs and to induce target gene expression. T3 and T4 also exert a negative feedback to the pituitary, in order to finely control Tsh expression. (**Figure 1.8** in introduction) (Brent, 2012; Dayan and Panicker, 2009; Oetting and Yen, 2007).

The growth retardation phenotype of homozygous mice can also be explained by the disruption of the thyroid hormone pathway. Interestingly, knock-out mice of the *Thra*, involved in the thyroid hormone pathway, show postnatal growth retardation evidenced at p14 and tend to die by four-five weeks of age, depending on the litter size. Also, *Thra* homozygous mice display a degenerated thyroid gland with reduced T3 and T4 hormone production (Fraichard et al., 1997). This phenotype closely resembles that of *Kdm3b* gene-trapped mice, as the growth retardation is already evidence from p14 and further, these mice do not thrive in adult life, with deaths occurring at 2, 4, 6 and rarely 10 weeks of age. Based on the qRT-PCR experiments, I found a statistically significant increase of *Tshb*-subunit expression in homozygous compared to the control mice, suggesting a perturbation of the thyroid hormone pathway.

Notably, it is already known that members of the Kdm3 subfamily interact with nuclear hormone receptors, acting as co-activators or co-repressors. Kdm3a and the s-Jmjd1c variant interact and function as co-activators of the androgen receptor-mediated gene activation (Wolf et al., 2007; Yamane et al., 2006). Hairless interacts and functions as a co-repressor of the thyroid receptor, the retinoic acid receptor-related orphan receptor and the vitamin D receptor (Thompson, 2009). Based on the published data and the qRT-PCR results, the following model can be put forward (**Figure 6.1**) where Kdm3b functions as a co-activator of the Thrα, via H3K9me2 promoter demethylation of T3 target genes. Like the *Thrα* knock-out mice, production and circulation of T3 and T4 hormones would be reduced in *Kdm3b* homozygous mice, resulting in the loss of the negative feedback loop to the pituitary gland. As a result, expression of the Tsh is significantly elevated.

This hypothesis is further re-enforced by the presence of an LXXLL domain in Kdm3b protein sequence, which is a signature motif of nuclear hormone binding proteins (Aranda and Pascual, 2001). In an alternative scenario. Kdm3b may control the expression of Thra by H3K9me2 demethylation. These hypotheses are very intriguing and require further experimentation, such as:

a) Validate the elevated expression of Tshb

b) Check the thyroid gland organ structure for any abnormalities in homozygous mice

c) Check the serum levels of T3 and T4

d) Investigate probable Kdm3b interaction with Tshα

e) Check whether Kdm3b functions to promote *Thra* expression

f) Gene expression analysis to investigate the downregulation of thyroid hormone target genes

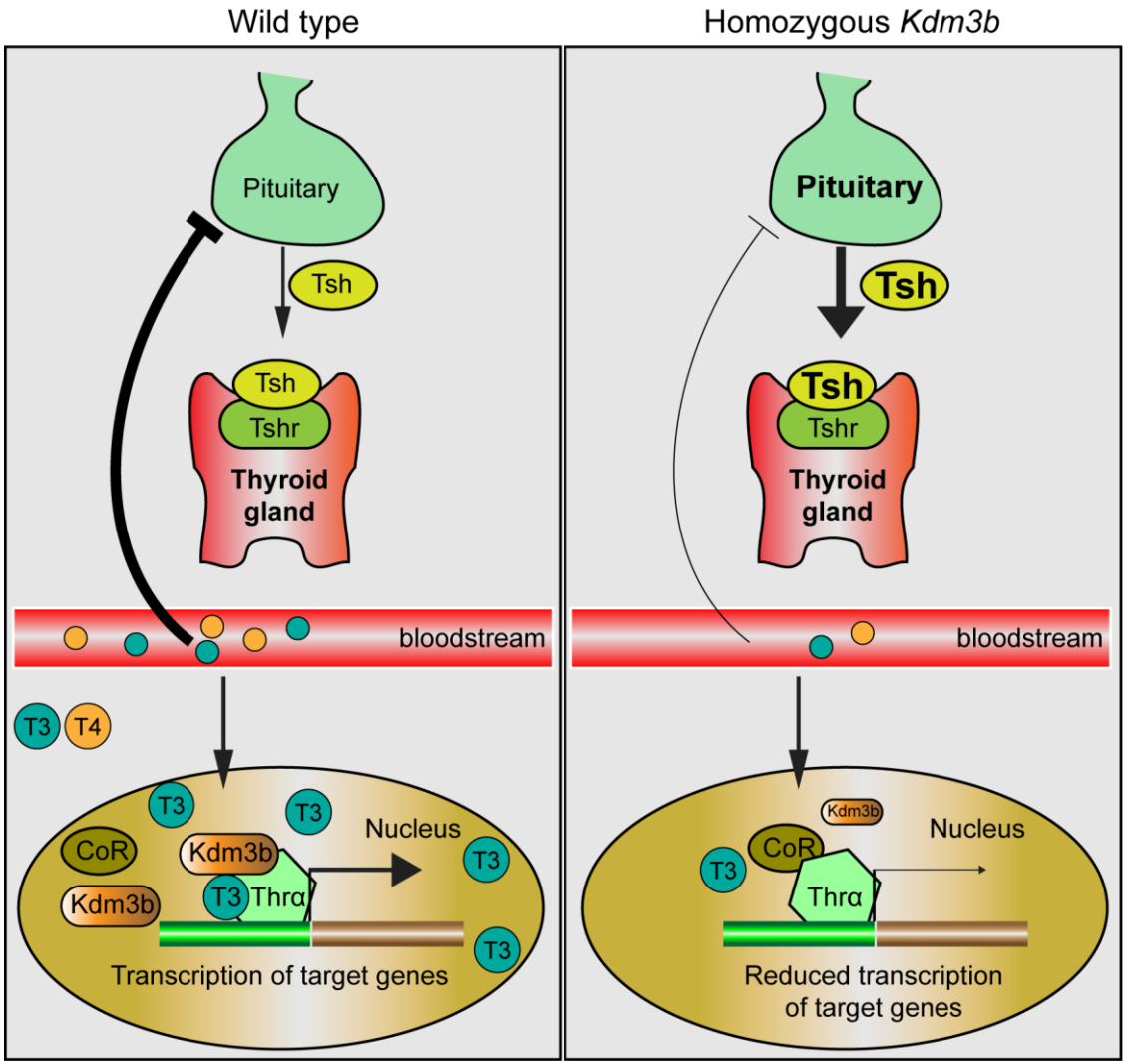

Figure 6.1: Proposed model for Kdm3b function in the thyroid hormone pathway.

In wild type mice, the pituitary gland expresses and releases thyroid stimulating hormone (Tsh), which binds to the thyroid stimulating hormone receptor (Tshr). The thyroid gland is stimulated to produce and release the thyroid hormones T3 and T4 in the bloodstream, which feed back to the pituitary to reduce Tsh expression. In the event of T3 binding to the Thrα, Kdm3b will interact with the receptor(s) and function as a co-activator of T3-mediated gene expression, via H3K9me2 promoter demethylation. In the homozygous Kdm3b gene-trapped mice, reduced Kdm3b expression results in the downregulation of T3 target genes, since gene promoters have increased H3K9me2 levels.. Furthermore, the thyroid gland produces less T3 and T4 and this results in the upregulation of Tsh expression.

6.4 Kdm3b as a candidate regulator of thymus development or maintenance

Kdm3b homozygous gene-trapped mice presented with reduced thymus/body weight ratio. Furthermore, for a proportion of homozygous-derived thymuses, the cortical layer was reduced or the two layers could not be clearly defined by H&E staining. This phenotype is reminiscent of thymic involution, an age-related process seen both in older mice and humans. In an age-related involuting thymus, the cortex and medulla lose their definition, as a result of thymic epithelial cell decrease. In addition, in this condition there is a reduction in lymphoid progenitor and differentiating thymocytes, as well as deposition of adipocytes that fill up the thymic space (Taub and Longo, 2005; Taub et al., 2010). However, *Kdm3b* homozygous mice were only three weeks of age when the thymic cell layer defect was observed, suggesting that Kdm3b may be necessary for the development and/or the maintenance of the organ. As revealed by immunohistochemistry, Kdm3b is expressed in the thymus (more densely in the medullary layer), implying a direct role for the proper function of the organ. Thus, it is possible that Kdm3b loss results in an age-accelerated decrease of progenitors being supplied to the organ, or that the thymic epithelial cells are not maintained due to the loss of Kdm3b-mediated gene expression. Suprisingly, however, the process of T-cell maturation was complete in the homozygous thymuses. As in some cases the homozygous mice express minimal levels of Kdm3b, it may be possible that these low levels are enough to support proper development and T-cell maturation. A knock-out mouse, where Kdm3b

expression is completely lost, may provide a clearer picture for the contribution of Kdm3b on thymopoiesis.

To further define the thymic defect, more experiments are necessary, such as:

a) More FACS sorting with surface markers CD4, CD8, CD25 and CD44 from the third post-natal week onwards, to investigate whether thymocyte development stalls at any time point.
b) H&E staining of thymuses at younger ages to investigate whether the cortico-medullary layers initially develop normally in the homozygotes and later lose their definition
c) Immunofluorescence with markers of the cortical and medullary cell epithelial layers to better define the defect
d) Identification of cell type(s) that express Kdm3b

6.4.1 Neuroendocrinology meets immunity

Both the growth retardation and thymus defects observed in *Kdm3b* homozygous mice are interesting, but is there any connection between them? Intriguingly, dwarf mice that lack anterior pituitary cells, therefore deficient in the production of the growth hormone and thyroxine, have several immunological defects. The thymuses of these mice show post-natal involution, already evidenced at 30 days of age, characterised by a reduced thymus weight relative to body weight. At this age, the cortex width is reduced and the cortico-medullary boundary becomes undefined. Additionally, all cell types present in the bone marrow are reduced in number, and the peripheral white blood cell count is lower than wild type littermates throughout life (Fabris et al., 1971). A closer inspection at thymic lymphocyte maturation revealed that dwarf mice show a deficiency in $CD4^+$ $CD8^+$ double positive cells, which becomes more pronounced with increasing age. Strikingly, treatment of these mice with recombinant human GH increases thymus size and results in the re-appearance of $CD4^+$ $CD8^+$ double positive cells in the thymus (Murphy et al., 1992).

Increase in thymus size and cellularity is also evidenced when Igf1, which functions as the downstream effector of the Gh, is administered in insulin deficient/diabetic rats, or rats whose immune system has been compromised by cyclosporine treatment (Beschorner et al., 1991; Binz et al., 1990; García-Suárez et al., 2003). Igf1 receptor is expressed in the thymus (García-Suárez et al., 2003), therefore systemic Igf1 can bind and exert its growth promoting/mitogenic effect on thymus epithelial cells. It is therefore possible that Kdm3b indirectly maintains the thymus architecture, by promoting expression of growth hormones. A way to investigate this possibility is to inject Igf1 in *Kdm3b* homozygous mice and check thymic cellularity about two weeks after administration.

6.5 Concluding remarks

In this study, I checked the demethylation potential and expression pattern of the zebrafish and mouse Kdm3b, during embryogenesis. I also dissected the phenotype of *Kdm3b* gene-trapped mice, the first mouse model for this demethylase, and attempted to uncover the plausible function(s) of an alternative murine Kdm3a isoform (Kdm3a-i2).

Both the zebrafish *kdm3b* morphants and the *Kdm3a* gene-trapped and knock-out mice resemble a ciliopathy syndrome phenotype. Furthermore, the murine Kdm3a-i2 isoform appears to have both a histone demethylation and a plausible unknown centrosomal function. In contrast, the phenotype of *Kdm3b* gene-trapped mice is not reminiscent of a ciliapathy syndrome. Rather, Kdm3b is involved in post-natal growth by promoting the expression of growth regulators, and in immunity, by maintaining the organisation of thymic layers. Based on these data, it is proposed that 1) functionally, the zebrafish kdm3b is closer to the murine Kdm3a and 2) the murine Kdm3a and Kdm3b paralogues are not redundant, but rather have distinct/non-overlapping biological roles.

Chapter 7. Appendix

Alignment of the human and mouse KDM3A and KDM3B paralogues


sp|Q7LBC6|KDM3B_HUMAN SSKLVSGVLGSALTSGGPSLSAMGNGRSSSPTSSLTQPIEMPTLSSSPTEERPTVGPGQQ 757
tr|B9EKS2|KDM3B_MOUSE SSKLVSGVLGSALSTGSPSLSAVGNGRSSSPTNSLTQPIEMPTLSSSPTEERPTVGPGQQ 758
sp|Q9Y4C1|KDM3A_HUMAN ----------SPS-DVSNAPEVKAGVN 460
sp|Q6PCM1|KDM3A_MOUSE ----------STSDDLSDKPEVKAGVT 462
sp|Q7LBC6|KDM3B_HUMAN DNPLLKTFSNVFGRHSGGFLSSPADFSQENKAPFEAVKRFSLDERSLACRQDSDSSTNSD 817
tr|B9EKS2|KDM3B_MOUSE DNPLLKTFSTVFGRHSGSFLSAPAEFAQENKAPFEAVKRFSLDERSLACRQDSDSSTNSD 818
sp|Q9Y4C1|KDM3A_HUMAN SDS----------PNNCS----------GKKVEPSALACRSQNLKESSVK 490
sp|Q6PCM1|KDM3A_MOUSE --S----------LNSCA----------EKKVEPSHLGSQSQNLKETSVK 490
sp|Q7LBC6|KDM3B_HUMAN LSDLSDSEEQLQAKTGLKGIPEHLMGKLGPNGERSAELLLGKSKGKQAPKGRPRTAPLKV 877
tr|B9EKS2|KDM3B_MOUSE LSDLSDSEEQLQAKSGLKGIPEHLMGKLGPNGERSAELLLGKGKGKQAPKGRPRTAPLKV 878
sp|Q9Y4C1|KDM3A_HUMAN ----------V----------DNESCCSRSNNKIQNAPS 509
sp|Q6PCM1|KDM3A_MOUSE ----------V----------DNESCCTRSSNKTQTPPA 509
sp|Q7LBC6|KDM3B_HUMAN GQSVLKDVSKVKKLKQSGEPFLQDGSCINVAPHLHKCRECRLERYRKFKEQEQDDSTVAC 937
tr|B9EKS2|KDM3B_MOUSE GQSVLKDVSKVRKLKQSGEPFLQDGSCINVAPHLHKCRECRLERYRKFKEQEQDDSTVAC 938
sp|Q9Y4C1|KDM3A_HUMAN RKSVLTDPAKLKKLQQSGEAFVQDDSCVNIVAQLPKCRECRLDSLRKDKEQ-QKDSPVFC 568
sp|Q6PCM1|KDM3A_MOUSE RKSVLTDPDKVRKLQQSGEAFVQDDSCVNIVAQLPKCRECRLDSLRKDKDQ-QKDSPVFC 568
sp|Q7LBC6|KDM3B_HUMAN RFFHFRRLIFTRKGVLRVEGFLSPQQSDPDAMNLWIPSSSLAEGIDLETSKYILANVGDQ 997
tr|B9EKS2|KDM3B_MOUSE RFFHFRRLVFTRKGVLRVEGFLSPQQSDPDAMNLWIPSSSLAEGIDLETSKYILANVGDQ 998
sp|Q9Y4C1|KDM3A_HUMAN RFFHFRRLQFNKHGVLRVEGFLTPNKYDNEAIGLWLPLTKNVVGIDLDTAKYILANIGDH 628
sp|Q6PCM1|KDM3A_MOUSE RFFHFRRLQFNKHGVLRVEGFLTPNKYDSEAIGLWLPLTKNVVGTDLDTAKYILANIGDH 628
sp|Q7LBC6|KDM3B_HUMAN FCQLVMSEKEAMMMVEPHQKVAWKRAVRGVREMCDVCETTLFNIHWVCRKCGFGVCLDCY 1057
tr|B9EKS2|KDM3B_MOUSE FCQLVMSEKEAMMMVEPHQKVAWKRAVRGVREMCDVCETTLFNIHWVCRKCGFGVCLDCY 1058
sp|Q9Y4C1|KDM3A_HUMAN FCQMVISEKEAMSTIEPHRQVAWKRAVKGVREMCDVCDTTIFNLHWVCPRCGFGVCVDCY 688
sp|Q6PCM1|KDM3A_MOUSE FCQMVISEKEAMSTIEPHRQVAWKRAVKGVREMCDVCDTTIFNLHWVCPRCGFGVCVDCY 688
sp|Q7LBC6|KDM3B_HUMAN RLRKSRPRSETEEMGDEEVFSWLKCAKGQSHEPENLMPTQIIPGTALYNIGDMVHAARGK 1117
tr|B9EKS2|KDM3B_MOUSE RLRKSRPRSETEEMGDEEVFSWLKCAKGQSHEPENLMPTQIIPGTALYNIGDMVHAARGK 1118
sp|Q9Y4C1|KDM3A_HUMAN RMKRKNC----QQGAAYKTFSWLKCVKSQIHEPENLMPTQIIPGKALYDVGDIVHSVRAK 744
sp|Q6PCM1|KDM3A_MOUSE RMKRKNC----QQGAAYKTFSWIRCVKSQIHEPENLMPTQIIPGKALYDVGDIVHSVRAK 744
sp|Q7LBC6|KDM3B_HUMAN WGIKANCPCISRQNKSVLRPAVTNGMSQLPSINPSASSGNETTFSGGGGPAPVTTPEPDH 1177
tr|B9EKS2|KDM3B_MOUSE WGIKANCPCISRQSKSVLRPAVTNGISQLPSVTPSASSGNETTFSSGGGAAAVTNPEPDQ 1178
sp|Q9Y4C1|KDM3A_HUMAN WGIKANCPCSNRQFKLFSKPASKEDLKQTSLAGEKPTLGAVL----------QQNPS-- 791
sp|Q6PCM1|KDM3A_MOUSE WGIKANCPCSNRQFKLFSKPALKEDLKQTSLSGEKPTLGTMV----------QQSSP-- 791
sp|Q7LBC6|KDM3B_HUMAN VPKADSTDIRSEEPLKTDSSASNSNSELKAIRPPCPDTAPPSSALHWLADLATQKAKEET 1237
tr|B9EKS2|KDM3B_MOUSE VPKGAGTDGRSEEPLKAEGSASNSNSELKAIRPPCPDTAPPSSALHWLADLATQKAKEET 1238
sp|Q9Y4C1|KDM3A_HUMAN ----------VLEPAAVGGE--AASKPAGSMKPACPAS---TSPLNWLADLTSGNVNKEN 836
sp|Q6PCM1|KDM3A_MOUSE ----------VLEPVAVCGE--AASKPASSVKPTCPTS---TSPLNWLADLTSGNVNKEN 836
sp|Q7LBC6|KDM3B_HUMAN KEAGSLRSVLNKESHSPFGLDSFNSTAKVSPLTPKLFNSLLLGPTASNNKTEGSSLRDLL 1297
tr|B9EKS2|KDM3B_MOUSE KDAGSLRSVLNKESHSPFGLDSFNSTAKVSPLTPKLFNSLLLGPTASNSKTEGSSLRDLL 1298
sp|Q9Y4C1|KDM3A_HUMAN KEKQPTMPILKNEIKCLPPLPPLSKS----STVLHTFNSTILTPVSNNN---SGFLRNLL 889
sp|Q6PCM1|KDM3A_MOUSE KEKQLTMPILKNEIKCLPPLPPLNKP----STVLHTFNSTILTPVSNNN---SGFLRNLL 889
sp|Q7LBC6|KDM3B_HUMAN HSGPGKLPQTPLDTGIPFPPVFSTSSAGVKSKASLPNFLDHIIASVVENKKTSDASKRAC 1357
tr|B9EKS2|KDM3B_MOUSE HSGPGKLPQTPLDTGIPFPPVFSSSSAVAKSKASLPDFLDHIIASVVENKKTSDPSKRSC 1358
sp|Q9Y4C1|KDM3A_HUMAN NSSTGKT----------ENGLKNTPKILDDIFASLVQNKTTSDLSKRPQ 928
sp|Q6PCM1|KDM3A_MOUSE NSSTAKT----------ENGLKNTPKILDDIFASLVQNKTSSDSSKRPQ 928
sp|Q7LBC6|KDM3B_HUMAN NLTDTQKEVKEMVMGLNVLDPHTSHSWLCDGRLLCLHDPSNKNNWKIFRECWKQGQPVLV 1417
tr|B9EKS2|KDM3B_MOUSE NLTDTQKEVKEMAMGLNVLDPHTSHSWLCDGRLLCLHDPSNKNNWKIFRECWKQGQPVLV 1418
sp|Q9Y4C1|KDM3A_HUMAN GLT----------IKPSILGFDTPHYWLCDNRLLCLQDPNNKSNWNVFRECWKQGQPVMV 978
sp|Q6PCM1|KDM3A_MOUSE GLT----------IKPSILGFDTPHYWLCDNRLLCLQDPNNKSNWNVFRECWKQGQPVMV 978
sp|Q7LBC6|KDM3B_HUMAN SGVHKKLKSELWKPEAFSQEFGDQDVDLVNCRNCAIISDVKVRDFWDGFEIICKRLRSE- 1476
tr|B9EKS2|KDM3B_MOUSE SGVHKKLKSELWKPEAFSQEFGDQDVDLVNCRNCAIISDVKVRDFWDGFEIICKRLRSE- 1477
sp|Q9Y4C1|KDM3A_HUMAN SGVHHKLNSELWKPESFRKEFGEQEVDLVNCRTNEIITGATVGDFWDGFEDVPNRLKNE- 1037
sp|Q6PCM1|KDM3A_MOUSE SGVHHKLNTELWKPESFRKEFGEQEVDLVNCRTNEIITGATVGDFWDGFEDVPNRLKNDK 1038

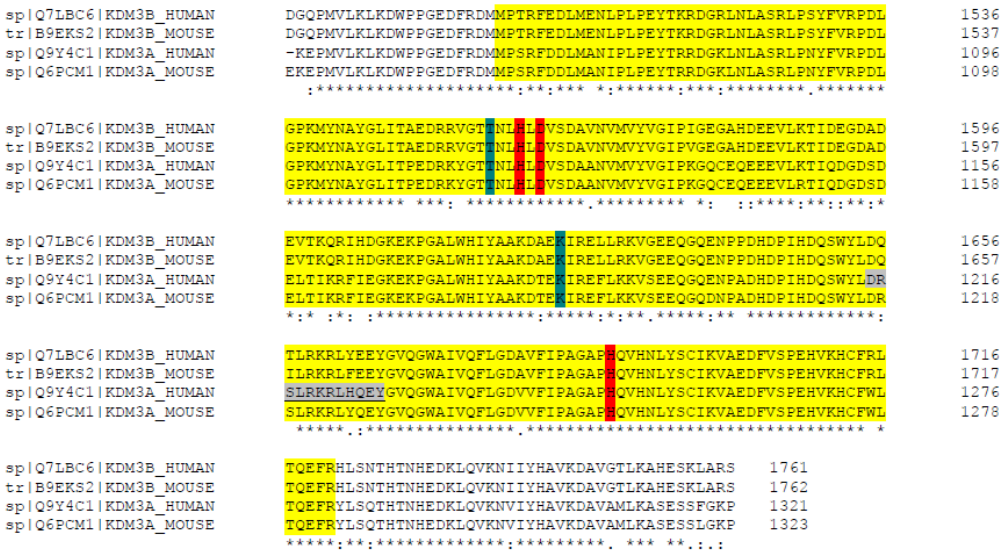

Figure 7.1: Alignment of the human and mouse KDM3A and KDM3B paralogues with Uniprot identifiers: Q7LBC6, B9EKS2, Q9Y4C1 and Q6PCM1.

Highlights: Grey: predicted NLS; light blue: zinc finger; green: nuclear receptor motif; yellow: JmjC domain; red: predicted iron binding sites and dark blue: α-ketoglutarate binding sites.

* indicates fully conserved residue
: indicates residues of strongly similar properties
. indicates residues of weakly similar properties

Alignment of the human and mouse KDM3A and the zebrafish prediction

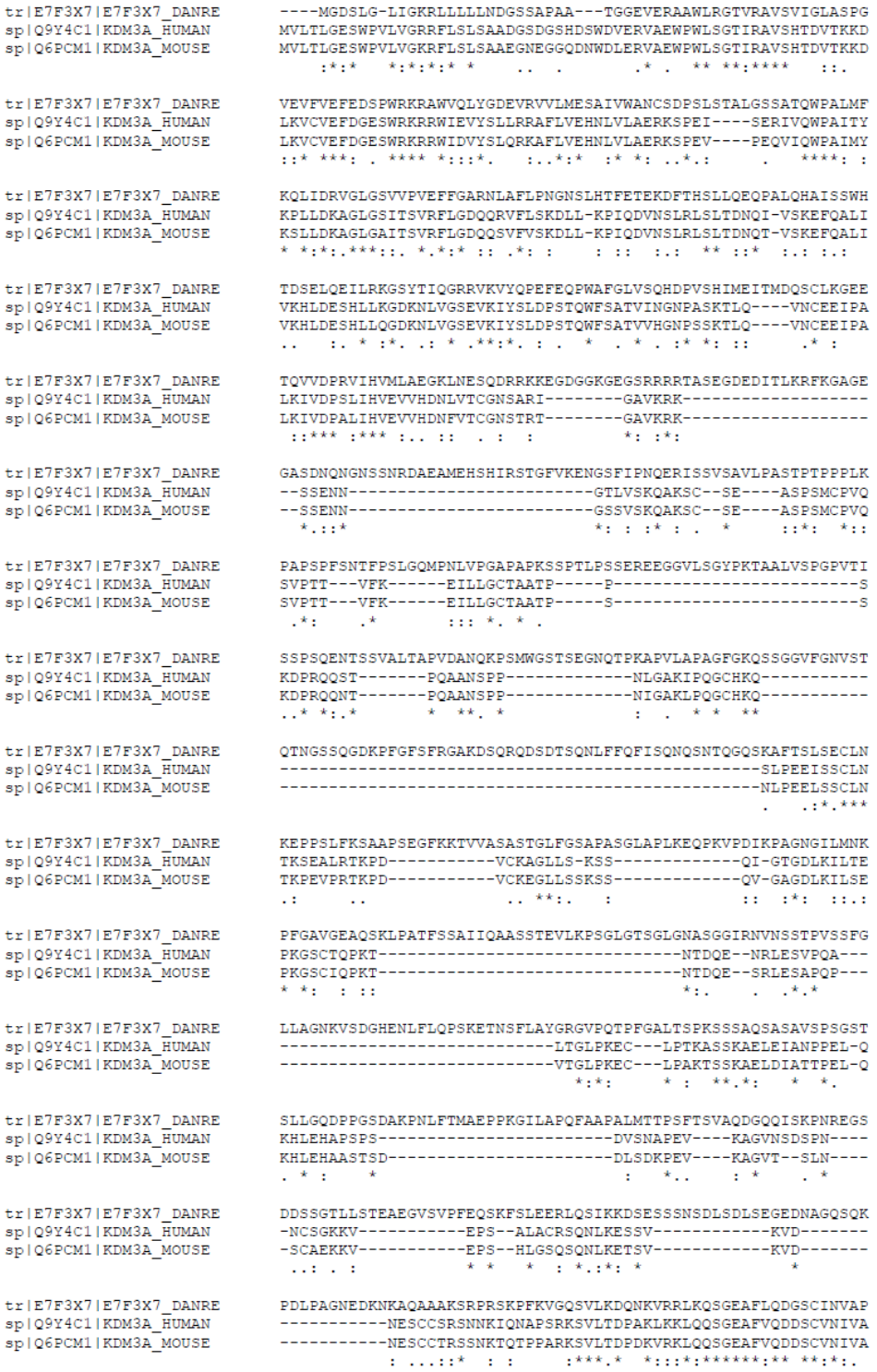

Figure 7.2: Alignment of human and mouse KDM3A and zebrafish prediction with Uniprot identifiers Q9Y4C1, Q6PCM1 and E7F3X7 respectively.

Highlights: Light blue: zinc finger with cysteine residues in grey; green: nuclear receptor motif; dark grey: the two amino acids missing in GFP-Zf-3bΔ2aa; yellow:

JmjC domain; brown: hypothetical zebrafish JmjC domain; red: predicted iron binding sites and dark blue: α-ketoglutarate binding sites.

* indicates fully conserved residue
: indicates residues of strongly similar properties
. indicates residues of weakly similar properties

Alignment of the human and mouse KDM3B and the zebrafish prediction

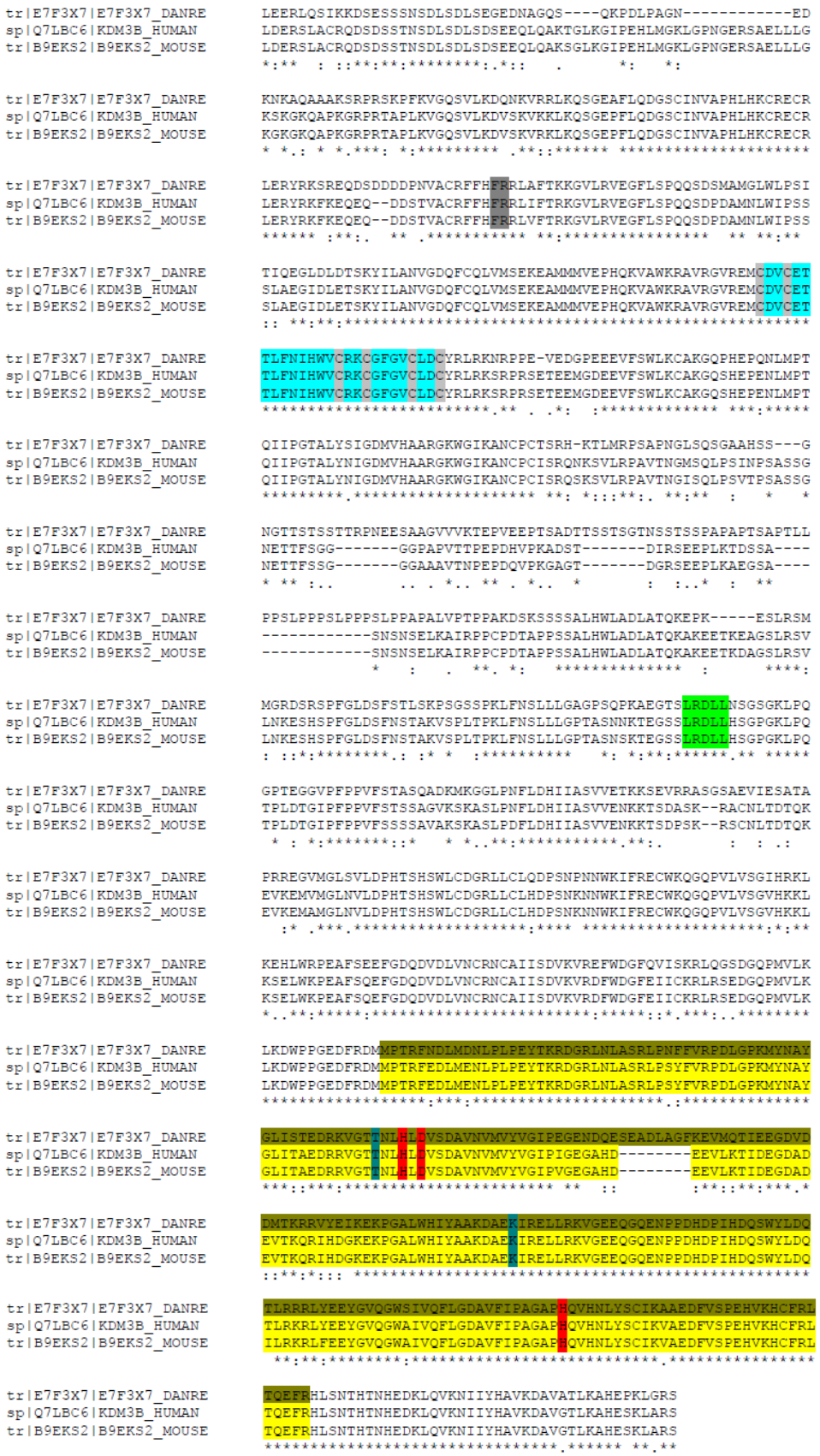
tr|E7F3X7|E7F3X7_DANRE
sp|Q7LBC6|KDM3B_HUMAN
tr|B9EKS2|B9EKS2_MOUSE

Figure 7.3: Alignment of human and mouse KDM3B and zebrafish prediction with Uniprot identifiers Q7LBC6, B9EKS2 and E7F3X7 respectively.
Highlights: Purple: predicted NLS by the NLStradamus software; blue: zinc finger with cysteine residues in grey; green: nuclear receptor motif; dark grey: the two amino acids missing in GFP-Zf-3bΔ2aa; yellow: JmjC domain; brown: hypothetical zebrafish JmjC domain; red: predicted iron binding sites and dark blue: α-ketoglutarate binding sites.

* indicates fully conserved residue
: indicates residues of strongly similar properties
. indicates residues of weakly similar properties

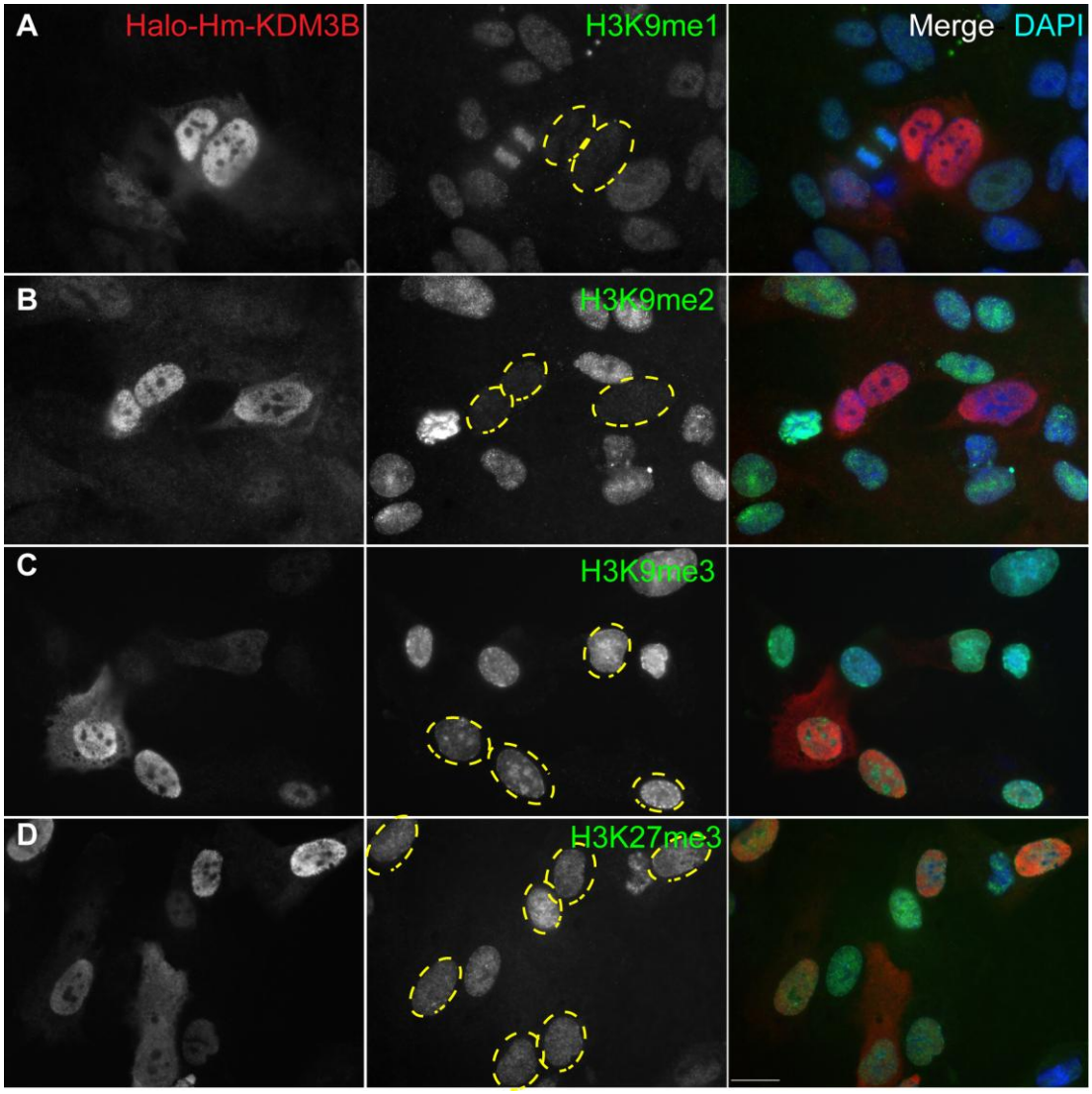

Figure 7.4: Halo-Hm-KDM3B can function as an H3K9me1/2 demethylase. (**A-B**) The Halo-Hm-KDM3B transfected cells reduce H3K9me1 and H3K9me2 fluorescence compared to neighbouring untransfected cells. (**C**) The H3K9me3 mark formed puncta in two out of four cells upon Halo-Hm-Kdm3b transfection. (**D**) The H3K27me3 mark remained unaffected. Yellow circles indicate nuclei of transfected cells. Scale bar: 20μm.

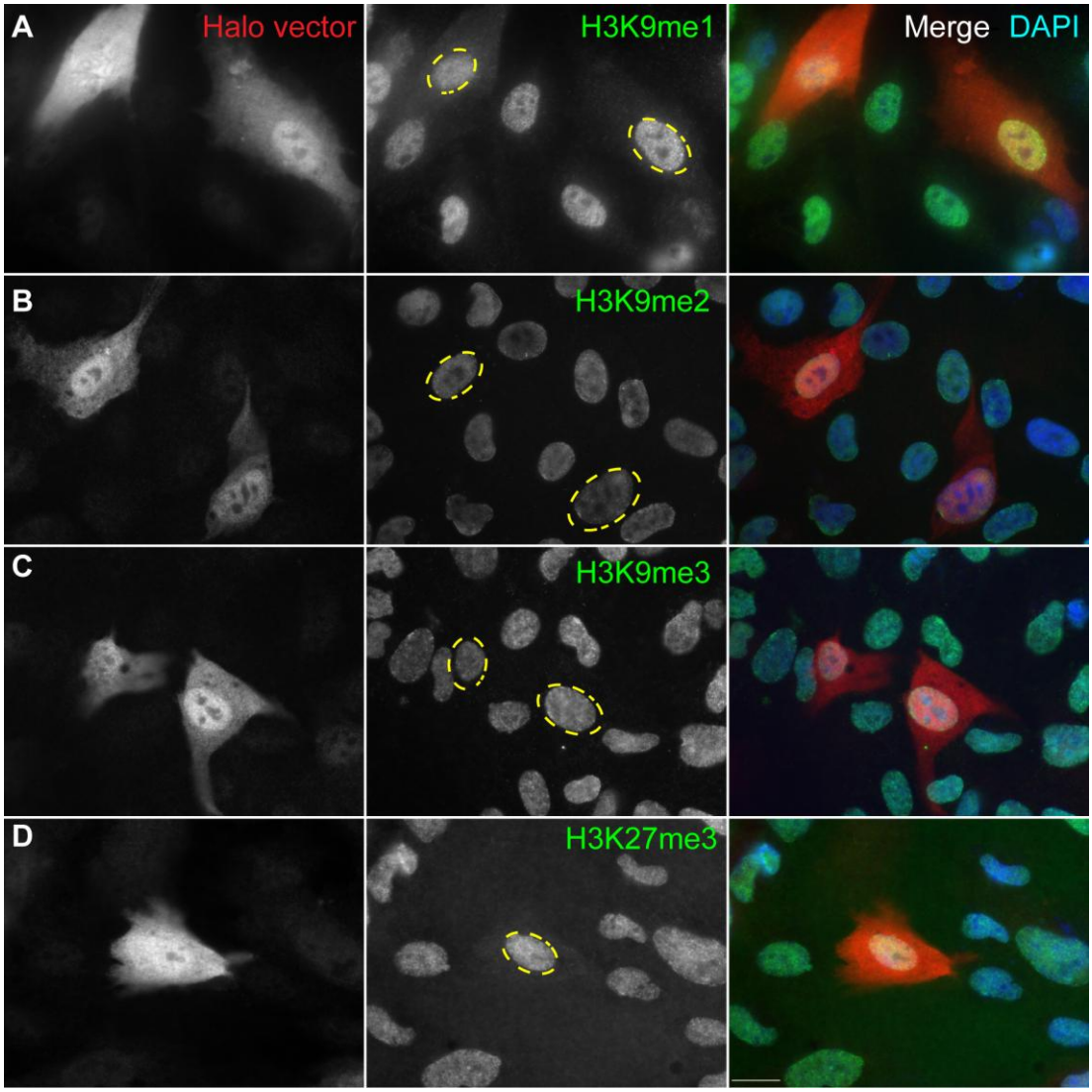

Figure 7.5: The Halo vector transfections did not affect the fluorescence of the epigenetic marks.
(**A-D**) The fluorescence of epigenetic marks remained unchanged in Halo vector transfected and neighbouring untransfected cells. Yellow circles indicate nuclei of transfected cells. Scale bar: 20μm.

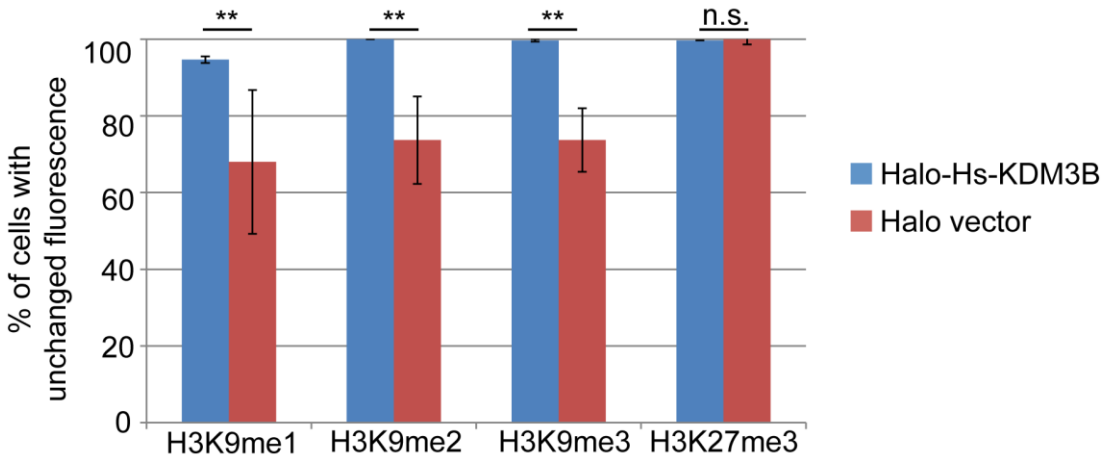

Figure 7.6: In 10% FCS growth media, the Halo-Hm-KDM3B can function as an H3K9me1 and H3K9me2 demethylase.
Thirty two percent (32%) and 26% of Halo-Hm-KDM3B transfected cells showed reduced H3K9me1 and H3K9me2 fluorescence respectively. In addition, 26% of Halo-Hm-KDM3B transfected cells showed a punctuated H3K9me3 pattern. There was no change in fluorescence for the control H3K27me3 mark. Compared to the Halo vector transfections, the results for H3K9me1, H3K9me2 and H3K9me3 were significant. The experiment was repeated in triplicate. ** = significant, Fisher's exact test $p < 0.05$. Error bars represent ± standard error.

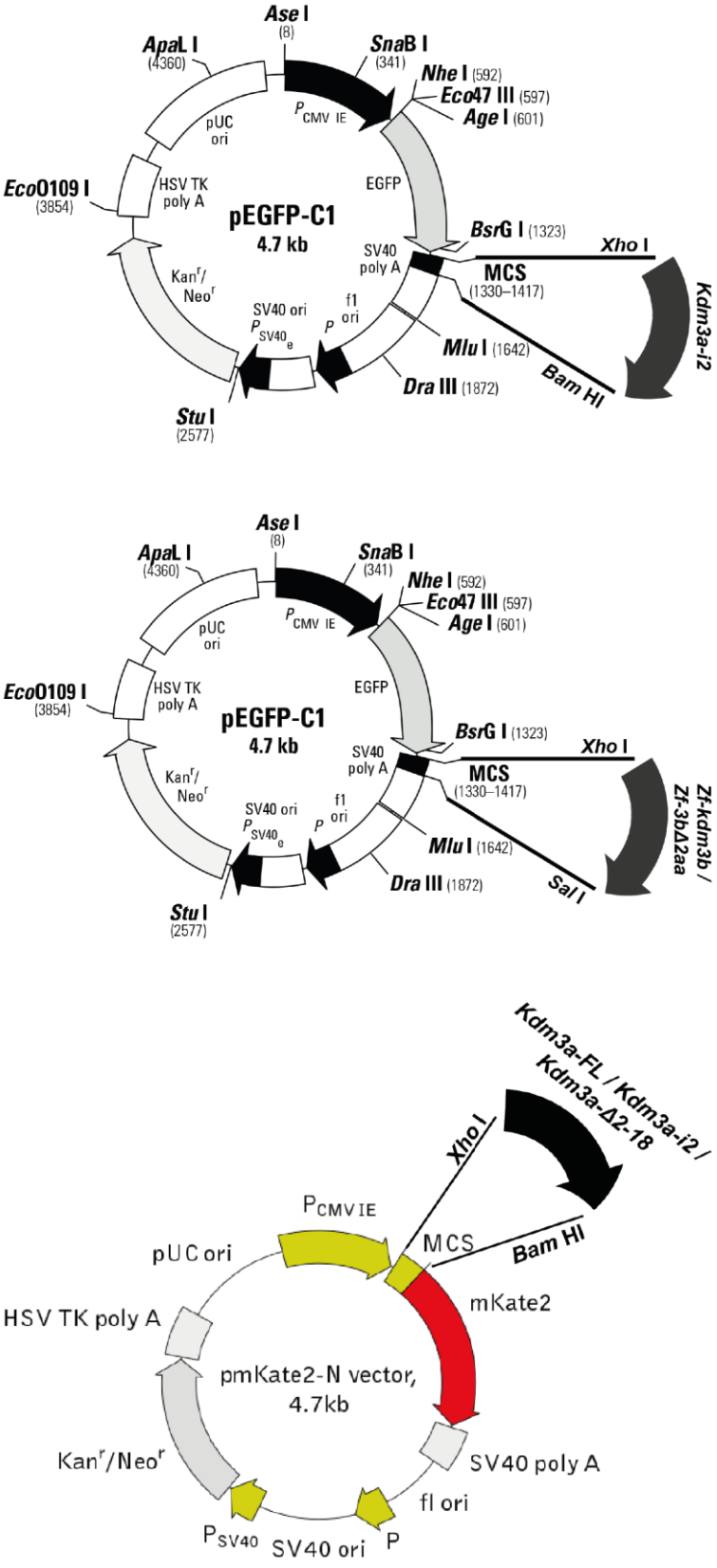

Figure 7.7: Vector maps with cloning sites for the Kdm3 constructs.

The murine *Kdm3a-i2* isoform and the zebrafish *kdm3b* transcripts were subcloned in the pEFGP-C1 vector (Clontech, 6084-1). The Kdm3a-FL, Kdm3a-i2 and Kdm3a-Δ2-18 transcripts were subcloned in an mKate2 (RFP) vector (Evrogen, FP182). Vector maps adapted from www.clontech.com and www.evrogen.com, and modified to show the site of transcript insertion, as well as the restriction sites utilised.

References

Abd-El-Barr, M. M., Sykoudis, K., Andrabi, S., Eichers, E. R., Pennesi, M. E., Tan, P. L., Wilson, J. H., Katsanis, N., Lupski, J. R. and Wu, S. M. (2007). Impaired photoreceptor protein transport and synaptic transmission in a mouse model of Bardet-Biedl syndrome. *Vision Res.* 47, 3394–3407.

Ahmad, W., Faiyaz ul Haque, M., Brancolini, V., Tsou, H. C., ul Haque, S., Lam, H., Aita, V. M., Owen, J., deBlaquiere, M., Frank, J., et al. (1998). Alopecia universalis associated with a mutation in the human hairless gene. *Science* 279, 720–724.

Alba, M. and Salvatori, R. (2004). A mouse with targeted ablation of the growth hormone-releasing hormone gene: a new model of isolated growth hormone deficiency. *Endocrinology* 145, 4134–4143.

Aranda, A. and Pascual, A. (2001). Nuclear hormone receptors and gene expression. *Physiol. Rev.* 81, 1269–1304.

Barrionuevo, F., Bagheri-Fam, S., Klattig, J., Kist, R., Taketo, M. M., Englert, C. and Scherer, G. (2006). Homozygous inactivation of Sox9 causes complete XY sex reversal in mice. *Biol. Reprod.* 74, 195–201.

Beaudoin, G. M. J., 3rd, Sisk, J. M., Coulombe, P. A. and Thompson, C. C. (2005). Hairless triggers reactivation of hair growth by promoting Wnt signaling. *Proc. Natl. Acad. Sci. U. S. A.* 102, 14653–14658.

Berbari, N. F., O'Connor, A. K., Haycraft, C. J. and Yoder, B. K. (2009). The primary cilium as a complex signaling center. *Curr. Biol. CB* 19, R526–535.

Beschorner, W. E., Divic, J., Pulido, H., Yao, X., Kenworthy, P. and Bruce, G. (1991). Enhancement of thymic recovery after cyclosporine by recombinant human growth hormone and insulin-like growth factor I. *Transplantation* 52, 879–884.

Bhandoola, A., von Boehmer, H., Petrie, H. T. and Zúñiga-Pflücker, J. C. (2007). Commitment and developmental potential of extrathymic and intrathymic T cell precursors: plenty to choose from. *Immunity* 26, 678–689.

Bicknell, L. S., Bongers, E. M. H. F., Leitch, A., Brown, S., Schoots, J., Harley, M. E., Aftimos, S., Al-Aama, J. Y., Bober, M., Brown, P. A. J., et al. (2011). Mutations in the pre-replication complex cause Meier-Gorlin syndrome. *Nat. Genet.* 43, 356–359.

Binz, K., Joller, P., Froesch, P., Binz, H., Zapf, J. and Froesch, E. R. (1990). Repopulation of the atrophied thymus in diabetic rats by insulin-like growth factor I. *Proc. Natl. Acad. Sci. U. S. A.* 87, 3690–3694.

Black, J. C., Van Rechem, C. and Whetstine, J. R. (2012). Histone lysine methylation dynamics: establishment, regulation, and biological impact. *Mol. Cell* 48, 491–507.

Brandt, S. J. and Koury, M. J. (2009). Regulation of LMO2 mRNA and protein expression in erythroid differentiation. *Haematologica* 94, 447–448.

Brauchle, M., Yao, Z., Arora, R., Thigale, S., Clay, I., Inverardi, B., Fletcher, J., Taslimi, P., Acker, M. G., Gerrits, B., et al. (2013). Protein complex interactor analysis and differential activity of KDM3 subfamily members towards H3K9 methylation. *PloS One* 8, e60549.

Bremang, M., Cuomo, A., Agresta, A. M., Stugiewicz, M., Spadotto, V. and Bonaldi, T. (2013). Mass spectrometry-based identification and characterisation of lysine and arginine methylation in the human proteome. *Mol. Biosyst.* 9, 2231–2247.

Brent, G. A. (2012). Mechanisms of thyroid hormone action. *J. Clin. Invest.* 122, 3035–3043.

Briggs, S. D., Bryk, M., Strahl, B. D., Cheung, W. L., Davie, J. K., Dent, S. Y., Winston, F. and Allis, C. D. (2001). Histone H3 lysine 4 methylation is mediated by Set1 and required for cell growth and rDNA silencing in Saccharomyces cerevisiae. *Genes Dev.* 15, 3286–3295.

Brooks, A. J. and Waters, M. J. (2010). The growth hormone receptor: mechanism of activation and clinical implications. *Nat. Rev. Endocrinol.* 6, 515–525.

Cachón-González, M. B., San-José, I., Cano, A., Vega, J. A., García, N., Freeman, T., Schimmang, T. and Stoye, J. P. (1999). The hairless gene of the mouse: relationship of phenotypic effects with expression profile and genotype. *Dev. Dyn. Off. Publ. Am. Assoc. Anat.* 216, 113–126.

Chaturvedi, C.-P., Somasundaram, B., Singh, K., Carpenedo, R. L., Stanford, W. L., Dilworth, F. J. and Brand, M. (2012). Maintenance of gene silencing by the coordinate action of the H3K9 methyltransferase G9a/KMT1C and the H3K4 demethylase Jarid1a/KDM5A. *Proc. Natl. Acad. Sci. U. S. A.* 109, 18845–18850.

Chuikov, S., Kurash, J. K., Wilson, J. R., Xiao, B., Justin, N., Ivanov, G. S., McKinney, K., Tempst, P., Prives, C., Gamblin, S. J., et al. (2004). Regulation of p53 activity through lysine methylation. *Nature* 432, 353–360.

Ciofani, M. and Zúñiga-Pflücker, J. C. (2007). The thymus as an inductive site for T lymphopoiesis. *Annu. Rev. Cell Dev. Biol.* 23, 463–493.

Clarke, S. G. (2013). Protein methylation at the surface and buried deep: thinking outside the histone box. *Trends Biochem. Sci.* 38, 243–252.

Clemmons, D. R. (1997). Insulin-like growth factor binding proteins and their role in controlling IGF actions. *Cytokine Growth Factor Rev.* 8, 45–62.

Clissold, P. M. and Ponting, C. P. (2001). JmjC: cupin metalloenzyme-like domains in jumonji, hairless and phospholipase A2beta. *Trends Biochem. Sci.* 26, 7–9.

Cloos, P. A. C., Christensen, J., Agger, K., Maiolica, A., Rappsilber, J., Antal, T., Hansen, K. H. and Helin, K. (2006). The putative oncogene GASC1 demethylates tri- and dimethylated lysine 9 on histone H3. *Nature* 442, 307–311.

Cooper, S. J., Trinklein, N. D., Anton, E. D., Nguyen, L. and Myers, R. M. (2006). Comprehensive analysis of transcriptional promoter structure and function in 1% of the human genome. *Genome Res.* 16, 1–10.

Coschigano, K. T., Clemmons, D., Bellush, L. L. and Kopchick, J. J. (2000). Assessment of growth parameters and life span of GHR/BP gene-disrupted mice. *Endocrinology* 141, 2608–2613.

Coschigano, K. T., Holland, A. N., Riders, M. E., List, E. O., Flyvbjerg, A. and Kopchick, J. J. (2003). Deletion, but not antagonism, of the mouse growth hormone receptor results in severely decreased body weights, insulin, and insulin-like growth factor I levels and increased life span. *Endocrinology* 144, 3799–3810.

Coster, G. and Goldberg, M. (2010). The cellular response to DNA damage: a focus on MDC1 and its interacting proteins. *Nucl. Austin Tex* 1, 166–178.

Dam, A. H. D. M., Feenstra, I., Westphal, J. R., Ramos, L., van Golde, R. J. T. and Kremer, J. A. M. (2007). Globozoospermia revisited. *Hum. Reprod. Update* 13, 63–75.

Dayan, C. M. and Panicker, V. (2009). Novel insights into thyroid hormones from the study of common genetic variation. *Nat. Rev. Endocrinol.* 5, 211–218.

DeChiara, T. M., Efstratiadis, A. and Robertson, E. J. (1990). A growth-deficiency phenotype in heterozygous mice carrying an insulin-like growth factor II gene disrupted by targeting. *Nature* 345, 78–80.

De Gendt, K., Swinnen, J. V., Saunders, P. T. K., Schoonjans, L., Dewerchin, M., Devos, A., Tan, K., Atanassova, N., Claessens, F., Lécureuil, C., et al. (2004). A Sertoli cell-selective knockout of the androgen receptor causes spermatogenic arrest in meiosis. *Proc. Natl. Acad. Sci. U. S. A.* 101, 1327–1332.

Delaval, B. and Doxsey, S. J. (2010). Pericentrin in cellular function and disease. *J. Cell Biol.* 188, 181–190.

D'Ercole, A. J., Stiles, A. D. and Underwood, L. E. (1984). Tissue concentrations of somatomedin C: further evidence for multiple sites of synthesis and paracrine or autocrine mechanisms of action. *Proc. Natl. Acad. Sci. U. S. A.* 81, 935–939.

Di Lorenzo, A. and Bedford, M. T. (2011). Histone arginine methylation. *FEBS Lett.* 585, 2024–2031.

Dunwell, J. M., Culham, A., Carter, C. E., Sosa-Aguirre, C. R. and Goodenough, P. W. (2001). Evolution of functional diversity in the cupin superfamily. *Trends Biochem. Sci.* 26, 740–746.

Dunwell, J. M., Purvis, A. and Khuri, S. (2004). Cupins: the most functionally diverse protein superfamily? *Phytochemistry* 65, 7–17.

Efstratiadis, A. (1998). Genetics of mouse growth. *Int. J. Dev. Biol.* 42, 955–976.

Egorova, K. S., Olenkina, O. M. and Olenina, L. V. (2010). Lysine methylation of nonhistone proteins is a way to regulate their stability and function. *Biochem. Biokhimiia* 75, 535–548.

Eicher, E. M. and Beamer, W. G. (1976). Inherited ateliotic dwarfism in mice. Characteristics of the mutation, little, on chromosome 6. *J. Hered.* 67, 87–91.

Ellis, P., Fagan, B. M., Magness, S. T., Hutton, S., Taranova, O., Hayashi, S., McMahon, A., Rao, M. and Pevny, L. (2004). SOX2, a persistent marker for multipotential neural stem cells derived from embryonic stem cells, the embryo or the adult. *Dev. Neurosci.* 26, 148–165.

Fabris, N., Pierpaoli, W. and Sorkin, E. (1971). Hormones and the immunological capacity. 3. The immunodeficiency disease of the hypopituitary Snell-Bagg dwarf mouse. *Clin. Exp. Immunol.* 9, 209–225.

Finkielstain, G. P., Forcinito, P., Lui, J. C. K., Barnes, K. M., Marino, R., Makaroun, S., Nguyen, V., Lazarus, J. E., Nilsson, O. and Baron, J. (2009). An extensive genetic program occurring during postnatal growth in multiple tissues. *Endocrinology* 150, 1791–1800.

Flurkey, K., Papaconstantinou, J., Miller, R. A. and Harrison, D. E. (2001). Lifespan extension and delayed immune and collagen aging in mutant mice with defects in growth hormone production. *Proc. Natl. Acad. Sci. U. S. A.* 98, 6736–6741.

Fraichard, A., Chassande, O., Plateroti, M., Roux, J. P., Trouillas, J., Dehay, C., Legrand, C., Gauthier, K., Kedinger, M., Malaval, L., et al. (1997). The T3R alpha gene encoding a thyroid hormone receptor is essential for post-natal development and thyroid hormone production. *EMBO J.* 16, 4412–4420.

Fuller, S. D., Gowen, B. E., Reinsch, S., Sawyer, A., Buendia, B., Wepf, R. and Karsenti, E. (1995). The core of the mammalian centriole contains gamma-tubulin. *Curr. Biol. CB* 5, 1384–1393.

García-Atares, N., San Jose, I., Cabo, R., Vega, J. A. and Represa, J. (1998). Changes in the cerebellar cortex of hairless Rhino-J mice (hr-rh-j). *Neurosci. Lett.* 256, 13–16.

García-Suárez, O., Pérez-Pérez, M., Germanà, A., Esteban, I. and Germanà, G. (2003). Involvement of growth factors in thymic involution. *Microsc. Res. Tech.* 62, 514–523.

Gerdes, J. M., Davis, E. E. and Katsanis, N. (2009a). The Vertebrate Primary Cilium in Development, Homeostasis, and Disease. *Cell* 137, 32–45.

Gerdes, J. M., Davis, E. E. and Katsanis, N. (2009b). The vertebrate primary cilium in development, homeostasis, and disease. *Cell* 137, 32–45.

Goetz, S. C. and Anderson, K. V. (2010). The primary cilium: a signalling centre during vertebrate development. *Nat. Rev. Genet.* 11, 331–344.

Greer, E. L. and Shi, Y. (2012). Histone methylation: a dynamic mark in health, disease and inheritance. *Nat. Rev. Genet.* 13, 343–357.

Guernsey, D. L., Jiang, H., Hussin, J., Arnold, M., Bouyakdan, K., Perry, S., Babineau-Sturk, T., Beis, J., Dumas, N., Evans, S. C., et al. (2010). Mutations in centrosomal protein CEP152 in primary microcephaly families linked to MCPH4. *Am. J. Hum. Genet.* 87, 40–51.

Guler, H. P., Zapf, J., Scheiwiller, E. and Froesch, E. R. (1988). Recombinant human insulin-like growth factor I stimulates growth and has distinct effects on organ size in hypophysectomized rats. *Proc. Natl. Acad. Sci. U. S. A.* 85, 4889–4893.

Herrington, J. and Carter-Su, C. (2001). Signaling pathways activated by the growth hormone receptor. *Trends Endocrinol. Metab. TEM* 12, 252–257.

Hildebrandt, F., Benzing, T. and Katsanis, N. (2011). Ciliopathies. *N. Engl. J. Med.* 364, 1533–1543.

Ho, L. and Crabtree, G. R. (2010). Chromatin remodelling during development. *Nature* 463, 474–484.

Holzenberger, M., Dupont, J., Ducos, B., Leneuve, P., Géloën, A., Even, P. C., Cervera, P. and Le Bouc, Y. (2003). IGF-1 receptor regulates lifespan and resistance to oxidative stress in mice. *Nature* 421, 182–187.

Höög, C., Schalling, M., Grunder-Brundell, E. and Daneholt, B. (1991). Analysis of a murine male germ cell-specific transcript that encodes a putative zinc finger protein. *Mol. Reprod. Dev.* 30, 173–181.

Hsieh, J.-C., Sisk, J. M., Jurutka, P. W., Haussler, C. A., Slater, S. A., Haussler, M. R. and Thompson, C. C. (2003). Physical and functional interaction between the vitamin D receptor and hairless corepressor, two proteins required for hair cycling. *J. Biol. Chem.* 278, 38665–38674.

Huang, J., Perez-Burgos, L., Placek, B. J., Sengupta, R., Richter, M., Dorsey, J. A., Kubicek, S., Opravil, S., Jenuwein, T. and Berger, S. L. (2006a). Repression of p53 activity by Smyd2-mediated methylation. *Nature* 444, 629–632.

Huang, J., Perez-Burgos, L., Placek, B. J., Sengupta, R., Richter, M., Dorsey, J. A., Kubicek, S., Opravil, S., Jenuwein, T. and Berger, S. L. (2006b). Repression of p53 activity by Smyd2-mediated methylation. *Nature* 444, 629–632.

Huang, J., Sengupta, R., Espejo, A. B., Lee, M. G., Dorsey, J. A., Richter, M., Opravil, S., Shiekhattar, R., Bedford, M. T., Jenuwein, T., et al. (2007). p53 is regulated by the lysine demethylase LSD1. *Nature* 449, 105–108.

Inagaki, T., Tachibana, M., Magoori, K., Kudo, H., Tanaka, T., Okamura, M., Naito, M., Kodama, T., Shinkai, Y. and Sakai, J. (2009). Obesity and metabolic syndrome in histone demethylase JHDM2a-deficient mice. *Genes Cells Devoted Mol. Cell. Mech.* 14, 991–1001.

Ishikawa, H. and Marshall, W. F. (2011). Ciliogenesis: building the cell's antenna. *Nat. Rev. Mol. Cell Biol.* 12, 222–234.

Iwamori, N., Zhao, M., Meistrich, M. L. and Matzuk, M. M. (2011). The testis-enriched histone demethylase, KDM4D, regulates methylation of histone H3 lysine 9 during spermatogenesis in the mouse but is dispensable for fertility. *Biol. Reprod.* 84, 1225–1234.

Jäger, R. J., Anvret, M., Hall, K. and Scherer, G. (1990). A human XY female with a frame shift mutation in the candidate testis-determining gene SRY. *Nature* 348, 452–454.

Jensen, L. R., Amende, M., Gurok, U., Moser, B., Gimmel, V., Tzschach, A., Janecke, A. R., Tariverdian, G., Chelly, J., Fryns, J.-P., et al. (2005). Mutations in the JARID1C gene, which is involved in transcriptional regulation and chromatin remodeling, cause X-linked mental retardation. *Am. J. Hum. Genet.* 76, 227–236.

Joshi, R. L., Lamothe, B., Cordonnier, N., Mesbah, K., Monthioux, E., Jami, J. and Bucchini, D. (1996). Targeted disruption of the insulin receptor gene in the mouse results in neonatal lethality. *EMBO J.* 15, 1542–1547.

Kappeler, L., De Magalhaes Filho, C., Dupont, J., Leneuve, P., Cervera, P., Périn, L., Loudes, C., Blaise, A., Klein, R., Epelbaum, J., et al. (2008). Brain IGF-1 receptors control mammalian growth and lifespan through a neuroendocrine mechanism. *PLoS Biol.* 6, e254.

Karytinos, A., Forneris, F., Profumo, A., Ciossani, G., Battaglioli, E., Binda, C. and Mattevi, A. (2009). A novel mammalian flavin-dependent histone demethylase. *J. Biol. Chem.* 284, 17775–17782.

Kasioulis, I., Syred, H. M., Tate, P., Finch, A., Shaw, J., Seawright, A., Fuszard, M., Botting, C. H., Shirran, S., Adams, I. R., et al. (2014). Kdm3a lysine demethylase is an Hsp90 client required for cytoskeletal rearrangements during spermatogenesis. *Mol. Biol. Cell*.

Kierszenbaum, A. L. and Tres, L. L. (2004). The acrosome-acroplaxome-manchette complex and the shaping of the spermatid head. *Arch. Histol. Cytol.* 67, 271–284.

Kim, S.-M., Kim, J.-Y., Choe, N.-W., Cho, I.-H., Kim, J.-R., Kim, D.-W., Seol, J.-E., Lee, S. E., Kook, H., Nam, K.-I., et al. (2010). Regulation of mouse steroidogenesis by WHISTLE and JMJD1C through histone methylation balance. *Nucleic Acids Res.* 38, 6389–6403.

Kim, J.-Y., Kim, K.-B., Eom, G. H., Choe, N., Kee, H. J., Son, H.-J., Oh, S.-T., Kim, D.-W., Pak, J. H., Baek, H. J., et al. (2012). KDM3B is the H3K9 demethylase involved in transcriptional activation of lmo2 in leukemia. *Mol. Cell. Biol.* 32, 2917–2933.

Kleine-Kohlbrecher, D., Christensen, J., Vandamme, J., Abarrategui, I., Bak, M., Tommerup, N., Shi, X., Gozani, O., Rappsilber, J., Salcini, A. E., et al. (2010). A functional link between the histone demethylase PHF8 and the transcription factor ZNF711 in X-linked mental retardation. *Mol. Cell* 38, 165–178.

Klingseisen, A. and Jackson, A. P. (2011). Mechanisms and pathways of growth failure in primordial dwarfism. *Genes Dev.* 25, 2011–2024.

Klose, R. J. and Zhang, Y. (2007). Regulation of histone methylation by demethylimination and demethylation. *Nat. Rev. Mol. Cell Biol.* 8, 307–318.

Klose, R. J., Yamane, K., Bae, Y., Zhang, D., Erdjument-Bromage, H., Tempst, P., Wong, J. and Zhang, Y. (2006a). The transcriptional repressor JHDM3A demethylates trimethyl histone H3 lysine 9 and lysine 36. *Nature* 442, 312–316.

Klose, R. J., Kallin, E. M. and Zhang, Y. (2006b). JmjC-domain-containing proteins and histone demethylation. *Nat. Rev. Genet.* 7, 715–727.

Klose, R. J., Gardner, K. E., Liang, G., Erdjument-Bromage, H., Tempst, P. and Zhang, Y. (2007). Demethylation of histone H3K36 and H3K9 by Rph1: a vestige of an H3K9 methylation system in Saccharomyces cerevisiae? *Mol. Cell. Biol.* 27, 3951–3961.

Kooistra, S. M. and Helin, K. (2012). Molecular mechanisms and potential functions of histone demethylases. *Nat. Rev. Mol. Cell Biol.* 13, 297–311.

Kornberg, R. D. (1977). Structure of chromatin. *Annu. Rev. Biochem.* 46, 931–954.

Kosugi, S., Hasebe, M., Tomita, M. and Yanagawa, H. (2009). Systematic identification of cell cycle-dependent yeast nucleocytoplasmic shuttling proteins by prediction of composite motifs. *Proc. Natl. Acad. Sci. U. S. A.* 106, 10171–10176.

Kouzarides, T. (2007). Chromatin modifications and their function. *Cell* 128, 693–705.

Kruse, R., Cichon, S., Anker, M., Hillmer, A. M., Barros-Núñez, P., Cantú, J. M., Leal, E., Weinlich, G., Schmuth, M., Fritsch, P., et al. (1999). Novel Hairless mutations in two kindreds with autosomal recessive papular atrichia. *J. Invest. Dermatol.* 113, 954–959.

Kulaga, H. M., Leitch, C. C., Eichers, E. R., Badano, J. L., Lesemann, A., Hoskins, B. E., Lupski, J. R., Beales, P. L., Reed, R. R. and Katsanis, N. (2004). Loss of BBS proteins causes anosmia in humans and defects in olfactory cilia structure and function in the mouse. *Nat. Genet.* 36, 994–998.

Kumpf, S., Mihlan, M., Goginashvili, A., Grandl, G., Gehart, H., Godel, A., Schmidt, J., Müller, J., Bezzi, M., Ittner, A., et al. (2012). Hairless promotes PPARγ expression and is required for white adipogenesis. *EMBO Rep.* 13, 1012–1020.

Kuroki, S., Matoba, S., Akiyoshi, M., Matsumura, Y., Miyachi, H., Mise, N., Abe, K., Ogura, A., Wilhelm, D., Koopman, P., et al. (2013a). Epigenetic regulation of mouse sex determination by the histone demethylase Jmjd1a. *Science* 341, 1106–1109.

Kuroki, S., Akiyoshi, M., Tokura, M., Miyachi, H., Nakai, Y., Kimura, H., Shinkai, Y. and Tachibana, M. (2013b). JMJD1C, a JmjC domain-containing protein, is required for long-term maintenance of male germ cells in mice. *Biol. Reprod.* 89, 93.

Kwan, A. Y. M. and Hartman, M. L. (2007). IGF-I measurements in the diagnosis of adult growth hormone deficiency. *Pituitary* 10, 151–157.

Lange, A., Mills, R. E., Lange, C. J., Stewart, M., Devine, S. E. and Corbett, A. H. (2007). Classical nuclear localization signals: definition, function, and interaction with importin alpha. *J. Biol. Chem.* 282, 5101–5105.

Laumonnier, F., Holbert, S., Ronce, N., Faravelli, F., Lenzner, S., Schwartz, C. E., Lespinasse, J., Van Esch, H., Lacombe, D., Goizet, C., et al. (2005). Mutations in PHF8 are associated with X linked mental retardation and cleft lip/cleft palate. *J. Med. Genet.* 42, 780–786.

Lee, V. D. and Huang, B. (1993). Molecular cloning and centrosomal localization of human caltractin. *Proc. Natl. Acad. Sci. U. S. A.* 90, 11039–11043.

Liang, G., Klose, R. J., Gardner, K. E. and Zhang, Y. (2007). Yeast Jhd2p is a histone H3 Lys4 trimethyl demethylase. *Nat. Struct. Mol. Biol.* 14, 243–245.

Lin, H., Wang, Y., Wang, Y., Tian, F., Pu, P., Yu, Y., Mao, H., Yang, Y., Wang, P., Hu, L., et al. (2010). Coordinated regulation of active and repressive histone methylations by a dual-specificity histone demethylase ceKDM7A from Caenorhabditis elegans. *Cell Res.* 20, 899–907.

Lind, E. F., Prockop, S. E., Porritt, H. E. and Petrie, H. T. (2001). Mapping precursor movement through the postnatal thymus reveals specific microenvironments supporting defined stages of early lymphoid development. *J. Exp. Med.* 194, 127–134.

Litt, M. D., Simpson, M., Gaszner, M., Allis, C. D. and Felsenfeld, G. (2001). Correlation between histone lysine methylation and developmental changes at the chicken beta-globin locus. *Science* 293, 2453–2455.

Liu, J. P., Baker, J., Perkins, A. S., Robertson, E. J. and Efstratiadis, A. (1993). Mice carrying null mutations of the genes encoding insulin-like growth factor I (Igf-1) and type 1 IGF receptor (Igf1r). *Cell* 75, 59–72.

Liu, Z., Zhou, S., Liao, L., Chen, X., Meistrich, M. and Xu, J. (2010a). Jmjd1a demethylase-regulated histone modification is essential for cAMP-response element modulator-regulated gene expression and spermatogenesis. *J. Biol. Chem.* 285, 2758–2770.

Liu, W., Tanasa, B., Tyurina, O. V., Zhou, T. Y., Gassmann, R., Liu, W. T., Ohgi, K. A., Benner, C., Garcia-Bassets, I., Aggarwal, A. K., et al. (2010b). PHF8 mediates histone H4 lysine 20 demethylation events involved in cell cycle progression. *Nature* 466, 508–512.

Liu, L., Kim, H., Casta, A., Kobayashi, Y., Shapiro, L. S. and Christiano, A. M. (2013). Hairless is a histone H3K9 demethylase. *FASEB J. Off. Publ. Fed. Am. Soc. Exp. Biol.*

Loenarz, C. and Schofield, C. J. (2008). Expanding chemical biology of 2-oxoglutarate oxygenases. *Nat. Chem. Biol.* 4, 152–156.

Lois, S., Blanco, N., Martínez-Balbás, M. and de la Cruz, X. (2007). The functional modulation of epigenetic regulators by alternative splicing. *BMC Genomics* 8, 252.

Louvi, A., Accili, D. and Efstratiadis, A. (1997). Growth-promoting interaction of IGF-II with the insulin receptor during mouse embryonic development. *Dev. Biol.* 189, 33–48.

Lowell, B. B. and Spiegelman, B. M. (2000). Towards a molecular understanding of adaptive thermogenesis. *Nature* 404, 652–660.

Lu, T., Jackson, M. W., Wang, B., Yang, M., Chance, M. R., Miyagi, M., Gudkov, A. V. and Stark, G. R. (2010). Regulation of NF-kappaB by NSD1/FBXL11-dependent reversible lysine methylation of p65. *Proc. Natl. Acad. Sci. U. S. A.* 107, 46–51.

Luger, K., Mäder, A. W., Richmond, R. K., Sargent, D. F. and Richmond, T. J. (1997). Crystal structure of the nucleosome core particle at 2.8 A resolution. *Nature* 389, 251–260.

Lui, J. C., Forcinito, P., Chang, M., Chen, W., Barnes, K. M. and Baron, J. (2010). Coordinated postnatal down-regulation of multiple growth-promoting genes: evidence for a genetic program limiting organ growth. *FASEB J. Off. Publ. Fed. Am. Soc. Exp. Biol.* 24, 3083–3092.

Lupu, F., Terwilliger, J. D., Lee, K., Segre, G. V. and Efstratiadis, A. (2001). Roles of growth hormone and insulin-like growth factor 1 in mouse postnatal growth. *Dev. Biol.* 229, 141–162.

Martin, C. and Zhang, Y. (2005). The diverse functions of histone lysine methylation. *Nat. Rev. Mol. Cell Biol.* 6, 838–849.

Mayo, K. E. (1992). Molecular cloning and expression of a pituitary-specific receptor for growth hormone-releasing hormone. *Mol. Endocrinol. Baltim. Md* 6, 1734–1744.

Metzger, E., Wissmann, M., Yin, N., Müller, J. M., Schneider, R., Peters, A. H. F. M., Günther, T., Buettner, R. and Schüle, R. (2005). LSD1 demethylates repressive histone marks to promote androgen-receptor-dependent transcription. *Nature* 437, 436–439.

Miller, S. A., Mohn, S. E. and Weinmann, A. S. (2010). Jmjd3 and UTX play a demethylase-independent role in chromatin remodeling to regulate T-box family member-dependent gene expression. *Mol. Cell* 40, 594–605.

Mochizuki, T., Wu, G., Hayashi, T., Xenophontos, S. L., Veldhuisen, B., Saris, J. J., Reynolds, D. M., Cai, Y., Gabow, P. A., Pierides, A., et al. (1996). PKD2, a

gene for polycystic kidney disease that encodes an integral membrane protein. *Science* 272, 1339–1342.

Müller, J., Hart, C. M., Francis, N. J., Vargas, M. L., Sengupta, A., Wild, B., Miller, E. L., O'Connor, M. B., Kingston, R. E. and Simon, J. A. (2002). Histone methyltransferase activity of a Drosophila Polycomb group repressor complex. *Cell* 111, 197–208.

Murphy, W. J., Durum, S. K. and Longo, D. L. (1992). Role of neuroendocrine hormones in murine T cell development. Growth hormone exerts thymopoietic effects in vivo. *J. Immunol. Baltim. Md 1950* 149, 3851–3857.

Nakayama, J., Rice, J. C., Strahl, B. D., Allis, C. D. and Grewal, S. I. (2001). Role of histone H3 lysine 9 methylation in epigenetic control of heterochromatin assembly. *Science* 292, 110–113.

Nguyen Ba, A. N., Pogoutse, A., Provart, N. and Moses, A. M. (2009). NLStradamus: a simple Hidden Markov Model for nuclear localization signal prediction. *BMC Bioinformatics* 10, 202.

Nigg, E. A. and Raff, J. W. (2009). Centrioles, centrosomes, and cilia in health and disease. *Cell* 139, 663–678.

Noma K, Allis, C. D. and Grewal, S. I. (2001). Transitions in distinct histone H3 methylation patterns at the heterochromatin domain boundaries. *Science* 293, 1150–1155.

Notini, A. J., Davey, R. A., McManus, J. F., Bate, K. L. and Zajac, J. D. (2005). Genomic actions of the androgen receptor are required for normal male sexual differentiation in a mouse model. *J. Mol. Endocrinol.* 35, 547–555.

O'Driscoll, M., Ruiz-Perez, V. L., Woods, C. G., Jeggo, P. A. and Goodship, J. A. (2003). A splicing mutation affecting expression of ataxia-telangiectasia and Rad3-related protein (ATR) results in Seckel syndrome. *Nat. Genet.* 33, 497–501.

Oetting, A. and Yen, P. M. (2007). New insights into thyroid hormone action. *Best Pract. Res. Clin. Endocrinol. Metab.* 21, 193–208.

Okada, Y., Scott, G., Ray, M. K., Mishina, Y. and Zhang, Y. (2007). Histone demethylase JHDM2A is critical for Tnp1 and Prm1 transcription and spermatogenesis. *Nature* 450, 119–123.

Okada, Y., Tateishi, K. and Zhang, Y. (2010). Histone demethylase JHDM2A is involved in male infertility and obesity. *J. Androl.* 31, 75–78.

Park, S. H., Zhu, P.-P., Parker, R. L. and Blackstone, C. (2010). Hereditary spastic paraplegia proteins REEP1, spastin, and atlastin-1 coordinate microtubule interactions with the tubular ER network. *J. Clin. Invest.* 120, 1097–1110.

Pasini, D., Cloos, P. A. C., Walfridsson, J., Olsson, L., Bukowski, J.-P., Johansen, J. V., Bak, M., Tommerup, N., Rappsilber, J. and Helin, K. (2010). JARID2 regulates binding of the Polycomb repressive complex 2 to target genes in ES cells. *Nature* 464, 306–310.

Pazour, G. J., Baker, S. A., Deane, J. A., Cole, D. G., Dickert, B. L., Rosenbaum, J. L., Witman, G. B. and Besharse, J. C. (2002). The intraflagellar transport protein, IFT88, is essential for vertebrate photoreceptor assembly and maintenance. *J. Cell Biol.* 157, 103–113.

Pekowska, A., Benoukraf, T., Zacarias-Cabeza, J., Belhocine, M., Koch, F., Holota, H., Imbert, J., Andrau, J.-C., Ferrier, P. and Spicuglia, S. (2011). H3K4 tri-methylation provides an epigenetic signature of active enhancers. *EMBO J.* 30, 4198–4210.

Petrie, H. T. and Zúñiga-Pflücker, J. C. (2007). Zoned out: functional mapping of stromal signaling microenvironments in the thymus. *Annu. Rev. Immunol.* 25, 649–679.

Plath, K., Fang, J., Mlynarczyk-Evans, S. K., Cao, R., Worringer, K. A., Wang, H., de la Cruz, C. C., Otte, A. P., Panning, B. and Zhang, Y. (2003). Role of histone H3 lysine 27 methylation in X inactivation. *Science* 300, 131–135.

Plotnikova, O. V., Pugacheva, E. N. and Golemis, E. A. (2009). Primary cilia and the cell cycle. *Methods Cell Biol.* 94, 137–160.

Potter, G. B., Beaudoin, G. M., 3rd, DeRenzo, C. L., Zarach, J. M., Chen, S. H. and Thompson, C. C. (2001). The hairless gene mutated in congenital hair loss disorders encodes a novel nuclear receptor corepressor. *Genes Dev.* 15, 2687–2701.

Potter, G. B., Zarach, J. M., Sisk, J. M. and Thompson, C. C. (2002). The thyroid hormone-regulated corepressor hairless associates with histone deacetylases in neonatal rat brain. *Mol. Endocrinol. Baltim. Md* 16, 2547–2560.

Pujic, Z., Omori, Y., Tsujikawa, M., Thisse, B., Thisse, C. and Malicki, J. (2006). Reverse genetic analysis of neurogenesis in the zebrafish retina. *Dev. Biol.* 293, 330–347.

Rauch, A. (2011). The shortest of the short: pericentrin mutations and beyond. *Best Pract. Res. Clin. Endocrinol. Metab.* 25, 125–130.

Reynolds, N., Latos, P., Hynes-Allen, A., Loos, R., Leaford, D., O'Shaughnessy, A., Mosaku, O., Signolet, J., Brennecke, P., Kalkan, T., et al. (2012). NuRD suppresses pluripotency gene expression to promote transcriptional heterogeneity and lineage commitment. *Cell Stem Cell* 10, 583–594.

Rose, S. R., Municchi, G., Barnes, K. M., Kamp, G. A., Uriarte, M. M., Ross, J. L., Cassorla, F. and Cutler, G. B., Jr (1991). Spontaneous growth hormone secretion increases during puberty in normal girls and boys. *J. Clin. Endocrinol. Metab.* 73, 428–435.

Rosen, E. D. and MacDougald, O. A. (2006). Adipocyte differentiation from the inside out. *Nat. Rev. Mol. Cell Biol.* 7, 885–896.

Rudolph, T., Beuch, S. and Reuter, G. (2013). Lysine-specific histone demethylase LSD1 and the dynamic control of chromatin. *Biol. Chem.* 394, 1019–1028.

Sandelin, A., Carninci, P., Lenhard, B., Ponjavic, J., Hayashizaki, Y. and Hume, D. A. (2007). Mammalian RNA polymerase II core promoters: insights from genome-wide studies. *Nat. Rev. Genet.* 8, 424–436.

Santos-Rosa, H., Schneider, R., Bannister, A. J., Sherriff, J., Bernstein, B. E., Emre, N. C. T., Schreiber, S. L., Mellor, J. and Kouzarides, T. (2002). Active genes are tri-methylated at K4 of histone H3. *Nature* 419, 407–411.

Sarjeant, K. and Stephens, J. M. (2012). Adipogenesis. *Cold Spring Harb. Perspect. Biol.* 4, a008417.

Schaft, D., Roguev, A., Kotovic, K. M., Shevchenko, A., Sarov, M., Shevchenko, A., Neugebauer, K. M. and Stewart, A. F. (2003). The histone 3 lysine 36 methyltransferase, SET2, is involved in transcriptional elongation. *Nucleic Acids Res.* 31, 2475–2482.

Schlaitz, A.-L., Thompson, J., Wong, C. C. L., Yates, J. R. and Heald, R. (2013). REEP3/4 ensure endoplasmic reticulum clearance from metaphase chromatin and proper nuclear envelope architecture. *Dev. Cell* 26, 315–323.

Schmitz, S. U., Albert, M., Malatesta, M., Morey, L., Johansen, J. V., Bak, M., Tommerup, N., Abarrategui, I. and Helin, K. (2011). Jarid1b targets genes regulating development and is involved in neural differentiation. *EMBO J.* 30, 4586–4600.

Schneider, L., Clement, C. A., Teilmann, S. C., Pazour, G. J., Hoffmann, E. K., Satir, P. and Christensen, S. T. (2005). PDGFRalphaalpha signaling is regulated through the primary cilium in fibroblasts. *Curr. Biol. CB* 15, 1861–1866.

Schotta, G., Lachner, M., Sarma, K., Ebert, A., Sengupta, R., Reuter, G., Reinberg, D. and Jenuwein, T. (2004). A silencing pathway to induce H3-K9 and H4-K20 trimethylation at constitutive heterochromatin. *Genes Dev.* 18, 1251–1262.

Shi, Y., Lan, F., Matson, C., Mulligan, P., Whetstine, J. R., Cole, P. A., Casero, R. A. and Shi, Y. (2004). Histone demethylation mediated by the nuclear amine oxidase homolog LSD1. *Cell* 119, 941–953.

Shi, X., Kachirskaia, I., Yamaguchi, H., West, L. E., Wen, H., Wang, E. W., Dutta, S., Appella, E. and Gozani, O. (2007). Modulation of p53 function by SET8-mediated methylation at lysine 382. *Mol. Cell* 27, 636–646.

Shin, S. and Janknecht, R. (2007). Activation of androgen receptor by histone demethylases JMJD2A and JMJD2D. *Biochem. Biophys. Res. Commun.* 359, 742–746.

Siddle, K. (2011). Signalling by insulin and IGF receptors: supporting acts and new players. *J. Mol. Endocrinol.* 47, R1–10.

Simon, J. A. and Kingston, R. E. (2009). Mechanisms of polycomb gene silencing: knowns and unknowns. *Nat. Rev. Mol. Cell Biol.* 10, 697–708.

Spicuglia, S. and Vanhille, L. (2012). Chromatin signatures of active enhancers. *Nucl. Austin Tex* 3, 126–131.

Sprecher, E., Bergman, R., Szargel, R., Friedman-Birnbaum, R. and Cohen, N. (1999). Identification of a genetic defect in the hairless gene in atrichia with papular lesions: evidence for phenotypic heterogeneity among inherited atrichias. *Am. J. Hum. Genet.* 64, 1323–1329.

Sroczynska, P., Cruickshank, V. A., Bukowski, J.-P., Miyagi, S., Bagger, F. O., Walfridsson, J., Schuster, M. B., Porse, B. and Helin, K. (2014). shRNA screening identifies JMJD1C as being required for leukemia maintenance. *Blood*.

Stearns, T., Evans, L. and Kirschner, M. (1991). Gamma-tubulin is a highly conserved component of the centrosome. *Cell* 65, 825–836.

Steger, D. J., Lefterova, M. I., Ying, L., Stonestrom, A. J., Schupp, M., Zhuo, D., Vakoc, A. L., Kim, J.-E., Chen, J., Lazar, M. A., et al. (2008). DOT1L/KMT4 recruitment and H3K79 methylation are ubiquitously coupled with gene transcription in mammalian cells. *Mol. Cell. Biol.* 28, 2825–2839.

Stooke-Vaughan, G. A., Huang, P., Hammond, K. L., Schier, A. F. and Whitfield, T. T. (2012). The role of hair cells, cilia and ciliary motility in otolith formation in the zebrafish otic vesicle. *Dev. Camb. Engl.* 139, 1777–1787.

Szymanska, K. and Johnson, C. A. (2012). The transition zone: an essential functional compartment of cilia. *Cilia* 1, 10.

Tan, M., Luo, H., Lee, S., Jin, F., Yang, J. S., Montellier, E., Buchou, T., Cheng, Z., Rousseaux, S., Rajagopal, N., et al. (2011). Identification of 67 histone marks and histone lysine crotonylation as a new type of histone modification. *Cell* 146, 1016–1028.

Taniguchi, C. M., Emanuelli, B. and Kahn, C. R. (2006). Critical nodes in signalling pathways: insights into insulin action. *Nat. Rev. Mol. Cell Biol.* 7, 85–96.

Taranova, O. V., Magness, S. T., Fagan, B. M., Wu, Y., Surzenko, N., Hutton, S. R. and Pevny, L. H. (2006). SOX2 is a dose-dependent regulator of retinal neural progenitor competence. *Genes Dev.* 20, 1187–1202.

Tateishi, K., Okada, Y., Kallin, E. M. and Zhang, Y. (2009). Role of Jhdm2a in regulating metabolic gene expression and obesity resistance. *Nature* 458, 757–761.

Taub, D. D. and Longo, D. L. (2005). Insights into thymic aging and regeneration. *Immunol. Rev.* 205, 72–93.

Taub, D. D., Murphy, W. J. and Longo, D. L. (2010). Rejuvenation of the aging thymus: growth hormone-mediated and ghrelin-mediated signaling pathways. *Curr. Opin. Pharmacol.* 10, 408–424.

Thompson, C. C. (2009). Hairless is a nuclear receptor corepressor essential for skin function. *Nucl. Recept. Signal.* 7, e010.

Thompson, C. C., Sisk, J. M. and Beaudoin, G. M. J., 3rd (2006). Hairless and Wnt signaling: allies in epithelial stem cell differentiation. *Cell Cycle Georget. Tex* 5, 1913–1917.

Toffolo, E., Rusconi, F., Paganini, L., Tortorici, M., Pilotto, S., Heise, C., Verpelli, C., Tedeschi, G., Maffioli, E., Sala, C., et al. (2014). Phosphorylation of neuronal Lysine-Specific Demethylase 1LSD1/KDM1A impairs transcriptional repression by regulating interaction with CoREST and histone deacetylases HDAC1/2. *J. Neurochem.* 128, 603–616.

Tsukada, Y., Fang, J., Erdjument-Bromage, H., Warren, M. E., Borchers, C. H., Tempst, P. and Zhang, Y. (2006). Histone demethylation by a family of JmjC domain-containing proteins. *Nature* 439, 811–816.

Tzschach, A., Lenzner, S., Moser, B., Reinhardt, R., Chelly, J., Fryns, J.-P., Kleefstra, T., Raynaud, M., Turner, G., Ropers, H.-H., et al. (2006). Novel JARID1C/SMCX mutations in patients with X-linked mental retardation. *Hum. Mutat.* 27, 389.

Ueki, I., Ooi, G. T., Tremblay, M. L., Hurst, K. R., Bach, L. A. and Boisclair, Y. R. (2000). Inactivation of the acid labile subunit gene in mice results in mild retardation of postnatal growth despite profound disruptions in the circulating insulin-like growth factor system. *Proc. Natl. Acad. Sci. U. S. A.* 97, 6868–6873.

Van Haaften, G., Dalgliesh, G. L., Davies, H., Chen, L., Bignell, G., Greenman, C., Edkins, S., Hardy, C., O'Meara, S., Teague, J., et al. (2009). Somatic mutations of the histone H3K27 demethylase gene UTX in human cancer. *Nat. Genet.* 41, 521–523.

Verrier, L., Escaffit, F., Chailleux, C., Trouche, D. and Vandromme, M. (2011a). A new isoform of the histone demethylase JMJD2A/KDM4A is required for skeletal muscle differentiation. *PLoS Genet.* 7, e1001390.

Verrier, L., Escaffit, F., Chailleux, C., Trouche, D. and Vandromme, M. (2011b). A New Isoform of the Histone Demethylase JMJD2A/KDM4A Is Required for Skeletal Muscle Differentiation. *PLoS Genet* 7, e1001390.

Voeltz, G. K., Prinz, W. A., Shibata, Y., Rist, J. M. and Rapoport, T. A. (2006). A class of membrane proteins shaping the tubular endoplasmic reticulum. *Cell* 124, 573–586.

Watanabe, S., Watanabe, K., Akimov, V., Bartkova, J., Blagoev, B., Lukas, J. and Bartek, J. (2013). JMJD1C demethylates MDC1 to regulate the RNF8 and BRCA1-mediated chromatin response to DNA breaks. *Nat. Struct. Mol. Biol.* 20, 1425–1433.

Weitzel, J. M., Hamann, S., Jauk, M., Lacey, M., Filbry, A., Radtke, C., Iwen, K. A. H., Kutz, S., Harneit, A., Lizardi, P. M., et al. (2003). Hepatic gene

expression patterns in thyroid hormone-treated hypothyroid rats. *J. Mol. Endocrinol.* 31, 291–303.

Whetstine, J. R., Nottke, A., Lan, F., Huarte, M., Smolikov, S., Chen, Z., Spooner, E., Li, E., Zhang, G., Colaiacovo, M., et al. (2006). Reversal of histone lysine trimethylation by the JMJD2 family of histone demethylases. *Cell* 125, 467–481.

White, J. M. (2003). ADAMs: modulators of cell-cell and cell-matrix interactions. *Curr. Opin. Cell Biol.* 15, 598–606.

Whyte, W. A., Bilodeau, S., Orlando, D. A., Hoke, H. A., Frampton, G. M., Foster, C. T., Cowley, S. M. and Young, R. A. (2012). Enhancer decommissioning by LSD1 during embryonic stem cell differentiation. *Nature* 482, 221–225.

Wissmann, M., Yin, N., Müller, J. M., Greschik, H., Fodor, B. D., Jenuwein, T., Vogler, C., Schneider, R., Günther, T., Buettner, R., et al. (2007). Cooperative demethylation by JMJD2C and LSD1 promotes androgen receptor-dependent gene expression. *Nat. Cell Biol.* 9, 347–353.

Wolf, S. S., Patchev, V. K. and Obendorf, M. (2007). A novel variant of the putative demethylase gene, s-JMJD1C, is a coactivator of the AR. *Arch. Biochem. Biophys.* 460, 56–66.

Wu, J. I., Lessard, J. and Crabtree, G. R. (2009). Understanding the words of chromatin regulation. *Cell* 136, 200–206.

Yamada, D., Kobayashi, S., Yamamoto, H., Tomimaru, Y., Noda, T., Uemura, M., Wada, H., Marubashi, S., Eguchi, H., Tanemura, M., et al. (2011). Role of the Hypoxia-Related Gene, JMJD1A, in Hepatocellular Carcinoma: Clinical Impact on Recurrence after Hepatic Resection. *Ann. Surg. Oncol.*

Yamane, K., Toumazou, C., Tsukada, Y., Erdjument-Bromage, H., Tempst, P., Wong, J. and Zhang, Y. (2006). JHDM2A, a JmjC-containing H3K9 demethylase, facilitates transcription activation by androgen receptor. *Cell* 125, 483–495.

Yeh, S., Tsai, M.-Y., Xu, Q., Mu, X.-M., Lardy, H., Huang, K.-E., Lin, H., Yeh, S.-D., Altuwaijri, S., Zhou, X., et al. (2002). Generation and characterization of androgen receptor knockout (ARKO) mice: an in vivo model for the study of androgen functions in selective tissues. *Proc. Natl. Acad. Sci. U. S. A.* 99, 13498–13503.

Zha, J. and Lackner, M. R. (2010). Targeting the insulin-like growth factor receptor-1R pathway for cancer therapy. *Clin. Cancer Res. Off. J. Am. Assoc. Cancer Res.* 16, 2512–2517.

Zhou, X. and Ma, H. (2008). Evolutionary history of histone demethylase families: distinct evolutionary patterns suggest functional divergence. *BMC Evol. Biol.* 8, 294.

Zhou, Y., Xu, B. C., Maheshwari, H. G., He, L., Reed, M., Lozykowski, M., Okada, S., Cataldo, L., Coschigamo, K., Wagner, T. E., et al. (1997). A mammalian model for Laron syndrome produced by targeted disruption of the mouse growth hormone receptor/binding protein gene (the Laron mouse). *Proc. Natl. Acad. Sci. U. S. A.* 94, 13215–13220.

Zibetti, C., Adamo, A., Binda, C., Forneris, F., Toffolo, E., Verpelli, C., Ginelli, E., Mattevi, A., Sala, C. and Battaglioli, E. (2010). Alternative Splicing of the Histone Demethylase LSD1/KDM1 Contributes to the Modulation of Neurite Morphogenesis in the Mammalian Nervous System. *J. Neurosci.* 30, 2521 – 2532.

Zlotoff, D. A. and Bhandoola, A. (2011). Hematopoietic progenitor migration to the adult thymus. *Ann. N. Y. Acad. Sci.* 1217, 122–138.